UNIVERSIDADE FEDERAL DO PARANÁ

LEONARDO MAIRINK BARÃO

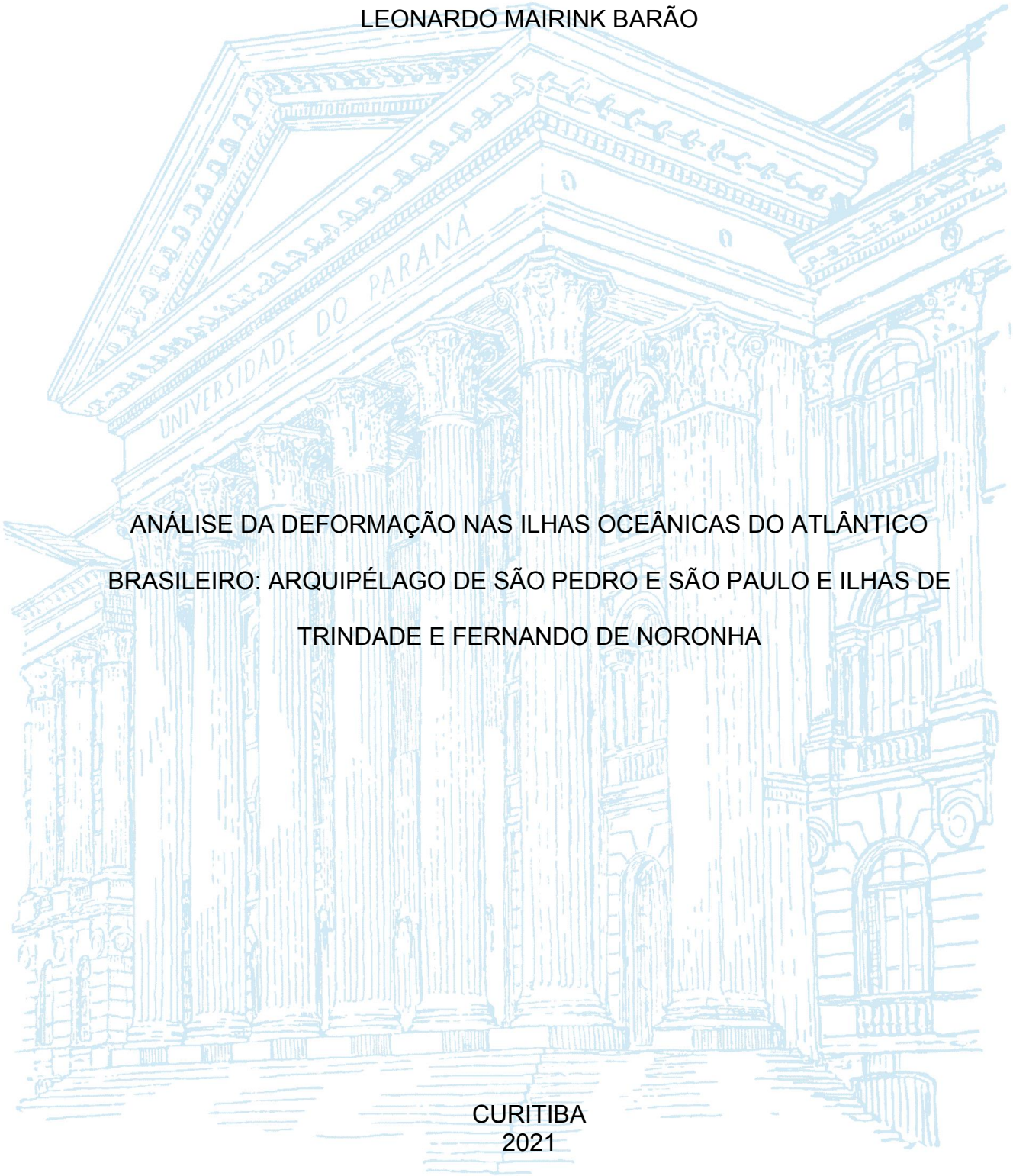

ANÁLISE DA DEFORMAÇÃO NAS ILHAS OCEÂNICAS DO ATLÂNTICO BRASILEIRO: ARQUIPÉLAGO DE SÃO PEDRO E SÃO PAULO E ILHAS DE TRINDADE E FERNANDO DE NORONHA

CURITIBA
2021

LEONARDO MAIRINK BARÃO

ANÁLISE DA DEFORMAÇÃO NAS ILHAS OCEÂNICAS DO ATLÂNTICO BRASILEIRO: ARQUIPÉLAGO DE SÃO PEDRO E SÃO PAULO E ILHAS DE TRINDADE E FERNANDO DE NORONHA

Tese apresentada ao curso de Pós-Graduação em Geologia, Setor de Ciências da Terra, Universidade Federal do Paraná, como requisito parcial à obtenção do título de Doutor em Geologia.
Orientadora: Profa. Dra. Barbara Trzaskos
Coorientadores:
Prof. Dr. Rodolfo José Angulo
Prof. Dr. Leonardo Evangelista Lagoeiro

CURITIBA
2021

Catalogação na Fonte: Sistema de Bibliotecas, UFPR
Biblioteca de Ciência e Tecnologia

B225a Barão, Leonardo Mairink
Análise da deformação nas ilhas oceânicas do atlântico brasileiro [recurso eletrônico] : arquipélago de São Pedro e São Paulo e ilhas de Trindade e Fernando de Noronha / Leonardo Mairink Barão. – Curitiba, 2021.

Tese - Universidade Federal do Paraná, Setor de Ciências da Terra, Programa de Pós-Graduação em Geologia, 2021.

Orientadora: Barbara Trzaskos.
Coorientadores: Rodolfo José Ângulo, Leonardo Evangelista Lagoeiro.

1. Arquipélagos. 2. Ilhas - Brasil. 3. Geologia estrutural. I. Universidade Federal do Paraná. II. Trzaskos, Barbara. III. Angulo, Rodolfo José. IV. Lagoeiro, Leonardo Evangelista. V. Título.

CDD: 551.8

Bibliotecária: Vanusa Maciel CRB- 9/1928

MINISTÉRIO DA EDUCAÇÃO
SETOR DE CIENCIAS DA TERRA
UNIVERSIDADE FEDERAL DO PARANÁ
PRÓ-REITORIA DE PESQUISA E PÓS-GRADUAÇÃO
PROGRAMA DE PÓS-GRADUAÇÃO GEOLOGIA - 40001016028P5

TERMO DE APROVAÇÃO

Os membros da Banca Examinadora designada pelo Colegiado do Programa de Pós-Graduação em GEOLOGIA da Universidade Federal do Paraná foram convocados para realizar a arguição da tese de Doutorado de **LEONARDO MAIRINK BARAO** intitulada: **ANÁLISE DA DEFORMAÇÃO NAS ILHAS OCEÂNICAS DO ATLÂNTICO BRASILEIRO: ARQUIPÉLAGO DE SÃO PEDRO E SÃO PAULO E ILHAS DE TRINDADE E FERNANDO DE NORONHA**, sob orientação da Profa. Dra. BÁRBARA TRZASKOS, que após terem inquirido o aluno e realizada a avaliação do trabalho, são de parecer pela sua APROVAÇÃO no rito de defesa.
A outorga do título de doutor está sujeita à homologação pelo colegiado, ao atendimento de todas as indicações e correções solicitadas pela banca e ao pleno atendimento das demandas regimentais do Programa de Pós-Graduação.

CURITIBA, 01 de Junho de 2021.

Assinatura Eletrônica
01/06/2021 13:32:00.0
BÁRBARA TRZASKOS
Presidente da Banca Examinadora

Assinatura Eletrônica
01/06/2021 13:15:05.0
WEBSTER UEIPASS MOHRIAK
Avaliador Externo (UNIVERSIDADE DO ESTADO DO RIO DE JANEIRO)

Assinatura Eletrônica
01/06/2021 12:51:50.0
DAVID LINO VASCONCELOS
Avaliador Externo (UNIVERSIDADE FEDERAL DE CAMPINA GRANDE)

Assinatura Eletrônica
01/06/2021 12:43:56.0
MARCIA MAIA
Avaliador Externo (FRENCH NATIONAL CENTRE FOR SCIENTIFIC RESEARCH)

Assinatura Eletrônica
01/06/2021 14:27:07.0
ANDREA TOMMASI
Avaliador Externo (UNIVERSITÉ DE MONTPELLIER)

À minha família, principalmente os meus pais, que investiram amor e tempo para conquista desses feitos.

AGRADECIMENTOS

Primeiramente gostaria de agradecer meus pais Rosana e Rogério e meu irmão Tiago, que sempre me incentivaram a completar mais essa conquista na minha vida e me auxiliaram em toda a minha carreira acadêmica. Gostaria de agradecer também a Betina Alencar que surgiu em minha vida e sempre me apoiou e suportou todas as barras da vida até aqui.

Gostaria de agradecer a minha orientadora Barbara Trzaskos por todo o incentivo, discussões e conselhos geológicos durantes esses seis anos de mestrado e doutorado. Além de me acolher no Laboratório de Análise de Bacias durante esse período. Agradeço também ao Prof. Fernando Vesely que sempre colaborou com meu projeto e em as todas as revisões de inglês e puxões de orelha durante esses anos.

Agradeço aos meus co-orientadores e co-autores professores Rodolfo J. Angulo, Leonardo Lagoeiro, Maria Cristina de Souza e Eleonora Vasconcellos, por participarem e apoiarem meu projeto de doutorado, além de darem assertivas contribuições ao texto da tese.

Aos meus colegas de LABAP, sala da pós e LAMIR, Renata, Fabio B., Thammy, Aurora, William, Camila, Lara N., Lara, L., Drag, Fabio D., Itararé, Farofa, Deisi, Merolyn, Hugo, Luís, Larissa, Gabriel F., Mayara, Fernanda B., Thailli, Amanda e Érika, esses que sempre apoiaram minha pesquisa e estavam no mesmo barco da geociências.

E também aos meus companheiros de campo em São Pedro e São Paulo, 2. Sargento Pereira, Cabo Adriano e o Marinheiro Ricardo, além dos pescadores que percorreram todo caminho até ASPSP em segurança e excelente hospitalidade. Aos meus colegas de Ilha de Trindade, Fernanda Avelar, Maurício Garcia, Luís Sielski, e

meu amigo Hérick Daufenbach que sempre auxiliaram nas pesquisas na ilha e fora dela. Gostaria de agradecer também as equipes da Marinha presentes na ilha Cabritadas Entrosados e Copa da Cabrita por todo auxílio nos trabalhos de campo e por tornar a pesquisa na ilha possível. Agradecendo especialmente ao suboficial enfermeiro Anderson Arcanjo, que nos acompanhou na ilha e acabou por falecer no mês abril (2020) nos esforços contra o COVID-19.

Agradeço as entidades Marinha do Brasil e SECIRM por propiciar a pesquisa científicas nas ilhas oceânicas brasileiras, além do CNPQ pelo financiamento dos projetos número 557299/05-5, 557141/2009-5 e 442865/2015-5. E também a CAPES por custear minha bolsa de estudo, apesar dos intensos cortes que a ciência vem passando.

Aos laboratórios ILAMIR, LAPEM, LAMIN e LECOST por todo apoio cedido ao incentivo da pesquisa geológica na UFPR. Ao Laboratório Serviço Geológico Finlandês (GTK), principalmente os técnicos e geólogos Akseli Torppa, Hannu T. Makkonen, Jukka Laukkanen e Dandara Ataide Salvador, a pareceria e disposição na realização de ensaios analíticos e discussões. Também agraço a Flavia Alonso por confeccionar com grande maestria as lâminas petrográficas do meu doutorado.

Ao Programa de Pós-Graduação em Geologia da Universidade Federal do Paraná pela oportunidade cedida e principalmente ao secretário da pós Kazu que quando solicitado agiu com eficiência, além de ser um grande amigo.

Por fim agradeço a todos meus amigos Eduardo Santos, Felipe Nadalin, Bruno Gaúcho, Jan Soares, Amanda Huck, Thomas e Diego pelos momentos de descontração do doutorado.

“The saddest aspect of life right now is that science gathers knowledge faster than society gathers wisdom.”

(Isaac Asimov)

"Don't do anything I would do, and definitely don't do anything I wouldn't do..."

(Tony Stark, 2017)

RESUMO

A tectônica do Atlântico Sul apresenta diversas peculiaridades, sendo controlada pelo magmatismo e pela ação das zonas transformantes e de fraturas que se desenvolveram desde a ruptura do Gondwana. As ilhas oceânicas brasileiras mais distantes da porção continental estão intimamente ligadas à evolução das zonas de fraturas que as circundam, sendo elas o Arquipélago São Pedro e São Paulo (ASPSP) e as ilhas de Trindade (IT) e Fernando de Noronha (IFN). Consequentemente essas estruturas causam a deformação dessas ilhas desde a sua formação até o presente momento. Através do mapeamento geológico e utilizando a análise multiescala foi possível identificar e detalhar estruturas como falhas, foliações miloníticas, feições cataclásticas, feições brechóides e bandas de deformação. Utilizando-se de estudos microtectônicos foram identificadas fases minerais e a presença de estilos deformacionais distintos em cada um dos arquipélagos estudados. Também foram executados estudos de paleotensões em planos de falhas, afim de recompor a evolução tectônica dos arquipélagos. Tratadas separadamente, em cada ilha se observou: (1) que o ASPSP apresenta evolução tectônica marcada pela rápida exumação mantélica, assinalando assim a transição de estruturas e microestruturas entre os regimes de deformação dúctil e *semi-britlle*. No regime dúctil houve intensa milonitização, em temperaturas entre 700º-800º, com a recristalização da olivina e ortopiroxênios presentes nos peridotitos. A interação com fluídos originados do manto, criam domínios ricos em anfibólios e óxidos, marcando a passagem para o estágio de deformação *semi-brittle*. A contínua compressão e soerguimento, causada pela ação da Falha Transformante São Paulo, culmina na maior presença de fluidos hidrotermais, controlando quatro fases de serpentinização, associadas aos regimes *semi-brittle* e rúptil, em temperaturas entre 300º e 400.ºC. O último estágio de exumação é marcado pelo estabelecimento do regime de deformação rúptil, levando assim a fase de precipitação carbonática alojada em falhas e juntas de direção E-W, com tensões voltadas para a direção NW-SE similares aos sismos registrados atualmente na região. (2) A IT marca o evento vulcânico mais recente do território brasileiro (3.7 a <0.17Ma), aonde foi constatada a presença de falhas, que evoluíram de um momento distensional, com a formação de conjuntos de grabens e horts de direção NNW-SSE ao longo de toda ilha, para um momento transtrativo, associado a formação dos diques alcalinos e a formação de falhas oblíquas de direção NE-SW. Esse arranjo configura a instalação de tensões NW-SE, similares à aquelas observadas para a Plataforma Sul-americana. A evolução tectônica e as tensões transtrativas levaram também a formação de bandas de deformação, causadas pela cisalhamento e catáclase das rochas piroclásticas. (3) Em IFN, foram observadas falhas semelhantes as observadas, remetendo a momentos distensionais e posteriormente momentos transtrativos associadas a falhas direcionais, que indicam tensões principais de direções NW-SE. A compilação dos dados de tensões nos três arquipélagos permitiu associar a presença de tensões principais de direção NW-SE, similares as observadas em movimentos neotectônicos na plataforma Sul-americana e em outras localidades com mesmos contextos tectônicos.

Palavras-chave: Regime de Transição Dúctil-Rúptil. Zonas de Fraturas Transformantes. Bandas de deformação. Ilhas vulcânicas. Rochas de Falha.

ABSTRACT

The South Atlantic tectonics has several controls of the deformation, being controlled by the magmatism and the action of the transforming and fractures zonesthat have developed since the Gondwana. The Brazilian oceanic islands furthest from the Brazilian mainland are closely linked to the evolution of the fracture zones that surround them, namely the São Pedro and São Paulo Archipelago (SPSPA) and the Trindade (TI) and Fernando de Noronha (FNI) Islands. Consequently, these structures lead to the deformation of these islands from their formation to the present moment. Through the geological mapping of tectonic structures and using a multiscale analysis it was possible to identify and detail structures such as faults, mylonitic foliations, cataclastic, breccia features and deformation bands. Using microtectonic approach on the rocks of these islands, distinct mineral phases and the presence of different deformational styles were identified in each of the studied archipelagos. Paleotension studies were also carried out on fault plans on these islands, in order to recompose the geological evolution of each of the studied archipelagos. Treated separately each island throughout this work was observed: (1) the ASPSP shows a tectonic evolution with rapid mantle exhumation, thus marking the transition of structures and microstructures between the ductile deformation regimes, causing intense milonitization, at temperatures between 700º-800º causing the intense recrystallization of olivine and orthopyroxenes present in peridotites. The interaction with fluids originating from the mantle creates domains rich in amphiboles and oxides, marking the passage to the semi-brittle deformation stage. The continuous compression and uplift caused by the action of the São Paulo Transformer Fault culminates in the greater presence of hydrothermal fluids, forming as a consequence four phases of veins, associated with semi-brittle to brittle regimes at temperatures between 300º and 400ºC. And the last stage of exhumation is marked by the establishment of the brittle deformation regime, thus leading to the phase of carbonate precipitation housed in faults and joints with E-W direction, with stresses strikes NW-SE direction similar to the earthquakes recalled for the region today. (2) IT marks the most recent volcanic event in the Brazilian territory (3.7 to <0.17Ma). On the island it was found by the presence of faults, evolving from an extensional moment, with the formation of sets NNW-SSW-striking grabens and horsts throughout the entire island, to a transtensional moment associated with the formation of alkaline dikes and the formation of faults oblique NE-SW direction, configuring the installation of NW-SE stresses, stresses similar to those observed for the South American Platform. The tectonic evolution and the transtensional stresses also led to the formation of deformation bands caused by the cataclase and the shear of the pyroclastic rocks. (3) In FN, faults similar to those observed in Trindade were observed, referring to extension moments and later transtractive moments associated with strike-slip faults, which indicate principal stresses strikes NW-SE. The compilation of stress data in the three archipelagos made it possible to associate the presence of main stresses strikes NW-SE, similar to those observed in neotectonic movements on the South American Plate.

Keywords: Ductile-brittle transition. Transformer Fault. Deformation Band. Volcanic Islands. Fault Rocks.

LISTA DE FIGURAS DA TESE

LISTA DE FIGURAS ARTIGO 1

LISTA DE FIGURAS ARTIGO 2

LISTA DE FIGURAS ARTIGO 3

LISTA DE TABELAS

LISTA DE TABELAS ARTIGO 2

LISTA DE ABREVIATURAS OU SIGLAS

Amp	Anfibólio (Amphibole)
ASPSP	Arquipélago São Pedro e São Paulo
Cb	Grupo dos carbonatos
Cpx	Clinopiroxênio (Clinopyroxene)
DB	Deformation Band
IFN	Ilha de Fernando de Noronha
IT	Ilha de Trindade
LEPLAC	Plano de Levantamento da Plataforma Continental Brasileira
Mag	Magnetita (Magnetite)
MAR	Middle Atlantic Ridge
Ol	Olivina (Olivine)
Opx	Ortopiroxênio (Orthopyroxene)
RTF	Romanche Transform Fault
Spl	Espinélio (Spinel)
Spr	Serpentina (Serpentine)
SPSPA	Saint Peter and Saint Paul Archipelago
SPTF	Saint Peter Transform Fault
TI	Trindade Isle
VTFZ	Vitória-Trindade Fracture Zone
ZFSP	Zona de Fratura São Paulo
ZFVT	Zona de Fratura Vitória Trindade

SUMÁRIO

CAPÍTULO I

1.1. Introdução

As ilhas oceânicas, pertencentes ao território nacional brasileiro, fazem parte do patrimônio geológico do Brasil e tratam-se de localidades estratégicas para o desenvolvimento científico devido a possibilidade de exploração de recursos naturais (Souza et al., 2009). Os aspectos deformacionais dessas ilhas são pouco discutidos na literatura atual, colocando essas ilhas como alvo potencial para o estudo do tectonismo recente e ainda atuante na região.

A formação do conjunto de ilhas oceânicas está relacionada a abertura do Oceano Atlântico Sul (Almeida, 2006), estando associada a processos unicamente vulcânicos, como o caso dos arquipélagos de Fernando de Noronha e Trindade e Martin Vaz (Almeida, 2006), ou pela exumação de corpos mantélicos, como ocorre no Arquipélago de São Pedro e São Paulo (Hekinian et al., 2000; Sichel et al., 2008; Maia et al., 2016).

Os arquipélagos são circundados por diversas estruturas transformantes que condicionaram o vulcanismo e a exumação de corpos mantélicos (Almeida, 2006). A tectônica atual se faz presente, visto a quantidade de pequenos abalos sísmicos que ocorrem, principalmente no Arquipélago São Pedro e São Paulo, associados possivelmente a acomodação tectônica de falhas transformantes (Campos et al. 2009a).

1.2. Estrutura da Tese

A tese está estruturada em quatro capítulos distintos. Este primeiro introdutório com foco na estrutura e localização da área de estudo (**Capítulo I**).

O **Capítulo II** no qual serão destacados os métodos utilizados para pesquisa, a geologia regional e local, além da fundamentação teórica sobre a formação de ilhas oceânicas semelhantes aos casos estudados.

O **Capítulo III** apresenta os resultados da pesquisa em forma de três artigos. O primeiro publicado no *Journal of Structural Geology (Vol. 133, abril 2020*, https://doi.org/10.1016/j.jsg.2020.103981*),* voltado para evolução tectônica do Arquipélago São Pedro e São Paulo e as deformações dúcteis-rúpteis (Seção 3.1). O segundo artigo relacionado ao arcabouço estrutural da Ilha de Trindade e sua relação com a tectônica Atlântica (Seção 3.2), publicado no *Journal of South American Earth Science* (Vol. 104, dezembro 2020, https://doi.org/10.1016/j.jsames.2020.102812). O terceiro artigo será voltado para as bandas de deformação observadas na Ilha de Trindade (Seção 3.3) a ser submetido ao *Journal of Structural Geology*. Em adição, são relatados os dados estruturais obtidos no arquipélago Fernando de Noronha (Seção 3.4).

O **Capítulo IV** trata das considerações finais e conexão entre os três artigos propostos nessa tese, além das referências bibliográficas compiladas dos três artigos.

1.3. Localização das Áreas de estudo

As áreas de estudo localizam-se na costa nordeste e sudeste do Brasil (Figura 1A, estando o Arquipélago de São Pedro e São Paulo (ASPSP) localizado a cerca de 1.000 km da cidade de Natal - RN (Figura 1B). As rochas desse arquipélago são limitadas pela Zona de Fratura São Paulo (Figura 1B), gerada durante a formação do Oceano Atlântico (Wilson, 1965). A segunda área de estudo, é a Ilha de Fernando de Noronha (IFN), situa-se a sudoeste do

ASPSP, distando-se cerca de 360 km da cidade de Natal (Figura 1B), sendo limitada pela Zona de Fratura de Fernando de Noronha (ZFN) (Figura 1B). A terceira área de estudo situa-se a 1170 km de cidade de Vitória (Espírito Santo), denominada como Cadeia Vitória-Trindade (Figura 1C), onde ocorrem as Ilhas de Vitória-Trindade e Martin Vaz.

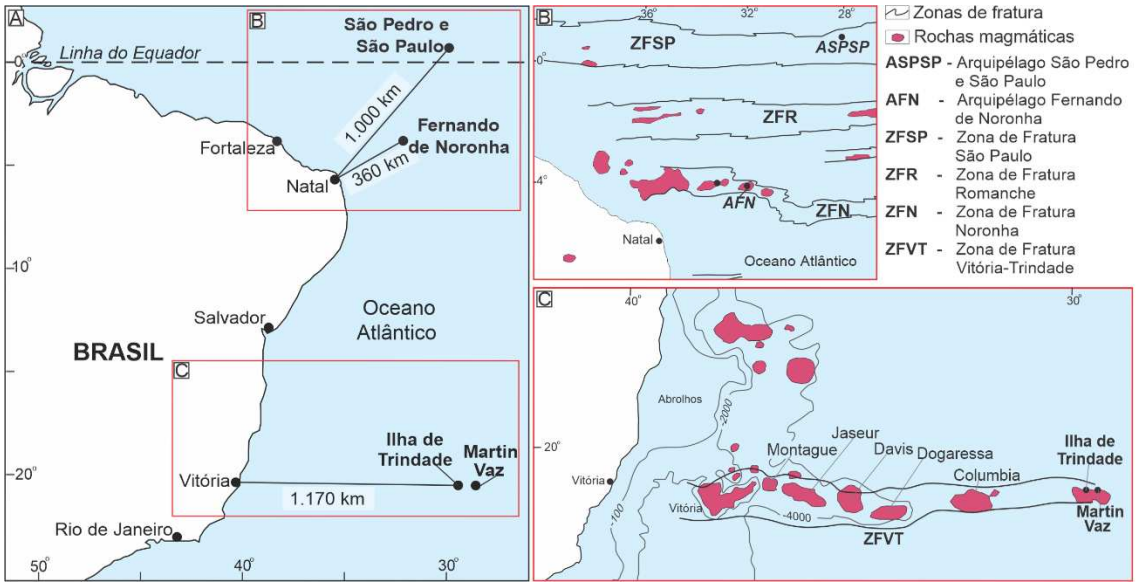

Figura 1 – A) Localização das áreas de estudo. B) Indicação da região dos arquipélagos São Pedro e São Paulo (ASPSP) e Ilha de Fernando Noronha (IFN). C) Arquipélago de Trindade e Martin Vaz. Modificado de Almeida (2006).

CAPÍTULO II

2.1. Objetivos

Esse trabalho tem por objetivo realizar o estudo da deformação nos arquipélagos de São Pedro e São Paulo, Fernando de Noronha e Trindade e Martin Vaz, utilizando a análise estrutural, afim de compreender o regime tectônico, e o campo de tensão atuante em cada uma das ilhas estudadas. Pretende-se também propor modelo de evolução tectônica conjunta para os três arquipélagos, contribuindo para o entendimento da colocação das ilhas no Atlântico Sul.

Desta maneira será possível alcançar abordagem regional e integrada da deformação no Atlântico Sul, incluindo a identificação dos paleoesforços e dos tensores atuais, com o objetivo de estabelecer a relação entre as zonas de falhas transformantes adjuntas e evolução tectônica de cada arquipélago. Para tanto alguns objetivos específicos são apontados:

- Detalhar a deformação em cada um dos arquipélagos;
- Definir regimes e fases de deformação;
- Reconstruir tensões exercidas durante os processos formadores e deformadores;
- Estabelecer relações e influência entre as zonas transformantes e os arquipélagos.

2.2. Justificativa

O estudo das ilhas oceânicas é essencial para a expansão do território brasileiro em milhas náuticas, sendo a pesquisa científica nessas áreas necessária para a compreensão dos diferentes contextos geológicos da

evolução da plataforma continental brasileira. A ação das zonas transformantes nessas ilhas ainda é pouco compreendida, sendo comum a ocorrência de sismos, que podem causar impacto à sobrevivência nesses arquipélagos.

A influência das zonas transformantes nas ilhas oceânicas brasileiras ainda é pouco estudada e os aspectos deformacionais não foram bem ilustrados ou compreendidos. A análise da deformação nessas ilhas servirá de suporte à correlação dos esforços tectônicos *in situ* com os paleoesforços responsáveis pela formação dos arquipélagos.

2.3. Hipótese

Espera-se que os principais e mais distantes arquipélagos brasileiros tenham se formado em taxas de deformação diferenciada. Cada arquipélago teve influência tectônica de diferentes zonas transformantes, essas podem ter atuado com distintas taxas de deformação ao longo de sua evolução e posterior deformação.

A variação de tensores tectônicos deve ter propiciado regimes tectônicos distintos, essa alteração já foi observada em estudos paleomagnéticos, para a Zona Transformante de Romanche, a norte de Fernando Noronha (Ernesto, 2005), e mais recentemente inversão de tensores observada para a deformação do arquipélago São Pedro e São Paulo (Maia et al., 2016). Esses tensores devem estar atuantes e devem ser a resposta para os sismos recorrentes na região litorânea e nordeste brasileira.

2.4. Materiais e Métodos

Para a realização desta pesquisa foram utilizadas diversas abordagens, explicitadas no fluxograma da Figura 2, no qual são ordenados as atividades desenvolvidas e os objetivos pretendidos durante o mestrado. No fluxograma (Figura 2) está elucidado a progressão da pesquisa em cada um dos métodos e arquipélagos. A seguir serão detalhados cada um dos métodos empregados durante a pesquisa.

2.4.1. Levantamento Bibliográfico

Consistiu no levantamento dos trabalhos históricos e atuais já executados nos arquipélagos de São Pedro e São Paulo e ilhas de Fernando de Noronha e Trindade (e.g. Darwin, 1844; Almeida, 1969; Almeida, 2006; Campos et al., 2009a; Palmiotto et al., 2017). Em adição, além de ilhas oceânicas, foram analisados artigos de outras ilhas formadas em mesmo contexto tectônico e magmático, tanto no Oceano Atlântico quanto no Oceano Pacífico .

O levantamento bibliográfico visou abranger o estudo das técnicas empregadas para o desenvolvimento da pesquisa, como os mecanismos de deformação.

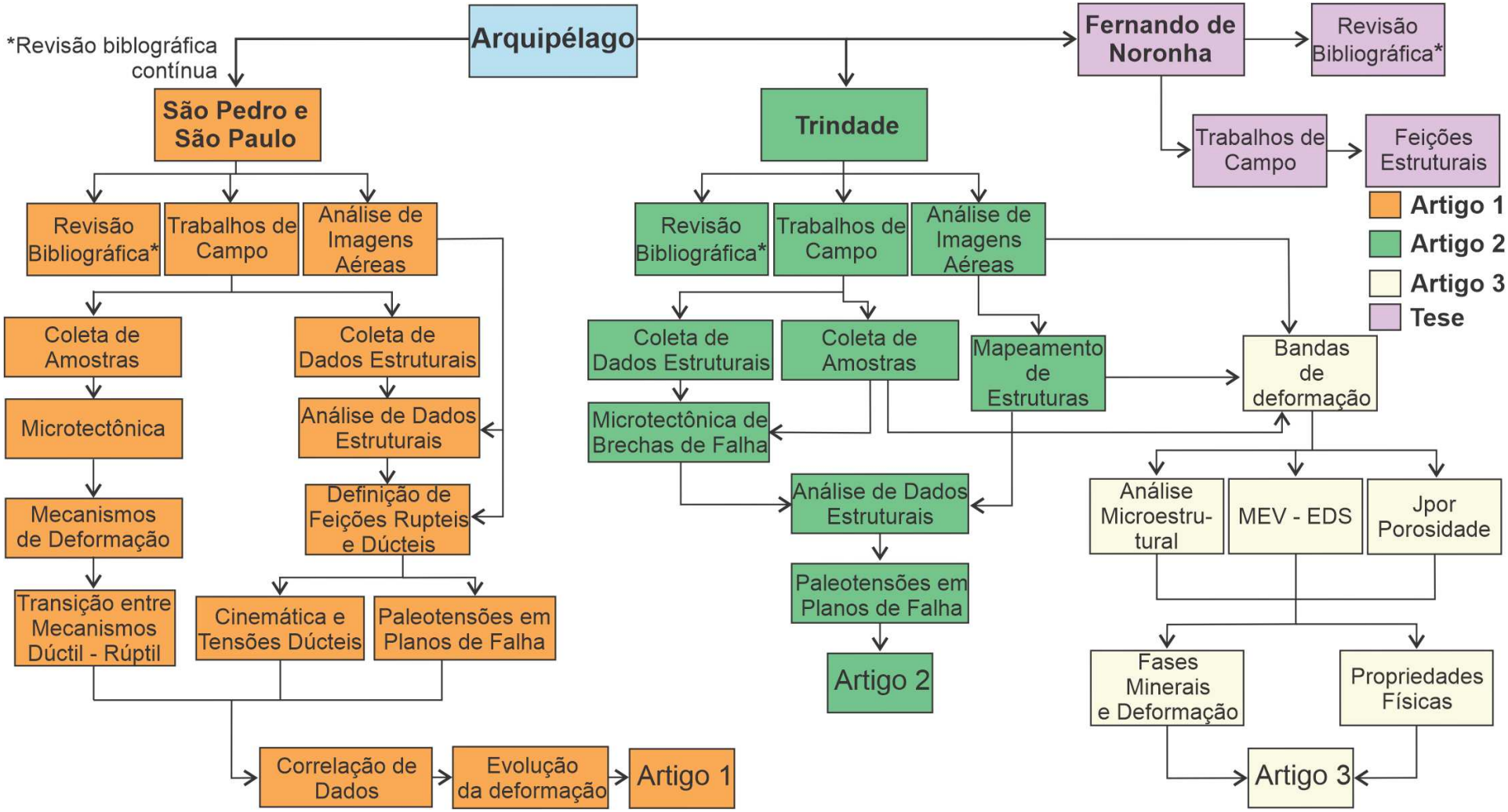

Figura 2 - Fluxograma de atividades desenvolvidas durante o doutorado.

2.4.2. Análise Espacial

A análise espacial em ambos os arquipélagos foi realizada a fim de se observar a distribuição das estruturas tectônicas nas ilhas. No Arquipélago São Pedro e São Paulo foi utilizada a imagem adquirida por drone pela Universidade Federal de Pernambuco, onde foi possível se distinguir a foliação milonítica, fraturas, falhas, corpos sedimentares e se identificar elementos fractais distribuídos no arquipélago (Barão et al., 2018a).

Já na Ilha de Trindade foram utilizadas duas fontes distintas de imagens, a primeira derivada de imagem aérea, capturadas pela Marinha do Brasil (2011). Foram utilizadas para se definir as principais estruturas da ilha, detalhando cerca 10 mil lineamentos presentes na ilha. Para maior detalhe foi ainda utilizada imagens adquiridas por levantamentos de drone realizado para Universidade Federal de Viçosa. A partir da imagem foi possível identificar fraturas, acamamento vulcânico e as bandas de deformação presentes na região do vulcão do Paredão.

2.4.3. Levantamentos de Campo

Foram efetuadas quatro etapas de campo para o mapeamento de estruturas tectônicas presentes nos arquipélagos. O tempo de permanência nos arquipélagos dependeu principalmente de órgãos federais como a Marinha e o ICMBio, totalizando 40 dias de campo divididos segundo a Tabela 1.

Tabela 1 - Tempo de permanência em campo nos arquipélagos. Não levando em conta o tempo de deslocamento e dias ociosos devido as atividades da Marinha.

Arquipélago	*Etapa*	*Dias de Campo*
São Pedro e São Paulo	Abril - Maio (2017)	16
Fernando de Noronha	Maio (2017)	3
Trindade	Junho de 2017 e Maio - Junho (2018)	21

Nestas etapas de campo foram tomadas atitudes estruturais de juntas, falhas, foliações, estruturas de fluxo e lineações (mineral, estiramento, intersecção), afim de elaborar diagramas estereográficos para a análise estrutural.

Em campo foram coletadas amostras orientadas de rochas deformadas, analisadas a luz dos mecanismos de deformação. As etapas de campo serviram para identificação de indicadores cinemáticos, no caso de indicadores rúpteis em zonas de falha como estepes e estrias, além de outros indicadores já relatados em extensa bibliografia (Petit, 1987; Doblas, 1998). No caso de indicadores de deformação em regime dúctil foram examinadas rochas miloníticas, observando a foliação, par S/C, feições dobradas, entre outras estruturas que poderiam indicar a cinemática e os paleoesforços responsáveis pelas estruturas.

2.4.4. Análise da deformação

Os dados estruturais obtidos nas etapas de campo foram tabelados e organizados em planilhas, posteriormente tratados e relacionados aos eventos deformacionais correspondentes. A partir da planilha de dados estruturais foram confeccionados diagramas estereográficos em *softwares* como *OpenStereo* (Grohmann and Campanha, 2010) e *Stereo32*, no qual foram plotados os dados de planos de falha, estrias e cinemática. Nesses diagramas foram plotados os

planos de fratura, foliações e lineações, com o objetivo de obter as principais direções dessas estruturas e suas relações espaciais.

No caso de indicadores cinemáticos rúpteis foram obtidas as direções dos paleoesforços a partir do método dos Diedros Retos idealizado inicialmente por (Angelier and Mechler, 1977) (Figura 3), e posteriormente desenvolvido para o *software Wintensor 5.0.6* (Delvaux, 2012). Através de ambos os métodos foi possível adquirir a componente triaxial (tensão máxima (σ_1), intermediária (σ_2) e mínimo (σ_3) para os planos de falha.

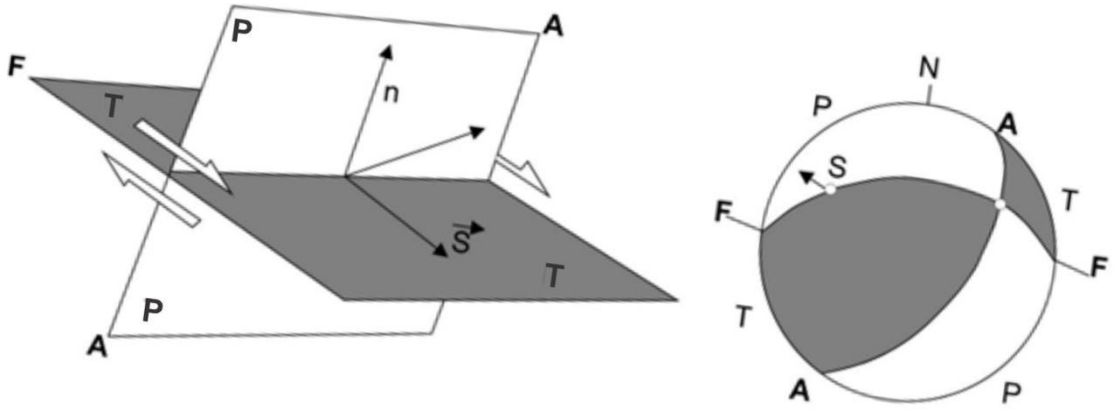

Figura 3 - Método dos diedros retos em falhas. A) Vista em perspectiva dos diedros. B) diagrama estereográfico representando os campos de tensão atuantes em uma falha. P=diedro de compressão (branco); T=diedro de extensão (cinza); A=plano auxiliar; F=plano de falha; s=vetor de movimentação (estria); n=plano de falha inversa; B=interseção dos planos a e b. Modificado de Angelier (1994).

2.4.5. Mecanismos de Deformação

Os mecanismos de deformação/recristalização representam o registro geológico dos parâmetros como temperatura, pressão, taxa de deformação, tamanho dos grãos, composição de fluidos (Knipe, 1989; Stipp et al., 2002a; Paschier e Trouw, 2005) vigentes durante a deformação da rocha. A conjuntura desses fatores é capaz de criar microestruturas diferenciadas segundo determinado regime tectônico, sendo ele dúctil ou rúptil.

A caracterização desses mecanismos, pela descrição de seções delgadas utilizando-se do microscópio petrográfico, é essencial para definir o regime deformacional das rochas. Em grande parte das ilhas, localizadas em nível crustal raso, espera-se o predomínio do regime rúptil, representado por brechas e cataclasitos (Sibson, 1977). As microestruturas geradas nessas rochas são as microfraturas e microfalhas, causando a cominuição dos grãos a baixas temperaturas (Knipe, 1989). Entretanto a deformação pode ocorrer também pelos mecanismos de transferência de massa (dissolução e precipitação), deformação intracristalina (geminações, estruturas em *kink*, recuperação e recristalização) e transferência de massa por difusão (recristalização estática). A distinção desses mecanismos auxilia a elucidação dos parâmetros controladores da deformação (Paschier e Trouw, 2005).

2.4.6. MEV – EDS - Raman

A seção petrográfica foi primeiramente polida até se atingir a espessura correta para o uso técnica de MEV-EDS (Microscópio Eletrônico de Varredura - Espectroscopia por Energia Dispersiva). Posteriormente a esse polimento foi utilizado o equipamento FEI Quanta 650 FEG-SEM MLA (Figura 4A) para analisar o conteúdo mineral do Serviço Geológico Filandes (GTK) no Laboratório de Processamento Mineralógico de Outokumpu (Finlândia).

O método de identificação mineral usado foi o MLA (*Mineral Liberation Analyzer*), que se trata de um sistema analítico computadorizado, que usa análise de imagens de elétrons retroespalhados (BSE - *Backscattered-Electron Imaging*) e espectros de raios-X (EDS) na identificação dos minerais, em secções petrográficas polidas (Carioca e Brandão, 2018). O microscópio

Renishaw InVia Qontor Raman (Figura 4B), foi usado para identificar principalmente fases minerais de granulação muito finas a finas, como a zeólita. O banco de dados Raman de minerais (RRUFF) foi usado para identificação de fases minerais específicicas e de granulação muito fina, como os minerais do grupo da zeolita.

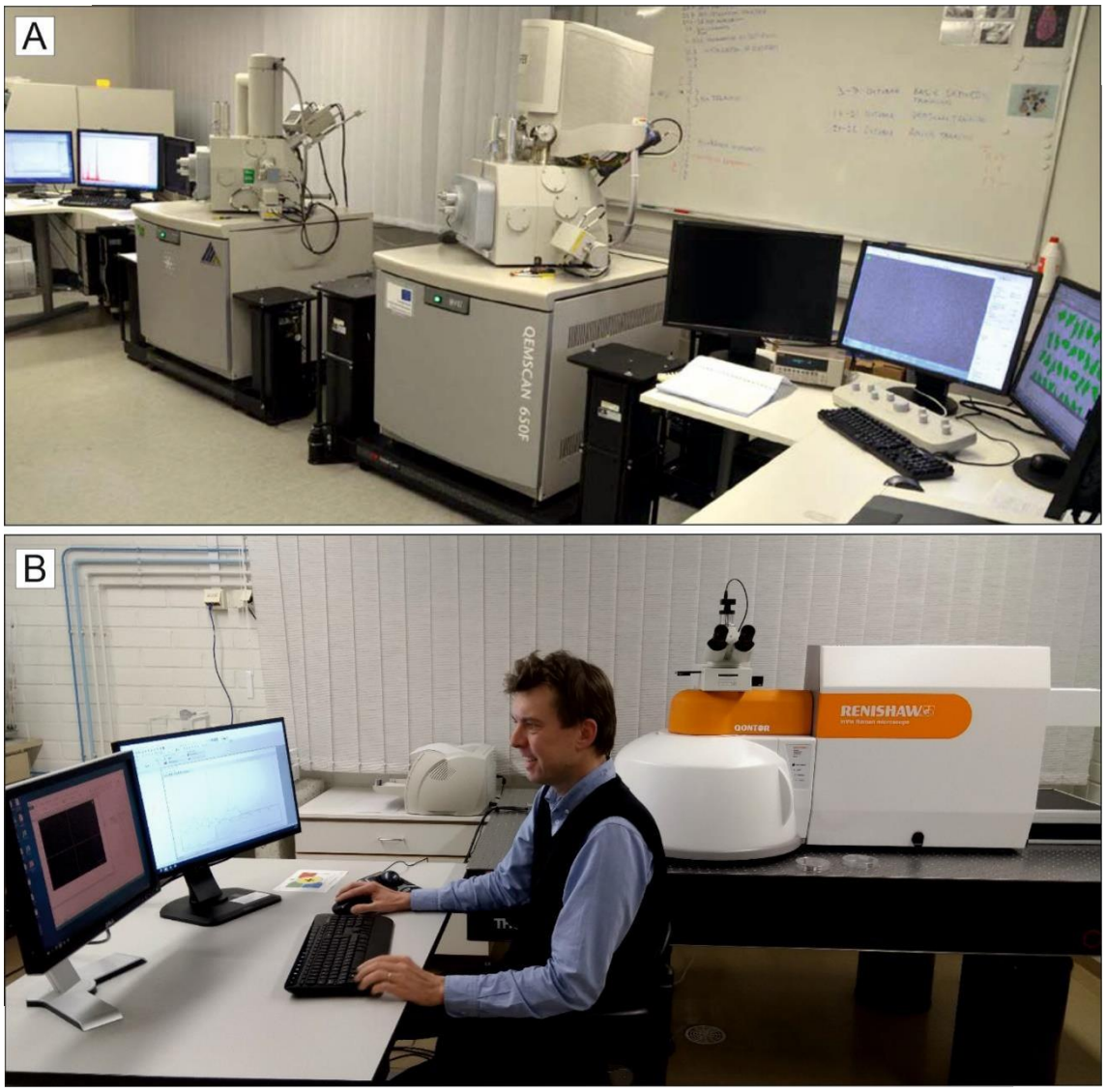

Figura 4 - Equipamentos usados para a obtenção dos aspectos microscópios das bandas de deformação. (A) Dois instrumentos MLA no Laboratório de Mineralogia de Processo do GTK em Outokumpu, Finlândia. (B) The Renishaw InVia Qontor Raman microscope.

Também foi usado método XMOD_STD, que trata-se da contagem de pontos de MLA em que a área da amostra é dividida sistematicamente em pontos

de amostragem e o espectro de raios-X é medido em cada ponto. Os espectros de raios-X são salvos para classificação. Os espectros coletados são comparados com uma biblioteca espectral coletada antes ou após a medição. Este método classifica modalmente a mineralogia, ou seja, o conteúdo dos componentes minerais na amostra.

Os conteúdos minerais obtidos por esse método são tabaleados e depois indexados para a construção de mapas de fase minerais (Item 3.3 – Artigo de Bandas de Deformação). Com base nos dados do MLA, o principal componente da amostra estudada é a massa fundamental, que é composto de partículas minerais de granulação muito fina. A indexação dos dos grãos menores do que 1 e 5μm ficou comprometida, por formarem uma massa muito fina o que dificulto sua detecção no MLA.

2.5. Contexto Geológico

2.5.1. Ilhas oceânicas a sua relação com a tectônica e magmatismo

As ilhas oceânicas podem ser divididas de acordo com sua origem, ao longo de todos os oceanos, com maior ocorrência nas proximidades das dorsais mesoceânicas (Islândia no Atlântico Norte) ou nas proximidades de anomalias mantélicas em placas oceânicas (Ilhas do Havaí no pacífico) (Wilson, 1963; Morgan, 1972).

Em geral as ilhas vulcânicas se desenvolvem seguindo o modelo proposto por Darwin (1844) (Figura 5). O modelo leva em conta que inicialmente o vulcanismo atinge o nível do mar acabando por formar uma ilha oceânica ativa (Figura 5A). Assim que cessada a atividade vulcânica a ilha passa por processos de soerguimento, culminando em plataformas de recifes ao redor do vulcão,

agradando e progredindo sobre as paredes do vulcão (Figura 5B). Processo semelhante ocorre nas ilhas de Fernando de Noronha e Trindade (Almeida, 2006). A partir de certo momento ocorre a subsidência tectônica com a erosão parcial do vulcão (Figura 5C), criando uma lagoa profunda dentro da parede de coral. A evolução dessa lagoa e da barreira de coral, bem como dos processos erosivos sobre o vulcão, acabam por gerar feição anelar denominada de atol (Figura 5D).

A completa erosão do cone vulcânico e a formação de extensa plataforma culmina no estágio final de evolução de uma ilha vulcânica, formando montes submarinos denominados como *guyots* (Figura 5E). Feição comum observada ao longa da cadeia Vitória-Trindade e nas proximidades do arquipélago de Fernando de Noronha (Almeida, 2006).

Em geral as ilhas vulcânicas possuem expectativa de vida variável entre 5 e 20 Ma, dependendo da velocidade e intensidade de movimentação da placa tectônica em que se forma a ilha (McDougall, 1964; McDougall e Chamalaun, 1969). Sendo que a maior concentração de atividade sísmica observada nessas ilhas ocorre principalmente durante a sua formação, sendo pouco registrada ao longo de sua existência (Palmiotto et al., 2017).

Já as ilhas tectônicas são associadas a movimentos verticais de porções litosféricas da placa oceânica, estão associadas a diretamente a tectônica falhas transformantes, circundantes a essas ilhas e formadas perpendiculares as dorsais oceânicas(Palmiotto et al., 2017), distribuindo-se ao longo dos oceanos Atlântico e Indico (Figura 6). Em geral são constituídas por rochas de derivação mantélica e por extensa plataforma de recifes que recobre essas rochas (Figura 7).

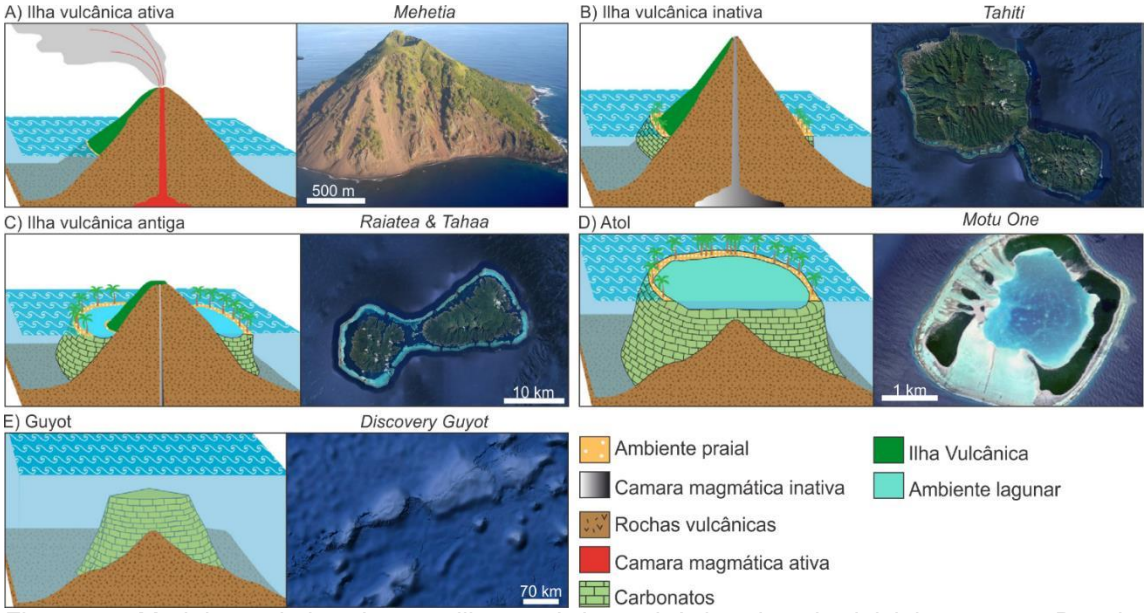

Figura 5 - Modelo evolutivo de uma ilha oceânica vulcânica descrito inicialmente por Darwin (1884). Modificado de Palmiotto et al. (2017).

A conjuntura dos esforços tectônicos gera grandes cadeias de montanha submarinas, como as que ocorrem no Arquipélago de São Pedro e São Paulo (Figura 7A), que possui mais de 4000 m de profundidade (Hekinian et al., 2000; Motoki et al., 2011), expondo as rochas peridotíticas do manto em superfície. Por se tratar de um local propício para abrigar vida em meio ao oceano, pode desenvolve alongada plataforma carbonática de topo plano (Figura 7B).

Devido a contínua subsidência térmica que ocorre na litosfera oceânica, a ilha fica propensa a criação de plataforma carbonática alongada segundo da cadeia submarinha (Palmiotto et al., 2017) (Figura 7C). Pode ser observada a variação de relevo ao longo dessa estrutura, gerado devido a tectônica instável e que afeta essas ilhas. Por final a completa subsidência leva a formação de extensa plataforma carbonática submersa, com pouca ou nenhuma atividade tectônica (Figura 7D), criando uma ilha vulcânica fóssil. Dessa maneira a existência dessas ilhas está intimamente relacionada a contínua taxa de soerguimento, provocada pela ação sísmica na região das zonas transformantes (Palmiotto et al., 2017).

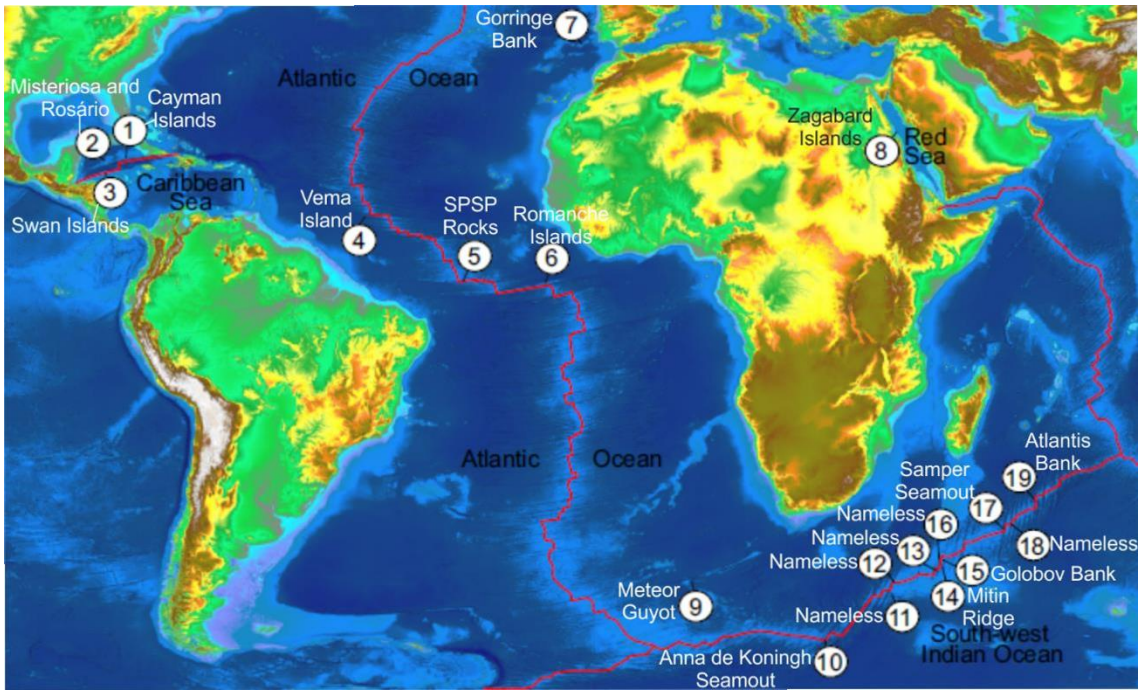

Figura 6 - Distribuição das ilhas tectônicas no Atlântico e porção sudoeste do Oceano Indico e nos mares vermelho e do Caribe. A linha vermelha indica o limite das placas tectônicas Modificado de Palmiotto et al. (2017).

2.5.2. Arquipélago São Pedro e São Paulo

O Arquipélago São Pedro e São Paulo (ASPSP) dista cerca de 1.000 km a nordeste da cidade de Natal-RN (Figura 1A), estando situado aproximadamente a 1° a norte da Linha do Equador (Almeida, 2006). O arquipélago é composto por 10 ilhas (Figura 2A), possuindo área total emersa de cerca de 17 km^2, com atitudes máximas de até 18m. Essas ilhas representam a porção emersa de uma cadeia submarina transversal a cadeia mesoceânica (Campos et al., 2009a).

A estrutura condicionante do ASPSP possui direção WSW-ENE denominada como Zona de Fratura São Paulo (ZFSP) (Figura 2B), essa zona de fratura possui cerca de 120 km largura, se estendendo no Oceano Atlântico desde a Meso Dorsal Atlântica e até próximo a região continental brasileira (Almeida, 2006). Próximo a região onde afloram as rochas do arquipélago as profundidades alcançam cerca de -3600 m, contudo são observadas profundidades de até -5.000 m (Hekinian et al., 2000).

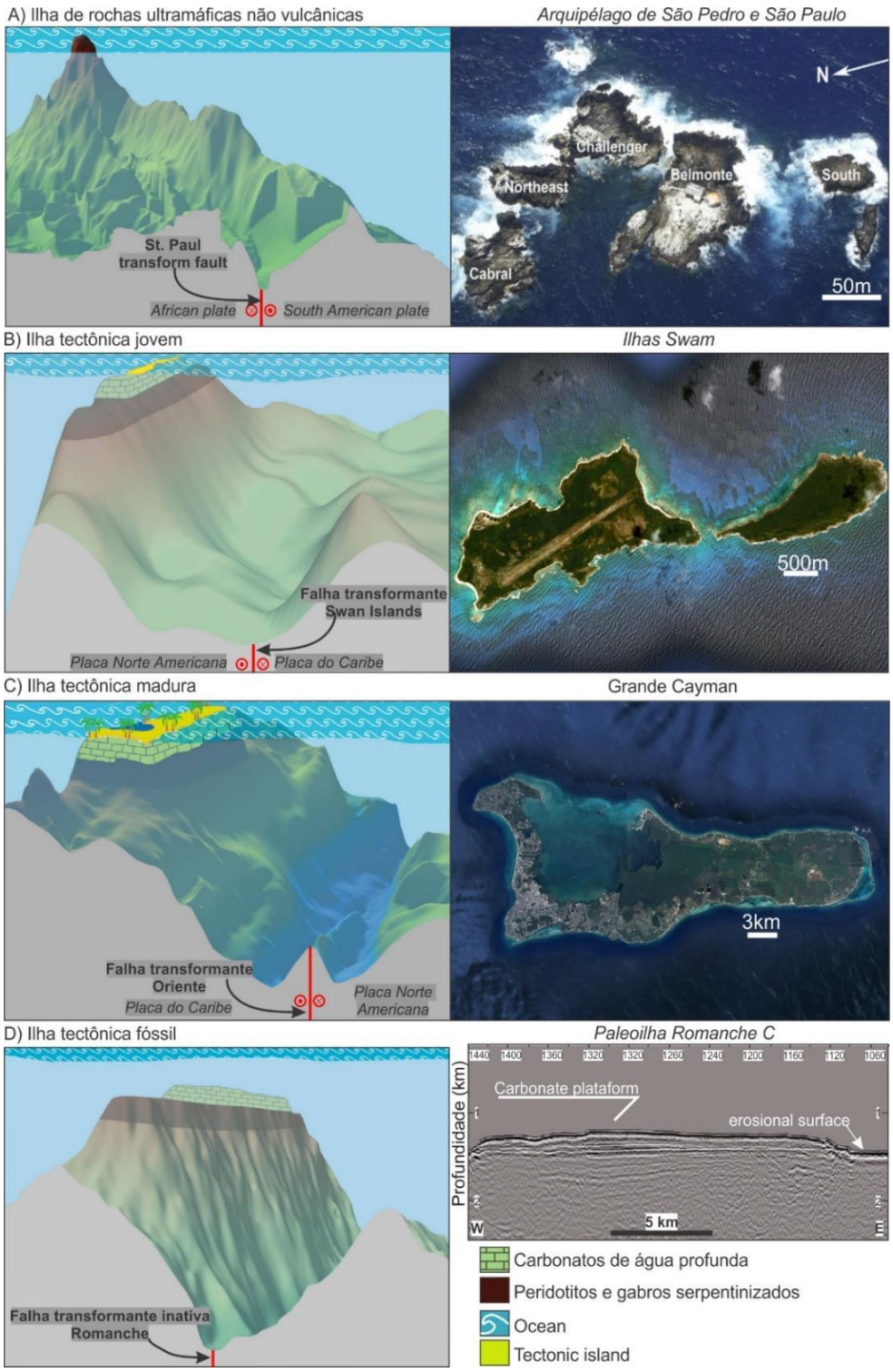

Figura 7 - Evolução de uma ilha tectônica, seguindo por etapas observadas em diferentes localidades pelo mundo. (A) exumação do manto, formando rochas peridotíticas; (B) formação a plataforma carbonática; (C) estabilidade tectônica e formação lagoa devido a subsidência; (D) completa subsidência e permanência de plataforma marinha. Modificado de Palmiotto et al. (2017).

O ASPSP é formado por rochas texturalmente muito finas de cor cinza escuro, aflorantes na porção noroeste da Ilha Belmonte (Figura 9) correspondendo ao peridotito milonitizado (Melson et al., 1967, 1972). Já ao sudeste da Ilha Belmonte e no restante das ilhas ocorre o predomínio de rocha heterogênea, de granulação fina, de cor variada e intensamente fraturada. Essa rocha trata-se do peridotito milonitizado onde ocorre o processo de intensa serpertinização, devido a ação de fluídos hidrotermais ao longo de microfraturas (Campos et al., 2003). A heterogeneidade presente nessa rocha se deve a interação entre a trama não serpertinizada e serpertinizada, desenvolvida a partir do fraturamento que causa o "consumo" da fase milonítica anteriormente formada (Campos et al., 2009b).

Na Ilha Challenger ocorre variante da rocha peridotítica denominada como milonito kaersutítico (Figura 9). Trata-se também de rocha de granulação fina a muito fina, de cor cinza, rica em kaersutita. Pode ocorrer a intercalação do material milonítico e da rocha rica em kaersutita, gerando bandamento composicional com níveis centimétricos a milimétricos (Campos et al., 2009b).

A foliação é obliterada pelos processos de serpentinização e halmirólise (ação da água salobra sobre as rochas) (Campos et al. 2003a). A paragênese dessas rochas ainda possui resquício de composição ígnea, sendo evidenciada pela presença de porfiroclastos de olivina, piroxênio, anfibólios e espinélios. Esses cristais são fortemente fraturados, fragmentados e envoltos por matriz fina a muito fina (Campos et al., 2003a). Melson et al. (1972) identificaram três distintas *fabrics* formadas devido a diminuição progressiva da temperatura e pressão: a) primária correspondente aos porfiroclastos deformados; b) minerais

não deformados, resposta da cristalização contínua; c) formada pelos processos posteriores a milonitização, ou seja, a serpentinização e a halmirólise.

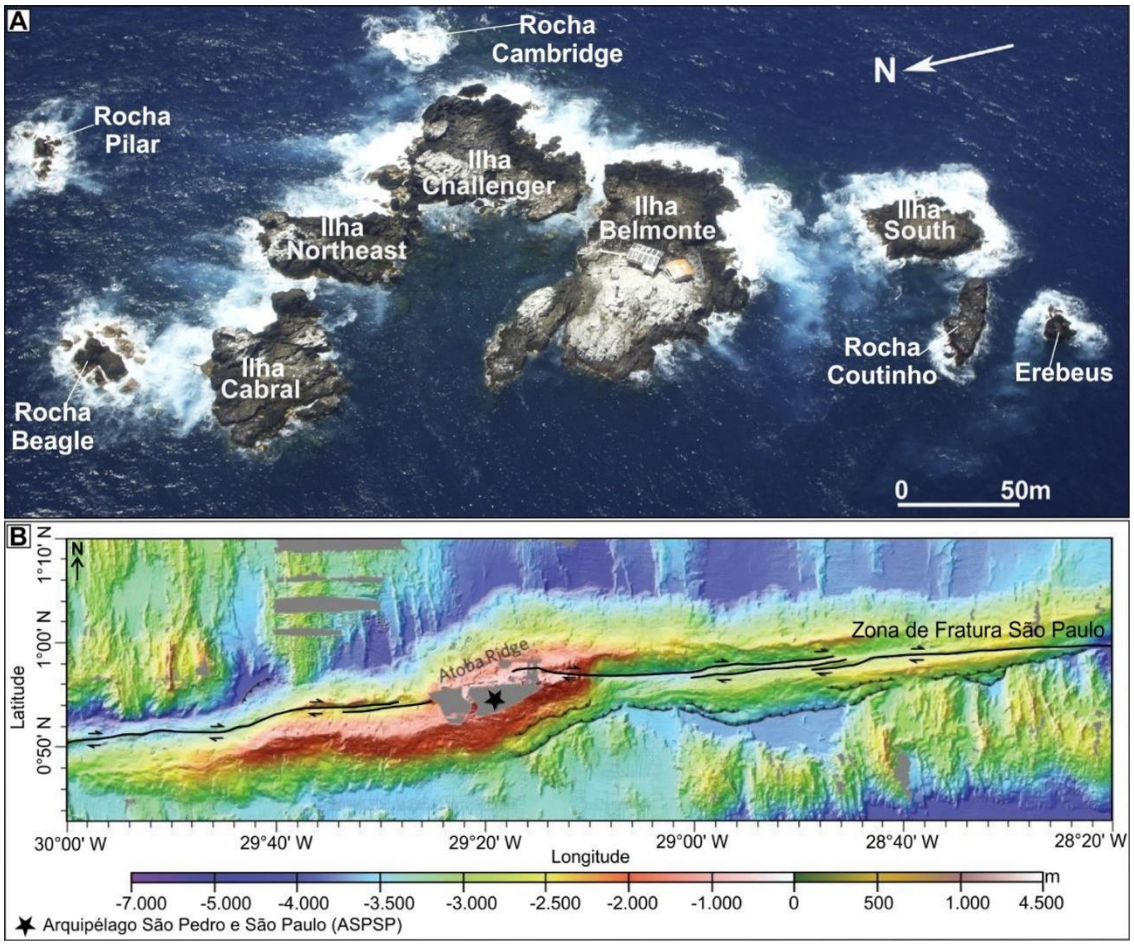

Figura 8 - (A) Distribuição das dez ilhas no Arquipélago São Pedro e São Paulo, modificado de Angulo et al. 2012. (B) configuração tectônica do ASPSP em relação a Zona de Fratura São Paulo (ZFSP), caracterizando a forma sigmoidal próxima a essa zona, modificado de Maia et al. (2016).

Segundo aspectos estruturais, os peridotitos estão intensamente cisalhados em estado dúctil, sendo representados por ultramilonitos, indicando inicialmente a deformação plástica, sendo estruturas relevantes para a compreensão da história tectônica do ASPSP (Simões et al., 2009).

Essas rochas encontram-se intensamente recristalizadas devido a ação tectônica, sendo marcante a intensa foliação que contorna os porfiroclastos de olivina e espinélio (Moraes, 1997; Andrade et al., 2006; Simões et al., 2009). A

foliação, detalhada por diversos autores (e.g. Melson et al., 1972; Hekinian et al., 2000; Moraes, 1997; Andrade et al., 2006), apresenta direção e mergulho varável entre N10-30W/70-45E (Figura 3), sendo essa direção discordante da Zona Transformante São Pedro e São Paulo, podendo estar intimamente associada as zonas de cisalhamento Sirius e Píer, que devem ter contribuído para a deformação local da estrutura, gerando padrão incoerente com a zona transformante (Simões et al., 2009).

Sobre as rochas peridotíticas da Ilha Challenger, ocorre a presença de pequena formação sedimentar marinha rasa de idade quaternária (Campos et al., 2003b; Campos et al., 2009a; Angulo et al., 2013), composta por sedimentos clásticos polimíticos de origem biológica e grãos das rochas peridotíticas adjacentes (Angulo et al., 2013). Campos et al. (2003a, 2009b) definiram essa unidade geológica como Formação São Pedro e São Paulo, subdivida em duas unidades distintas:

- Unidade Atobás: posicionada discordantemente sobre os peridotitos, composta por conglomerados, arenitos e brechas e rochas com cimentação carbonática. Sendo comum a presença de fósseis de corais disseminados na matriz das brechas.
- Unidade Viuvinhas: situada discordantemente sobre as rochas da Unidade Atobás, formada por brechas e paraconglomerados, em geral possuem fósseis coralíferos.

Assume-se que essas rochas foram depositadas aproveitando as zonas de fraqueza de direção NW-SE e existentes no peridotito. Com a invasão da água marinha ocorreu a deposição inicialmente da Unidade Atobás e posteriormente da Unidade Viuvinhas. Essas unidades passaram por expressivo evento

tectônico, que deve ter basculhado as camadas dessas unidades (Campos et al., 2003b, 2009b).

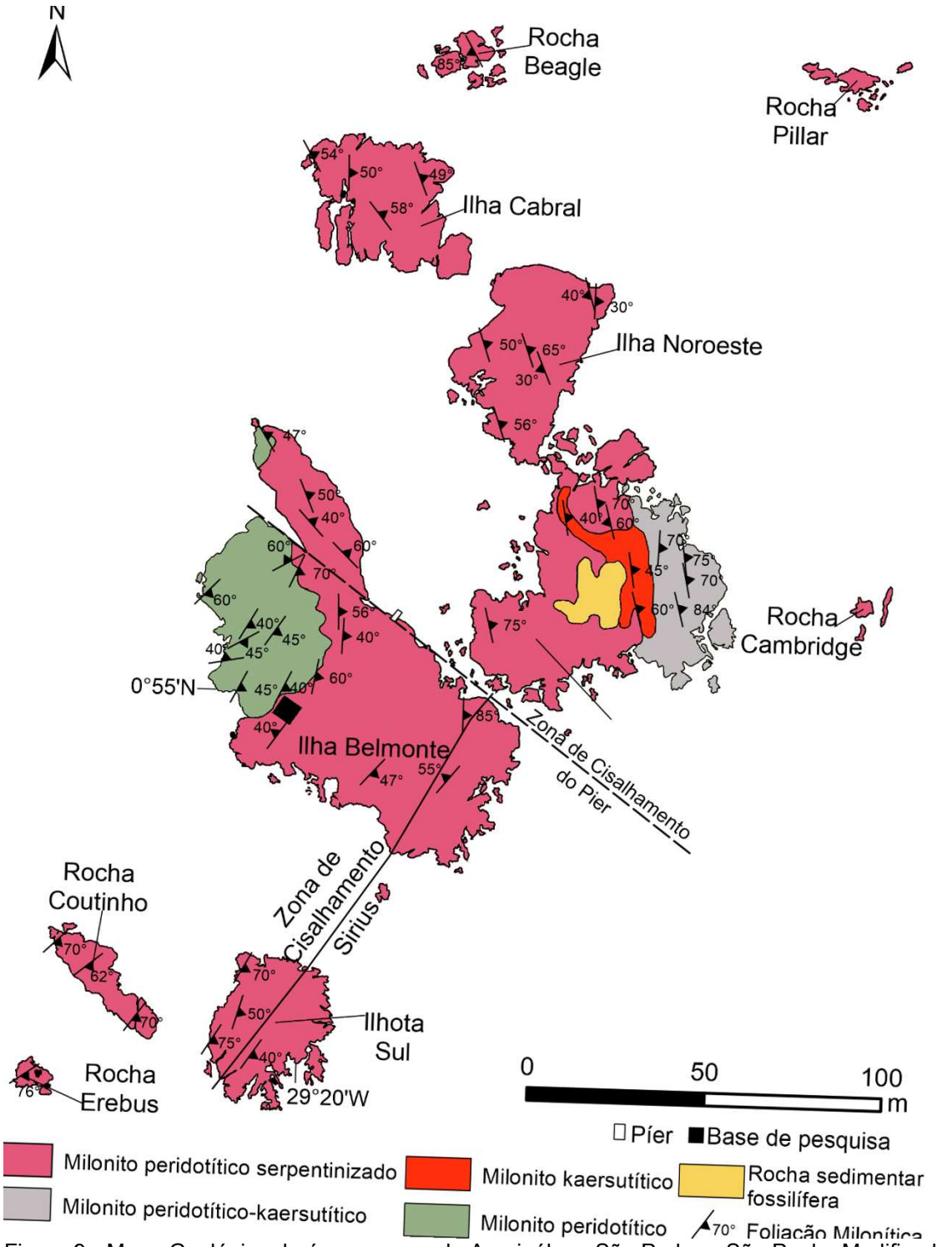

Figura 9 - Mapa Geológico da área emersa do Arquipélago São Pedro e São Paulo. Modificado de Campos et al. (2003b), Campos et al. (2009a,b) e Simões et al. (2009).

- Modelos Tectônicos Propostos para o ASPSP

Apesar de estudado a mais de 200 anos o ASPSP passou por diversas modificações conceituais sobre a sua evolução tectônica. Darwin (1844) foi o primeiro a constatar que essas rochas eram de derivação mantélica, diferentemente de estudos propostos anteriormente. Posteriormente Tilley (1947), através de estudos petrográficos, descreveu as rochas do arquipélago como peridotito serpentinizado, confirmando a teoria de Darwin (1844) e colocando assim o ASPSP como alvo de estudo geológicos e tectônicos. Melson et al. (1967) e posteriormente Bonatti (1971) propuseram que a evolução tectônica e a abertura do Oceano Atlântico (Figura 10A), que permitiu a ascensão do manto por esforços extensional que permitiram a formação da cadeia de montanha do ASPSP, consequentemente a sua evolução a partir da dorsal Mesoceânica, através da diferenciação do magma plutônica que intrude na crosta continental recém-formada. Todavia o modelo proposto não leva em conta a evolução da Zona Transformante São Paulo e sua deformação e a formação de milonitos e ultramilonitos do arquipélago.

Bonatti (1990) constata que as rochas observadas no ASPSP apresentam derivação do manto abissal, devido a sua composição geoquímica diferenciada, se comparada ao manto atual e a falta de remobilização e diferenciação magmática terrestre. Posteriormente Hekinian et al. (2000) a partir mergulhos utilizando o submersível *Nautile*, constaram que ao redor da cadeia de montanha do ASPSP foi observado intenso enxame de diques gabroícos e de basaltos, que se diferenciaram a partir do manto peridotítico seccionando a crosta oceânica. Foi definido que a região constitui estrutura sigmoidal, causada pela movimentação diferencial dextral da ZFSP durante a formação da porção Sul e

norte da cadeia de montanha submarina (Figuras 8B e 10B). Devido a essa movimentação diferenciada, Hekinian et al. (2000) constataram que o soerguimento da porção norte foi mais intenso e consequentemente foi maior a deformação exercida sobre as rochas dessa região, do que sobre a porção sul do sigmoide (Figura 10B).

Com a evolução dos estudos batimétricos (Sandwell e Smith, 1997), e os mergulhos realizados pelo *Nautile* foi possível caracterizar melhor a estrutura sigmoidal do ASPSP, confirmando também a teoria de Bonatti et al. (1990) da origem mantélica abissal das rochas do ASPSP. Nessa configuração Sichel et al. 2008 sugerem que a Zona Transformante São Paulo constitui a feição de descolamento (Figura 10C), que permitiu a exumação do manto abissal formando a estrutura denominada como *megamullion* (Tucholke et al., 1998). Essa estrutura nada mais seria que a feição semelhante ao “casco de tartaruga”, que ascende na superfície sobre as condições do regime compressivo que afetou a ZFSP.

Segundo Sichel et al. (2008) constituem uma lasca tectônica formada durante o fechamento do Oceano Rheic durante o cretáceo (Figura 10C). Esse manto ficou estável e sua ascensão se deu a partir da abertura do Oceano Atlântico no Cretáceo por regimes distensionais (Sichel et al., 2008).

Com o avanço de novas técnicas e a aquisição de dados sísmicos e gravimétricos de melhor qualidade para a região do ASPSP, Maia et al. (2016) propõe a evolução sistemática do ASPSP a partir da evolução tectônica da Zona Transformante São Paulo (Figura 10D). As tensões tectônicas impostas sobre o arquipélago sugerem a inicial rotação sinistral a cerca de 11 Ma, permitindo o

soerguimento transtrativo e flexura tectônica que levou a formação do arquipélago e o seu contínuo soerguimento e deformação atual.

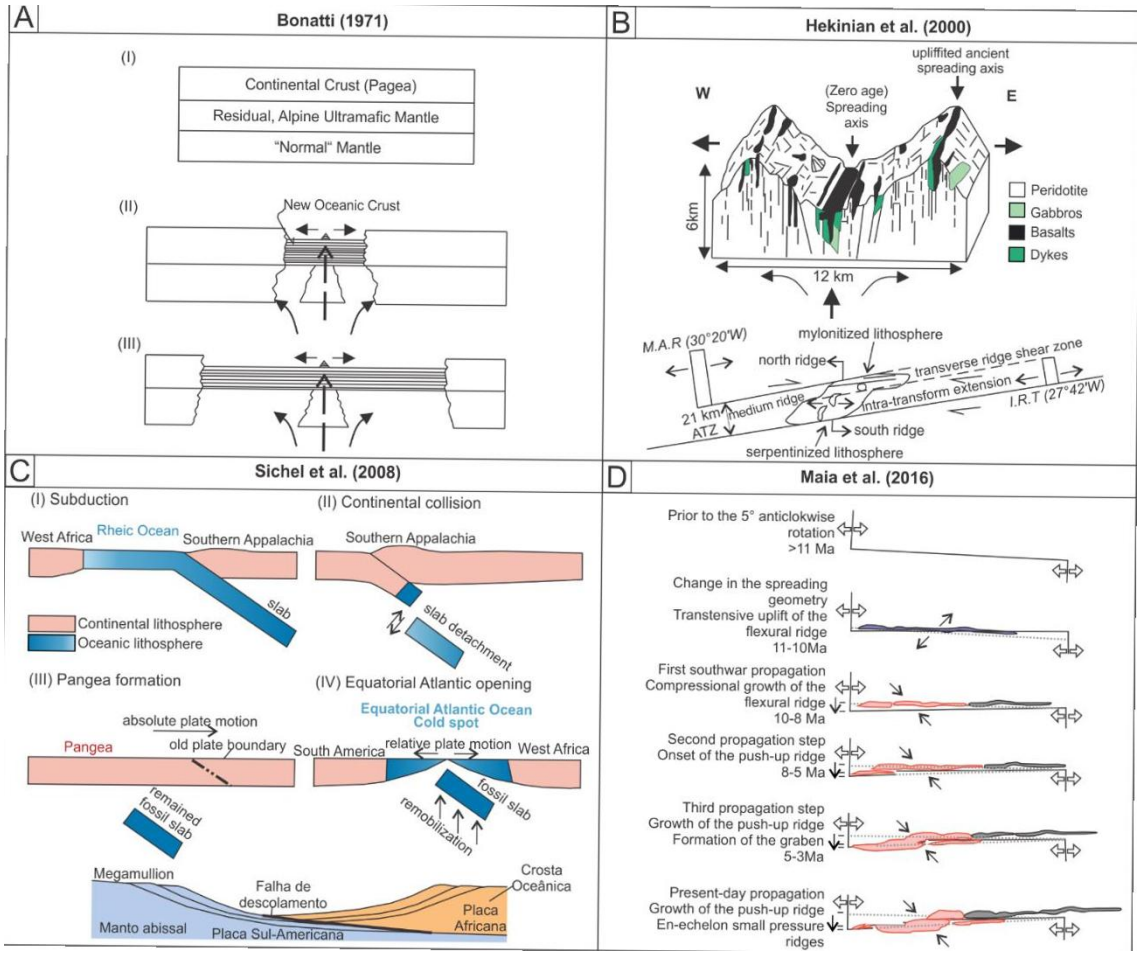

Figura 10 - Histórico de modelos tectônicos propostos para os ASPSP. (A) modelo proposto por Bonatti (1971); (B) modelo de Hekinian et al. (2000); (C) modelo observado por Sichel et al. (2008); (D) último modelo tectônico proposto por Maia et al. (2016).

2.5.3. Ilha de Trindade

O Arquipélago de Trindade e Martin Vaz ou a Cadeia Vitória-Trindade tem seu início no talude continental próximo a cidade de Vitória e possui continuidade a norte até a região de Abrolhos (Figura 11). O arquipélago é formado por diversos montes submarinos (*guyots*) alinhados e alongados segundo a direção

E-W (Figura 11), na Zona de Fratura de Vitória-Trindade (ZFVT) (Alves et al., 2006).

A Cadeia Vitória-Trindade trata-se de importante atividade tectono-magmática oceânica que ocorreu durante o Cenozoico, possivelmente devido a reativação da ZFVT (Almeida, 2006; Alves et al., 2006). Essa estrutura foi descrita e mapeada por Alves et al. (2002), utilizando-se de métodos sísmicos, no qual foi comprovada a sua continuidade até a costa Africana, seccionando a Dorsal-Mesoceânica e produzindo localmente o deslocamento de cerca de 6 km.

Figura 11 - Mapa geológico proposto por Almeida (1961) da Ilha de Trindade. Modificado de Almeida (1961) e Pires e Bongiolo (2016).

A principal ilha da cadeia é denominada como Trindade (IT), composta pela sucessão de depósitos piroclásticos e grande conjunto de rochas subvulcânicas,

geomorfologicamente expostas na forma de domos, *necks* e diques (Ulbrich et al., 2004). Essas rochas vulcânicas foram subdivididas em quatro formações: Desejado, Morro Vermelho, Valado e Paredão (Figura 11). Ainda na IT são observados domos, diques e *necks* vulcânicos de composição fonolítica (Pires e Bongiolo, 2016). A cerca de 50 km da IT encontra-se a Ilha de Martin Vaz, feição geológica e geomorfológica semelhante a IT (Almeida, 2006).

Segundo a análise espacial dos diques e fraturas (Ferrari e Riccomini, 1999), os eixos de tensão possuem direção ENE-WSW a E-W, para a formação dos diques de direção NW-SE, sendo estes concordantes com a forma da ilha e de seu principal edifício vulcânico, sugerindo mesmo controle tectônico para a formação da ilha. A ação da ZFVT é registrada por Alves et al. (2006), a zona propicia a formação de regimes transcorrente e distensivos na região da Cadeia Vitória-Trindade. A ZFVT deve ter servido como um local favorável para o desenvolvimento de esforços alternados, ora compressivos e ora distensivos associados a vulcanismo e falhas (Alves et al., 2006).

2.5.4. Ilha de Fernando Noronha

A Ilha de Fernando de Noronha (IFN) é constituído da ilha principal, com cerca de 16 km², e vinte outras ilhas menores (Ulbrich et al. 2004). A ilha é constituída por sucessão vulcânica, vulcanoclástica e rochas alcalinas de idade miocênica (Almeida 2002) (Figura 12). A unidade geológica mais antiga da ilha principal é a Formação Remédios (Almeida 1955), composta por rochas alcalinas como álcali basaltos, fonolitos, traquitos tufos, brechas vulcânicas (Figura 12), além de diversos diques alcalinos verticais que seccionam toda a ilha.

As rochas alcalinas da Formação Quixaba são encobertas por espesso derrame, chegando a cotas de até 180 m acima do nível do mar (Almeida 2002,2006). Essa unidade é composta por melanefenilinitos (ankatritos), intercalados com rochas piroclásticas de mesma composição (Ulbrich et al., 2004). São observados também derrames de basanitos.

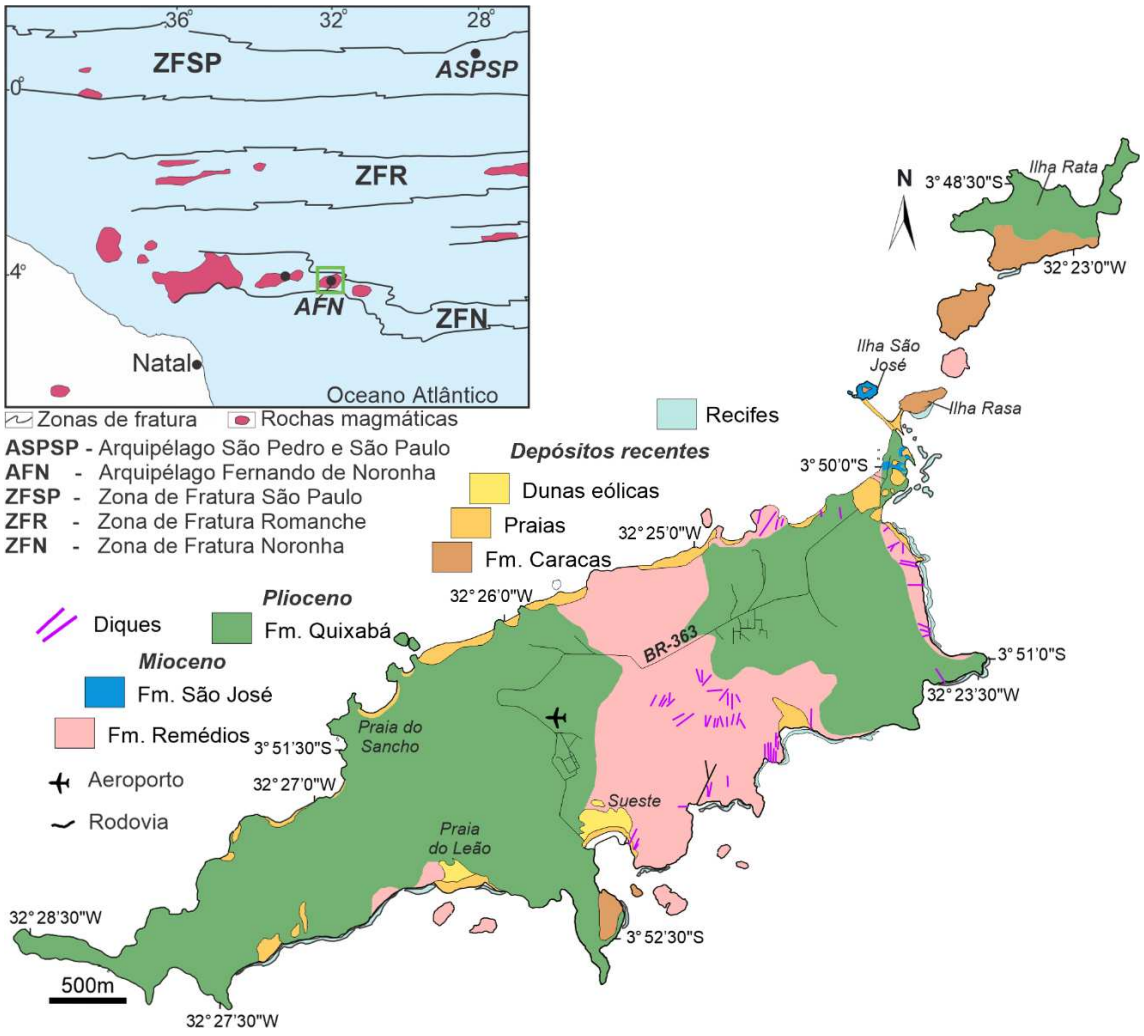

Figura 12 - Mapa geológico proposto por Almeida (1955) da Ilha de Fernando de Noronha. Modificado de Ulbrich et al. (2004).

Adjacente a IFN encontra-se a Zona de Fratura de Noronha (ZFN), zona transformante de direção E-W (Figura 12). Costa et al. (2002) relatou que essa estrutura apresenta continuidade para a região litorânea brasileira entre Fortaleza e Acaraú (Figura 1), caracterizando um sistema de fraturas e falhas de

cinemática dextral. Segundo Carneiro et al. (1989), essa zona registra a ocorrência de grande fluxo térmico e gradiente geotérmico, sendo denominada como Zona Sísmica de Fortaleza.

CAPÍTULO III

3.1. Artigo 1

DEFORMATION AND STRUCTURAL EVOLUTION OF MANTLE PERIDOTITES DURING EXHUMATION ON TRANSFORM FAULTS: A FORCED TRANSITION FROM DUCTILE TO BRITTLE REGIME

*Journal of Strucutural Geology, Vol. 133, abril 2020, DOI: **https://doi.org/10.1016/j.jsg.2020.103981***

Leonardo Mairink Barão[1], Barbara Trzaskos[1], Rodolfo José Angulo[1], Maria Cristina de Souza[1]

Highlights

- Transitional structures formed between ductile-brittle domains marking exhumation of ultramafic rocks in São Pedro and São Paulo Archipelago;
- Fluids influenced the formation of serpentine and carbonate veins phases; it also associates to semi-brittle to brittle stage;
- Faults kinematics and paleostress indicate the rotation of main tensions, establishing the actual tensions NW-SE;
- Multiple events of transpression and transtension generate a diversity of structures and microstructures, variable in ductile to brittle domain.

Abstract

The exhumation of peridotite rocks in oceanic transform zones passes by the rheological transition between the ductile and brittle deformation until the complete emplacement in the oceanic lithosphere. The São Pedro and São Paulo Archipelago (SPSPA), in the Equatorial Atlantic, records the deformational products of ductile, brittle and the rocks/fluid interaction generating specific structures in each domain. The deformational stages are related to the transpressional and transtensional geodynamics of São Paulo Transform Fault. Firstly, during transpression, exhumation occurs associated with the ductile domain causing intense mylonitization in temperatures between ~700°-800°C, defined by olivine and orthopyroxene recrystallization. The interaction with fluids initially originated from the mantle generates amphibole and oxide-rich layers marking the passage to a semi-brittle deformation. The continuation of peridotite exhumation, associated with an NW-SE shortening and transpressional led to a higher availability of hydrothermal fluids. As a consequence, four serpentinization episodes are recorded, which are associated with semi-brittle to brittle transition under temperatures between 300° and 400° C. Finally, the complete exhumation and establishment of brittle mechanisms led to carbonatation phase near the surface, with temperatures ranging from 300° to 150° C. The active NW-SE tectonic stress generated E-W strike-slip faults that were filled by carbonates recording the final exhumation stage.

Keywords: Ultramylonites; serpentinite; cataclastic flow; São Pedro and São Paulo Archipelago

1. Introduction

The deformation processes in the upper continental crust have been relatively well studied (Richard H. Sibson, 1977, 1983; Evans, 1988; Scholz, 1988; Knipe, 1989; Post and Tullis, 1999; Paschier and Trouw, 2005; Fossen et al., 2018a). These studies address shallow process associated with brittle deformation mechanisms, concerning fracturing, brecciation and cataclasis (Ramsay, 1980; Hancock, 1985; Blenkinsop and Rutter, 1986; Sibson, 1986; Hadizadeh and Tullis, 1992; Lloyd and Knipe, 1992; Genna et al., 1996; Jébrak, 1997; Crider and Peacock, 2004; Bestmann et al., 2012), and deep deformation processes related to ductile deformation in rocks composed predominantly of quartz and feldspar (Tulis, 1970; Urai et al., 1986; Grady and Kipp, 1987; Carter et al., 1990; Hirth and Tullis, 1992; Lloyd and Knipe, 1992; Mainprice et al., 1993; Lloyd, 2000; Stipp et al., 2002b; Ceriani et al., 2003; Law, 2014; Rahl and Skemer, 2016). Ductile to brittle deformational process are also documented on the oceanic crust associated with transform zones and fluid/rock interaction (MacLeod et al., 2002; Schroeder and John, 2004; Andreani et al., 2007; C. Prigent et al., 2018a,b; Peuble et al., 2018).

However, there are limited studies on how peridotitic rocks formed and deformed in the transition from ductile to brittle regime associated with transforming zones, which is mainly because of the lack of outcrop information. This paper aims to discuss deformation processes in mantle rocks in the ductile, semi-brittle and brittle regime. We studied the deformation mechanisms within the São Pedro and São Paulo Archipelago - SPSPA (Figure 1.1A), which exposes one of the few aerial mantle exposures still in formation in the Atlantic Ocean (Palmiotto et al., 2013).

The SPSPA was first described as a peridotitic rock body (Darwin, 1844). Based on this description, there was a series of studies addressing its formation, composition, sedimentation, and tectonics (Tilley, 1947; Wiseman, 1966; Melson et al., 1967, 1972; Moraes, 1997; Hekinian et al., 2000; Sichel et al., 2008; Campos et al., 2009b; Motoki et al., 2009; Simões et al., 2009; Angulo et al., 2013; Maia et al., 2016). The peridotitic body exhumation on transform zones is frequent in the Atlantic Ocean, as is the case for the Romanche Transform Fault (Bonatti, 1978; Bonatti et al., 1994; Ligi et al., 2002; Palmiotto et al., 2017) and Vema Transform Fault (Bonatti and Crane, 1982; Bonatti et al., 1992; Palmiotto et al., 2013). These structures are located nearby the SPSPA (Figure 1.1A) and show similar mantle exhumation associated with active transforming faults, carbonate platform formation and erosional process (Bonatti et al., 1974; Gasperini et al., 1997; Palmiotto et al., 2013, 2017).

The SPSPA displays a rare record of ductile deformation superimposed by brittle structures. The archipelago also exhibits features commonly observed in oceanic-continent transition (Skelton and Valley, 2000; Manatschal et al., 2006; Picazo et al., 2013), in ophiolites (e.g. Quesnel et al., 2013, 2016; Iseppi et al., 2018; Prigent et al., 2018) and in transform zones (MacLeod et al., 2002; Schroeder and John, 2004; Andreani et al., 2005; Palmiotto et al., 2013, 2017). The examination of tectonic products formed during the exhumation of the mantle rocks exposed in the SPSPA contributes to understand the formation and deformation of peridotite rocks in similar settings that are not accessible to traditional field-based geological surveys.

2. Geological Setting

The governing structure of the SPSPA is the São Paulo Transform Fault (SPTF) (Figures 1.1A and 1.1B), trending in the WSW-ENE direction. The SPTF extends in the Atlantic from the Mid-Atlantic Ridge (MAR) to the Brazilian continental margin (Almeida, 2006), at depths of up to 5,000 m (Hekinian et al., 2000), and has about 100km along the E-W direction in the São Pedro e São Paulo chain (Figure1.1B). The SPSPA consists of a sigmoidal outcrop ridge (Figure 1.1B) composed of one peridotite massif; it was formed due to dextral movement, associated with multiple-stages of transpressional and transtensional uplifting, related with an oceanic flexure and hot-spots influence (Hekinian et al., 2000; Maia et al., 2016); and later, to compressional events that modified tectonic tensions, inducing the current uplift of the ridge (Motoki et al., 2009; Maia et al., 2016).

This tectonic arrangement allowed the exhumation of mantle rocks, which starts close to the ridge-transform intersection. The evolution of transform faults promotes transpression and transtension as a result of changes in tectonic plate motion (Bonatti, 1978; Bonatti et al., 1994; Palmiotto et al., 2013, 2017). The uplift produces extremely deformed portions in the northern part of the ridge, and less deformed ones in the southern (Hekinian et al., 2000) (Figure 1.1C). The thrust faults formation, nearby the SPTF (Figure1.1B), uplift significant reliefs and expose deep rocks distributed along with bands parallel to the SPTF, forming positive flower structures (Maia et al., 2016) (Figure 1.1D). It is also the most deformed region, which originated from the transpression that emplaced the peridotites.

The SPSPA is formed by fine to very fine-grained (< 1cm) rocks of dark gray color, with oriented minerals such as olivines, characterized as mylonitic peridotites (Melson et al., 1967, 1972). In general, these rocks are intensely serpentinized and display interaction between the serpentine with the previously generated fabric, which in some cases caused the consumption and cataclasis of the mylonitic fabric (Campos et al., 2009b) (Figure 1.2).

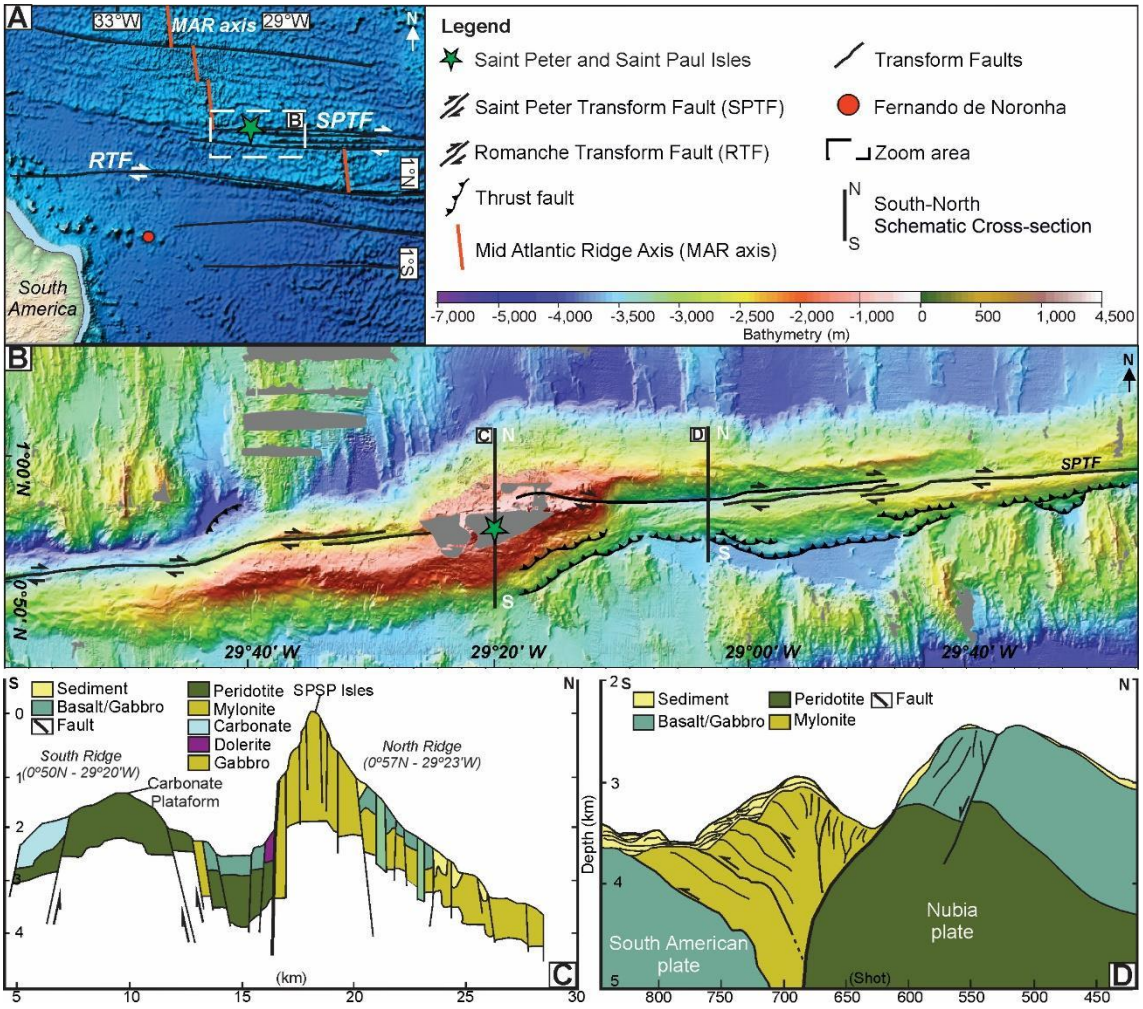

Figure 1.1 - Location of the São Pedro and São Paulo Archipelago (SPSPA) in the Mid-Atlantic Zone. (A) Location of the SPSPA, with indication of the São Paulo (SPTF) and the Romanche Transform Faults (modified from Sandwell and Smith, 1997); (B) Shaded bathymetric relief map of the SPTF where it intersects the SPSPA (modified from Maia et al., 2016); (C) Schematic cross-section of the SPSPA drawn by Hekinian et al. (2000); (D) Tectonic model based on seismic data drawn by Maia et al. (2016).

Although overprinted by serpentinization and halmirolysis (Campos et al., 2003b; Campos et al., 2009), the rock paragenesis are evidenced by the presence of porphyroclasts of olivine, pyroxene (orthopyroxene and diopside), amphibole, spinel, and traces of magnetite. A variety of peridotite characterized by kaersutite in restricted mylonitic bands (Campos et al., 2009b) occurs locally mainly in the Belmonte Isle (Figure 1.2).

Moreover, this mylonite-peridotite fabric is strongly recrystallized (Melson et al., 1972; Moraes, 1997; Andrade et al., 2006; Campos et al., 2009b). Melson et al. (1972) identified three mineral phases formed due to the progressive decrease of temperature and pressure: a) a primary phase, corresponding to porphyroclasts composed mainly of olivine, orthopyroxene and amphibole; b) recrystallized and secondary mineral associated with mylonitization; c) a last one with minerals associated with peridotite serpentinization and carbonatation.

The sedimentary units of the São Paulo Formation were deposited along NW-oriented weak zones in the peridotite. Under wave action, the deposition of the Atobás unit took place, consisting of conglomerates, sandstones and breccias cemented by carbonates, followed by the Viuvinhas unit, composed of breccias and conglomerates (Campos et al., 2003; Campos et al., 2009; Angulo et al., 2013)

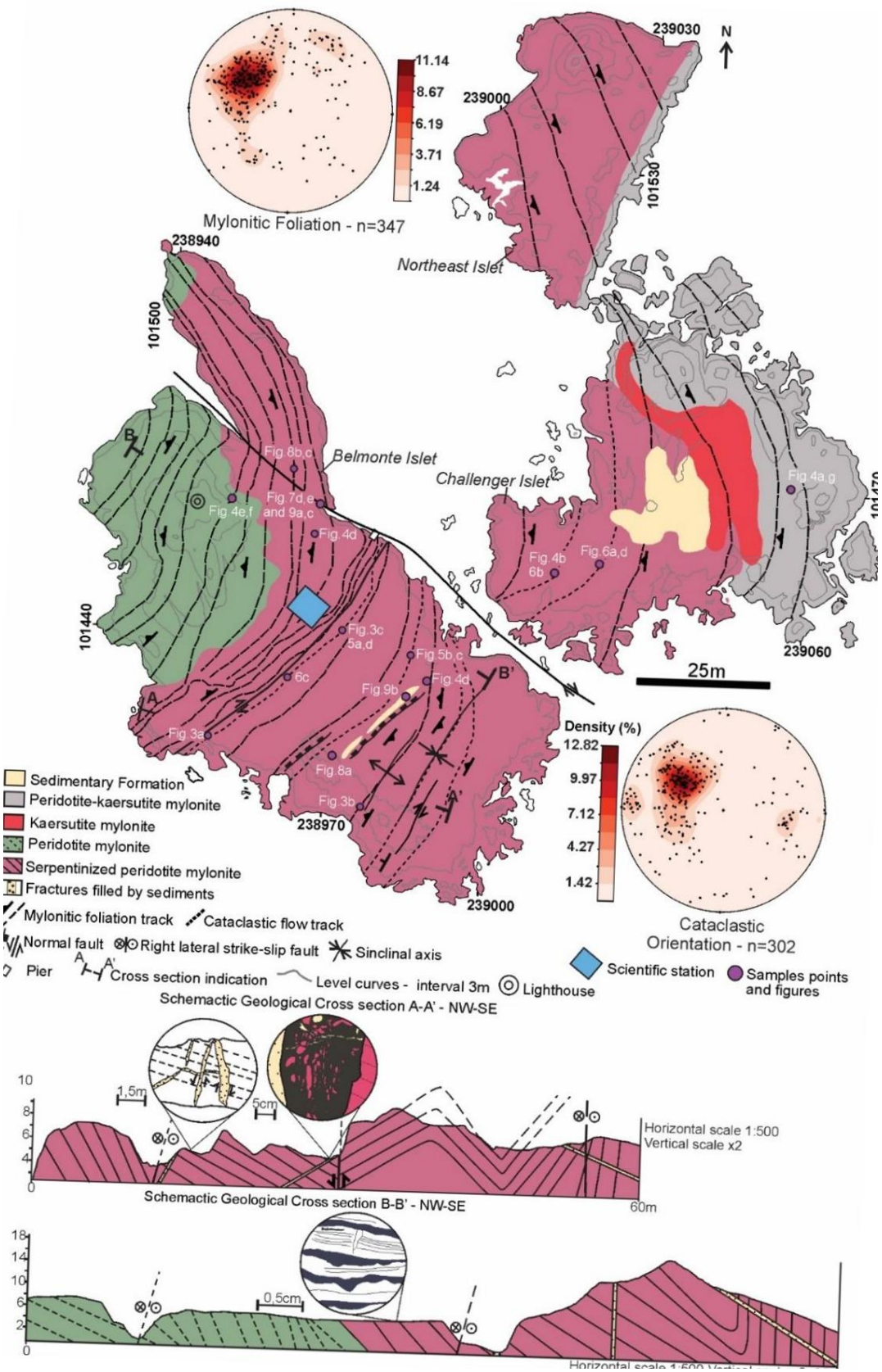

Figure 1.2 - Geological map (modified from Campos et al., 2003) and geological cross-sections A-A' and B-B' of the Belmonte, Challenger and Northeast islets of the SPSPA; and lower-hemisphere, equal-area projections, indicating the trending of the mylonitic foliation and the cataclastic orientation in the SPSPA.

3. Methods

In order to identify and characterize the deformation mechanisms of the peridotites from the SPSPA, we mapped structures such as mylonitic foliation, cataclastic flow and fractures (Anexo 1). Based on this mapping, we defined the structural control and possible kinematic indicators associated with these tectonic domains. Data from the fault planes, such as steps and striations, were processed using the Wintensor software 5.8.6 (Delvaux, 2012). We used the straight dihedral-angle method (Angelier and Mechler, 1977; Angelier, 1994) to determine the main tectonic shortening and extensional fields of the fault planes. The samples collected in the field were oriented and microstructurally analyzed to identify deformational microstructures of mylonitic, cataclastic and brittle domains, and also to look for kinematic indicators.

4. Results

Field mapping allowed us to estimate the main deformational domains that the rocks of the SPSPA passed through (Figure 1.3A). These domains involve the abrupt transition from ductile to the brittle regime, initially forming peridotite mylonites to ultramylonites (Figure 1.3B), and later cataclasites and breccia faults (Figure 1.3C).

4.1. Mylonitic domain

The mylonitic domain is characterized in the field by the preservation of the mylonitic foliation (Figure 1.3B) oriented to N30E-20W, with different orientations in the SPSPA isles (Figure 1.2). Also, the foliation is gently folded with axis oriented to the northeast (Figure 1.2)

Similar to observed in the field, thin sections exhibit gentle folds (Figure 1.4A and Anexo 1), which are remarkable in the mylonitic foliation. In terms of texture, the rock exhibits a fine to a very fine-grained matrix (Figures 1.4A-D), composed of minerals such as olivine, orthopyroxene, spinel and amphibole. This foliation may be locally replaced by serpentine-rich layers (Figures 1.4B and D), with the same orientation observed for non-serpentinized rocks.

The porphyroclasts are olivine (Figures 1.4A and B), spinel (Figure 1.4C), orthopyroxene (Figures 1.4D and E) and amphibole (Figure 1.4F). In general, olivine porphyroclasts form asymmetric recrystallization tails, which indicate their predominantly left-lateral kinematics (Figures 1.4A and B); locally, however, they can display right-lateral kinematics. These crystals commonly exhibit pressure shadows, and their tails are associated with remarkable mineral recrystallization. In the case of spinel porphyroclasts, the crystal trail is formed in between the foliation (Figure 1.4C), indicating kinematics similar to that of crystals of olivine.

Orthopyroxene and olivine porphyroclasts (Figures 1.4D and E) tend to have distinct rheological behavior: the former seems to be more resistant to deformation and is surrounded by foliation; but the crystals are internally deformed. In general, the orthopyroxene exhibits deformation lamellae (Figures 1.4D and E), with the presence of clinopyroxene exsolution lamellae (Champness and Lorimer, 1973; Frets et al., 2012; Wang et al., 2012). Kink bands are also formed along these crystals (Figure 1.4D).

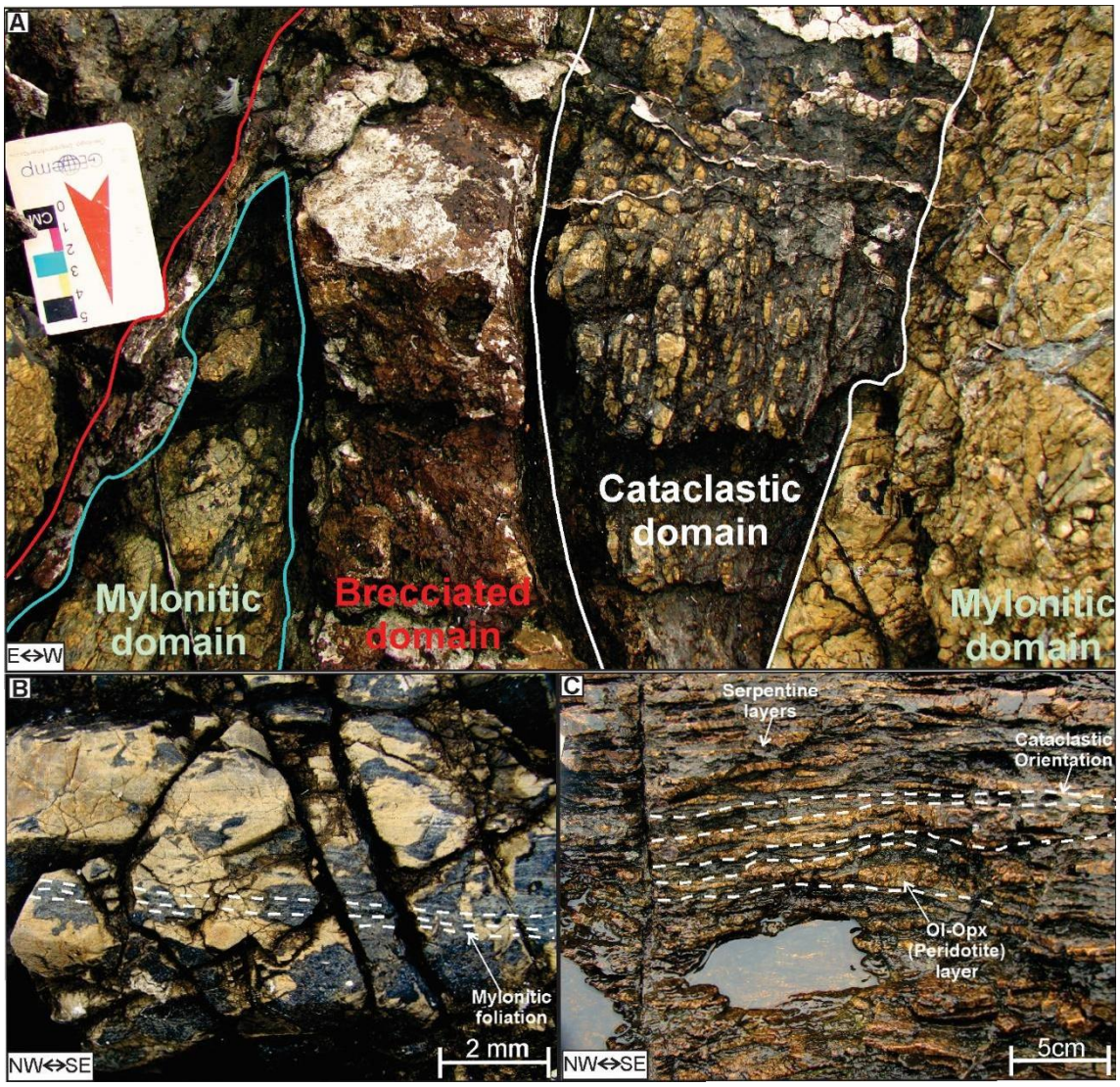

Figure 1.3 - Photographs of deformational domains imposed in SPSPA rocks. (A) Distribution and relationship between tectonic domains (mylonitic, cataclastic and brecciated); (B) Fine mylonitic foliation observed in mylonites and peridotitic ultramylonites; (C) Cataclastic orientation, marked by oriented peridotite fragments and by the presence of predominantly serpentine bands (dark bands).

Subgrains of orthopyroxene may occur (Figure 1.4E). This is a result of deformational process, forming subgrains with interdigitated contacts and intense recrystallization. Magnetite and clinopyroxene are also associated with this process (Figure 1.4E). These minerals have interdigitated contacts with orthopyroxene, representing the mineral modification during deformation, probably resulting from temperature and pressure change (Champness and Lorimer, 1973; Frets et al., 2012; Wang et al., 2012).

The observed reacting layer intercalated with the mylonitic and ultramylonitic levels. The fluid penetration may have been facilitated by the mylonitic foliation (Figures 1.4A and G). These fluids interact with the rock, forming amphibole, magnetite, and oxides (Figure 1.4G). Locally, there is the formation of porphyroblasts and crystals of amphibole with no preferred orientation, at times presenting angular or rounded shape, some cases presenting a fragmented shape (Figure 1.4G).

4.2. Cataclastic domain and serpentinization

4.2.1. Serpentine Cataclasite

In the field, the cataclastic domain is marked mainly by the formation of cataclastic orientation and cataclasites associated with serpentine, imposed by the cataclastic flow process. This domain tends to follow pre-existing structures, developing parallel to the mylonite domain (Figures 1.2 and 1.3A). The serpentine-filled fractures crosscut fragmented peridotites. Fragments can be elongated (Figures 1.3A and C), which may divides the rock into serpentinite bands and bands rich in elongated peridotite fragments (Figure 1.3C).

In some cases, the process of cataclasis may be random, producing angular fragments of varying dimensions (1 to 10cm) and forming tectonic breccias (Figure 1.3). The serpentinization phase overlays the previously formed mylonitic fabric. We also observed angular-shaped, asymmetrical domino boudins along a shear band, which are oblique-oriented to the main foliation (Figure 1.2) and indicate right-lateral kinematics. Breccia, in turn, are visible in areas of localized microfaults (Figures 1.4A and 1.5B) filled with serpentine, oxides or peridotite fragments (Figures 1.3A and 1.5B).

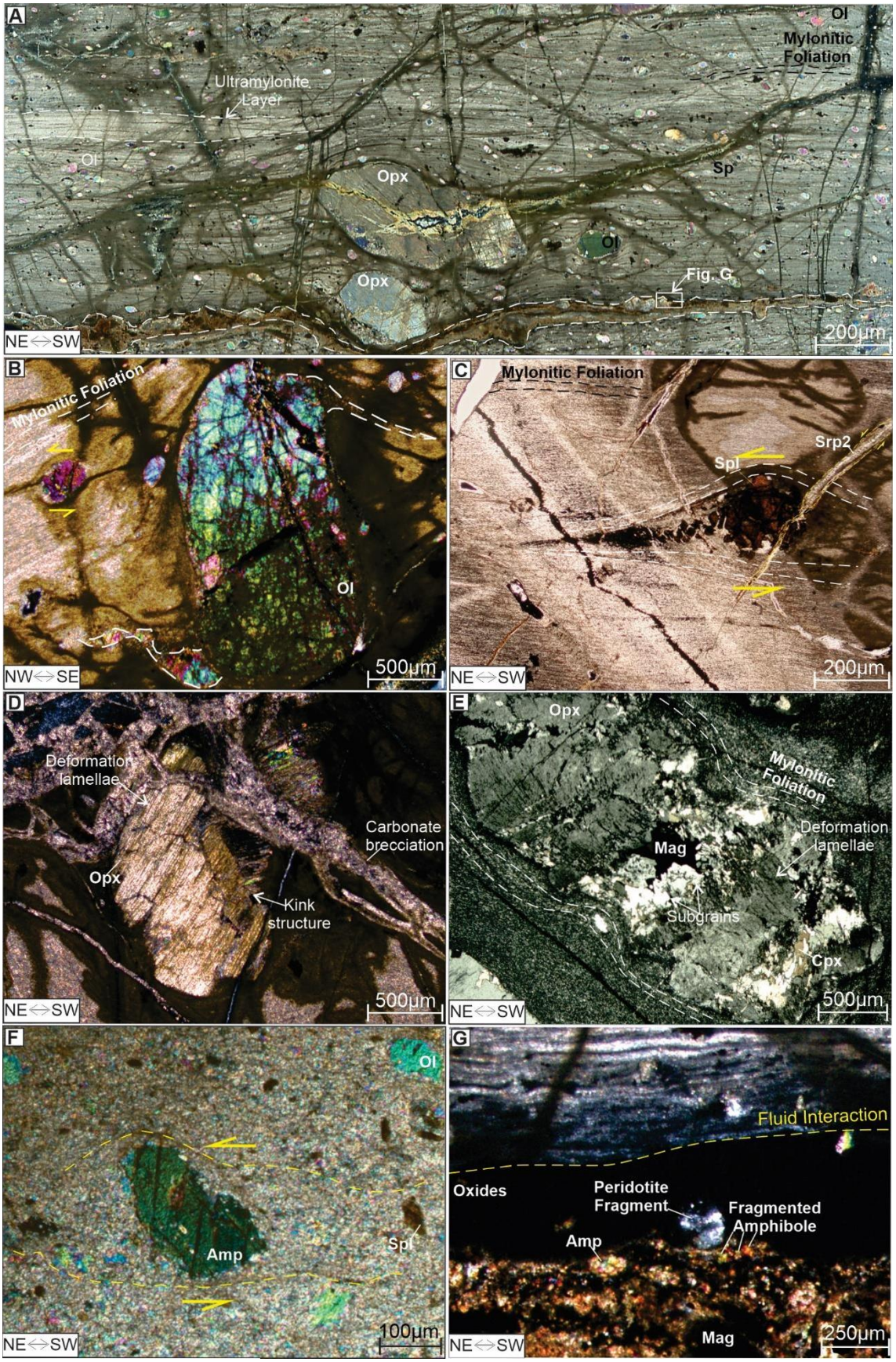

Figure 1.4 - Photomicrographs of the mylonitic domain, all thin sections are perpendicular to mylonitic foliation. (A) Overview of the ultramylonites to mylonites bands, It is highlight the orthopyroxene (OPX) and olivine (Ol) porphyroclasts surrounded by the fine-grained recrystallized matrix; (B) Olivine porphyroclasts showing left-lateral kinematics and pressure

shadow; (C) Spinel surrounded by mylonitic foliation, also it is observed a fragmented Spl; (D) Opx porphyroclast with kink structure and clinopyroxene exsolution lamellae, superimposed by the carbonate brecciation ; (E) Orthopyroxene porphyroclasts bypassed by mylonite foliation. It is observed the formation of Cpx subgrains associated to magnetite and opaque minerals; (F) amphibole porphyroclasts bypassed by the mylonitic foliation, the crystal exhibits cleavage intersect between 120°; (G)Reaction band with a formation of disoriented amphiboles, oxides and magnetite, caused by fluid percolation between the banded mylonite. Opx: Orthopyroxene, Cpx: Clinopyroxene, Ol: livine, Spl: Spinel, Srp: Serpentine, Mag: Magnetite, Amp: Amphibole. Abbreviations (Whitney and Evans, 2010).

The serpentine-filled microfaults (Figure 1.5C) have different generations overlapping each other and forming distinct serpentine veining episodes in the peridotites. In this context, serpentine gash veins take place (Figure 1.5D), which consists of elongated sigmoidal features, parallel to the main shortening direction (Lajtai, 1969; Paschier and Trouw, 2005; Coelho et al., 2006) and approximately oriented NW-SE. These gash veins underwent extreme cracking events, which produced microfaults that were filled by crosscutting carbonate veins forming millimetric residues (up to 0.25μm).

4.2.2. Serpentine phases

Four different phases of serpentine were identified in the field and in thin sections. Their recognition was based on crosscutting relationships between the veins as well as their relationship with the existing minerals in each generation.

The first phase (Srp1) is linked mainly to the replacement of olivine, orthopyroxene and ferromagnesian minerals (Figure 1.5D). The interaction with hydrothermal fluids led this modification to serpentine phases probably near the Mid Atlantic Ridge. The rock/fluid interaction allows the formation of the second type of veins (Srp2 - Figure 1.6A and B). These veins display the largest width among the four observed (100-500μm). Moreover, they generally present regular shape and higher pervasiveness, both in outcrop and microscale. Their crystals

exhibit an orderly wavy pattern toward the vein walls (Figures 1.6A, B); therefore, we can classify them as syntaxial veins, following Bons et al. (2012). They may also present a more fibrous aspect, in which their growth direction is identifiable (Figure 6A).

We identify multiple veining episodes associated with Srp2 (Figure 1.6A, B). They could crosscut each other (Figure 1.6B) in different phases of formation, but the most common aspect is its association with oxides, that fill the central portion of the vein (Figure 1.6A, B). Also, those veins are ramified following different paths during their formation (Figure 1.6B). Srp2 veins are associated with cataclastic flow process (Fig 1.3C and 1.5A), which causes peridotite fragmentation along with percolation of serpentine.

The continuos serpentinization process associated with deformation and tectonic setting change causes the formation of veins with various morphologies, such as phase Srp3 (Figure 1.6C). The serpentine veins exhibit interdigitated features between the crystals. Spr2 veins are generated in microfaults (Figures1. 5C and 1.6C) and gash veins (Figure 1.5D). The hydraulic fracturing patterns generated in Srp3 crosscut previous serpentine episodes (Figure 1.6C). Srp3 veins display right-lateral kinematics (Figure 1.5C), marking a continuous deformation, without kinematic variation during its generation. These veins, unlike Srp2, show very fine micro crystals of serpentine (1 to 5μm) without specific shape; therefore, it was not possible to identify crystals employing conventional techniques. Crystal shape and morphology suggest that vein has a syntaxial morphology: they grow from the host rock wall (following Bons et al., 2012). The Spr3 vein differs from the Spr2 vein due to the lack of oxide association, with the central portion of the Spr 3 axis being completely sealed (Figure 1.6C).

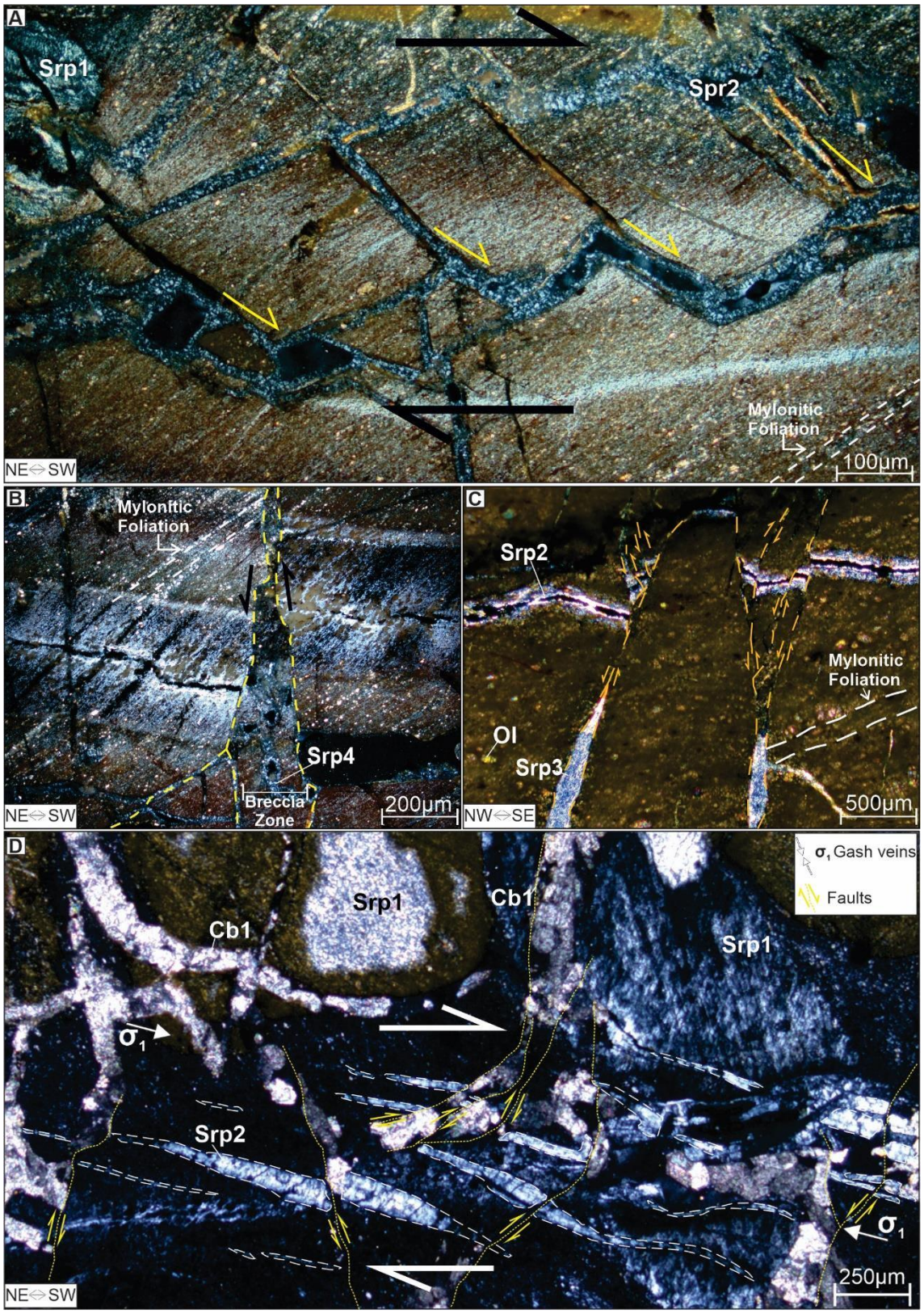

Figure 1.5 - Photomicrograph of the cataclastic domain.(A) Domino faults formed by the cataclastic flow process;(B) Microfaults producing tectonic breccias cemented by granular-shaped serpentine (Srp4); (C) Microfaults filled by microcrystalline serpentine veins (Srp3), causing the displacement of another serpentine phase (Srp2);(D) Serpentine gash veins formed by the crack-seal process (Srp2), displaying right-lateral kinematics. Srp1: Serpentine phase 1,

Srp: Serpentine phase 2, Srp3: Serpentine phase 3, Srp4: Serpentine phase 4 Cb1: Carbonate phase 1, Ol: Olivine.

The last vein phase (Srp4) crosscuts all previously formed phases (Figure 1.6D). These veins are 100 to 200μm wide and the crystals are coarser-grained (5 to 20μm) when compared to the veins formed in previous phases (Figure 1.6). The characteristic morphology is that of granular-shaped and isotropic serpentine crystals (Rouméjon et al., 2014), with well-defined rectilinear contacts and no preferred orientation. The veins Srp4 fill extensional fractures, allowing the formation of granular-shaped serpentine due to the space available (Figure 1.6D).

4.3. Brecciated domain and carbonation

4.3.1. Sedimentary bodies and brecciation

The brecciated domain is highlighted by peridotite fragments and carbonate cement that fill previous structures such as mylonitic foliation, cataclastic flow and faults. In general, when observed in map view, the sedimentary bodies are elongated and randomly arranged (Figure 1.7A – Anexo 1), with no preferred orientation. They are composed of conglomerate with peridotite clasts, shells and shell fragments all bounded by a carbonate-rich matrix. Such sedimentary material may surround large fragments of peridotite, isolating them from the host rock (Figure 1.7B).

Sometimes the sedimentary bodies are interconnected forming a complex anastomosing network. Shear zones (Figures 1.2 and 1.3C) seem to have facilitated the sedimentary bodies formation (Figure 7C). Besides, some bodies are predominantly composed of carbonate, lacking clasts. These sedimentary bodies dip at variable angles, from vertical (Figure 1.3A) to 40°, as a consequence of the different fractures they fill. The applied stress created open

spaces for sedimentation, forming bodies initially perpendicular to the main shortening direction and subsequently parallel to the main stress exerted on the shear zones (Figure 1.7C).

4.3.2. Carbonate veins

We identify two different phases of carbonate veins through petrography. They were named Cb1 and Cb2 (Figure 1.8) due to their temporal and crosscutting relationships with each other. The first phase (Cb1) directly crosscuts serpentinite veins, in some cases forming gash veins with the indication of right-lateral kinematics (Figure 1.8A), which may be limited by microfaults (Figure 1.5D) intersecting other veining events. Crystals inside veins are poorly defined and sometimes display fibro-radial features (Figure 1.8A) toward the center of the veins.

4.4. Faults and paleostresses

We observed the predominance of strike-slip faults (Figures 1.2 and 1.9), commonly associated with oblique components. The fault planes are mainly associated with sedimentary bodies described in section 4.3, in which kinematic indicators and striations can be observed (Figure 1.9).

The kinematic indicators (following Petit, 1987; Doblas, 1998) are predominantly right-lateral, with an oblique component (Figure 1.7B). These structures are linked to EW-directed fault planes crosscutting Belmonte isle (Figure 1.2); they are not pervasive belong to the archipelago, presenting spacing between 0.50 and 1.00m (Figure 1.7C). Locally, these features can produce

breccia faults along fault planes – extending for 5 to 10 cm (Figure 1.7C), and not associated with the cataclastic domain observed in the peridotites (Figure 1.3A).

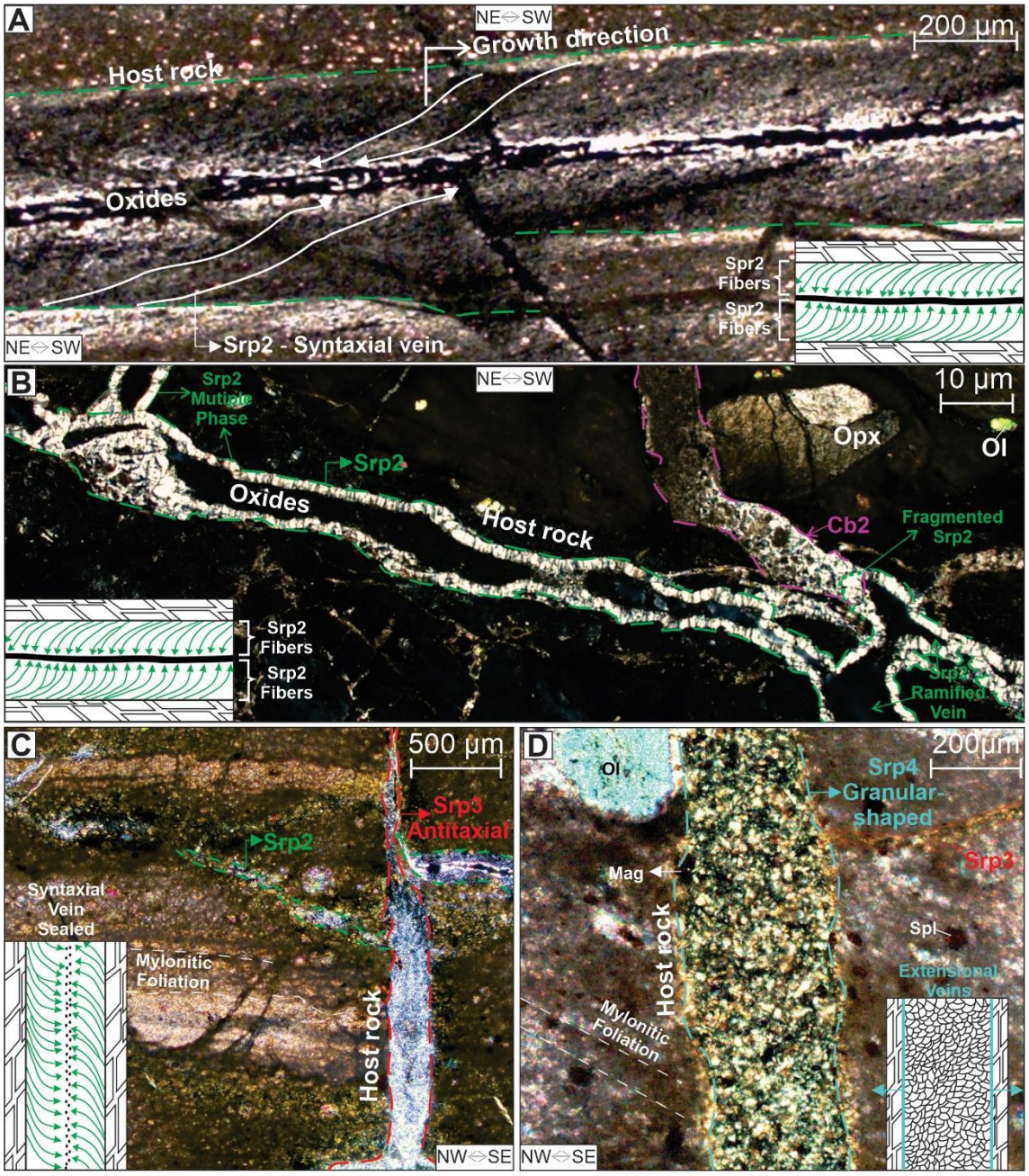

Figure 1.6 - Examples of the types of veins observed. (A) and (B) type Srp2, characterized by generally fibrous and syntaxial morphology, growing from the walls of the host rock toward the center of the vein; (C) Type Srp3, with very fine micro crystals of serpentine (1 to 5µm) without specific shape serpentine infill, characterized of syntaxial vein with sealed center; (D) Type Srp4, with granular-shaped serpentine infill and disoriented pattern. Srp1: Serpentine phase 1, Srp2: Serpentine phase 2, Srp3: Serpentine phase 3, Srp4: Serpentine phase 4 Cb2: Carbonate phase 2, Ol: Olivine.

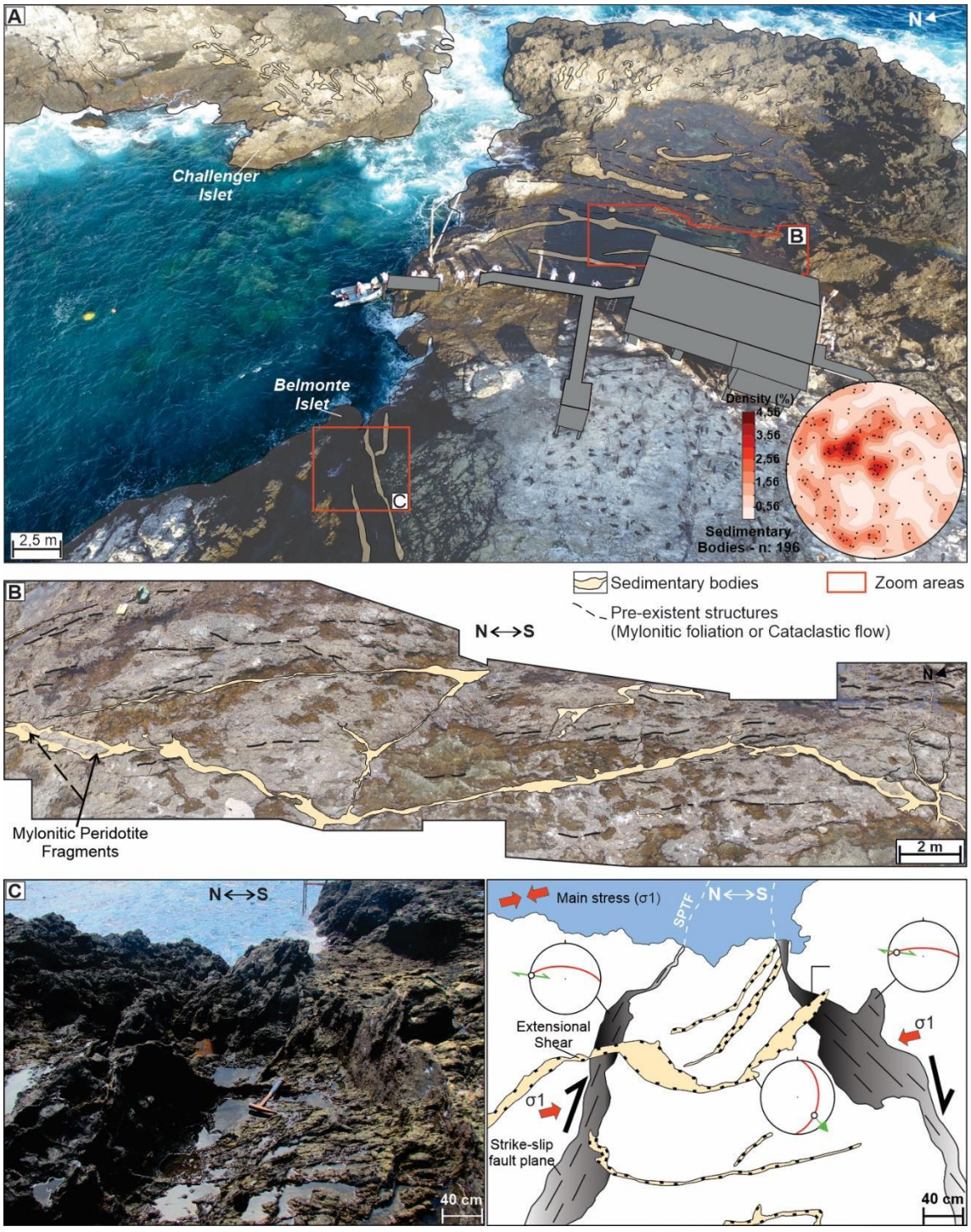

Figure 1.7 - Photographs and photomosaics of the Belmonte and Challenger islets. (A) Drone photographs, outlining some sedimentary bodies. Lower-hemisphere, equal area projection indicating the direction of sedimentary bodies in the SPSPA (modified from Barão et al., 2018); (B) Photomosaic outlining the sedimentary bodies, indicating the fragments of peridotite enclosed by them, parallel to the mylonitic foliation (Barão et al., 2018); (C) Zoom area of the strike-slip fault zone with a oblique component, alongside extensional shears oblique to the main fault zone.

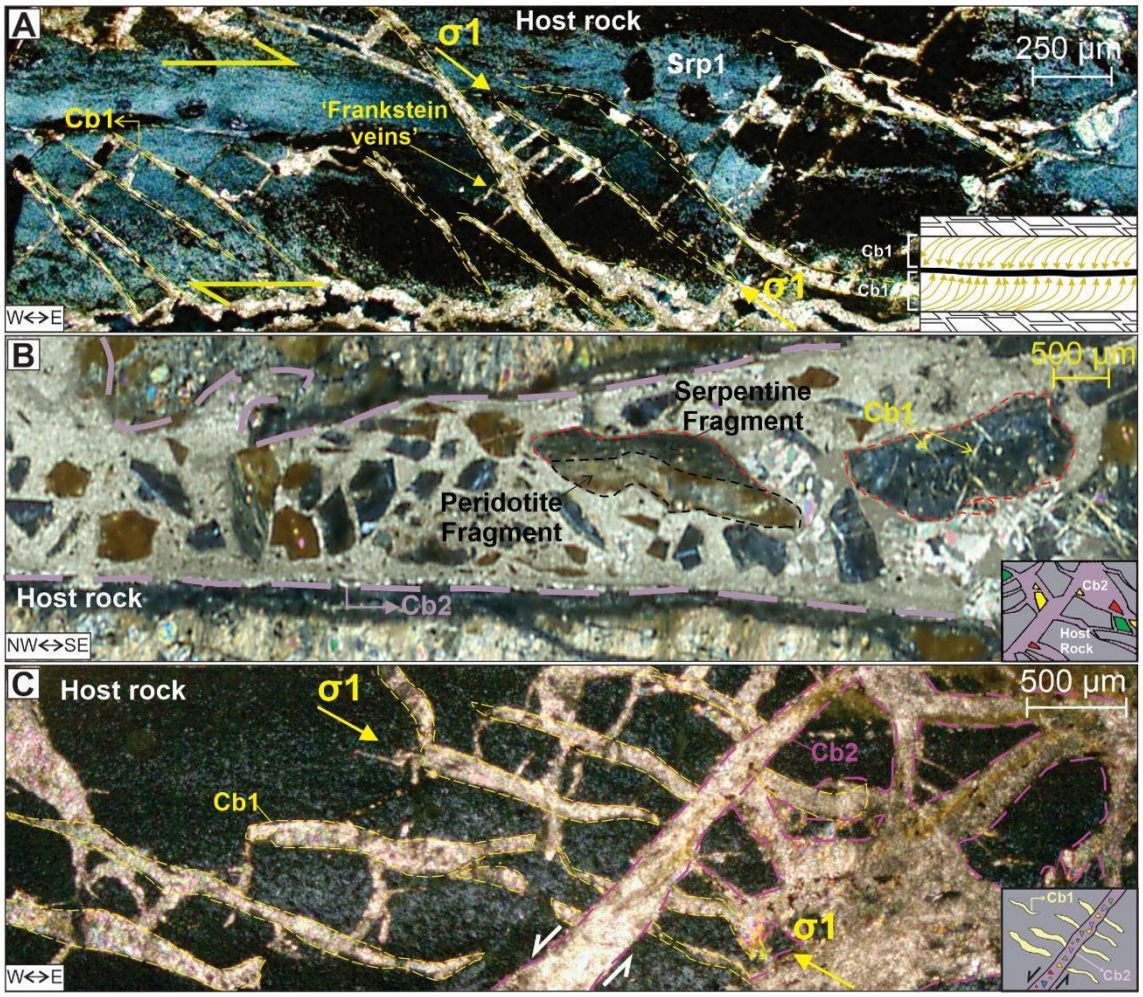

Figure 1.8 - Examples of carbonate veins observed in rocks in the SPSPA. (A) Cb1 veins marked by gash veins with right-lateral kinematics and syntaxial morphology (Bons et al., 2012) and "Frankenstein" veins (Kelemen et al., 2018), overlapping Srp1 phase; (B) Cb2 veins, associated with fluid brecciation process, creating fragments of peridotite, of serpentine veins and Cb1 veins;crosscutting relationship between the Cb1 and Cb2 veins. Srp1: Serpentine Phase 1, Cb1: Carbonate phase 1, Cb2: Carbonate phase 2.

Tension faults, variably orientated N10W-N10E and oblique to the strike-slip faults suggest a structural arrangement with the EW-directed fault planes (Figure 6C). Fault plane data collected in the field and processed by the straight dihedral-angle method suggest that the main tensor (σ1) has an approximate direction of NW-SE and a marked extension trending NE-SW (Figure 1.7D).

We identified a progressive deformation by the shortening tensor (σ1) rotation. Rotation of σ1 occurred locally (Figure 1.7D), causing the formation of predominantly right-lateral strike-slip structures oriented around N30E-N45W.

They can be mapped mainly on Belmonte islet (Figure 1.2) and fill large sediment bodies of up to 8m thick (Figures 1.2 and 1.6A, B). The main paleostress, in this case, is directed NE-SW, whereas the extension is NW-SE and may be associated with normal faults.

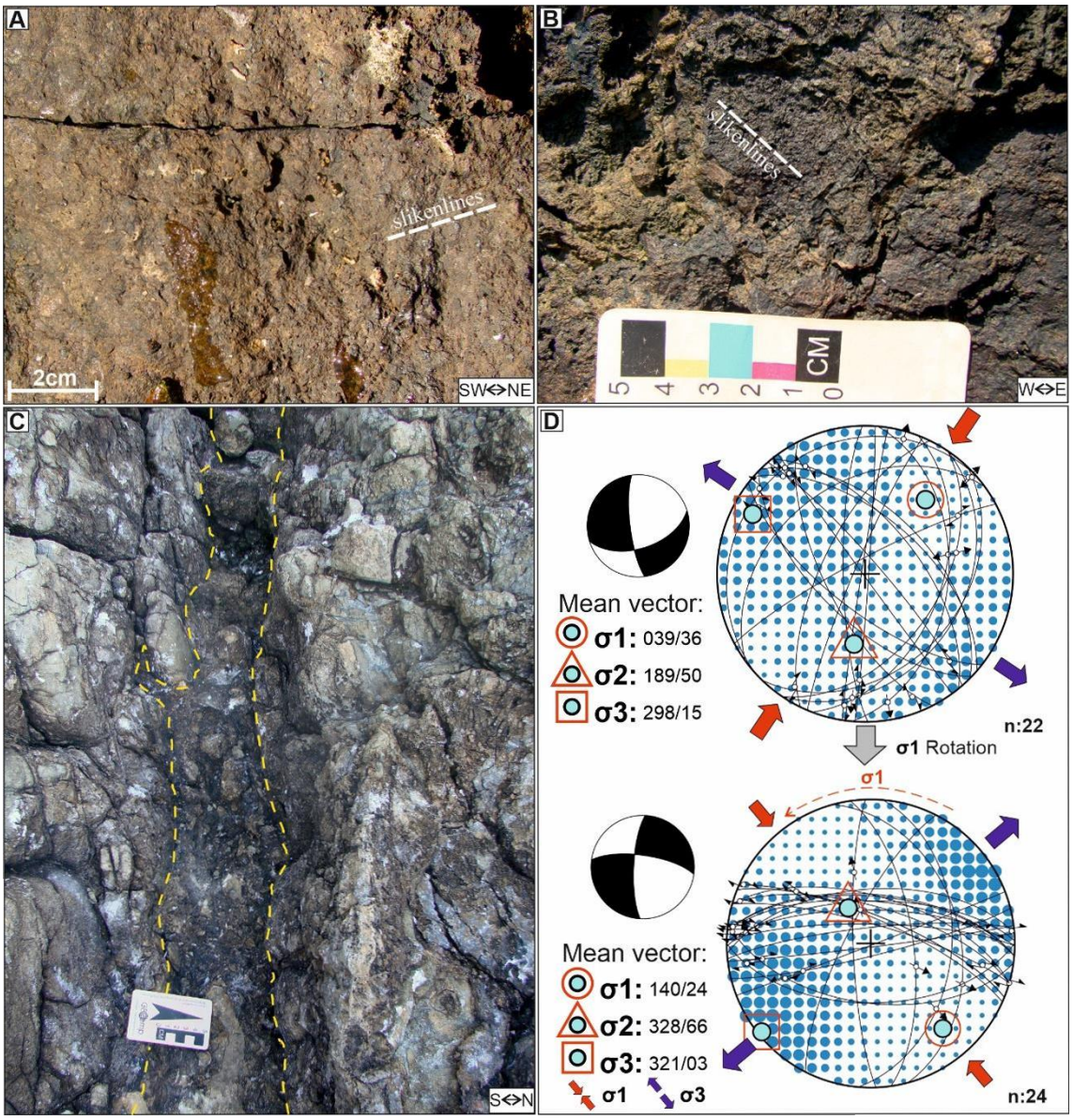

Figure 1.9 - Field photos of fault planes in the field. (A) and (B) Fault planes observed in sedimentary bodies, with marked slickenlines indicating an oblique component; (C) Breccia fault (15cm), with fragments cemented by oxides and serpentine; (D) Lower-hemisphere, equal-area projections using the straight dihedral-angle method, showing the two different main shortening direction observed in the faults of the SPSPA.

5. Discussion

5.1. Ductile-brittle transition

The structures and microstructures recognized in the deformation domains (Figure 1.3) record the progressive transition between deformation regimes in the SPSPA (Figure 1.10). This transition has been demonstrated in deformed rocks along shear zones (Searle et al., 2017; Papeschi et al., 2018) and locally associated with hydrothermal fluids in high-angle shear zones (Compton et al., 2017).

In the ductile regime, SPSPA rocks are possibly associated with the conjunction of different deformation mechanisms (Drury et al., 2011; Czertowicz et al., 2016; Park and Jung, 2017). These processes produce rotated porphyroclasts (Figure 1.4A) and intense olivine recrystallization - which generate fine to very fine-grained matrix, with specific crystallographic orientation. Orthopyroxene is more sensitive to the regime transition. It displays subgrains and locally modifies its composition to clinopyroxene and opaque minerals such as magnetite (Figures 1.4E and 1.10). The presence of exsolution lamellae is frequent (Figure 1.4D), as well as, at the last stage, the formation of kink structures (Borg and Handin, 1966; Starkey, 1968; Centrella et al., 2018).

Ductile deformation is associated with folding observed both in macro (Figure 1.2) and in microscale (Figure 1.10). These folds are possibly associated with peridotitic body exhumation in a transpressive SPTF context (Maia et al., 2016), allowing the formation of gently folds. However, Simões et al (2009) report the formation of folds and the change in the direction of foliation (Figure2) due to SPTF activity. This causes local rotation of mylonitic foliation, consequently leading to gentle folding in peridotitic rocks.

Also, the intercalation of fine (mylonitic) and ultrafine-grained (ultramylonitic) bands is evident (Figures 1.4A and 1.10). This layering is possibly linked to compositional differentiation formed during the exhumation of these rocks to the surface (Sichel et al., 2008), resulting in intercalated orthopyroxene-rich and olivine-rich bands (Dick and Sinton, 1979; Tubía et al., 2004; Ueda et al., 2008; Frets et al., 2012).

This layering became even more evident with the circulation of fluids, which locally cause mineralogical modification, mainly generating layers with amphibole grains, oxides and magnetite (Figure 1.4A, G). The amphibole grains generated in this phase have no specific organization, as occurs in the previously deformed phases with Ol and Opx (Figure 1.4A, G). This arrangement allows the passage to the semi-brittle or transitional regime (Figure 1.10), possibly associated with a fluid derived from the mantle, leading to changes in the deformation regime (Picazo et al., 2013; Prigent et al., 2018).

The transitional stage is marked by features that show mineral traces without associated recrystallization, forming fragments of spinel enclosed by the rock matrix (Figure 1.4C); as well as by *Riedel* shears, which indicate the gradual transition toward brittle deformation mechanisms (Papeschi et al., 2018).

The hydrothermal fluids penetration associated with the mantle block uplift and the possible penetration of seawater leading to rock/fluid interaction (Picazo et al., 2013; Birner et al., 2016), would culminate in the formation of serpentines. This process can be related to the transitional stage, with the presence of serpentine within the veins and the generation of gash veins oriented parallel to the tectonic tension (Bons et al., 2012). The penetration of fluids, concomitant with tectonic deformation, induced the formation of domino faults (Moreira and

Dias, 2018), resulting in the precipitation of serpentine (Figures 1.5A and 1.8). The tension veins formed in this context (Figure 1.5D), also indicate the presence of the fluid associated with tectonic efforts, forming sigmoidal features parallel to the main tension applied to the archipelago. These structures are also associated with a brittle-ductile transition regime (Hodgson, 1989; Mcclay, 1991; Leeder and Pérez-arlucea, 2006), thus contributing to the identification of this domain in SPSPA.

Therefore, the forced transition caused by the exhumation of the mantle block and its subsequent interaction with mantle fluids (Hensen et al., 2019) led to the formation of brittle structures, with the generation of cataclastic flow conditioned by serpentinite veins (Figure 1.10). Serpentine facilitates shearing between fragments, causing mainly the formation of cataclastic flow (Figures 1.2 and 1.3C) in a context of semi-brittle deformation (Hadizadeh and Tullis, 1992; Gumbsch, 2001; Pec et al., 2012; Prigent et al., 2018; Reber and Pec, 2018). This flow running parallel to the mylonitic foliation exploits previously formed structures. The rapid passage to a transitional regime culminates in the predominant formation of faults (Motoki et al., 2011), marking a complete progress to the brittle regime. Consequently, these structures are associated with the formation of fracture and/or fault planes filled with carbonates and breccia (Figures 9 and 10).

5.2. Hydrothermal phase and the transition to the brittle regime

The presence of fluids may have been essential for the ductile-brittle transition, serving as a lubricant in the mantle exhumation along a fault zone (Hirauchi and Katayama, 2013). Fluids, probably derived from deep regions in

preferential pathways, interacted with peridotites during their exhumation (Précigout et al., 2017; Mehouachi and Singh, 2018; Hensen et al., 2019).

The orthopyroxene-rich layers modified by the action of fluids generate mainly amphibole and oxides (Figure 1.4G), stabilizing the fluid/rock system along these layers (Précigout et al., 2017). The newly formed porphyroblast amphibole has no specific orientation (Figure 1.4G, 1.10), as observed for fabric generated during the ductile stage. The presence of magnesio-hornblende amphibole suggests a deformation temperature between ~700° and 800°C (Prigent et al., 2018), since olivine and pyroxene typically break down at this temperature, forming fractures that can be filled by amphibole. (Prigent et al., 2018).

The amphibole stability in this phase is an essential indicator of mylonitization temperature and the fluid reaction with a predefined layer (Picazo et al., 2013; Getsinger and Hirth, 2014). The reactive layers (Figure 1.4A, G) formed in this context mark a probable temperature of formation nearby ~800° (Dollinger and Blacic, 1975; Getsinger and Hirth, 2014), and also configures the imposition of new deformational regime related to semi-brittle stage (Babaie and La Tour, 1994; Prigent et al., 2018). However, the presence of amphibole porphyroclasts (Figure 1.4F) indicates the reaction stability during the mylonitization and possibly the mantellic fluid derivation able to react with orthopyroxene and olivines, likely related to metasomatism process (Wallace and Green, 1991; Campos et al., 2003b).

The temperature limit for the semi-brittle deformational stage comprises the maximum temperature for the stability of serpentine, ranging from 300° to 400°C (Andreani et al., 2007; Picazo et al., 2013) – possibly marking the abrupt

transition of semi-brittle to brittle regime (Hirose et al., 2006). The serpentine stability could be led by the hydrostatic, temperature and lithostatic conditions (Soda and Takagi, 2010). In the case of SPSPA, the serpentine should establish as veins when the hydrothermal system is open, possibiliting the transport of elements and the serpentinization process (Andreani et al., 2007). The establishment of temperature between 300 to 400°C suggests a change in tectonic configurations associated with peridotite body exhumation (Maia et al., 2016).

The pressure conditions, that also influence serpentine formation to make it possible to establish the semi-brittle to brittle mechanisms (Soda and Takagi, 2010; Andreani et al., 2007), genere microfaults, tension gashes and breccias locally (Figure 1.5).

The complete mantle exhumation and the continuous deformation led to the formation of fractures, generally filled by carbonates at distinct phases. The presence of faults (Figure 1.10), linked with carbonate veins (Figures 1.8 and 1.9), shows the onset of the brittle regime imposed on these rocks, associated with the SPTF. The brittle setting developed in SPSP associated with a carbonation process led to fluid flow and CO_2 transportation by fractures and faults (Peuble et al., 2015; Kelemen et al., 2018), resulting in carbonate precipitation in fractures and fault planes.

5.2.1. The relationship between serpentine and carbonate phases

The carbonatation and serpentinization phases appear to be closely associated, as has already been described by several authors (Wicks, F J; Whittaker, 1977; Morandi and Felice, 1979; Andreani et al., 2007, 2009; Rudge et al., 2010; Noort et al., 2013; Peuble et al., 2015, 2018). The direct influence of

hydrothermal fluids, as well as the interaction of seawater with the exhumation of SPSPA peridotite rocks, leads precisely to the formation serpentine and carbonate veins (Andreani et al., 2013; Godard et al., 2013).

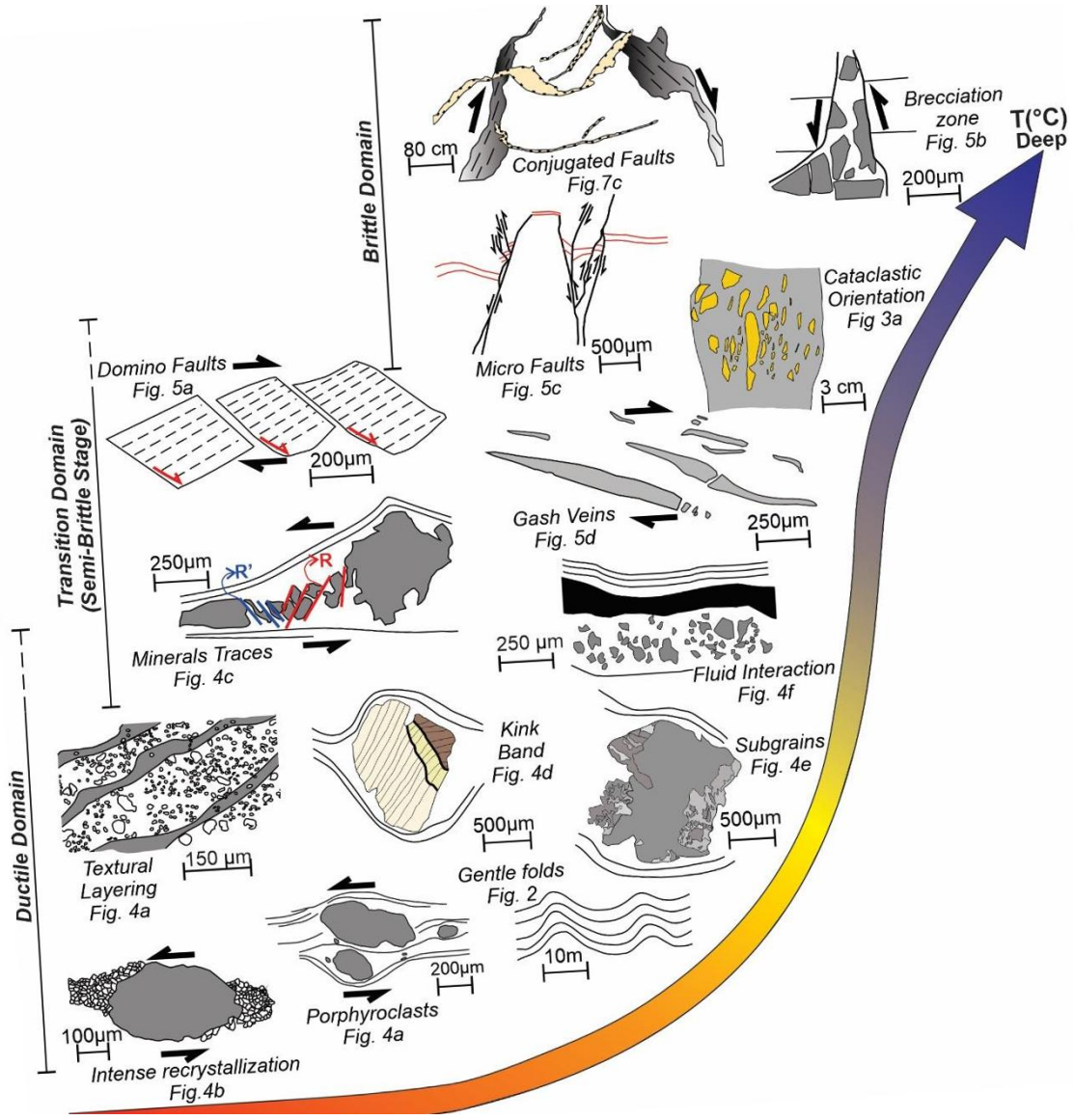

Figure 1.10 - Table of microstructures and structures observed in peridotites in the SPSPA. These structures describe the ductile-brittle transition in the archipelago; they are sensitive to the change in temperature, as well as to the depth of formation and exhumation of the ultramafic body.

These veins are oriented according to the tectonic tensions exerted on the archipelago rocks and exhibit similar right-lateral kinematics compatible with the SPTF motion (Figures 1.5D, 1.7C and 1.11). However, the sequence of

serpentinization and carbonatation seems to have occurred at a different tectonic moment when compared to the peridotite exhumation from the mantle to the oceanic lithosphere. The initial serpentinization, induced by a mantle alteration, sometimes turns the peridotite into olivine and orthopyroxene pseudomorphs (Dungan, 1979; Andreani et al., 2007) (Figure 1.11).

The transition to the semi-brittle regime leads to the formation of Srp2 and Spr3 veins (Figure 1.11). The crystals formed in the Srp2 phase exhibit an ordered and slightly undulating pattern toward the vein walls (Figures 1.6A, B). They are possibly associated with the crack-seal mechanism from microfaults being sealed by crystalline material (Ramsay, 1980; Andreani et al., 2004; Renard et al., 2005; Virgo et al., 2014).

The Srp2 veins tend to run parallel to the mylonitic foliation, isolating fragments of peridotite and olivine crystals from the rock matrix. They exhibit the right-lateral kinematics, therefore syntectonic to the current SPTF right-lateral movement. In this case, the semi-brittle to brittle transition prevails, causing the cataclastic flow process (Figures 1.3C, 1.5A, D). This circumstance marks the transition from the semi-brittle to the brittle regime in SPSPA.

As previously mentioned, the hydrodynamics impinged to peridotite causes the formation of various veins morphologies and types during the fluid flow process. On their part, the Srp4 veins (Figure 1.6D) show a fracture-filled with fluid, evidencing continuous deformation, without kinematic variation during crystal growth. This phase likely corresponds to the complete hydrothermal system opening, with the circulation of elements capable of forming granular-shaped serpentine (Rouméjon et al., 2014), whereas its granular aspect may be due to greater tectonic stability. Therefore, with space, time and fluids available,

serpentine tends to form in granular-shaped grains (Andreani et al., 2007; Rouméjon et al., 2014) .

The semi-brittle deformation creates a different vein morphology and phases (Andreani et al., 2007), that crosscut each other (Figures 1.6B, C and 1.9C). Initially, there is a serpentinization process predominance associated with the cataclasis of peridotites and formation of serpentine Srp1 and Srp2 phase (Figure 1.10). Both serpentine phases appear to be generated by the association of mineral substitution and cataclastic flow process, similar to described by Picazo et al (2013) to the formation of serpentines. The fluid hydrodynamics associated with tectonics allows the formation of Srp3 and Srp4 (Figure 1.4).

These last phase of serpentinization (Srp4) are time-equivalent to the carbonatation phases (Cb1 and Cb2) (Figure 1.10) and marks a progressive change to the carbonatation process predominance and peridotite exhumation to the surface (Andreani et al., 2007; Picazo et al., 2013). It also means evolution of hydrothermal process and chemical completion between carbonatation and serpentinization (Peuble et al., 2018).

The first phase of carbonatation Cb1 (Figure 1.11) is possibly related to the formation of ophicalcite associated with fluid flow and metamorphic reaction, with alkaline fluid derivated from serpentines (Trommsdorff et al., 1980; Picazo et al., 2013). This fluid took advantage of spaces generated by tectonic action in brittle deformation (Figure 1.8), creating an anastomosed fabric of these carbonate rocks (Schroeder and John, 2004; Kelemen et al., 2018).

However, Cb2 (Figure 1.11) marks a final carbonatation stage related to the formation of tectonic breccias (Bonatti et al., 1974; Picazo et al., 2013). This phase is associated with the formation of sedimentary bodies (Figure 1.7) and

the faults planes developed in these bodies (Figure 1.9). The breccia generated in this context is wholly associated with a brittle deformation setting (Figure 1.11) (Schroeder and John, 2004; Picazo et al., 2013).

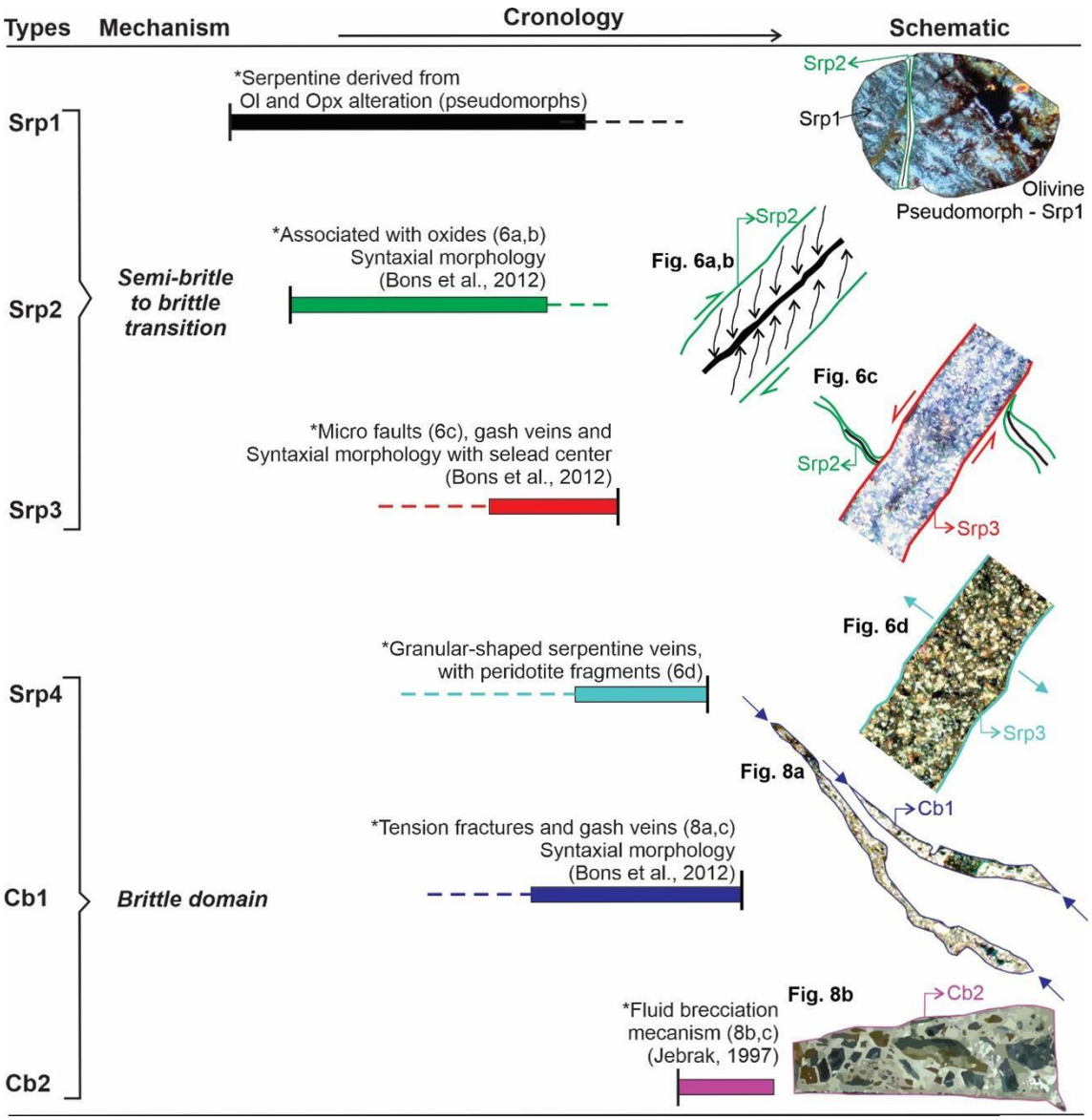

Figure 1.11 - Chronology of the formation of serpentine and carbonate phases in the SPSPA and their relation to the ductile-brittle transition. Srp1: serpentine phase 1; Srp2: serpentine phase 2; Srp3: serpentine phase 3; Srp4: serpentine phase 4; Cb1: carbonate phase 1; Cb2: carbonate phase 2.

5.3. Evolution of deformation mechanisms in the SPSPA

The SPSPA evolutionary history shows different deformational styles during peridotite exhumation, varying from ductile to brittle regimes. According to

the model proposed by Maia et al. (2016), the SPSPA passed by multiple stages of transtension and transpression, producing a positive flower structure (Figures 1.12A and 1.1B).

The deformational evolution illustrated in Figure 1.12 (schematic 3D model) is based on the concepts of progressive deformation from ductile to brittle regime in quartz-feldspar and peridotitic rocks (Scholz, 1988; Schroeder and John, 2004; Andreani et al., 2007; Piazolo et al., 2012; Picazo et al., 2013; Compton et al., 2017; Magott, et al., 2017; Fossen et al., 2018a; Hartman et al., 2018; Papeschi et al., 2018). According to the data obtained in this work, four relevant evolutionary stages in the archipelago being defined.

The first **stage (I)** (Figure 1.12B) comprises the ductile to semi-brittle deformational phases (Figure 1.10) of the São Paulo Transform Fault (Maia et al., 2016), involving transtension to transpression (Figure 1.12A). The mylonitization between the temperatures of ~700 – 800°C, causing olivine and orthopyroxene recrystallization (Figure 1.4A), by the conjunction of different deformation mechanisms (Drury et al., 2011; Czertowicz et al., 2016; Park and Jung, 2017).

The combination of these mechanisms creates a very fine-grained matrix in mylonitic and ultramylonitic bands along the archipelago (Figure 1.4A) (Melson et al., 1972; Simões et al., 2009), possibly as a reflection of the relict layering generated during the peridotite formation under lithospheric mantle (Tubía et al., 2004; Ueda et al., 2008; Frets et al., 2012). Also, the kinematic indicators observed in this phase display left-lateral kinematics (Figures 1.3 and 1.10), corresponding to the internal massif rotation at the beginning of exhumation, as described by the tectonic model proposed by Maia et al. (2016).

Firstly, the evidence of exhumation process is associated with amphibole-rich levels (Figure 1.4A, G), which were likely composed mostly of pyroxene at first, before they reacted with fluids and crystallized as the former (Prigent et al., 2018). This process limits the temperature of mylonitizaiton to 700º and marks the fluid/rock interaction with the formation of magnesium-amphiboles (Picazo et al., 2013; Précigout et al., 2017; Prigent et al., 2018).

The presence of fluids that possibly emerged at the beginning of exhumation, as well as the contact of peridotites with mantle-derived fluids and eventually associated with hydrothermalism, led to the semi-brittle regime (Birner et al., 2016) characterized by the formation of microfabrics attributed to the SPSPA initial exhumation. This latter process may have facilitated the peridotitic body uplift, leading to the transition from ductile to brittle mechanisms (Schroeder et al., 2002; Andreani et al., 2007; Picazo et al., 2013).

The stage (II) (Figure 12B) refers to the semi-brittle to brittle transition of rocks in the SPSPA, with the formation of cataclastic features (Figures 1.3C and 1.5A) and it is mainly associated with cataclastic flow process, which tends to follow a similar direction to the mylonitic foliation produced in **stage (I)**.

The fabric generated by the cataclastic flow processes is closely linked to the presence of fluid flow in the peridotite, developing the cataclastic orientation (Figures 1.4C and 1.12) and the first 3 phases of serpentinization process (Figures 1.11 and 1.12). The temperatures during this stage vary between 300 – 400°C related to serpentine stability (Andreani et al., 2007; Picazo et al., 2013) and the deformational settings established to uplift the peridotite body on oceanic lithosphere (Hirauchi and Katayama, 2013).

However, veins generated in the semi-brittle to brittle transition (Figure 1.11) show dynamic control that is compatible with the transpressional movement in the SPTF, with NW-SE shortening direction (Figure 1.10). Picazo et al. (2013) suggest that a temperature close to 350°C is responsible for the formation of cataclastic and gouge fabric (Figure 1.6), possibly generating serpentine in the interstices created by the peridotite fragmentation (Iyer et al., 2008). Andreani et al. (2007), in turn, locate the serpentine generation at the semi-brittle mechanisms, i.e., the intermediate regime. The same seems to occur in the SPSPA in three-phases of serpentinization generated in semi-brittle to brittle settings.

The **stage (III)** marks deformation under brittle regime (Figure 1.12B), where we observe the presence and intensification of faults, generated due to transpressional SPTF movements. This process forms mainly right-lateral faults with an oblique component and main shortening directed NW-SE (Figure 7D). In this phase, there is an absolute predominance of the formation of brittle features, such as fractures (Motoki et al., 2011) and microfaults (Figure 1.5B), which tend to be filled by Srp4 veins (Figure 1.11). These veins has a granular texture, thus indicating a moment of greater tectonic stability. The formation of Srp4 it is related to the brittle deformation due to tectonic space generated by microfractures (Andreani et al., 2007; Rouméjon et al., 2014).

The final phase of deformation results in **stage (IV)** (Figure 1.12B), during which faults and fractures oriented E-W and filled with carbonate-rich fluids have formed at temperatures about 150°C (Früh-Green et al., 1990; Peuble et al., 2018). The variation in tensions identified in the fault planes (Figure 1.9D)

corroborates the distribution of earthquakes as described for the SPSPA region (Wolfe et al., 1993; Hekinian et al., 2000; Melo and Nascimento, 2015, 2018).

The shortening direction evolves from NE-SW to NW-SE (Figure 1.9D). This direction is similar to the one observed in fault planes, which suggests a continuous deformation mechanism in the EW-directed fault planes. On the other hand, the initial NNW-SSE-directed event observed in the fault planes (Figure 1.9D) should be attributed to a moment, when tensions in the South American Platform prevailed and occurred according to shortening tensions in the northeast direction (Assumpcao, 1992; Heidbach et al., 2016, 2018).

The verified kinematic indicators point to a right-lateral movement for these structures (Figures 1.7C, 1.8A, 1.9D), which is compatible with the SPTF at present (Hekinian et al., 2000; Maia et al., 2016).

Common hydrothermal fluids in ultramafic rocks (Peuble et al., 2015; Kelemen et al., 2018; Menzel et al., 2018) led to the formation of breccia bodies that cross the SPSPA, fragmenting, at times randomly, the rocks in the archipelago. The Pier Shear Zone addressed by Simões et al. (2009) (Figure 1.2) may be related to this process: it consists of a brittle shear zone (Figure 1.6C) with a strike-slip oblique component. This fault and fracture network must has led to the deposition of the São Paulo Formation during a period of higher relative sea level (Campos et al., 2003a; Angulo et al., 2013).

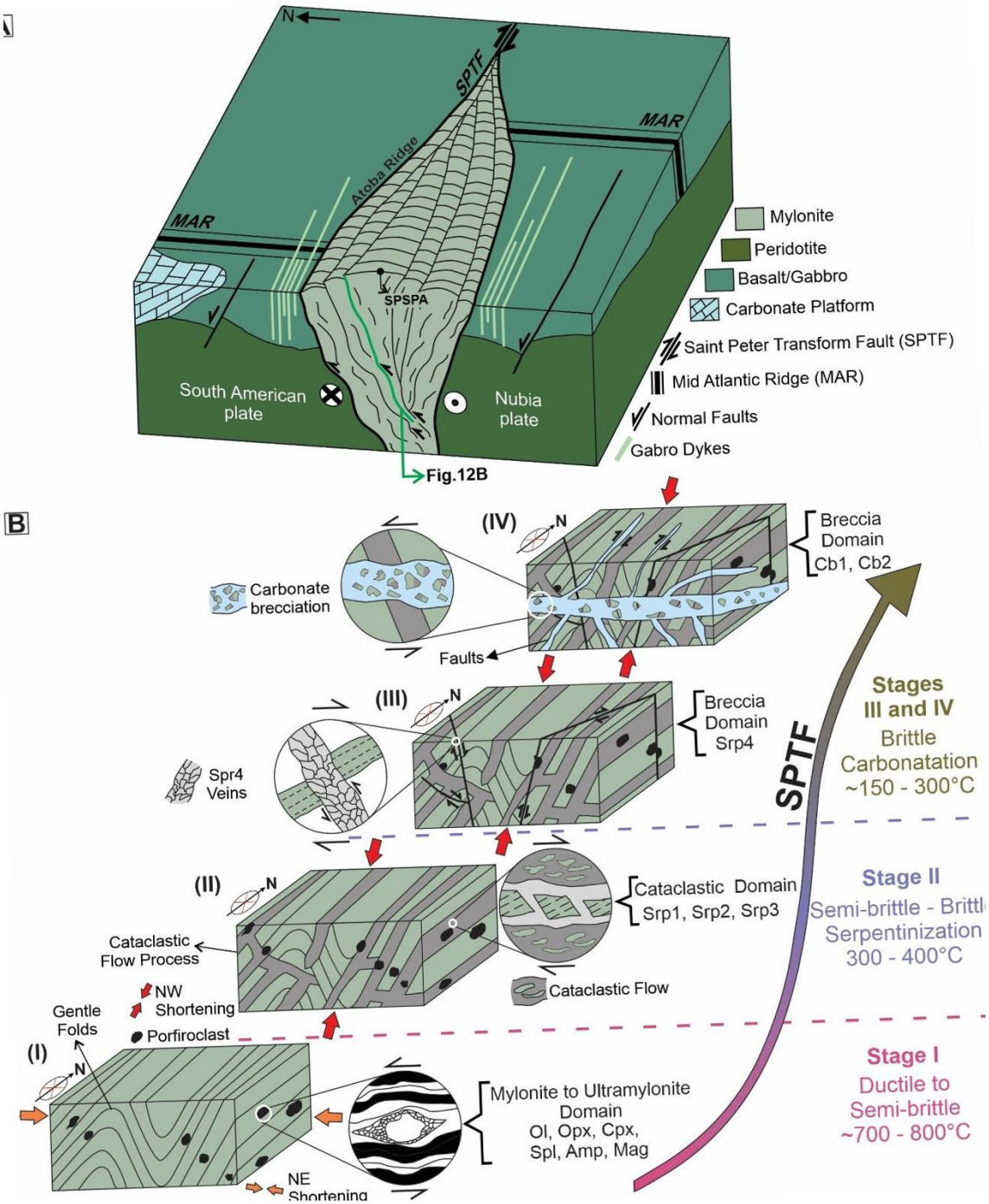

Figure 1.12 - Schematic evolution of the deformation events of the SPSPA. (A) Models for the formation of the SPSPA, based on seismic information obtained by Maia et al. (2016); (B) Evolutionary models of the deformation of the SPSPA (I) to (IV), marking the ductile-brittle deformational transition. Stages: (I) Ductile to semi-brittle deformation with (~700° - 800), (II) Semi-brittle to brittle deformation (300° - 400°), (III) and (IV) Brittle (300°C). Opx: Orthopyroxene, Cpx: Clinopyroxene, Ol: Olivine, Spl: Spinel, Srp: Serpentine, Mag: Magnetite, Amp: Amphibole, Srp1: serpentine phase 1; Srp2: serpentine phase 2; Srp3: serpentine phase 3; Srp4: serpentine phase 4; Cb1: carbonate phase 1; Cb2: carbonate phase 2.

6. Conclusions

Exhumation of the São Pedro and São Paulo Archipelago to the ocean lithosphere imprinted features that record deformation mechanisms during a transition from ductile to brittle regime. The analysis of different structures and microstructures in the deformed peridotitic rocks led us to conclude that:

- In the first stage, the rocks were affected by the ductile to semi-brittle deformation, which caused intense recrystallization of minerals such as olivine and orthopyroxene and the formation of the ultramylonitic features. This deformation is associated with temperatures ranging between 700-800°C;
- The continuous and rapid uplift led to the superposition of deformation mechanisms, with reactivation of pre-existing structures and predominance of semi-brittle to brittle deformation mechanisms, dominating by cataclastic flow process;
- The presence of fluids seems to have been essential both for the deformation and for the tectonic block uplift that sustains the SPSPA. These fluids initially reacted with the peridotites, forming amphibole-rich levels. Furthermore, the fluid is also closely related to the formation of four different generations of serpentine in brittle deformational context;
- Rapid exhumation is related to high pressures. Consequently, there was a high pressure of fluids, which in turn produced tectonic features such as faults and microfaults. These are mainly related to phases of carbonates and serpentine;
- We observed mainly faults associated with carbonate bodies. The direction of NW-SE of their main tensor is compatible with the current

compressive field observed in earthquakes nearby SPSPA, which indicates that this situation is still active.

7. Acknowledgments

We thank CNPq for the financial support through grants 557299/05-5, 557141/2009-5 and 442865/2015-5, CAPES for providing scholarship to the first author, Fundação Araucária by RJA for providing a senior grant (45725), CNPq process number 302913/2018-1 research scholarship RJA the Brazilian Navy and SECIRM for support during fieldwork, and LABAP, LECOST, LAMIR and PPGeol-UFPR for infrastructure. We also thank the anonymous reviewers for their helpful suggestions and reviews. The authors would also like to thank the Academic Publishing Advisory Center (Centro de Acessoria de Publicação Acadêmica – CAPA) of the Federal University of Paraná for language support for this version of the article.

3.2. Artigo 2

DEFORMATIONAL STRUCTURES DEVELOPED IN VOLCANIC SEQUENCES AS A PRODUCT OF TECTONIC ADJUSTMENTS IN THE SOUTH ATLANTIC OCEAN

Leonardo Mairink Barão[1*], Barbara Trzaskos[1], Rodolfo José Angulo[1], Maria Cristina de Souza[1], Herick Faust Daufenbach[1], Fernanda Avelar Santos[1], Eleonora Maria Gouvêa Vasconcellos[1]

Journal of South American Earth Sciences, Vol. 133, abril 2020, DOI: https://doi.org/10.1016/j.jsames.2020.102812

Abstract

The Atlantic Tectonics, associated with volcanic processes, allowed the formation of the Vitoria-Trindade Chain seamounts, and consist in a recent volcanic manifestation event in the Atlantic Ocean (3.7 to <0.17 Ma). The chain is aligned in the E-W direction, parallel to the Vitória-Trindade Fracture Zone (VTFZ), the structure that controls the deformation on and around the seamounts of Vitoria-Trindade Chain. The Trindade Island, a still rising outcrop of the chain, allow us to outline tectonic features and to get the paleostress acting on the island. We used a multiscale approach integrating regional seismic reflection, spatial analysis, fieldwork, paleostress analysis and petrography to refine and detail the structural control and the deformational settings in Trindade Island. The pyroclastic deposits and phonolite intrusions formed during the lower Pleistocene, which belong to the Trindade Complex, and comprise the basal unit of the island. This unit is affected by extensional phases capable of creating sets

of NNW-SSE direction horsts and grabens. These structures are associated with strike-slip faults with left-lateral kinematics and NE-SW direction. The structural arrangement between those sets of structures enable them to establish the main shortening direction as vertical, suggesting active tectonics during the first volcanic event of the Island. The tectonic events progression support the establishment of the transtensive regime, mainly due to the deformation caused by NE-SW strike-slip faults, where the main drainages of the island are currently located, and also associated with the emplacement of vertical alkaline dikes following mainly en chelon pattern with NW-SE direction, which intrude the pyroclastic sequences of the Trindade Complex. This transition from the extensional to the transtensive regime establishes the rotation of tensions, where initially the tensions are vertical during the lower Pleistocene, similar to what occurred in the southeastern Brazilian basins. The progression to the transtensional regime associated with direction NNW-SSE stresses suggests in the establishment of similar tectonic stress imposed on the South American Plate continental portion.

Keywords: Oceanic fracture zone, normal faults, strike-slip faults, Trindade Island, Vitória-Trindade Fracture Zone, alkaline dikes

1. Introduction

Oceanic volcanic complexes and volcanic islands present a complex evolutionary history involving emplacement process controlled by tectonics and magmatic activity(e.g., De Rita et al., 1983; Carracedo, 1996; Cimarelli and De Rita, 2006; Mathieu and van Wyk de Vries, 2009; Bistacchi et al., 2012; Sibrant et al., 2015). The tectonic influence of oceanic fractures zones on offshore islands

and continental regions is still little studied. However, these structures can influence the paleocontinents configuration (Reuber and Mann, 2019; Vasconcelos et al., 2019), rift zones (Mascle et al., 1988; Mohriak and Rosendahl, 2003; Torsvik et al., 2009; Wilson, 1965), continental deformation (Mohriak and Barros, 1990; Pinheiro et al., 2019), and volcanic islands (Långbacka and Gudmundsson, 1995; Ventura et al., 1999; Alves et al., 2006).

South Atlantic tectonics involves a diversity of tectonic settings and the various genetic mechanisms to the offshore island formation (Davison, 1999; Torsvik et al., 2009; Mohriak, 2020). This differentiation of tectonic context is associated with the geometry and configuration of oceanic fractures (Mohriak and Rosendahl, 2003), generating crustal deformation as tectonic stresses are applied (Palmiotto et al., 2017). This kind of deformation was not well characterized in volcanic sequences developed in volcanic islands.

In this paper, we outline the structural framework of Trindade Island (TI) (Figure 2.1). We based in structures identified in previous studies (e.g., Almeida, 1961; Pires and Bongiolo, 2016; Angulo et al., 2018) and we applied a multiscale approach using 2D seismic reflection data, spatial analysis, and fieldwork data, paleostresses analysis and petrographic data to understand the tectonic events and mechanisms that controlled the evolution of the Vitória-Trindade Chain. Our results allowed us to improve the knowledge about the inherited tectonic control from oceanic fracture zones during the Quaternary in the South Atlantic Ocean.

2. Geological Context

The Vitória-Trindade Chain has a complex evolutionary history, beginning in the Brazilian continental slope, with continuity to the east towards the Atlantic

Ocean (Figure 1A). The Vitória-Trindade Chain is composed of several aligned and elongated seamounts oriented to E-W direction (Figure 2.1A), parallel to the Vitória-Trindade Fracture Zone (VTFZ) (Almeida, 1961; Alves et al., 2006). This feature marks an important oceanic tectonic-magmatic activity that occurred during the Cenozoic (Cordani, 1970), possibly due to VTFZ reactivation (Almeida, 2006). Alves et al. (2006) emphasized the continuity of this structure to the African coast, sectioning the Dorsal-Mesoceanic and producing the local displacement of 6km.

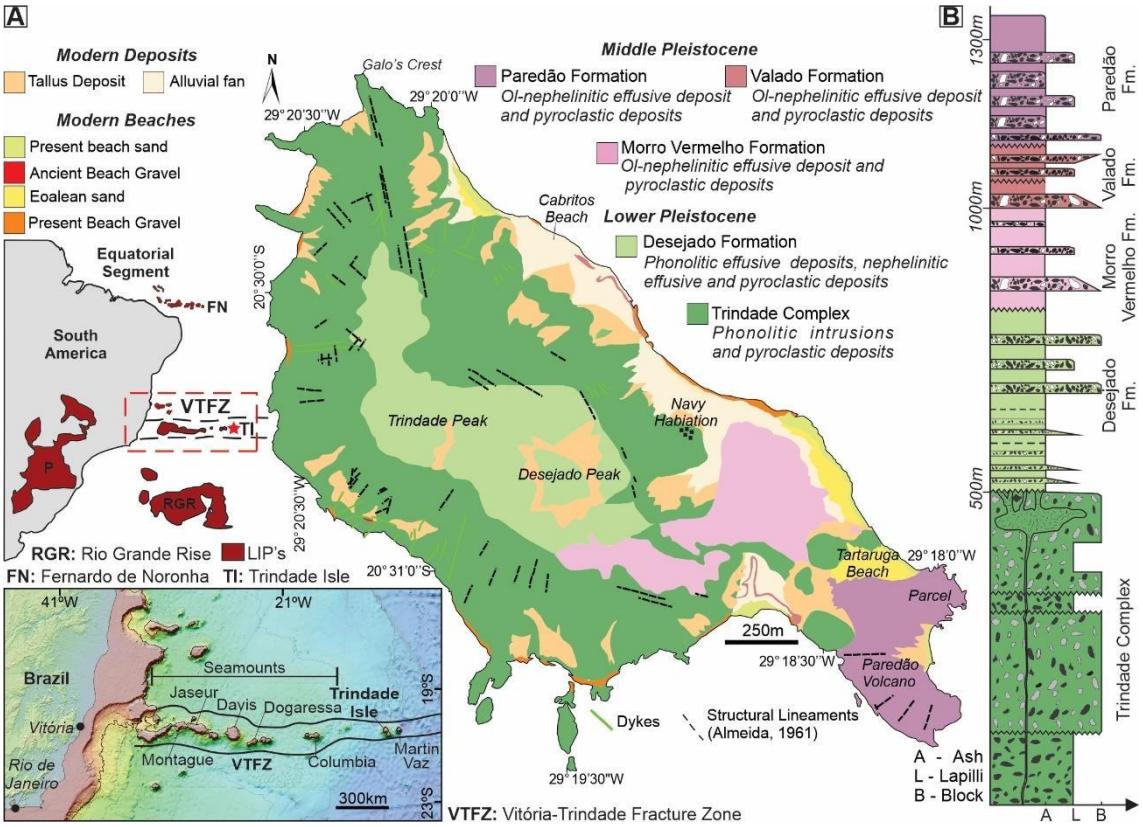

Figure 2.1 - (A) Simplified geological map of Trindade Island (TI) and lineament distribution observed by Almeida (1961) (After Almeida, 1961; Pires and Bongiolo, 2016; Angulo et al., 2018; (B) Stratigraphic column proposed for TI geological units by Pires and Bongiolo (2016).

The main outcrop in the Vitória-Trindade Chain seamount is the TI. The TI is composed of pyroclastic deposits successions and a large set of shallow intrusive rocks, exposed in the form of domes, necks and dikes (Almeida, 1961) (Figure 2.1A). The volcanic rocks are subdivided into five distinct geological units

(Figure 2.1B) with formation ages between the lower and middle Pleistocene (Almeida, 1961; Pires and Bongiolo, 2016), thus comprising: the Trindade Complex (phonolytic necks and pyroclastic rocks) and the Desejado (pyroclastic rocks interspersed with effusive rocks), Morro Vermelho (volcanic plateaus and small pyroclastic deposits), Valado (volcanic effusive and pyroclastic rocks) and Paredão formations (effusive and pyroclastic deposits) (Figure 2.1).

The volcanic processes varied according to the Strombolian and Vulcanian styles (Pires and Bongiolo, 2016), with the phonolytic-nephelinite volcanic episodes associated with relative viscosity processes and gas-enriched magmas, generating pyroclastic deposits and low volume of effusive rocks (Pires and Bongiolo, 2016). Volcanic plateaus, on the other hand, are associated with low viscosity stages and continuous overflow, linked to the Hawaiian volcanic style (Pires and Bongiolo, 2016).

The spatial analysis of dikes and fractures, performed by Ferrari and Riccomini (1999), demonstrated the main shortening direction ENE-WSW to E-W, for the dike formation. These tensors corroborate to the shape and island's axis orientation (Ferrari and Riccomini, 1999), which suggests tectonic control in the island formation. The VTFZ provides the role of strike-slip and compressional regimes in the Vitória-Trindade Chain region (Alves et al. 2006). VTFZ served as a favorable location for the development of tectonic stresses associated with volcanism and fault formation (Alves et al. 2006).

3. Methods

Initially, we define the regional structures nearby the TI based on the interpretation of multi-channel reflection seismic 2D sections of the LEPLAC II

and VII projects (Plano de Levantamento da Plataforma Continental Brasileira - Brasil, 1989) (Figure 2.2 and Supplementary Figure 2.1), carried out between the 1980s and 1990s, acquired from the Diretoria de Hidrografia e Navegação (DHN), the project covers the area of VTFZ not specifically the area near TI. However, we can observe similar tectonic features in TI. It will be associated with structures defined on the spatial analysis and fieldwork.

The tectonic and volcanic structures mapped on TI were initially observed by the interpretation of aerial photograph captured by the Brazilian Navy in 2011 (Marinha do Brasil, 2011 - Supplementary Figure 2) and the relief map obtained by the interpolation of topographic data (DHN, 1971), which were used in the construction of the digital elevation model (DEM). Based on these data, structural lineaments were delineated, thus allowing them to establish the directions that prevail in the island's structuring.

In the outcrops, we perform a multiscale approach (Davy et al., 2008), observing tectonic features as a fault plane, fractures, conjugate pairs, and deformation bands. Fault planes and striations were measured, in addition to kinematic criteria for fault planes (Petit, 1987; Doblas, 1998). The dynamic analysis was performed using the straight dihedral method (Angelier and Mechler, 1977; Angelier, 1994) and Win-tensor 5.8.8 software (Delvaux, 2012) to obtain the paleostress responsible for the fault planes.

4. Results

4.1. Regional fault framework

The 2D seismic lines cut off much of the Vitória-Trindade Chain seamounts region (Figure 2A and Supplementary Figure 2.1A), in those sections, we

highlight the lower Pliocene Layer identified by Alves et al 2006 and the volcanic basement (Mohriak, 2003, 2020). The presence of faults is frequent for the selected sections (Figure 2.2) and they are generally vertical when observed in sections perpendicular to the VTFZ (Figure 2.2B). In them, there are strike-slip structures, with the formation of negative flower structures (Figure 2.2B), displaced blocks, and wedge features, indicating the right-lateral kinematics for fault zone movement.

Successive sets of grabens and horsts that reach the newly sedimentary sections and resulting modifications of the ocean floor topography are common (Figure 2.2C). The triangular features geometry delimited by normal fault planes shows that the performance of regional events with similar stresses affected the entire Vitória-Trindade Chain region. The blocks tilting caused by faults is sometimes so intense that it causes displacement in sedimentary sections (Figure 2.2D), causing significant displacements that effect until newly sedimentary sections.

Igneous intrusions, which are common throughout the chain, frequently appear as vertical features that locally affect sedimentary sections and cause the tilting of seismic reflectors (Figure 2.2E). Normal faults with moderate dip angles (45° - 60°) and secondarily reverse faults may be related to these intrusions. The fault planes endings culminate in intrusions or at greater depth in the volcanic basement (Figure 2.2E and). Thrust faults with a low dip angle (≤30°) are less expressive, thus affecting the sediment locally and generating small high features on the ocean floor topography (Figure 2.2C).

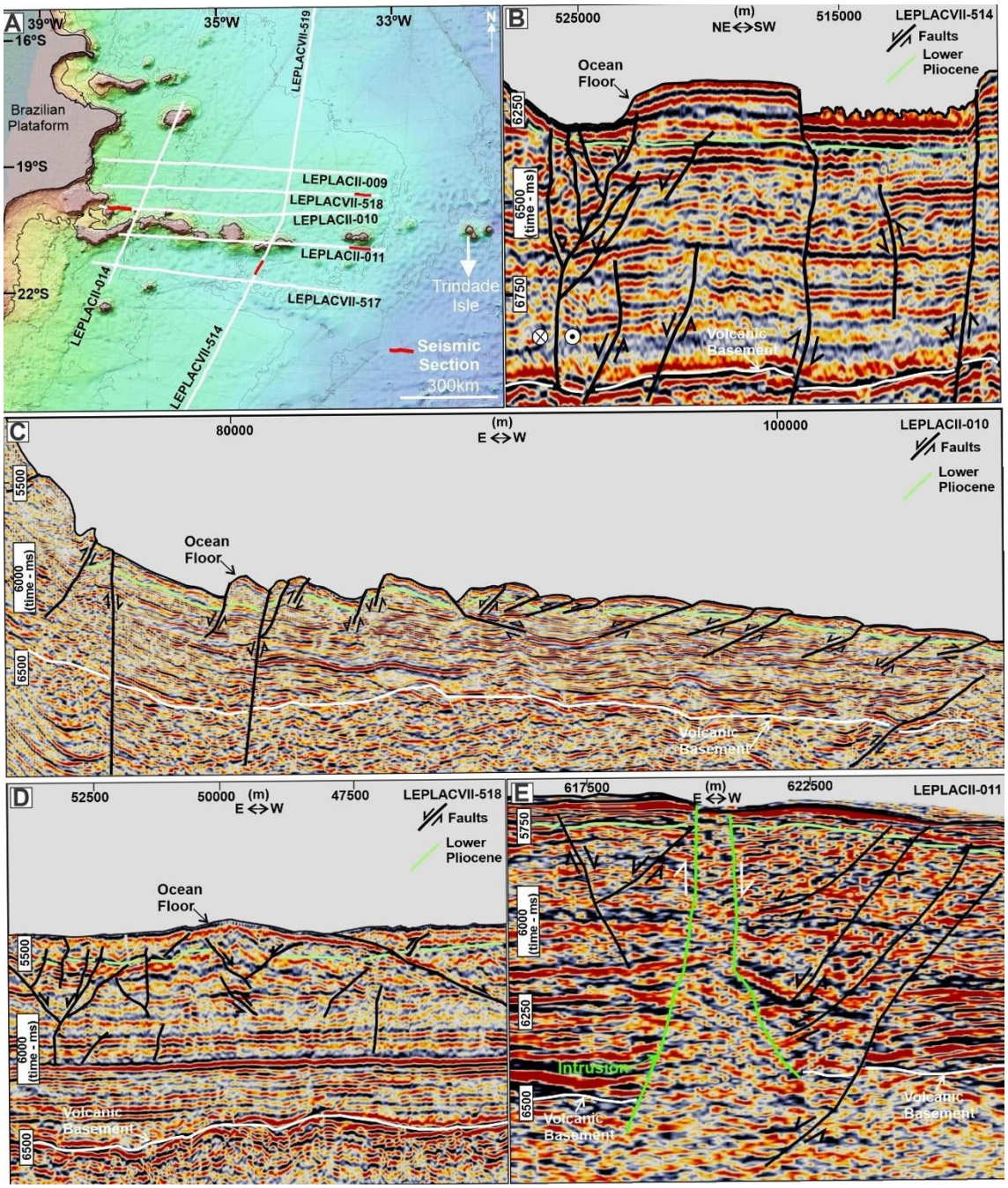

Figure 2.2 - Seismic features observed in the Vitória-Trindade Chain region. (A) Location of the LEPLAC seismic lines near the Vitória-Trindade Chain seamounts; (B) Strike-slip faults by severing the seismic reflectors, these faults suggest the presence of faults in negative flower and right-lateral kinematics; (C) Horsts and grabens geometry modifying ocean floor geometry; (D) Normal moderate-to-low dip angle faults, possibly marking planar or sliding block features; (E) Intrusions are affecting the region and forming normal faults and features representing the passage of hydrothermal fluids derived from intrusions. The uninterpreted seismic sections are available in Supplementary Figure 1.

4.2. Mapped structural features

The interpretation of tectonic structures allowed the verification of structural styles throughout TI. In the first sample, the dispersed pattern of the

structures was verified without lineaments specific direction (Figure 2.3A and Supplementary Figure 2A), as described by Ferrari and Riccomini (1999). However, the typical pattern reflected the presence structures oriented to N30-45W, and the main drainages generally appear to be allocated in the NE direction (Supplementary Figure 2) and possibly should refer to tectonic features.

By selecting specific areas and structures already mapped by Almeida (1961), revealed dispersed structural lineaments in Crista do Galo region (Supplementary Figure 2B). In this region, the presence of phonolytic dikes of the Trindade Complex (Pires and Bongiolo, 2016) with direction N20-30W are a constant feature that controls the relief and the region's geomorphology (Green line with two arrows in Figure 2.3A). The intrusive bodies are forming elongated ridges, which cut pyroclastic deposits. Although these structures control the relief of the island, the lineaments showed fan pattern, with mean N-S direction (Supplementary Figure 2.2B), unlike the regional pattern observed throughout the rest of TI.

The second area selected is the Paredão Volcano region (Supplementary Figure 2.2C). In this region it is possible to observe a possible volcanic cone from the last remarkable Trindade volcanism event, which ended up generating the Paredão Formation tuffs and lapilli tuffs (Almeida, 1961) (Supplementary Figure 2C). The image analysis will be delineated to define a circular structure arrangement in the aerial image. However, the remarkable accumulated frequency has the northwest direction (Supplementary Figure 1C), similar to that observed on the structural trend in TI (Supplementary Figure 2A).

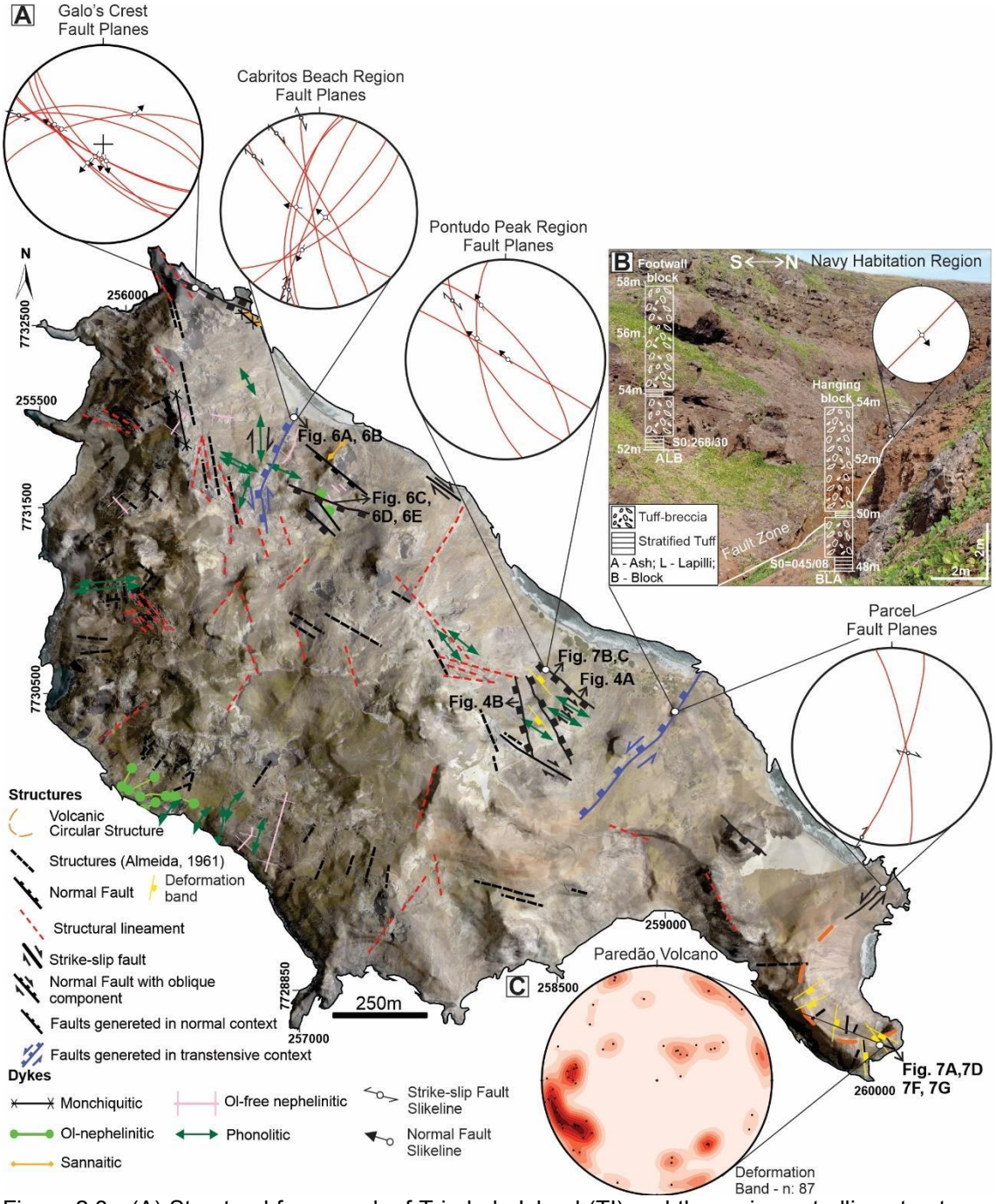

Figure 2.3 - (A) Structural framework of Trindade Island (TI) and the main controlling structures of the island, as well as structural faults, dikes and lineaments. Defined using the aerial image (Marinha, 2011) associated with the digital elevation model based on 20m contour lines (DHN - Diretoria de Hidrografia e Navegação, 1971). (B) Vertical displacement caused by NE oriented fault and settled close to drainage; (C) Lower-hemisphere, equal-area projections observed for deformation bands features generated in TI pyroclastic rocks.

The dispersion pattern observed in the structures (Figure 3A) can refer to existing volcanic structures, such as magmatic flow features and intrusive bodies, such as stocks and dikes, which intrude the rocks of TI (Leonardo M. Barão et

al., 2018). The pattern of NW-SE oriented structures is constant throughout the island. It exerts substantial structural control in observed locations highlighted on the map (Figure 2.3A – Pontudo Peak, Cabritos Beach and Galos Crest). Spatial analysis of deformational structures, based on image analysis, enabled the identification and distribution of these features in the field. The mapped structures correlation showed a variable direction pattern between NNW-SSE and secondarily NE-SW (Figure 2.3A – Pontudo Peak and Navy Habitation regions).

These mapped structures are mainly normal faults and secondarily strike-slip faults with a normal oblique component. The northwestern features (N10-45W) control the island relief and generate clusters of grabens and horsts in their region (Figure 2.3A – Pontudo Peak Region), mainly sectioning the pyroclastic and phonolytic sequences of the Trindade Complex. This fault system locally controls geological contacts, placing phonolites and tuffs side by side (Figure 2.4 – Pontudo Peak Region) and locally modifying stratigraphic stacking. The faults present continuity along the island, showing a straight line with varying dip angles between 45° - 70° (Figure 2.4A – Pontudo Peak Region). These structures generate tilted blocks that tend to rotate along the fault planes (Figure 2.4B) and form triangular facets in the outcrops described (Figures 2.4A and 2.4B).

The N to NE-SW direction structural features (Figure 3A) are associated with the main drainage zones of TI (Supplementary Figure 2). The incised valley case (Figures 2.1 and 2.3B), where the controlling structure is an extensional feature that vertically displaces Morro Vermelho Formation volcanic unit. This vertical displacement generates a slope about 4m (Figure 2.3B - Navy Habitation) from the footwall and hanging wall of the fault, causing the abrupt dip change of the volcanic bedding from the stratified tuffs in that outcrop portion (Figure 2.3B).

In the region of Cabritos Beach (Figure 2.3A), we mapped a similar structure (Figure 2.3A and Supplementary Figure 2), where the tectonic must have directly influenced the drainage fitting in the region, as well as the formation of breccia features.

The Paredão volcano region has a circular feature observable in aerial images (Figure 2.3A – the orange volcanic circular structure and Supplementary Figure 2), and the remnant of the precursor volcanic cone is identified (Almeida, 1961; Pasqualon et al., 2019). Normal faults sectioned this cone structure (Figure 2.3A – orange volcanic circular structure), sometimes featuring cataclastic features and deformation bands (Figures 2.3A and 2.3C), as well as structures as conjugate pairs that section pyroclastic deposits.

The dikes that cut the Trindade Complex rocks are associated with fault planes (Figures 2.3 and 2.4A), making it possible to observe striation and steps in the contacts. These dikes are related to the passage of fluid, causing the rocks to fragment and forming hydrothermal and tectonic breccias. In the following section, we will report the different aspects generated in each distinct rheological response on the island.

4.2.1. Tectonic features in phonolytic rocks

The phonolytic rocks of Trindade Complex are marked by light gray to dark gray. These rocks are composed of nepheline or alkali feldspar phenocrysts surrounded by a thin matrix composed mainly by sanidine, nepheline, aegirine-augite, without specific crystal orientation (Figure 2.5).

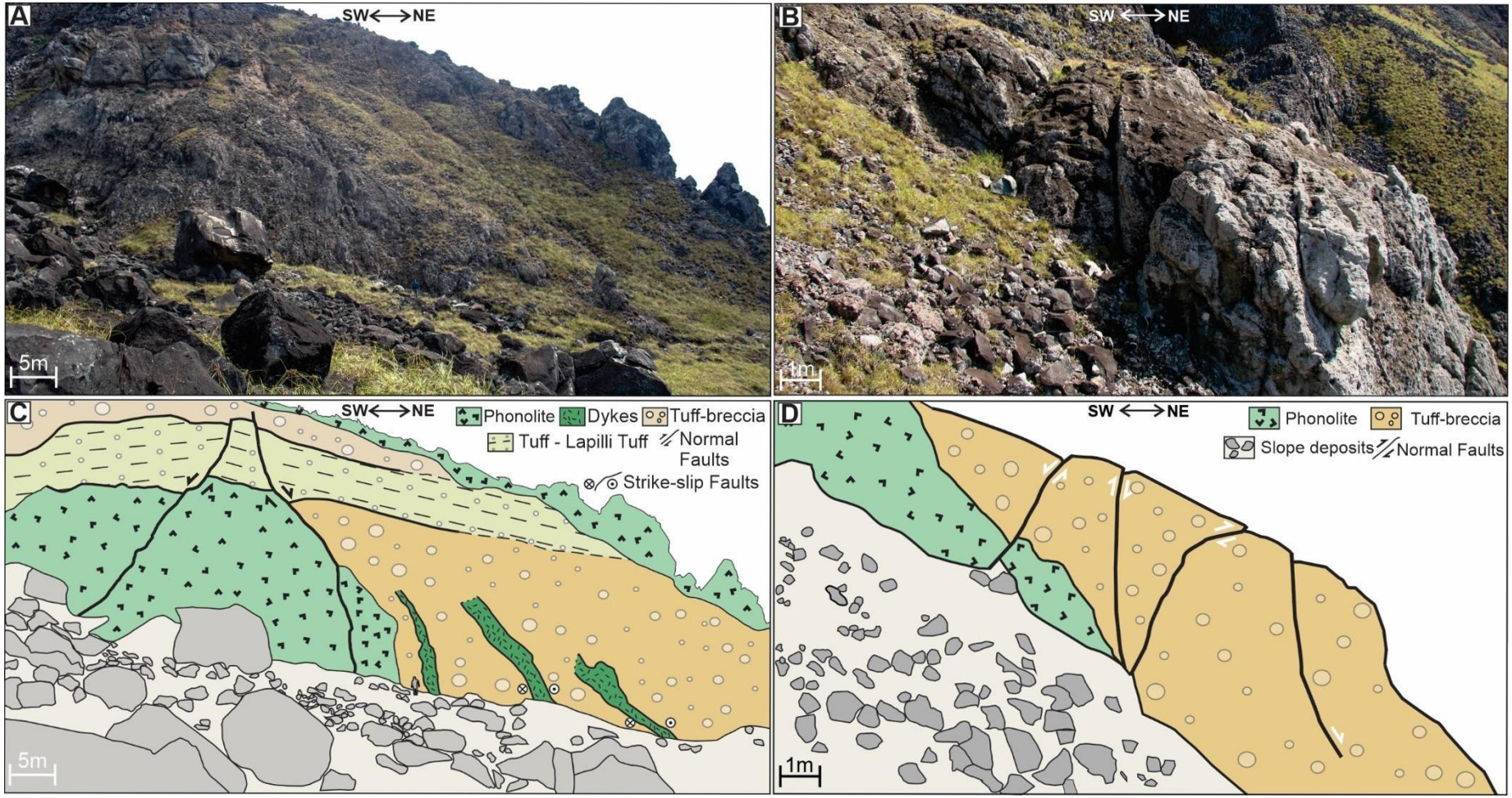

Figure 2.4 - Interpreted photomosaics of representative outcrops of the grabens and horst system. (A and B) Normal NW oriented faults that end up tipping geological contacts; (C and D) Triangular features caused by the displacement of normal fault planes.

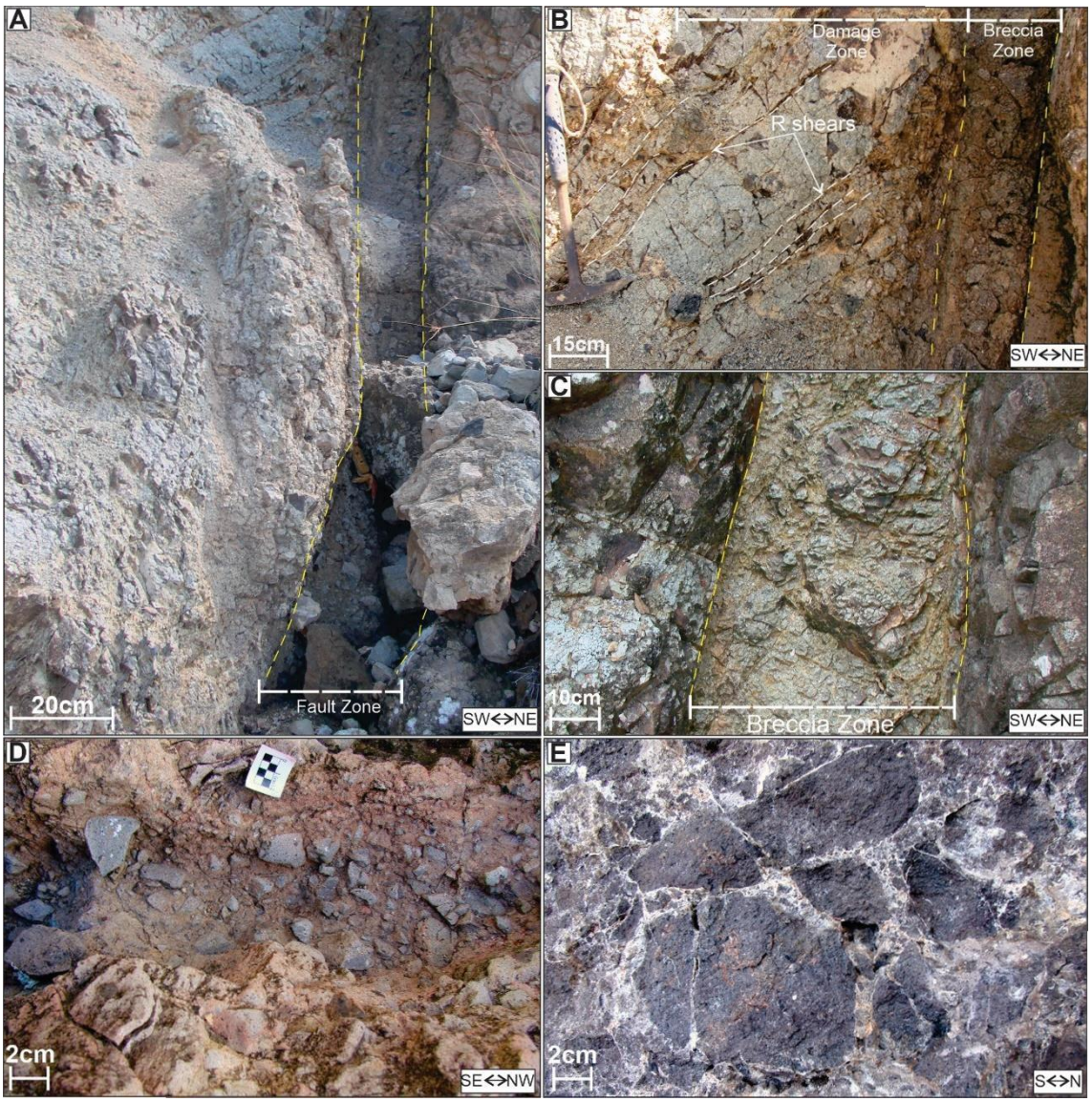

Figure 2.5 - Features generated along phonolytic rock fault planes. (A) NW oriented and vertical fault plane; (B) R type fractures formed obliquely to the main fault zone; (C) Breccia developed along the fault plane; (D) Breccia formed by angular fragments associated to iron oxide rich cement; (E) Carbonate-cemented hydraulic breccia.

The faults presence in phonolytic rocks is marked by centimeter fault zones (30 to 40 cm), usually vertical (Figure 2.5A) and associated with local fragmentation and breccia generation (Figure 2.5B). Riedel-type fractures damage zones, are the oblique-slip direction to the main shear zone (Figure 2.5B) and are associated with fault breccias. The cataclasis caused by the tectonics in the phonolites generating angular and fractured fragments without specific orientation (Figure 2.5C). Fragment sizes range from 4 to 10 cm, which is

commonly cemented by reddish-colored oxides that support the fault rock (Figure 2.5D). Locally, it is possible to observe the blocks fragmentation that composes the breccia, caused by the percolation of hydrothermal fluids, subsequently cemented by carbonate (Figure 2.5E).

The dikes are associated with the regional tectonic stresses, generating the subvertical phonolytic intrusions (Figure 2.4A). Internally, the dykes can present sub-horizontal fractures and can be described as a columnar disjunction caused by cooling (Figure 2.6A). Also, the dikes might be allocated by normal faults, which intrude in pyroclastic rocks (lapillistone and tuff-breccias) and are parallel to the phonolites intrusion direction (Figure 6B). Occasionally the shape of these structures is sigmoidal (Figures 2.6B and 2.6C), probably a response for the tectonics imposed by the dike generation. Sometimes the deformation is so intense that it causes the dike rupture and the formation of fault breccias (Figure 2.6B).

Another tectonic indicator on these dikes is their parallelism with shear features that cut the outcrop (Figure 2.6C) and restrict continuity of these bodies in the fault plane (Figures 2.6B and 2.6C). Internally to the dikes, it is possible to observe the parallel fractures fabric, which is slightly undulating (Figure 2.6D), enabling the interaction with fluids and, consequently, internal fracturing. The intrusion base is marked by the breccia features development in contact with the dike host rock, in this case pyroclastic rocks (Figure 2.6E).

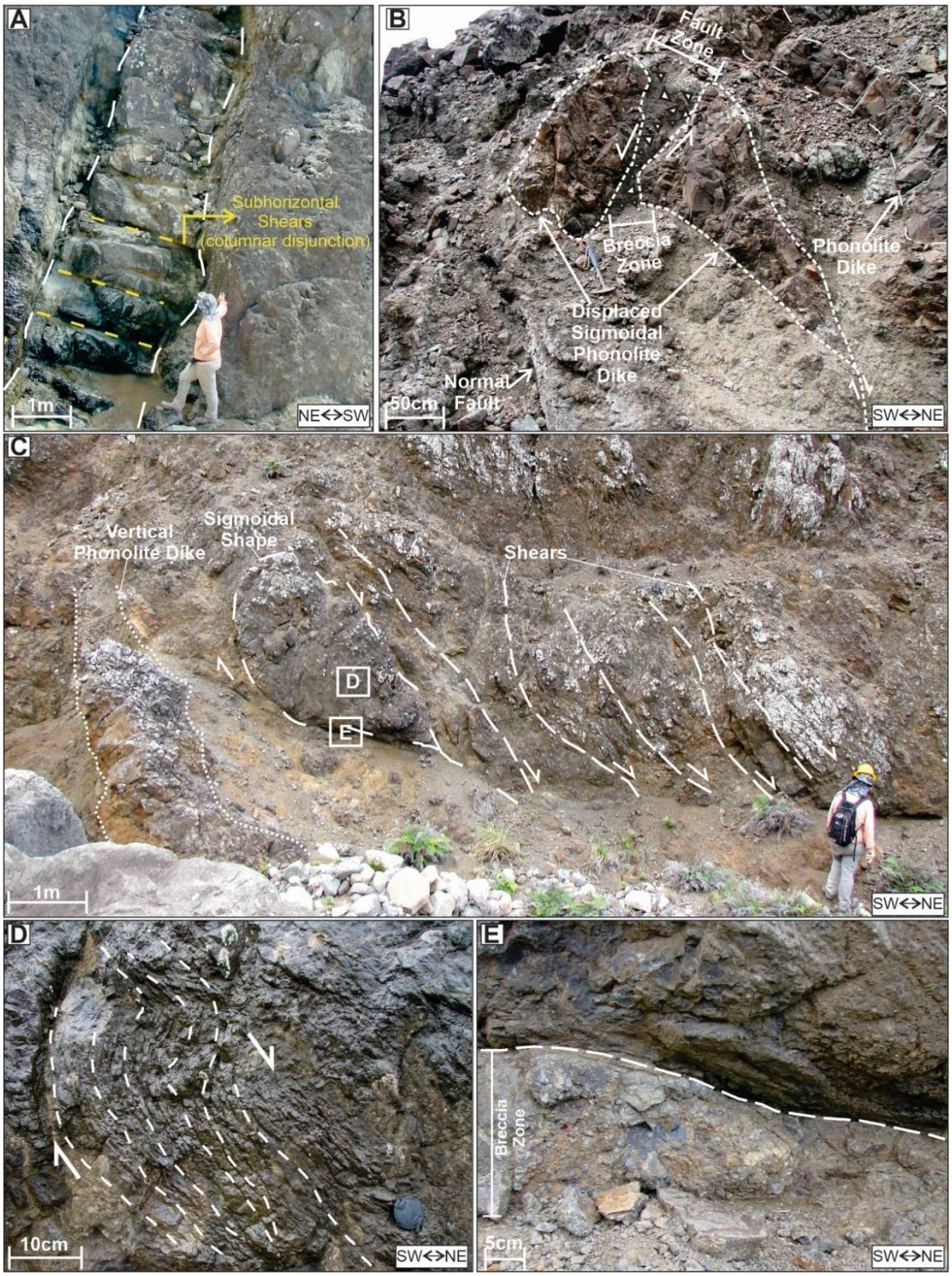

Figure 2.6 - Phonolytic dikes associated with fault plans. (A) and (B) in general, faults appear to be closely linked to these structures, and these bodies tend to become parallel to the fault planes; (C) Sigmoidal dike parallel to fractures and faults; (D) Zoom area showing internal features formed in dikes, probably slightly undulating cooling fractures indicating right-lateral shear; (E) Fault breccia zoom generated along the basal plane of the fault.

4.2.2. Tectonic features in pyroclastic sequences

Unlike phonolytic rocks, pyroclastic deposits (lapilli-tuff, lapillistone and tuff-breccias – Figure 2.7) affected by faults tend to form millimetric thickness fault planes, which cause centimeter displacements (2 to 7cm) between volcanic lamination (Figure 2.7A). This type of feature is commonly observed in lapillistone, lapilli-tuffs and tuff-breccias (Figures 2.7B and 2.7C) in the Trindade Complex and the Paredão Fm. (Figures 2.7A). The average directional pattern of these structures is NW-SE (Figure 2.3C – Paredão Volcano), following the normal fault pattern observed for the island (Figure 2.3A). However, these structures section the entire wall of the Paredão volcano in a concentric form.

It is common to observe conjugated pairs (Figure 2.7D) associated with these features, usually associated with extensional deformation, which should enable fluid passage and internal shear to these structures. The deformation bands formed along these planes have a variable thickness (2 and 8cm), presenting less porous zones than the host rock (Figure 2.7E).

Throughout these deformation bands are possible to identify broken minerals and rock fragments and rarely elongated crystals (Figure 2.7E). Re-cementing in the deformation bands is common by filling voids that were previously composed of vesicles and pores of the host rock (Figure 2.7F), oxides and secondarily carbonates composes the cement-containing material. The sigmoid features present so-called eye structures (Figure 2.7G), which formed from two collinear fault plane segments that connect and form a single fault plane (Antonellini and Aydin, 1995), thus indicating normal kinematics for these structures.

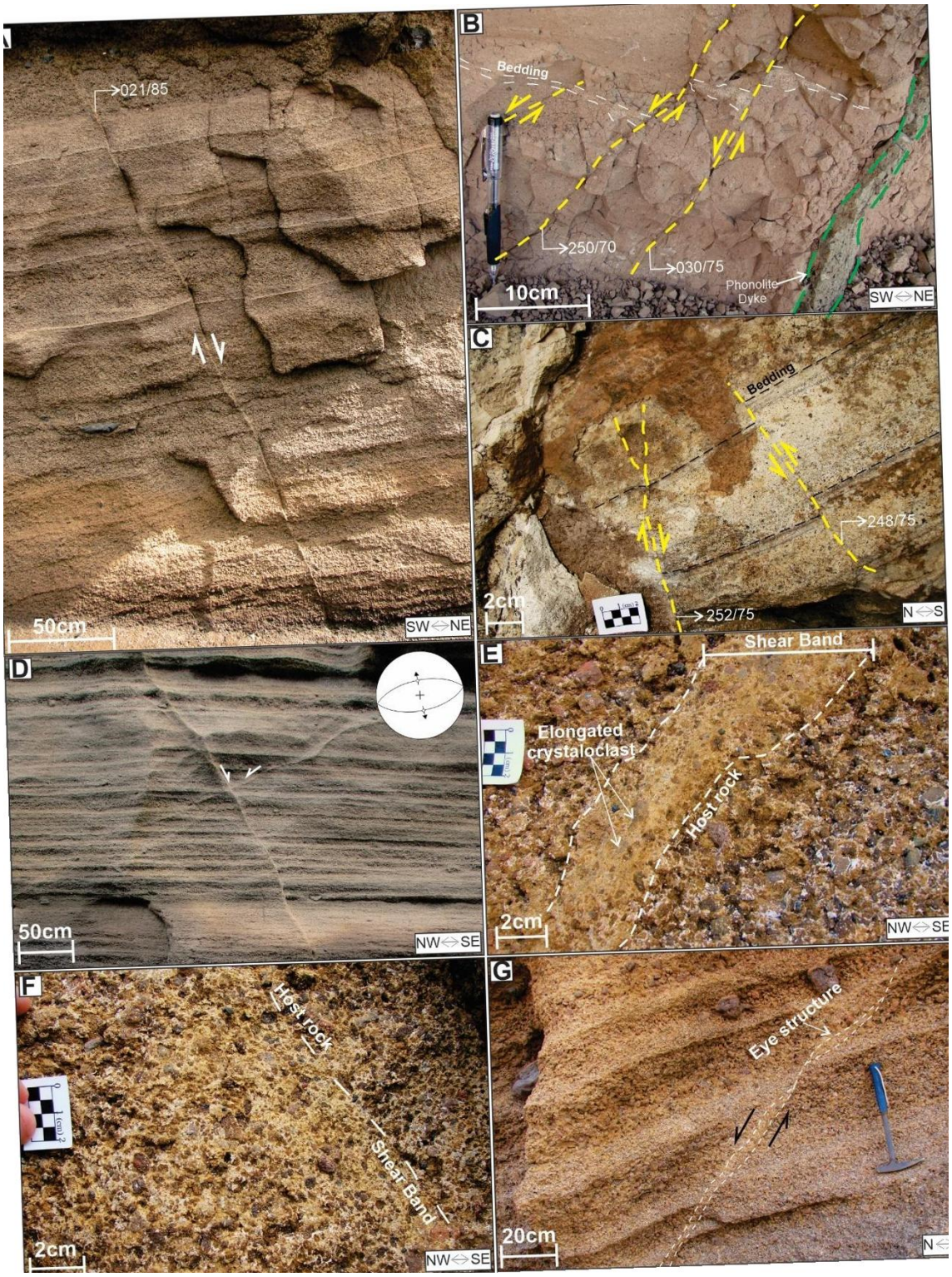

Figure 2.7 - Deformational features formed in pyroclastic deposits affected by fault zones. (A) Fault plane intersecting lapilli tufts of Paredão Fm. oriented to NW; (B and C) Sequences of planar features in horst and grabens in Trindade Complex outcrops; (D) Conjugate pair oriented to EW, marking the extensional tectonics through which the pyroclastic sequences of the Paredão Volcano passed; (E) Deformation band with crystalloclast and lithoclast fragments; (F) Differentiated pyroclastic cementation in the deformation band showing the different porosities in the rock; (G) Normal fault commonly observed in lapilli tufts of Fm. Paredão, which makes it possible to observe the eye structure, a reflection of the junction of two shear planes.

4.3. Microstructural analysis of breccias and deformation bands

Faults observed in TI generate different features along the fault plane, with the passage of fluids, still associated with the volcanism. Breccia mechanisms occur by the friction of fragments or the passage of hydrothermal fluids. These processes cause the cataclasis and comminution of phonolitic rocks. The fragments generated by the rock friction have dimensions ranging between 1 and 10cm, surrounded by the matrix composed of thin comminuted fragments (> 1cm). The cementation of these rocks is composed of carbonates and clay minerals (Figure 2.8A), which gives a “dirty” aspect to the rock (Figure 2.8B). Otherwise, the clay minerals develop from the wall of the fault plane (Figure 2.8A), possibly associated with the percolation of hydrothermal fluids in the rock (Wintsch et al., 1995).

The progressive entry of fluids leads to the formation of rotated features (Figure 2.8C) and the probable mineral reorientation parallel and perpendicular to the principal tensor (Jébrak, 1997). The formation of cataclastic flow in phonolites is observed (Figures 2.8B and 2.8C), as well as the formation of rounded fragments, resulting from the interaction of fluids with a fractured rock. The deformation imposed on these rocks generates pseudotachylite (Sibson, 1977), formed as a result of high internal friction and fracturing in fault gaps (Figure 2.8D), small films with amorphous material along these existing fractures in the rock, especially in contact between the main shear plane and the breccia zone (Figure 2.8D).

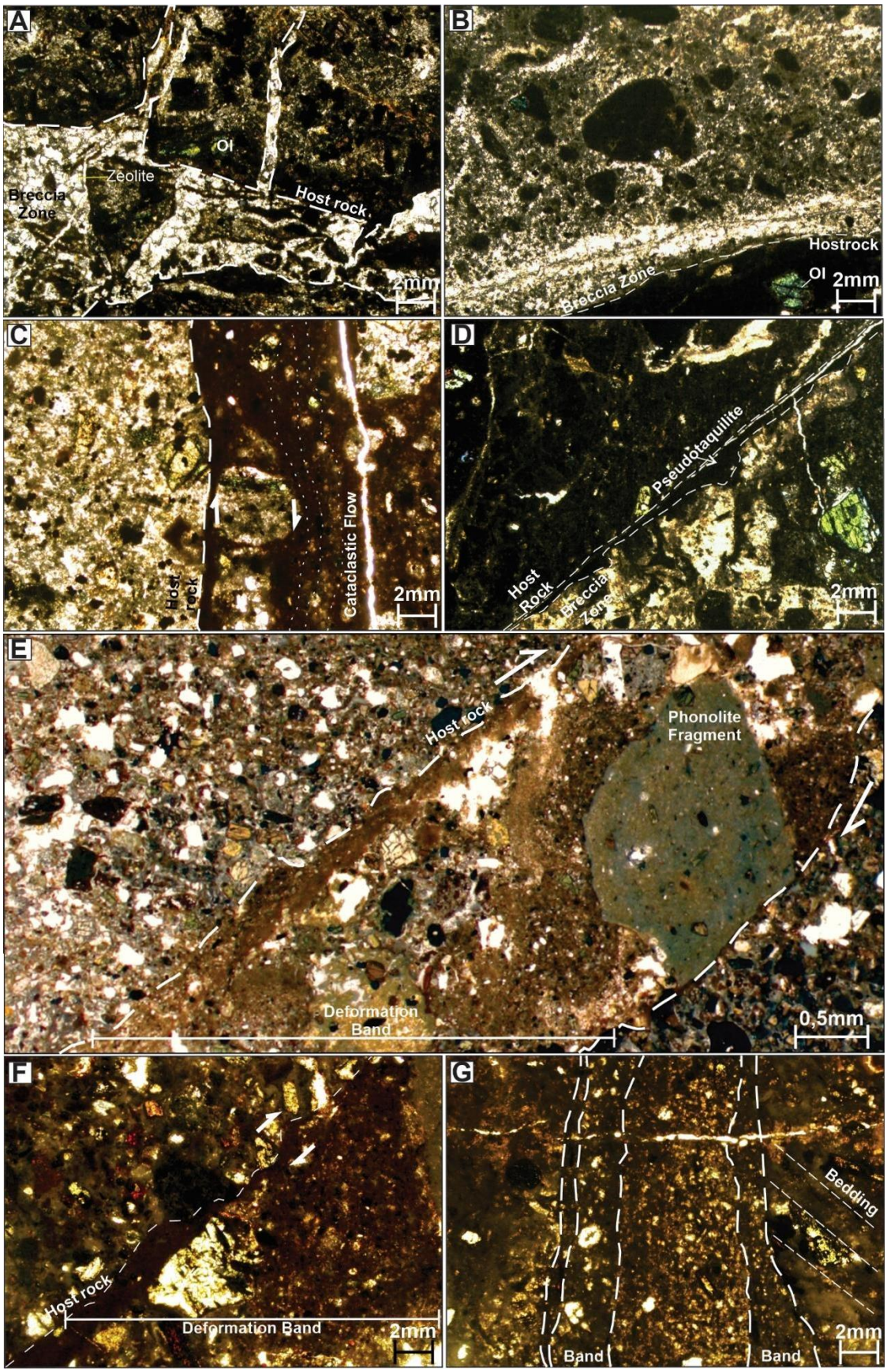

Figure 2.8 - Photomicrography of deformed rocks observed in Trindade Island. (A) Polarized photomicrography of fault breccia with angular lithic fragments and cemented by clay minerals and carbonates; (B) Development of fault zones and generation of pseudotachylite along the fault plane; (C) Formation of incipient foliation in the new matrix generated in the brecciated zone, and

the rotation of fragments generated by the fragmentation of the host rock can be verified; (D) Cataclastic feature observed in the brecciated zone, the fragments appear to react with the fluid, causing the fragments to become rounded; (E) General aspect of the interaction of the deformation band and the host rocks, with the presence of angular and recessed fragments (F) Deformation band observed by the abrupt decrease of rock porosity and by angular and rectilinear fragments along the fault rock; (G) Shear bands developed perpendicular to the rock bedding, where the thin matrix involving pyroclastic rock fragments and crystalloclasts.

The deformation band presence is relevant because they are the reflection of the tectonics exerted on volcanoclastic and pyroclastic rocks of TI. The first structural observation is the difference between the deformation bands and the host rocks with the abrupt change in cementation and the rupture of rock fragments (Figure 2.8E) and crystalloclasts (Figure 2.8F), which suggests the brittle regime imposition.

Local porosity modification in pyroclastic rocks is associated with deformation bands (Figures 2.7E,F), the same pattern seems to reflect microscopically (Figures 2.8F,G) the empty spaces are compacted and filled by oxides. The fragmented crystalloclasts (Figures 2.8E,F) indicate kinematics similar to that observed in outcropping (Figure 2.7A). The presence of oxides is clear (Figures 2.8E,G), showing the interaction with fluids as the fault occurs. The bands can configure different fracture frames interspersed with undeformed rock (Figure 2.8G).

4.4. Dynamic and kinematic analysis

Data acquired in the field included the fault plane orientation and linear structures (Figure 2.9) such as slickenlines, as well as kinematic indicators such as steps (Doblas, 1998), for example. Data collection on TI totaled 75 fault planes, with their kinematic indicators (Table 2.1).

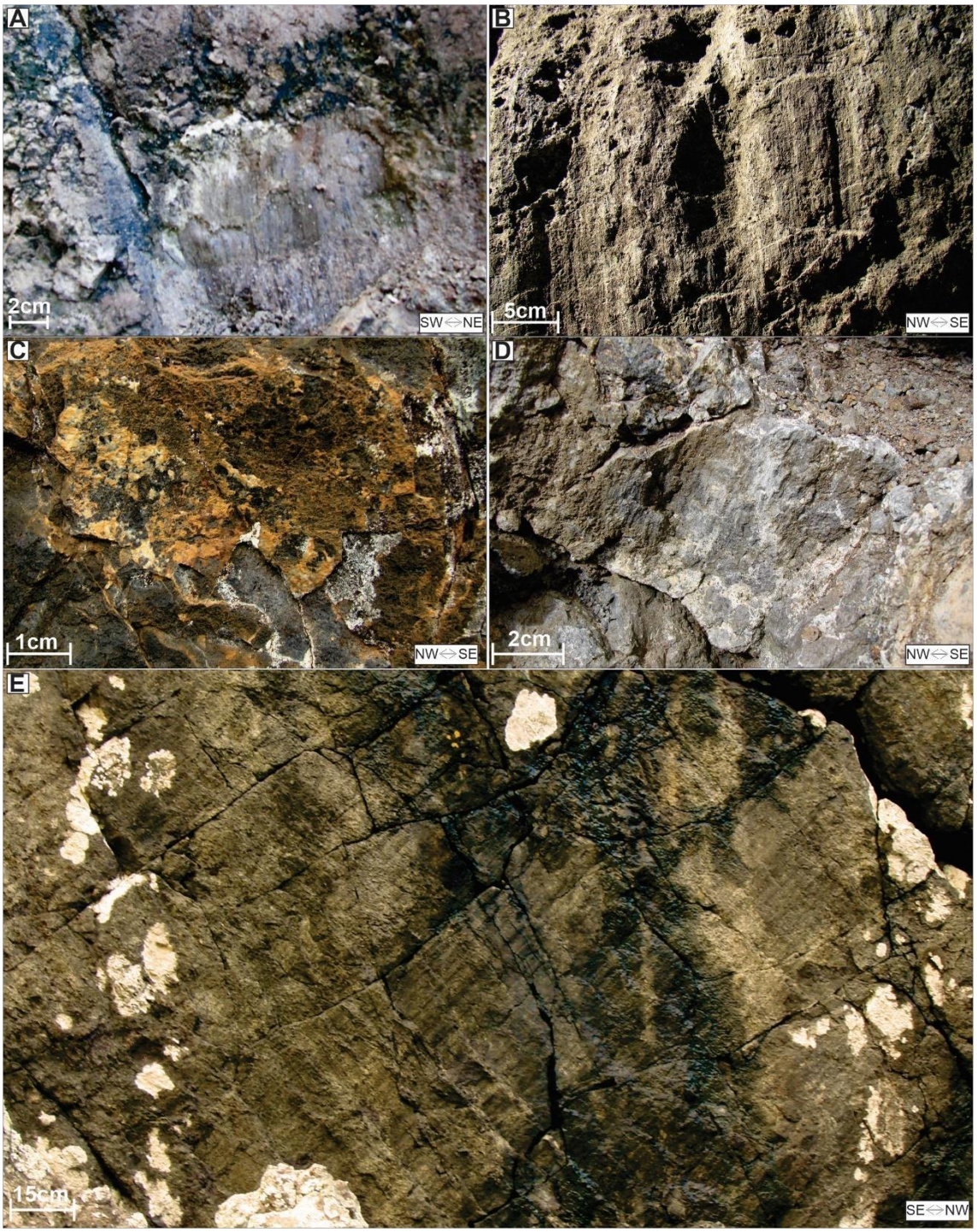

Figure 2.9 - Fault planes observed in Trindade Island. (A) and (B) Normal fault planes with vertical striations observed in the Pico Pontudo region and the Crista do Galo; (C) Fault plane with normal oblique kinematics in Praia dos Cabritos; (D) Right-lateral fault plane observed in the Northwest region; (E) Normal oblique fault plane in phonolytic dike in the northwest region.

The main fault planes observed in the field are polished surfaces with sub-vertical striations (Figures 2.9A,B), where they sometimes have clay minerals (Figure 2.9A) and oxides. The fault planes with subvertical striations refer to

extensional tectonics, with normal faults formation mainly turned to NW-SE direction (Figure 2.3A – Pontudo Peak and Galos Crest regions), forming geometries of horst and grabens observed in the field (Figure 2.4). The first set of fault planes cataloged in the field, presents in general NW-SE direction, secondarily strike-slip fault planes with left-lateral kinematics and NE-SW direction. The shortening direction (σ1) is vertical (Figure 2.10A), marking the relevant extensional event on TI, thus establishing the structural arrangement outlined mainly by extensional NW direction structures associated with NE-SW left-lateral kinematics. This geometry enables horst and grabens creation along the entire island in an NW-SE direction (Figure 2.3A – Pico Pontudo and Cabritos Beach regions).

The second data set of fault planes enabled the paleostresses modification identification. We have observed predominantly strike-slip faults with subhorizontal slickenlines (Figure 2.9C) to a normal oblique component (Figure 2.9D), pointing to the greatest influence of directional tectonics on these fault planes. The strike-slip NE direction faults presence (Figure 2.3A – Navy Habitation and Cabritos Beach regions), which control the main island slopes (Figure 2.3A - Navy Habitation Region), shows a different geometry if compared to that observed by extensional faults, configuring elongated features in which the local fault zones displacement occurs, causing the movement of fault blocks (Figure 2.3B), characterized as transtensional faults.

Thus, about 24 fault planes were observed in the transtensional fault context with mainly NE-SW direction (Figure 2.10B), and secondarily Riedel R fractures orthogonal to the main shear (Figure 2.10B), in general with variable kinematics between right-lateral and left-lateral. The observed tensions for the

formation of this event mark shortening direction (σ1) oriented to NNW-SSE, and the extension (σ3) is mostly oriented to WNW-ESE, compatible with the opening of transtensional faults in a predominantly left-lateral kinematic context.

The vertical alkaline dikes (Figure 2.6A) play a significant role in the regional structuring of TI. They can fit into brittle fault zones (Figures 2.4A and 2.6), with the clear presence of kinematic indicators as striations and steps (Figure 2.9E). They also vary from strike-slip to normal oblique kinematics (Figure 2.9E). The fault planes recorded in this context, mainly associated with the right-lateral kinematics for the intrusion of these bodies (Figure 2.10C). The shortening (σ1) exerted on the alkaline intrusions are WNW-SSE, with vertical σ2, and extensional vector (σ3) directed to NNE-SSW, allowing the evolution of strike-slip tectonics, with main paleostresses parallel to the dike's preferential direction WNW-ESE.

Table 2.1 - Fault plans collected in Trindade Island and its associated mean vectors.

Fault Nature	**Fault Data**	**σ1 mean**	**σ2 mean**	**σ3 mean**
Extensional	32	N037/71	N174/14	N267/12
Transtensional	24	N015/12	N155/75	N283/09
Dikes associated to faults	18	N295/09	N160/77	N027/09

Dike intrusion comprises various body emplacement processes according to their geometric characteristics, namely intrusion dynamics, hydraulic influence, and tectonic context (Delaney and Pollard, 1981; Rivalta et al., 2015). In Trindade, the dike morphology, the presence of hydraulic features, as well as the tectonic context exerted should directly influence the arrangement of these bodies on the island and the temporality of their formation.

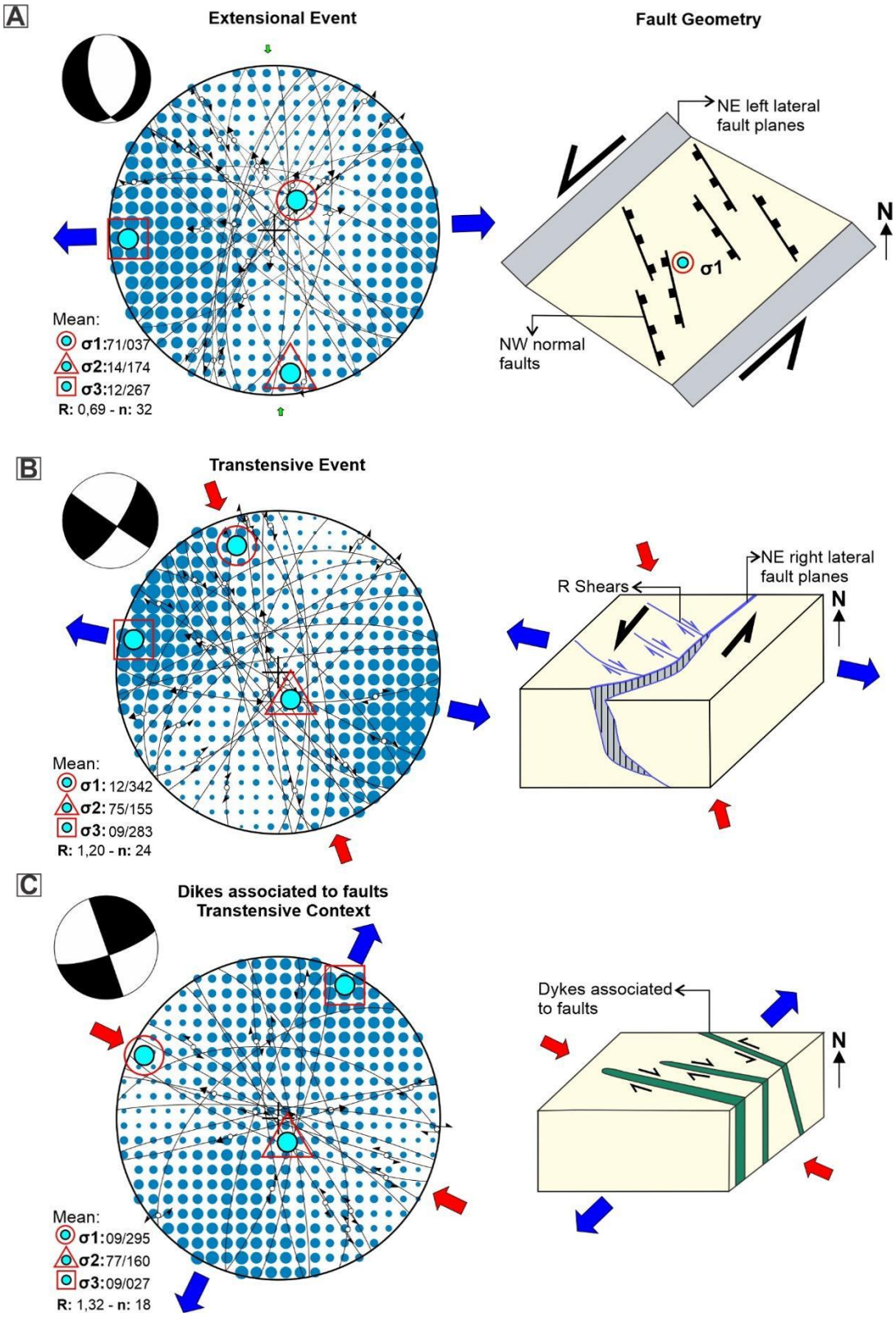

5.

Figure 2.10 - Lower-hemisphere equal-area projections generated from the fault planes collected in Trindade Island, generated on Win-tensor software 5.8.8 (Delvaux, 2012). (A) Fault planes associated with extensional features,

being directly linked to left-lateral kinematic, the shortening direction (σ1) is vertical in this case; (B) Transtensional features observed in the field associated with predominantly left-lateral tectonics and in some cases forming scissor geometry along the fault; (C) Dike-associated fault planes, where right-lateral kinematics with shortening (σ1) direction WNW-ESE predominates.

5. Discussions

5.1. Structural evolution of Trindade Island

The deformational aspects described in this research led to the proposal of an evolutionary history for TI since the lower Pleistocene (Figure 2.11). The presence of normal faults is evident throughout the island, but their highest occurrence is observed in the rocks of Trindade Complex. These structures are closely associated with phonolytic intrusions (Figure 2.11A), similar to the evolution model proposed by De Rita et al. (1983).

The structural pattern and fault geometry indicates that the main tectonic stress σ1 is vertical (Figure 2.10A), thus composing the grabens and horst fault system, as observed in the regional framework of seismic lines (Figure 2.2C). The structures may also be associated with the post-volcanic moment (Anderson, 1936; De Rita et al., 1983; Forslund and Gudmundsson, 1992; Långbacka and Gudmundsson, 1995). These fault systems are also associated with tectonic stress, which generates a normal faults in the Trindade Complex rocks. The tectonic blocks movement generated breccia zones (Figures 2.5 and 2.11) associated with the inflow of hydrothermal fluids, which in turn favored the precipitation of clay minerals and oxides, subsequently to the rock cataclasis

(Delaney and Pollard, 1981; Forslund and Gudmundsson, 1992; Lorilleux et al., 2002).

Progression of transtensional tectonics (Figure 2.11B) is noticed by the presence of kinematic indicators on vertical phonolytic dikes sectioning the island (Figure 2.9E), as well as by the presence of strike-slip faults with an oblique component (Figures 2.3A and 2.10A). These faults also influence the local stratigraphy, especially the Morro Vermelho Fm. (middle Pleistocene - Pires and Bongiolo, 2016).

They are usually longer length faults compared to the previously generated normal NW-oblique component faults (Figure 2.3A – Pontudo Peak), suggesting paleostresses oriented to NNW-SSE (Figures 2.10B and 2.10C). The breccias formed in this phase are generated by hydraulic fracturing and the fluids passage, culminating in the rich carbonate cementation (Jébrak, 1997; Lorilleux et al., 2002).

The final event observed in TI is marked in the volcanoclastic rocks of Paredão Fm. (Figures 2.3A and 2.3C) (middle Pleistocene - Pires and Bongiolo, 2016), associated with normal faults and conjugated pairs (Figure 2.11C), which locally displace the volcanic bedding. These structures are mainly oriented to NW-SE, similar to the structural pattern observed in grabens and horst systems, thus forming structures that may have facilitated the passage of fluids and formed deformation bands in normal fault planes.

The deformation bands (Figures 2.8E,F and 2.8G) are mainly associated with mineral breakage and fluid passage, with the imposition of stresses (Fossen et al., 2007). Even though these structures are commonly described as present in porous sedimentary rocks, such as sandstones (Aydin, 1978; Aydin and

Johnson, 1978; Fossen et al., 2007; Soliva et al., 2016), some authors have reported their existence in porous volcanoclastic rocks, such as ignimbrites and tuffs (Wilson et al., 2003; Cavailhes and Rotevatn, 2018).

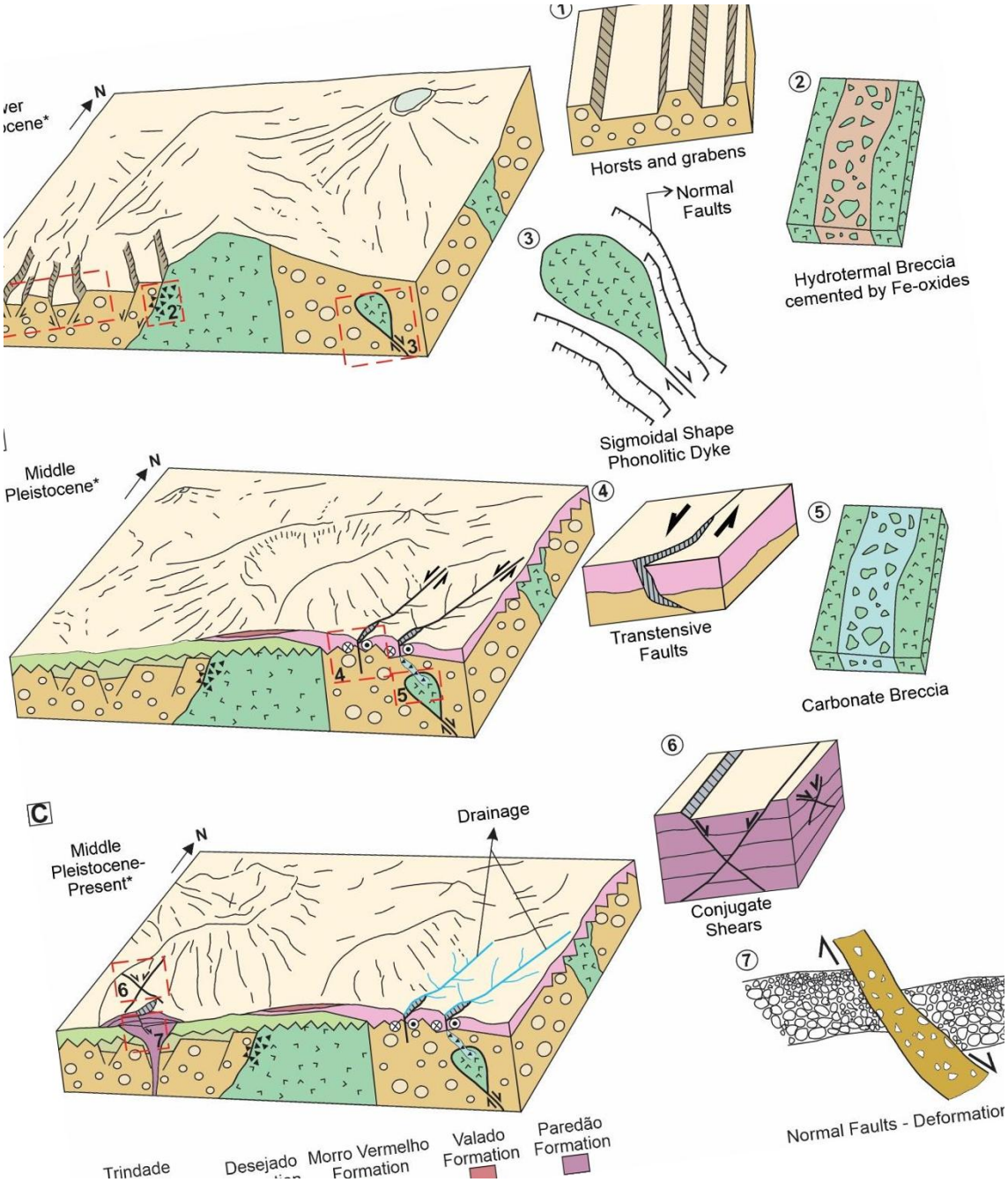

Figure 2.11 - A proposed evolutionary model for the structural evolution of Trindade Island, based on the stratigraphy proposed by Pires and Bongiolo (2016). (A) The first structural event observed on the island, mainly affecting the rocks of the Trindade Complex. Grabens and horst formation, breccias associated with oxides and sigmoidal dikes formed in the extensional context; (B) Transtensional faults associated to a formation of carbonate breccias; (C) Last extensional event observed in the basin, with the formation of conjugated pairs and lapilli tuft deformation bands in Paredão Formation.

Volcanic fluid can cause the chemical and mineralogical change around the deformation bands (Antonellini and Aydin, 1995; Wilson et al., 2003), as well as local reduction of visual porosity along the bands. The deformation bands formed in this context differ from those formed in sandstones (Aydin and Johnson, 1978; Fossen et al., 2007), due to the rheological difference of minerals therein, as they may or may not break in preferential planes, such as those of mineral cleavage and fractures (Cavailhes and Rotevatn, 2018). The same occurs for nepheline and olivine, which have distinct rheological behavior from quartz. The bands' formation should mark the final phase of volcanic fluid passage or even the hydraulic influence on the rocks (Dinwiddie et al., 2006, 2012; Wilson et al., 2003), as well as more significant tectonic impositions to date.

5.2. The tectonics control in alkaline intrusions

Understanding the dikes and stocks installation of TI is hugely relevant for structural and geomorphological studies, as they represent a considerable part of the mapped structures (Fig. 3A - green line with two arrows). They play a fundamental role in the formation of faults under the regime to the shearing imposed by deformational regimes. Although Ferrari and Riccomini (1999) detailed the stresses involved in the TI dikes placement, with shortening tension ($\sigma 1$) parallel to the main direction NW-SE, the authors did not take their morphology and the relationship with the shear features in TI.

Dike intrusion comprises various body emplacement processes according to their geometric characteristics, namely intrusion dynamics, hydraulic influence, and tectonic context (Delaney and Pollard, 1981; Rivalta et al., 2015). In Trindade, the dike morphology, the presence of hydraulic features, as well as the

tectonic context exerted should directly influence the arrangement of these bodies on the island and the temporality of their formation.

Initially, these intrusions were influenced by the extensional regime, in which normal faults were formed (Figure 2.10A), generating displacements capable of accommodating intrusions and facilitating the entry of bodies (Figure 2.12A). The imposition of this regime eventually generated sigmoidal dikes (Figures 6B and 6C), sin deformational to normal fault zones (Figure 2.12B), with stresses σ1 vertical and σ3 towards the most significant dike extension (Hoek, 1991; Forslund and Gudmundsson, 1992; Re et al., 2015; Dering et al., 2019). Accompanied by the dikes, there is great hydraulic fluid pressure, which generates internal fractures, features of internal cataclasis (Figure 2.6D), and hydraulic breccias in their edges (Figure 2.6E) (Correa-Gomes et al., 1991; Petronis, 2013; Misra and Mukherjee, 2016; Dering et al., 2019).

The dykes and stocks generated in this phase are possibly associated with extensional structures, such as the horst and graben system in Trindade Complex. Such configuration seems familiar in volcanic complexes (White et al., 2011; Márquez et al., 2017). Subvertical stresses can facilitate intrusion accommodation and the gravitational force acting on the dike-forming fluid flow (Delaney and Pollard, 1981; Pollard and Townsend, 2018), facilitating the filling of faults and shear fractures.

The evolution of right-lateral transtensional tectonics observed on the TI (Figure 2.10C), propitiates the subvertical dikes formation (Figures 2.4A and 2.6A) associated with strike-slip faults (Figure 2.12C). The presence of striated features on these dikes (Figures 2.9D and 2.9E) indicates the influence of right-lateral in a transtensional tectonics context. These dikes intruded perpendicularly

to the previously generated structures, possibly taking advantage of the shear fractures (Mathieu et al., 2008; Dering et al., 2019), or even creating new vertical structures that are directly influenced by the shearing (Misra and Mukherjee, 2016; Woods et al., 2019).

The shortening direction is horizontal, which means stress sub-parallel to the dike longest axis (Figure 2.12C), a fact already described by Ferrari and Riccomini (1998). On map (Figure 2.3A - green line with two arrows), these dikes may appear to present the en echelon pattern (Delaney and Pollard, 1981; Hoek, 1991), which may be influenced by the same intensity directional stresses along their formation process. The presence of radial dikes and radial lineaments (Leonardo M. Barão et al., 2018) (Figure 2.3A and Supplementary Figure 2.2) on the TI may correspond to the first phase of the evolution of volcanic caldera (Gudmundsson, 2011; Ribeiro et al., 2019).

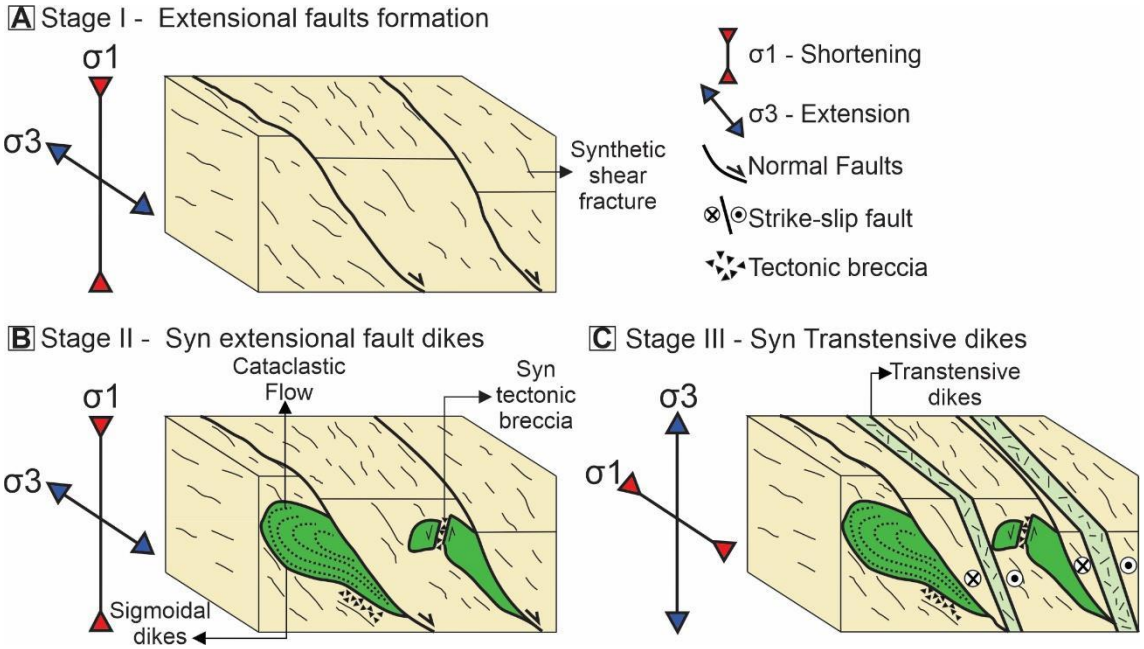

Figure 2.12 - Evolutionary stages of the dikes and their relationship with the tectonic structures present on the island. (A) Formation of normal faults and the relationship between shortening and extension; (B) Intrusion of sigmoidal dikes parallel to the normal fault zones, which internally generate cataclasis features and fault breccias by shearing these dikes and continuing the action

of vertical stresses; (C) Generation of subvertical dikes related to the transtensional context that surrounds Trindade Island, with shortening directions of the largest along its length.

5.3. South Atlantic tectonics influence on volcanic sequences

South Atlantic Ocean tectonic events are closely associated with the Atlantic Ocean opening (Torsvik et al., 2009; Moulin et al., 2010; Blaich et al., 2011) and the oceanic fracture zones evolution (Almeida, 2006; Davison, 1999; Francheteau and Pichon, 1972; Mohriak and Rosendahl, 2003; Vasconcelos et al., 2019; Wilson, 1965), forming a specific complex structural arrangement in conjunction with the igneous provinces (Figure 2.13A).

The oceanic fracture zones conditioned volcanism and contributed to the Vitória-Trindade Chain generation (Alves et al., 2006; Mohriak, 2020), which also caused local deformation of sedimentary successions (Mohriak and Rosendahl, 2003) and volcanic rocks adjacent to these structures. Similar aspects also observed in the equatorial region, associated with Romanche Fracture Zone, where the neotectonics controls the seamounts evolution and deformation settings (Tavares et al., 2020).

This configuration is associated with Pleistocene extensional tectonics with the formation of normal faults in the regional context (Figure 2.2C), as well as in the local context of TI (Figures 2.3A and 2.4). The presence of these structures leads to vertical shortening stresses (Figure 2.12B) capable of generating the grabens and horst geometry features during the possible active volcanism, which contributes to a more significant accumulation of fluids capable of generating the fault breccias (Figure 2.5).

In southeastern Brazil, similar rift features are recognized. They are related to local extensions and associated with the southeastern rift basins (Riccomini,

1989; Salvador and Riccomini, 1995; Riccomini et al., 2004), mainly during the Pleistocene with the formation of structures oriented to WNW-ESE. The faults also tilting the sediments present in the southeastern basins and are related to left-lateral tectonics, which is similar to the VTFZ left-lateral kinematics (Figure 2.13B). Tectonics also observed by other authors (Szatmari and Mohriak, 1995; Mohriak, 2003), these authors observe extensional and compressional features, associated with left-lateral rotation between VTFZ and Rio Grande Ridge (Figure 2.13A).

Analogous tectonics is also found on the African continent with widespread extension in sedimentary basins (Haddon and McCarthy, 2005), with main vertical shortening (σ1) associated with extensions oriented to WNW-ESE at the lower Pleistocene (Viola et al., 2012) (Figure 2.10A).

The main shortening direction evolution oriented to NW-SE (Figure 2.10C), marks the formation of strike-slip structures predominance. It is associated with the subvertical dikes observed in Trindade (Ferrari and Riccomini, 1999; Ribeiro et al., 2019) (Figure 2.6A) and by faults sectioning the seismic sections deforming sedimentary sequences already deposited in the seamounts vicinity (Figure 2.2E). This fact indicates that tectonic stresses are stabilized (Figure 2.13C), with similar tensions to those observed in the South American Plate (Assumpcao, 1992; Riccomini and Assumpção, 1999; Heidbach et al., 2016). The transtensional event also seems to affect the seamounts and the ocean floor (Figure 2.2B), and it is a possible reflection of the ocean fracture zones acting during the South Atlantic Ocean opening (Alves et al., 2006; Mohriak and Rosendahl, 2003; Tavares et al., 2020; Vasconcelos et al., 2019).

The NW-SE stresses installation suggests the predominance of right-lateral kinematics on VTFZ, similar to that observed in the South American continental portion (Riccomini and Assumpção, 1999; Pinheiro and Queiroz Neto, 2014; Pinheiro et al., 2019). The evolution from left lateral to the right lateral kinematics may probably correspond to the installation of stresses on the South American plate with stresses facing NW-SE as occurs in the continental portion of the plate (Assumpcao, 1992; Riccomini and Assumpção, 1999; Heidbach et al., 2016). In this way, it may be possible to indicate the action of these structures in the South American continent (Figure 2.13C), enabling neotectonics stresses in the southeastern region of Brazil.

6. Conclusions

The evolutionary history of TI corresponds to successive volcanic events and distinct deformational stages with progressive stress field modifications acting in the South Atlantic Ocean. Therefore, it is possible to conclude that:

(1) It is initially associated with extensional tectonics, with the formation of normal faults oriented to NW. The stresses are similar to those described in recent southeastern Brazilian (Riccomini, 1989; Riccomini et al., 2004) and African sedimentary basins (Viola et al., 2012) during Pleistocene;

(2) The normal faults allow the emplacement of sigmoidal phonolytic dikes, which took advantage of these zones of brittleness generated in the extensional context, developing in parallel to the axis of lowest tension exerted during its formation;

(3) The stresses development oriented to NW-SE with a transtensional tectonics predominance, imposed by VTFZ, corresponds to the generation

of faults observed in the seismic sections along the Vitória-Trindade Chain. Also, these faults are related to the intrusion of vertical dikes, the formation of carbonate breccias in Trindade fault zones;

(4) The strike-slip tectonic stage, currently active, is related to the Brazilian coast and oceanic islands evolution, with the structural fabric mainly associated with the movement of the oceanic fracture zones in the South Atlantic Ocean;

(5) The formation of deformation bands in the Paredão Formation, the most recent volcanic TI unit, marks the influence of tectonics in the control of hydrothermal fluids and faults associated with these deformation bands.

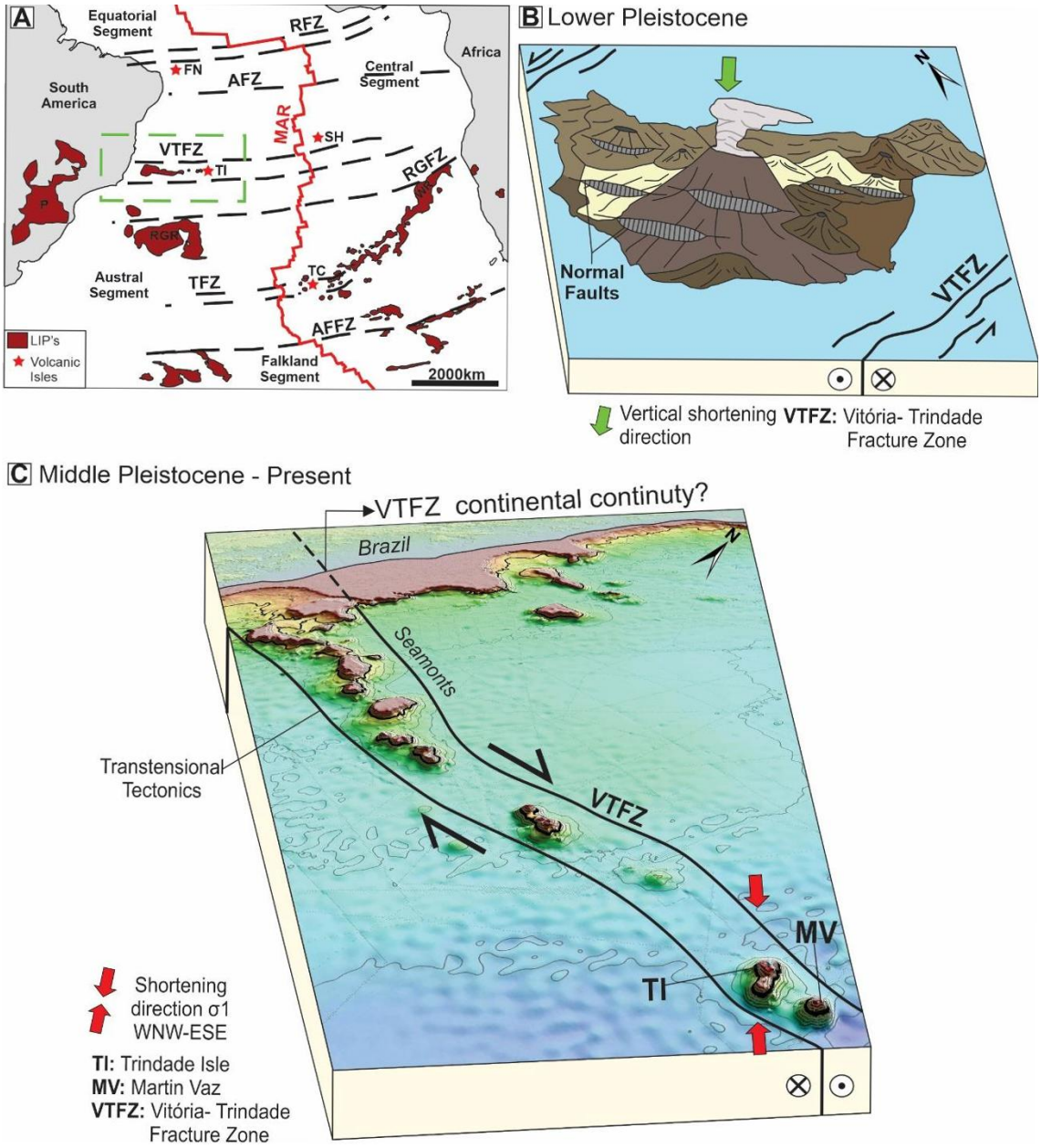

Figure 2.13 - Regional tectonic features influenced by the transforming zones in the South Atlantic. (A) Regional configuration of the transforming zones and their structural control over volcanic islands (After Alves et al., 2006; Davison, 1999; Torsvik et al., 2009; Vasconcelos et al., 2019); (B) Vertical tectonic stresses (σ1) exerted during the Pleistocene, with the generation of normal faults concomitant with Trindade Isle volcanism; (C) Tectonic stresses exerted during the middle Pleistocene to the Present, with NW-SE main direction affecting the Trindade and Martin Vaz islands. FN: Fernando de Noronha, SH: Santa Helena, TI: Trindade Island, MV: Martin Vaz, TC: Tristan da Cunha, RFZ: Romanche Fracture Zone; AFZ: Ascencion Fracture Zone, VTFZ: Vitória-Trindade Fracture Zone, TFZ: Tristan da Cunha Fracture Zone, AFFZ: Agulhas Falkland Fracture Zone, P: Paraná, RGR: Rio Grande Rise, WR: Walvis Ridge.

6. Acknowledgments

We would like to thank CNPq for the financial support through projects 557299/05-5, 557141/2009-5 and 442865/2015-5. To CAPES for the scholarship

(88882382075/2019-01), the Brazilian Navy for support and transportation during the fieldwork and the Directorate of Hydrography and Navigation for the assignment of seismic data from the LEPLAC project. To LABAP, LECOST and LAMIR Laboratories for all the infrastructure provided. We would also like to thank Professor Leonardo Lagoeiro for his collaboration in this work. To the Academic Publishing Advisory Center (Centro de Assessoria de Publicação Acadêmica, CAPA – www.capa.ufpr.br) of the Federal University of Paraná for assistance with English language translation. RJA is a research fellow of the CNPq (PQ 302913/2018-1) and Fundação Araucária senior fellowship (45725). BT is a CNPq researcher (PQ 306780/2019-4). The authors also thank the Editor-in-Chief Andres Folguera and the two anonymous reviewers for the suggestions, which improved the previous version of this paper.

3.3. Artigo 3

The structural aspects of cataclastic bands associated with a recent volcanogenic deposit, Paredão Volcano - Trindade Island

Leonardo Mairink Barão, Barbara Trzaskos, Leonardo Evangelista Lagoeiro, Jukka Laukkanen, Dandara Ataide Salvador, Natália Gauer Pasqualon, Herick Faust Daufenbach, Maria Cristina de Souza, Rodolfo José Angulo

1. Introduction

Deformation bands (DB) affect porosity of rocks in many geological and tectonic contexts (Fossen et al., 2007, 2018b; Rodrigues et al., 2015), marked by a change in petrophysical characteristics of porous rocks (Balsamo et al., 2010; Alikarami et al., 2013; Ballas et al., 2015). They are directly interfere with fluids percolation, increasing or decreasing the fluid's transport capacity (Antonellini and Aydin, 1995; Parry et al., 2004; Okubo et al., 2009). The fluid flow in DB's is very well studied by the oil industry, due to its relevant role for the oil industry, as a sealant and fluid flow mechanisms (Torabi et al., 2013).

Most of these structures are nucleated in porous sandstones (Aydin, 1978; Aydin and Johnson, 1978; Antonellini and Pollard, 1995; Zuluaga et al., 2014; Rodrigues et al., 2015; Soliva et al., 2016; Fossen et al., 2018b) and carbonate grainstones (Tondi et al., 2006; Cilona et al., 2012; Dimmen et al., 2017; Del Sole and Antonellini, 2019), however, the DB's are not common in volcaniclastic rocks (Kjenes, 2018). These structures are firstly described in volcaniclastic rocks by Wilson et al., 2003, demonstrating the influence of hydraulic dynamics on those

bands, followed by others authors in a similar setting (Evans and Bradbury, 2004; Dinwiddie et al., 2006; McGinnis et al., 2009)

Recently, Cavailhes and Aydin (2018) also describe the DB's associated with compressional tectonics in volcaniclastic rocks. However, the DB's identified in stratified tuffs of Trindade Isle (TI), represent structures formed in the upper crust during Pleistocene volcanic activity (Pasqualon et al., 2019). The bands observed in TI represents the tectonic influence of the transform zone surrounding the archipelago, the Vitória-Trindade Fracture Zone (VTFZ), in a transtensive context (Barão et al., 2020b). This paper aims to define the main characteristics, the petrophysical properties of the DB's such as porosity and permeability and its relationship to the volcanism and tectonism of the islands in the context of the Vitoria-Trindade Fracture Zone, in addition we evaluated the presence of fluids and the mechanism of formation of those bands associated with the tectonic context of the volcanism and tectonics significance.

2 Geological Context

The Trindade Island and Martin Vaz Archipelago are the only emerged volcanic place of Vitória-Trindade Fracture Zone (VTFZ) (Figure 1A), which trends in the E-W direction and represents the latest alkaline volcanism in the Brazilian Territory (ca. 3.7 to <0.17 Ma) (Cordani, 1970). This magmatism is associated with post Gondwana break-up and South Atlantic opening (Hawkesworth et al., 1999; Almeida, 2006; Gibson et al., 2006) and is related to a mantellic plume activity (Hartnady and le Roex, 1985; Siebel et al., 2000).

The tectonic context of the Trindade Island is related to the presence of VTFZ, which controls the alignment of the Vitória Trindade Ridge (Figure 3.1A). The TI has the major axis turned into NW-SE, by fractures, faults and dike

emplacement of NW-oriented (Almeida, 1961) (Figure 3.1B). The direction of maximum compression (σ1) was determined as being parallel to these structures during its formation (Ferrari and Riccomini, 1999; Barão et al., 2018). Although the first tectonic event is associated to an extensional event is registered mainly in the in basal unities of the island.(Barão et al., 2020b).

The volcanic history in the the TI, started at the Middle Pliocene, lasting until the Pleistocene (Cordani, 1970; Pires and Bongiolo, 2016; Pires et al., 2016). The island was formed by lava flows, phonolitic intrusions and pyroclastic deposits with a strongly sodic alkaline, SiO_2 undersaturated magma. The first mapping was executed by Almeida (1961), who identified five distinct geological units: Trindade Complex, Desejado Sequence, and the Morro Vermelho, Valado and Paredão Volcano formations (Figure 3.1B).

The first volcanic event started around 3.85 Ma (Ar/Ar - Pires et al., 2016) and was associated with the formation of pyroclastics deposits and phonolites intrusions of Trindade Complex, configuring the basal unit of the Trindade Island (Marques et al., 1999; Pires and Bongiolo, 2016). The sequence of volcanic events involves a variety of volcanic styles between Strombolian to Vulcanian, marking a highly explosive active in some cases (Pires and Bongiolo, 2016).

The last volcanic event in the TI took place in a restricted area in southeast edge of the TI (Figure 3.1B), leading to a deposition of a succession of pyroclastic sediments, with a minor contribution of effusive eruption (Pires and Bongiolo, 2016). The morphology resulting from this volcanic activity are well preserved and consists of volcanic cone agglomerates (Almeida, 1961; Pasqualon et al., 2019) it is denominated Paredão Volcano (Figure 3.1B). This score cone exposes

the intercalation of lapilli-tuffs, tuff-breccias, pyroclastic breccias and agglomerates (Pires and Bongiolo, 2016).

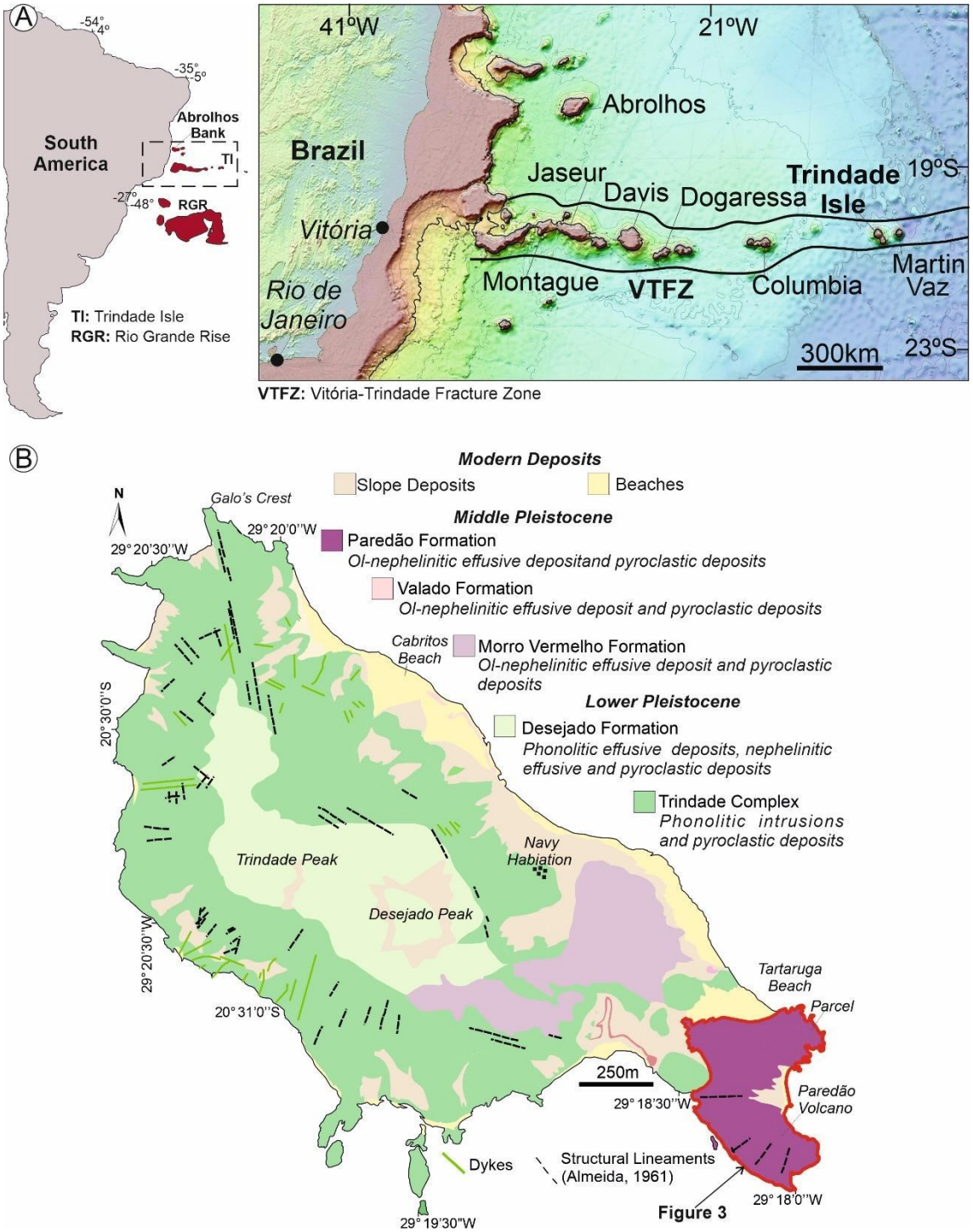

Figure 3.1 – (A) Location of Trindade Island in the South America comprising one of the only outcrops of the E-W direction Vitória-Trindade Chain (Alves et al., 2006); (B) The Island is composed of five distinct geological units with ages varying between Lower Pleistocene to Middle Pleistocene (3.7 to <0.17Ma) (Almeida, 1961; Bongiolo et al., 2016; Cordani, 1970; Pires and Bongiolo, 2016). The Paredão Volcano is highlighted in the map, the most recently volcanic activity in TI(<0.17Ma).

3 Host Rock characterization

Pasqualon et al. (2019) defined five facies associations in the Paredão Volcano Formation: proximal pyroclastic deposits, distal pyroclastic deposits, pahoehoe, rubbly pahoehoe and ‘A’a. This work focused on the proximal pyroclastic deposits and dealt mostly on the DB’s in pyroclastic rocks of TI. The association comprises the intercalation of planar layers of massive and reverse grading lapilli-breccias, lapillistones and lapilli-tuffs (Figure 3.2), composed of volcanic ash, lapillitic scoria and bombs of nephelinitic lava (Pasqualon et al., 2019). The presence of these deposits leaded to the interpretation of the volcanic edifice as a scoria cone formed by a dominant Strombolian volcanic style, with subordinate phreatomagmatic activity (Figures 3.2A,B,C) (Pires and Bongiolo, 2016; Pasqualon et al., 2019).

This volcanic sequence is affected by fault surfaces, causing the tilting of the volcanic layers (Figure 3.2C and D)), in which the DB’s reported in this article were developed. Generally, these surfaces have variable dips between 45º and 80º, associated with normal faults, reflex of transtensional stress over the TI (Barão et al. 2020).

4 Methods

4.1. Spatial Analysis and outcrop characterization

The DB’s and faults were firstly characterized using an aerial view, as these structures can be well-delineated using aero photogrammetry surveys (Bemis et al., 2014). The Unmanned Aerial Vehicle (UAV) survey was executed by Universidade Federal de Viçosa (UFV), acquiring a high-quality definition image

(Figure 3.3). The UAV image was treated, shaded and interpreted using the software ArcGis 10.6.1.

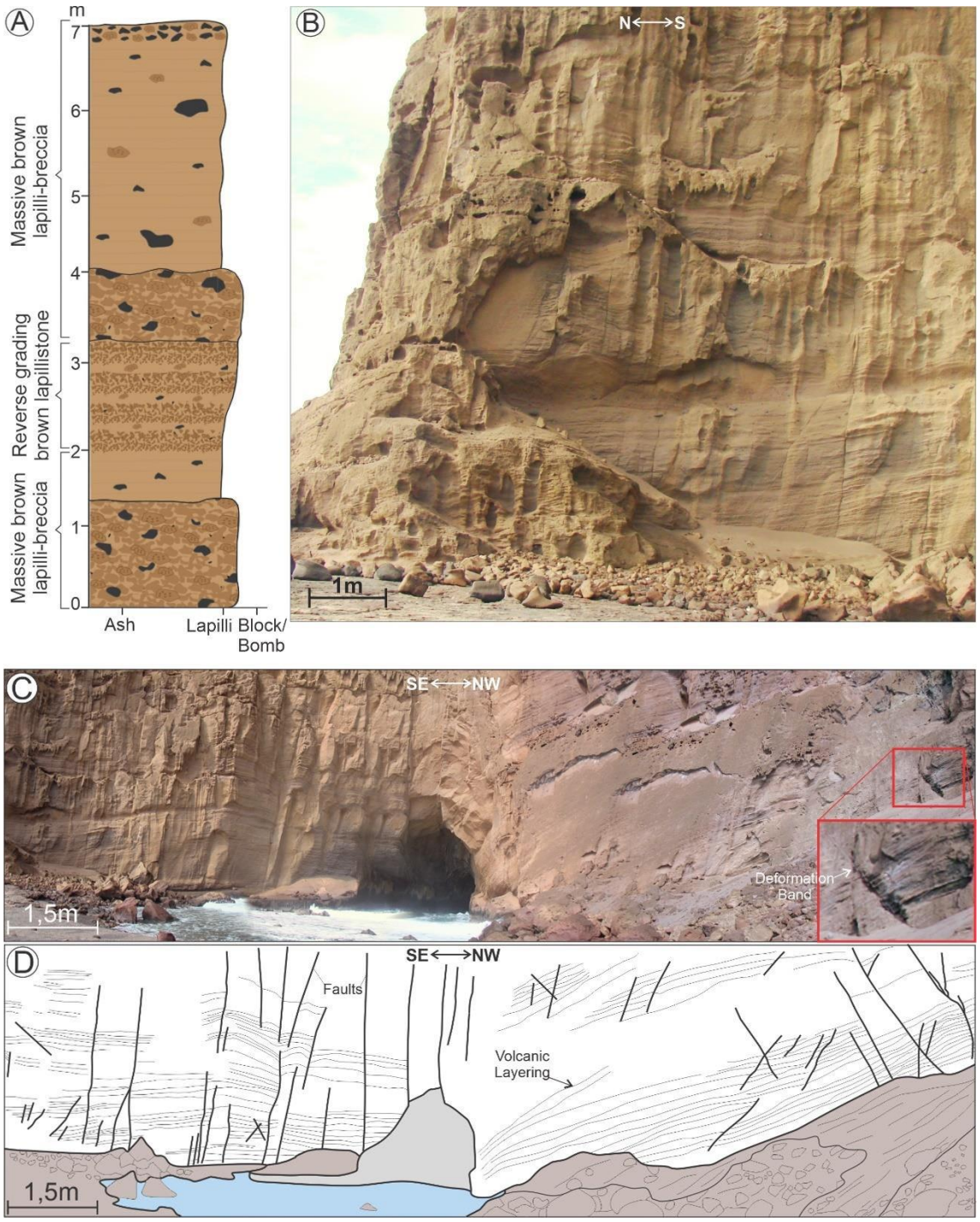

Figure 3.2 - The Paredão Volcano photos and schemes. (A) Stratigraphic column of the proximal facies of pyroclastic deposits (modified from Pasqualon et al., 2019); (B) Photo, in which the deformational bands are concentrated; (C, D) Volcanic layering and stratification of the Paredão Volcano, sectioned by fractures and faults, where the deformation bands can be seen.

The identification of linear structures in UAV images and its interpretation, allow to divide into primary structures as volcanic layering and secondary structures as joints and DB's. Azimuthal directions were extracted from these structures using the plugin Azimuthfinder (Queiroz et al., 2014) for ArcGis, and they were used to construct directional rosettes using the Dips software (Rocsience). The local arrangement of structures could be characterized in the Volcano Paredão, allowing us to asses the local arrangement of structures (Figure 3.3).

The structural analyses of the outcrop involved the observation, description and mapping of the DB's. All of them the structural data were collected (dip and direction), as well as oriented sample for laboratory studies involving optical and electron microscopy. Photomosaics were buit and over them all skecths and drawing were perfomed. Also we collected oriented samples to do the petrography and SEM and EDS analysis were executed in the samples.

4.2. Microscopic Analysis

The samples collected were analyzed under a petrographic microscope using thin sections to delineated the microstructures, the fluids reaction, cementation and compaction processes along and outside the DB's with the goal to identify the deformation mechanism operating during the band formation. The thin sections of the DB's were also scanned to give a bigger picture of the relationship between the DB's and the host rocks (HR.

4.2.1. ImageJ porosity analysis of light microscope pictures

We the aid of the Image J-software DB were differentiated from HR applying the method. Also to define the HR and DB porosity we used the analysis software

ImageJ (Ferreira and Rasband, 2012; Schneider et al., 2012) and the methodology applied by Dimmen (et al., 2017) and Kjenes (2018) for the 2D macroporosity of the DB's and HR. Areas of the same dimensions (300x1200 pixels) of HB and DB in thin sections were selected to define and compare porosity of equivalent areas. The selected areas are performed using two different macros to provide porosity estimations for the photomicrographs (Grove and Jerram, 2011; Kjenes, 2018).

The macro converts RGB images (Red, Green, Blue) to HSB (Hue, Saturation, Brightness). This transformation helps to discriminate the blue epoxy in the empty spaces from the rest of the matrix color spectrum by setting a threshold color to red (Kjenes, 2018). Further, the threshold image is converted into black and white, and set to a binary image for "particle" analysis, measuring pore space area (%) and the total area of pores (Kjenes, 2018). The data from the image analysis together with the fieldwork data helps supports to define the porosity of the DB and HR, by the relationship with the arrangement of the grains and pores in both analyzed areas.

4.2.2. SEM-EDS Analysis

The scanning electron microscope (SEM) FEI Quanta 650 FEG-SEM MLA instrument of the Geological Survey of Finland (GTK) was used to conduct investigations of the thin sections to increase the resolution of the porosity measurements. The Mineral Liberation Analysis (MLA) measurement method was XMOD_STD, used to store de backscatter image and separated the mineral phases. The XMOD_STD method is a point counting method of MLA in which the area of specimen is divided systematically into sampling points and the X-ray spectrum is measured at every point. The X-ray spectra are saved for off-line

classification (Supplementary Material 1 – ANEXO 3 - EDX Spectrum for matrix and Zeolite). The collected spectra are compared with a spectral library collected before or after the measurement. This method produces modal mineralogy information, i.e. the contents of the mineral components in the sample. (Supplementary Table 1 – ANEXO 3).

Additionally, Renishaw InVia Qontor Raman microscope was used to identify zeolite type (Supplementary Material 2). The backscattered electrons (BSE) images were also used to identify and map the new-formed phases inside pores in the DB's. The observations and descriptions of the DB's microstructure were accomplished with the aid of the BSE images.

5 Structures of the Paredao Volcano

5.1. Spatial distribution

The spatial distribution of structures in Paredão Volcano (Figure 3A) varies along with the circular structure of volcano and three main features can be separated (Figure 3.3B): volcanic layering (stratifications – Figures 2B, C), fractures and faults (Figure 3.2C) and DB's (Figure 3.3). The volcanic layer observed in the UAV image (Figure 3.3A), represents a subhorizontal surface (Figure 3.2B) with main direction N30-50W (mean azimuth value: 342.8º - Figure 3.3B). These structures represent a stratified layer with the intercalation between lapilli breccias to lapilli stone as described by Pasqualon et al. (2019).

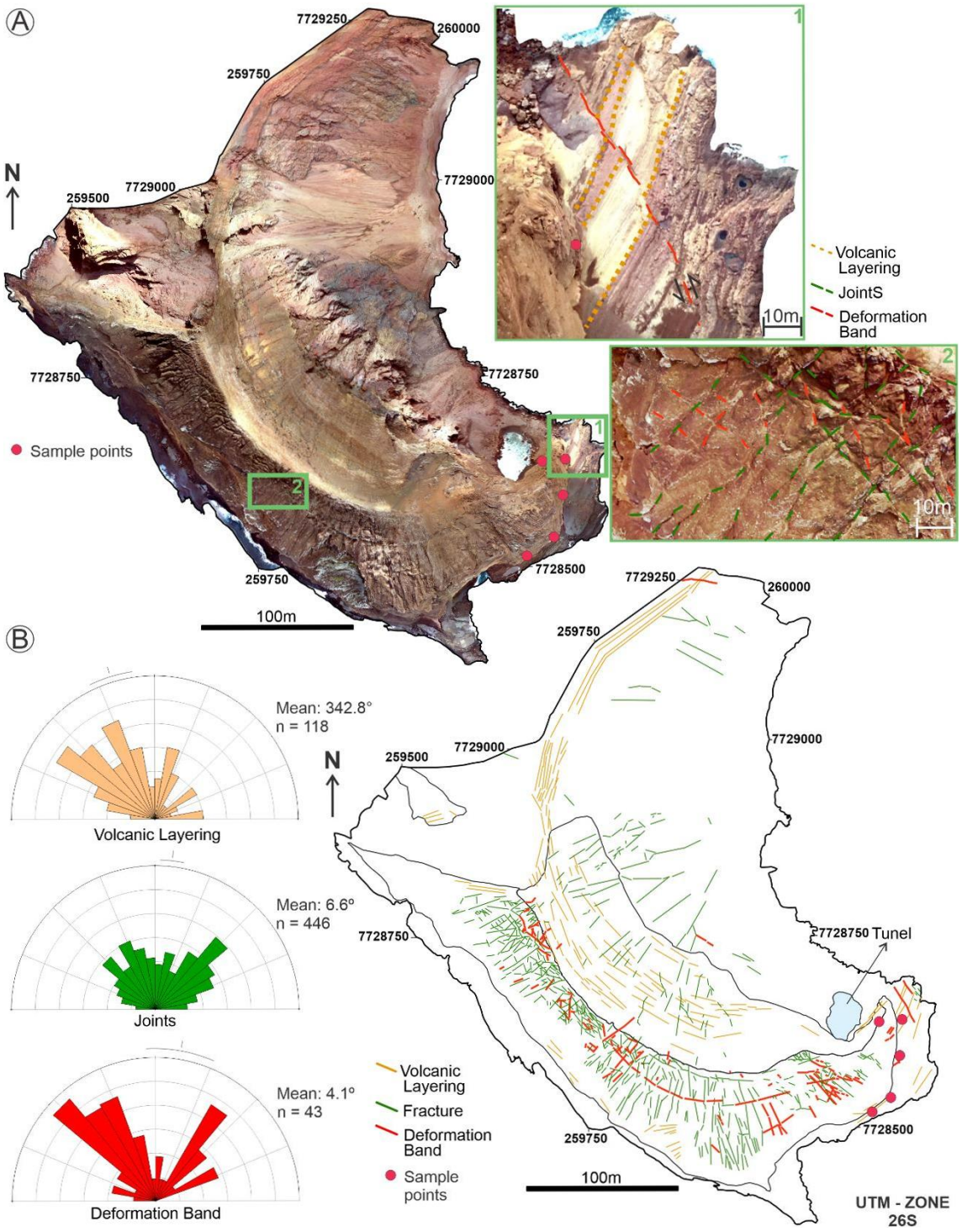

Figure 3.3 - Spatial analysis of the Paredão Formation. (A) UAV image of Paredão Volcano, highlight the main features fractures, volcanic layering, and deformation bands; (B) Interpreted structures in drone image with rose diagrams marking the circular structural trend of volcanic layering and the vertical structure sectioning the stratifications, interpreted as fractures and deformation bands.

Faults and DB's are distinct in UAV images. While faults appear dark in the image, the DB's are lighter which facilitates their separation (Figures 3.3A).

Furthermore, the DB's are more widely spaced (0.30 to 1.5 m) than the joints (0.10 to 0.60 m). However, these structures observed in Paredão Volcano are closed related to each other (Figure 3).

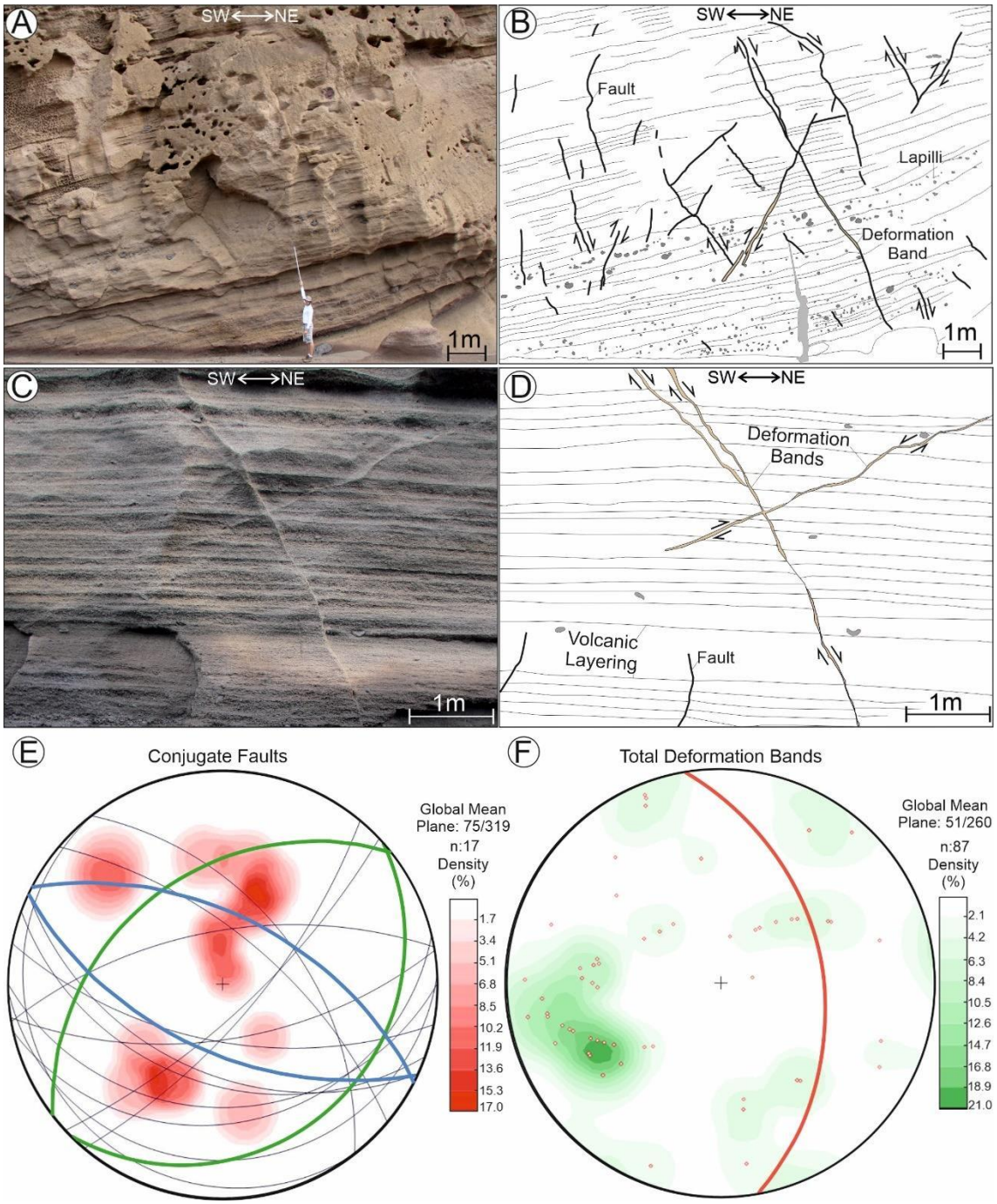

Figure 3.4 - Conjugate pairs structures observed in the Paredão Volcano. (A to D) Photos and schemes of deformation bands localized in conjugate structures; (E) Equal-area projection of conjugate faults associated with an angular opening between planes around 60°, blue and green planes indicate de mean values for the conjugate pair; (F) The equal-area projection of total deformation bands collected in fieldwork with mean direction NW-SE and moderate dip angles.

5.2. Field descriptions and structural control

The structural arrangement as observed in the UAV image, has patterns similar to observed in the field outcrops, characterized by pairs of conjugated structures and normal faults (Figures 3.4 and 3.5). A pair of conjugated DB's is shown in the Paredão Formation and it appears as a regular spacing in the outcrop causing an offset of the stratification with a total displacement of 3-5 cm. The conjugate pair is the best expositions of the DB's in the Paredão Fm. (Figure 3.4), they appear with regular spacing on the outcrop (≅1,5m) sectioning the stratification and causing a local vertical displacement between 3 to 5cm (Figure 3.4A to D). These structures are associated with fault zones with similar fault geometry and direction (Figure 3.4A and B).

The conjugate pair has a scattered direction (Figure 3.4E) with moderate to high dip angles (45° to 75°). The mean direction of those structures is N45E and N45W with an average angle between the fault planes about 45º. However, when compared to the total DB's measured in the field, the DB's are installed in the normal faults.

In the case of DB's releated to normal faults, the local displacement of the lapilli tuff stratification varies between 3 to 10cm (Figures 3.5A to D), and it is more expressive when compared to DB's in the conjugate pair. Also, the dimension of the DB associated with normal faults is more more pronounced than the DB formed in conjugate faults, ranging from 2 to 10cm (Figures 3.5C to F). The mean direction to the normal faults varies between N05-30W with moderate dip angles (≅30° to 45°). Locally in normal faults, we observe the Eye Structure (Figures 3.5C, 3.5D), formed from two collinear fault plane segments that

connected each other. It is usually observed vertical newly formed faults (Figures 3.5E, 3.5F).

We also observed in restricted locations the reverse faults associated with DB's (Figures 3.5G, 3.5H). In this case, the local displacement varies between 2 and 3cm, with a sinuous fault planes having similar morphology to the normal faults.

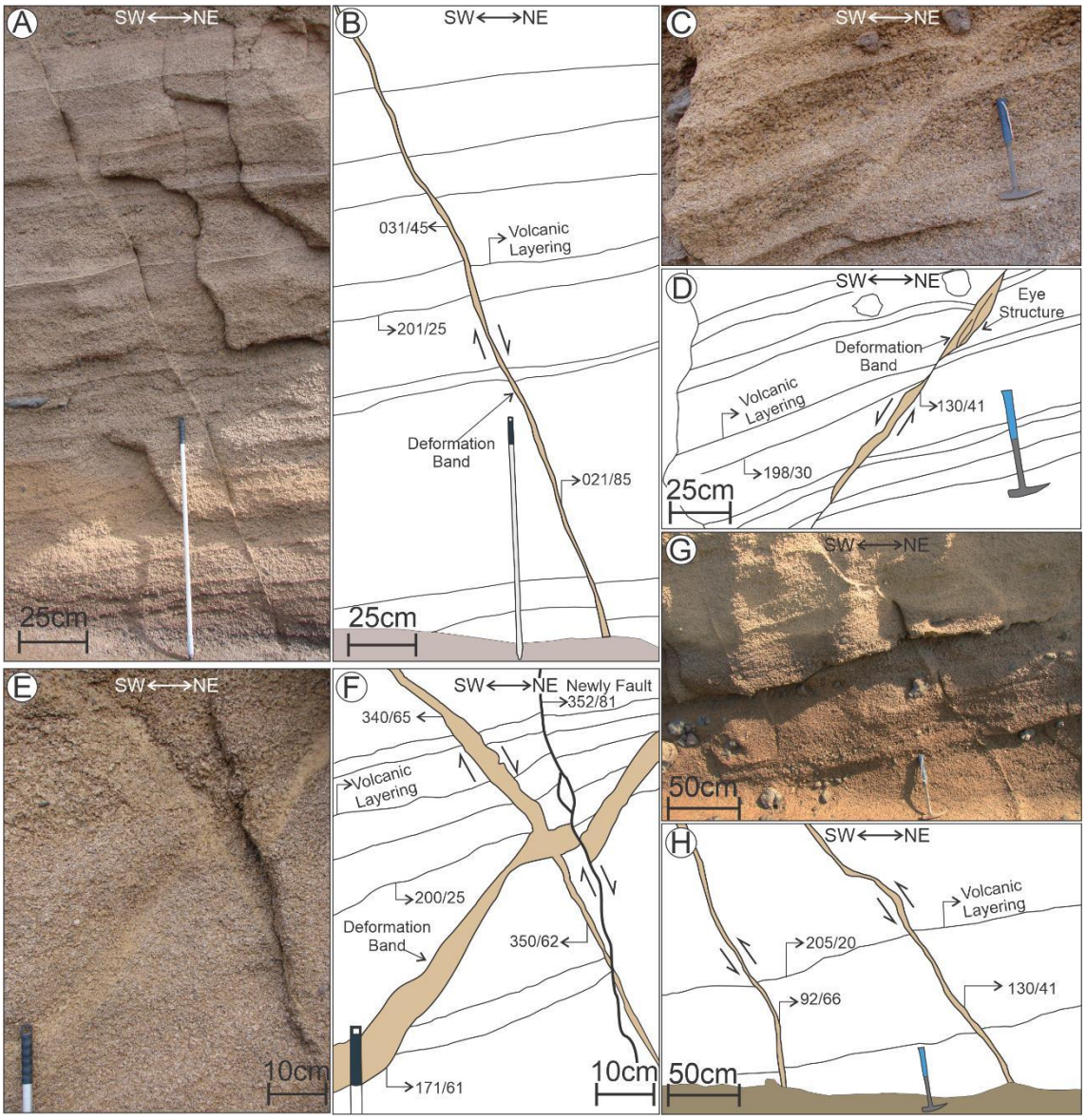

Figure 3.5 - Outcrop view of deformation bands. (A, B) normal faults associated with the deformation bands, causing a local displacement of the stratifications (5 to 10cm); (C, D) the eye structure formed by joining different fault planes it's a common structure in the DB's formed in normal faults; (E, F) zoom of conjugate DB sectioned by a newly formed fault, as a response of the active tectonics; (G, H) Inverse faults also associated to the DB's causing a local displacement (about 3cm).

5.2.1. Internal structures

DB's are milimetric scale structures that consists of fragments of the HR as well as of individual minerals (feldspar, pyroxene and amphibole). Crushed grains are embedded in a fine-grained matrix of cohesive aspect. Comparing to the HR, the DB's are more compacted and seems to have porosity reduction due to compaction and cementation. The DB's exhibit internally a structural fabric that would involve the mineral and lithoclast fragmentation/cataclasis, newly cementation, grain and pore reduction (Figure 3.6). These characteristics allow us to separate HR from the DB in outcrop analysis. In some outcrops, we were able to define the DB – main damage zone, the transition zone (TZ – about 1 to 5 cm from the main damage zone) and the preserved HR (Figure 3.6).

The bands are commonly affected by an intense cataclasitic process, causing a grain-size reduction and a production of a fine matrix (Figures 3.6). Grains and fragments are rotated and reoriented by the fault displacement producing an internal orientation (Figures 3.6A to D), observed by filaments stretched around rotated mineral fragments (Figures 3.5A,B), with kinematic observed by stratification displacement (Figure 3.4C). They are (a)symmetrically disposed around fragments of angular shapes and can also be observed features similar to pressure shadows involving the fragmented mineral, probably associated with a mineral rotation and fragmentation (Figures 3.6A,B).

The comminution process produces small angular fragments of phonolites (Figures 3.5C to 3.5F) with a weakly shape preferred orientation. Some of them show a microfaults with the same sense of shear observed in the deformed bands (Figures 3.6E, 3.5F).

Another observed characteristic to differentiate the DB of the HR is the cementation process that occurs in the bands (Figure 3.6). The bands are

majority filled with a light brown to light gray cement, of oxides (Figures 3.6 A to D) and carbonate in some cases (Figures 3.6E, F) compositions. The process of cementation associated with the deformation process causes a local reduction of porosity (cavities and vesicles) when compared to the HR (Figure 3.6).

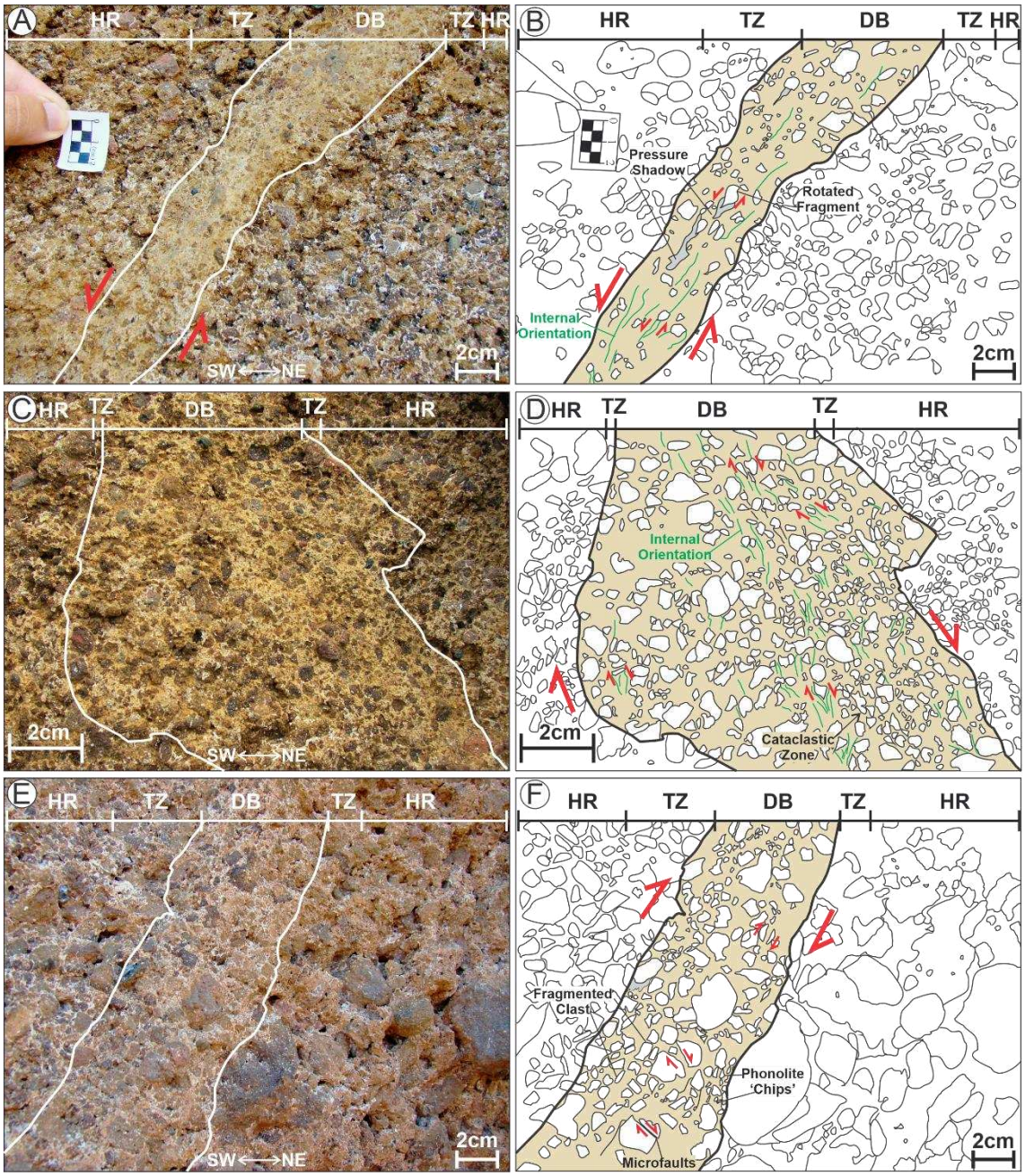

Figure 3.6 - Zoom of the internal structures observed in the deformation bands and the zonation of the deformation bands in outcrop. (A, B) It is possible to observe the internal orientation caused by cataclastic process, leading to the matrix reduction, rotation of fragments and pressure shadow formation, showing a similar kinematic of the DB displacement in outcrop; (C, D) irregular morphology of deformation bands, with the cataclastic matrix and formation of internal orientation associated to cataclasis; (E, F) fragmentation process causing the formation of microfaults with

local displacement of the clasts, with similar kinematic to the deformation band. HR: Host Rock, TR: Trasition Zone, DB: Deformation Band.

6 Microstructures

The microstructures within the DB's involves a structure sectioning the tuff stratifications, causing a local displacement (Figure 3.7A). The succession described allowing the formation of the mineral assemblage composed of pyroxene, K- Feldspar, amphibole, glass and magnetite, probably an unaltered assemblage for the lapilli tuff.

The focused-on microstructures of DB within the DB's consists of mineral grains and fragments of rocks of irregular shapes randomly distributed in a fine-grained matrix of of cohesive materials of redish colors. Grain aggregates do not have shape preferred orientations. Theses fragments are roughly equidimensional.

They are not also show any optical microstructures indicative of intracrystalline deformation such undulose extinction or subgrains. The DB's exhibit tabular shape and they do not show the development of any kind foliation. In fact grain are loosely distributed in the matrix in a varied of shapes and sizes. At the optical scale the matrix has a low porosity and mostly have a massive aspect indicating a high degree of compaction and cohesion. DB has as main characteristics in the scanned thin section: 1) the presence of oxides of a reddish color, 2) local matrix and porosity reduction, 3) fragmentated minerals and phonolite clasts and 4) fine to very fine cataclastic matrix formation (Figure 3.7).

Fluids seem to have a major control in development of the DB's. Where is observed the concentration of reddish material at the deformation along the band walls (Figures 3.7 and 3.8A, B), interacting with the minerals and volcanic glass

leading to the dissolution of the minerals (Figure 3.7). Sometimes causing the comminution and the fragmentation of the minerals, generating fine and angular grains of K-Feldspar and clinopyroxenes (<1mm) which are surrounded by iron hydroxides (Figures 3.8A,B). Casually the oxides can fill the primary porosity, which gives the reddish color the DB matrix (Figure 3.7).

Also is observed the matrix grain size reduction in the DB's when compared to HR (Figures. 3.7 and 3.8), in response to the cataclastic processes, causing a rupture, fragmentation and fracturing of minerals (Figure 3.8C,D). In some cases, microstructures similar to pressure shadow develop around large fragments of phonolites generate structures similar to pressure shadows wrapping fragments of phonolites (Figures 3.8A, 3.8B) affected by the cataclasis process and fluid flow.

Inside the DB's large fragments of feldspar grains are crosscut by shear fractures with the same sense of shear of the bulk DB's. It is observed the formation of shear fractures parallel to the main shear zone (Figures. 3.9A,B), this fractures sectioned K-Feldspar and opaque minerals giving kinematic similar to developed the DB.

The deformation observed in microscopic scale is sometimes is concentrated in specific layers where predominate the cataclasis. Mainly observed by the K-Feldspar crystals involved by a fine matrix and oxides (Figure 3.9C). In some DB's the porphyroclasts of amphyboles are fracture and rotated and involved by iron hydroxides, probably result by the process of dissolution and cataclasis along the DB (Figure 3.9D).

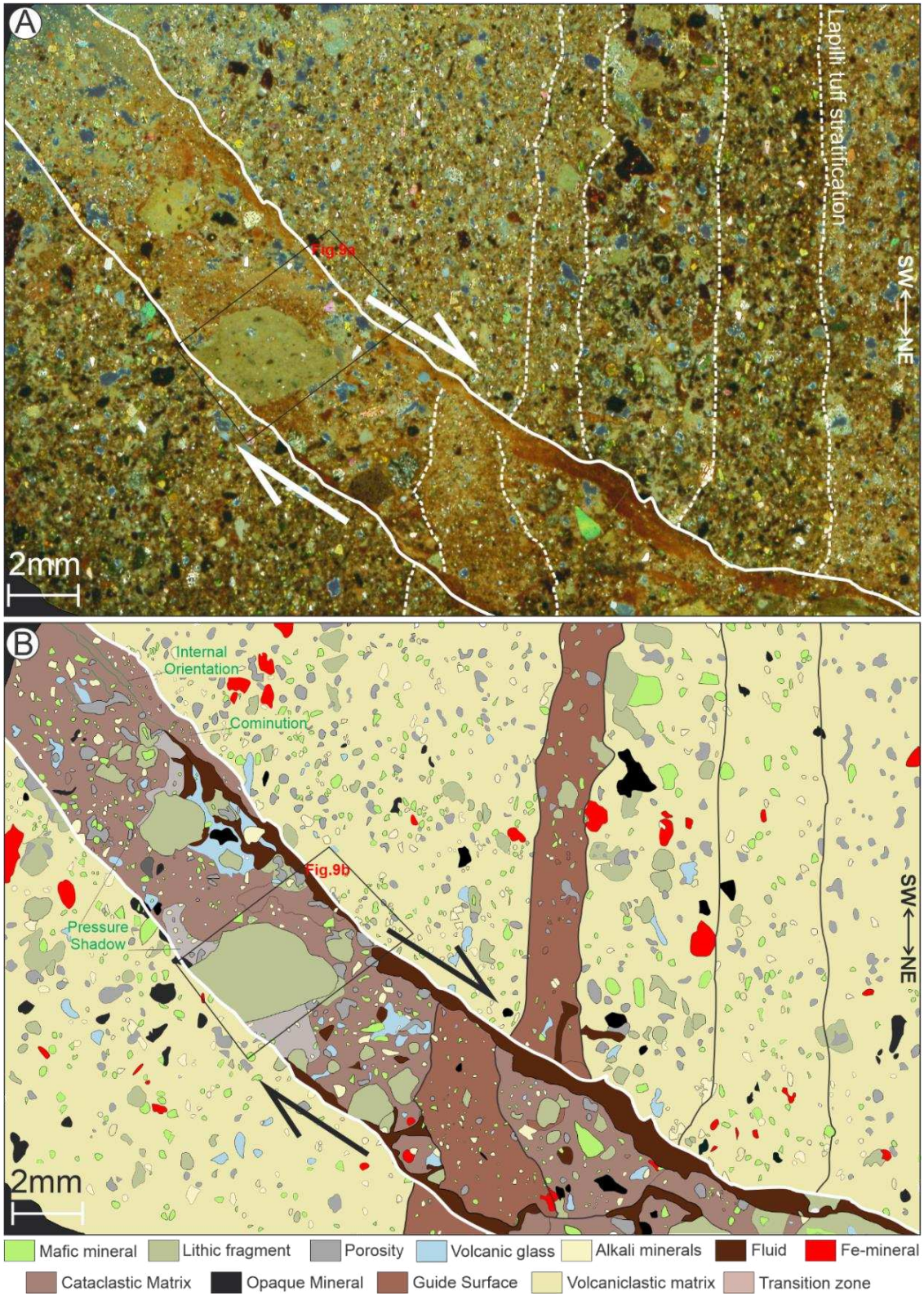

Figure 3.7 - (A) Scanned thin section of the HR and the deformation band; (B) Interpreted thin section with the indication of the main deformation band zone, highlighting the principal mineral groups and structures present in the DB.

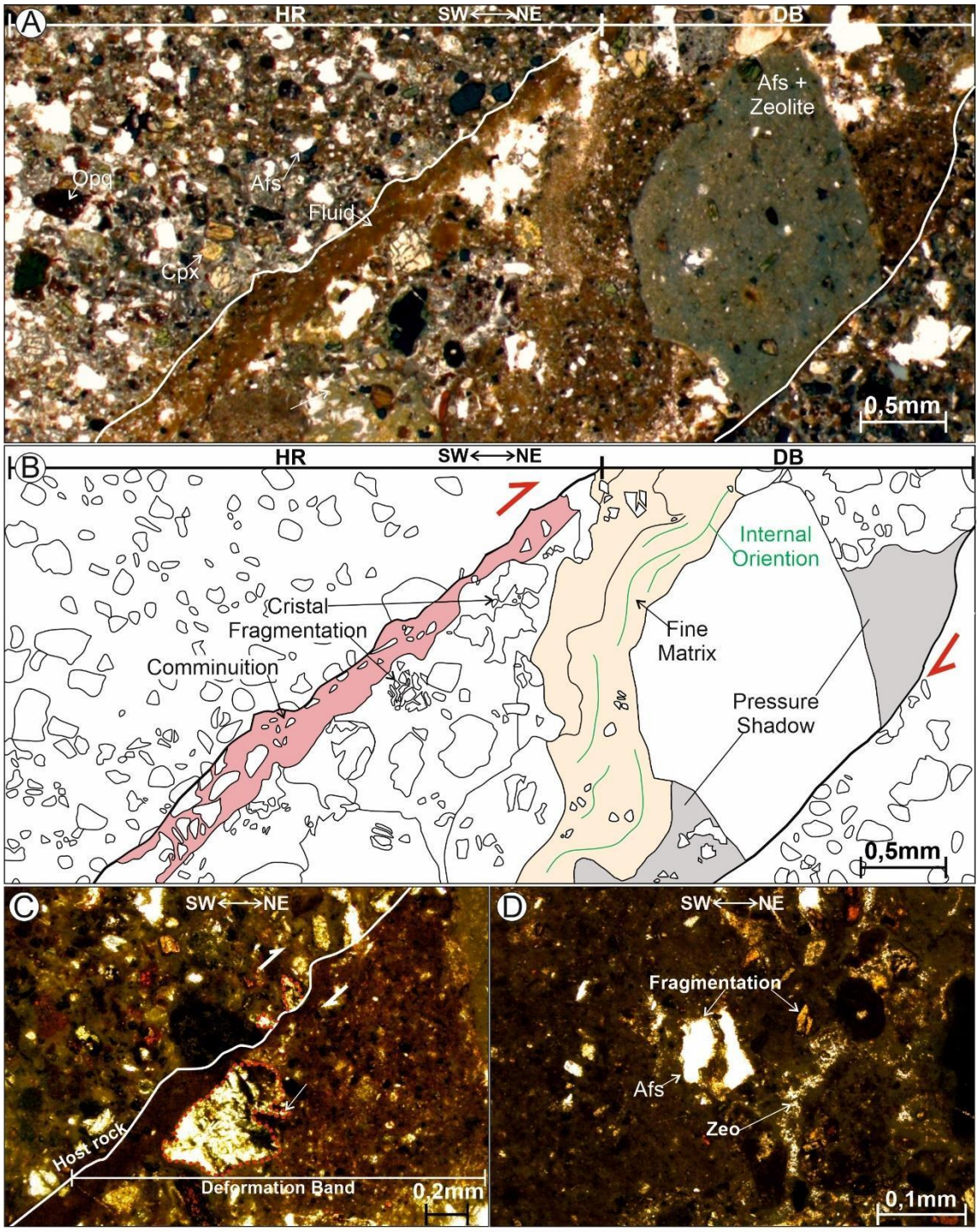

Figure 3.8 - Photomicrographs of deformation bands showing their interaction with the HR. (A, B) Zoom area of deformation, highlighting the presence of pressure shadows around the phonolite fragment and the fine matrix generated by cataclastic and comminution process. It also possible to observe the weak orientation in the fine matrix; (C) Local displacement of fragments in the deformation band; (D) Fragmentation of nepheline crystals and zeolite veins formation within the deformation. Opq: Opaque mineral, Cpx: Clinpyroxene, Zeo: Zeolite, Afs: Alkali Feldspar.

6.1. 2D Porosity analysis

The porosity was analyzed using the JPor in the DB and HR. Photomicrographs of 18 samples of HR and 14 of DB were acquired using petrography microscope (examples in Figure 3.10). In the HR the porosity is marked by the presence of vesicles and rounded cavities with sizes varying between 50 and 400μm. The porosity exhibits low connectivity in the HR (Figure 3.10A), with mean values around 16%. However, the connection between pores can be as higher as 40% when the distribuition of fracture in HR's is denser, but in some cases (Figure 3.10C), it can reach 40% because of the presence of fractures.

Pores in the DB are reduced by cominuition and just a fraction of open spaces is not filled by mineral precipitation, remaining only a few vesicles that are not sealed (Figure 3.10B). The pore spaces in the DB respond for up to 13 % of volume space, with an average of 6%, along the DB (Figure 3.10C). The connection between pores in the DB's case are poor or absent having most of the pore space left isolated, the pores are filled and have no connection between the pores, being isolated from each other possibly marking the low permeability between the pores. In contrast to the HR where the pores tend to be rounded, the pores of the DB's are apparently elongated and even rectangular without a specific orientation.

When compared, the distribution of porosity in DB and HR (Figure 3.10C), is observed a reduction of porosity inside the DB's caused by fluid circulation along these bands and the interaction with the fragments of minerals and rocks, which ultimately led to the dissolution of minerals and precipitation and cementation of pore space along the DB's. This demonstrated that in the region

of the bands the reduction of porosity occurs, due to the deformational processes and the passage of fluids in the bands, which possibly has sealed the lapilli tuffs primary porosity.

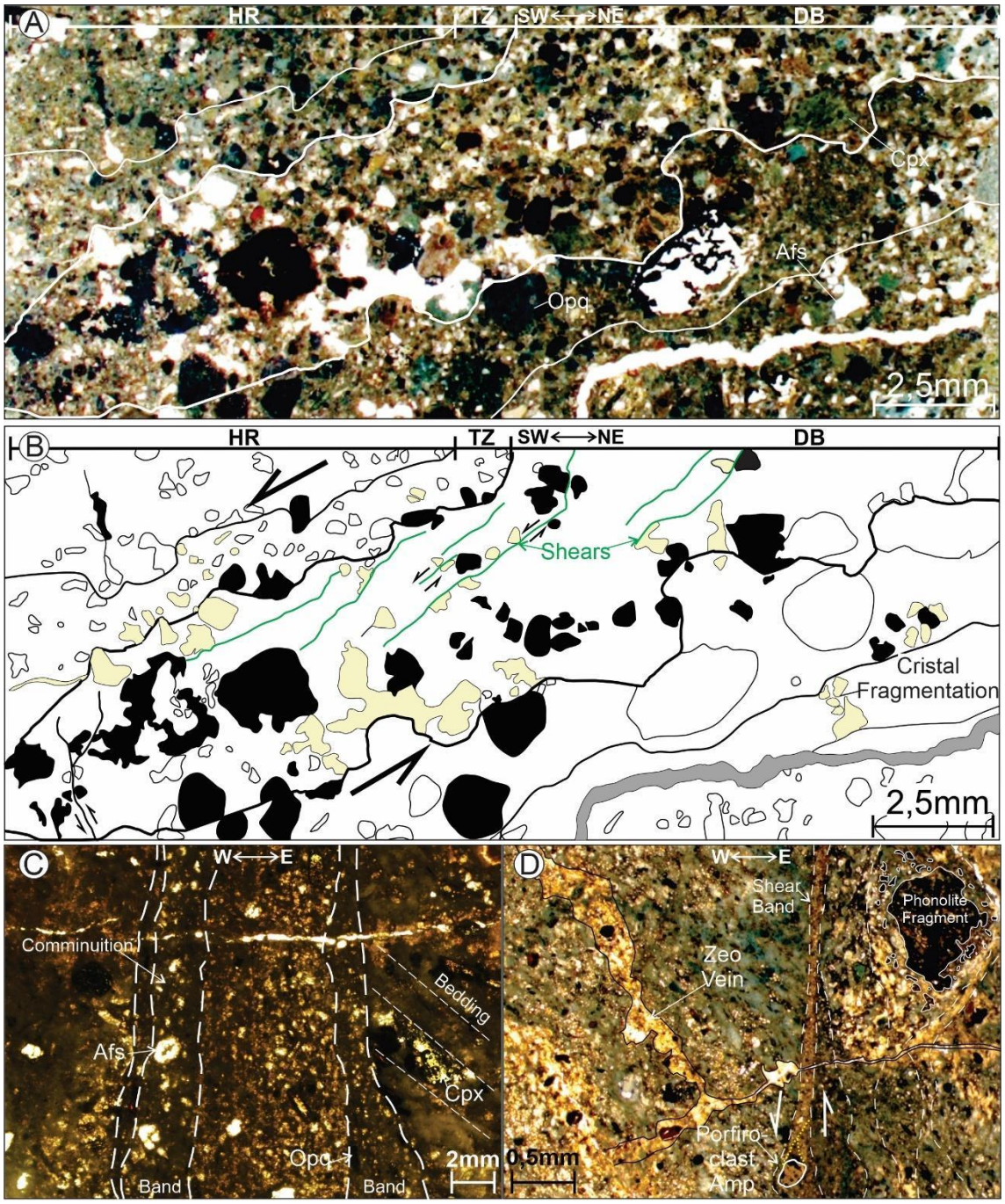

Figure 3.9 - Figure 9: Photomicrographs of the deformation bands. (A, B) Well defined deformation band zone, with matrix reduction and recementation of the DB region. Also, the formation of shear fractures occurs parallel to the wall of the DB and with similar kinematic. (C) Shear bands, in which comminution and fluid flow are concentrated, causing matrix reduction and fracturing minerals, such as alkali feldspar (Afs). (D) Bands in which amphibole (Amp) porphyroclasts and pressure shadow around those crystals were developed. Note the matrix reduction and the comminution of phonolite fragments. HR: Host Rock, DB: Deformation band, TZ: Transition Zone, Opq: Opaque mineral, Cpx: Clinpyroxene, Zeo: Zeolite.

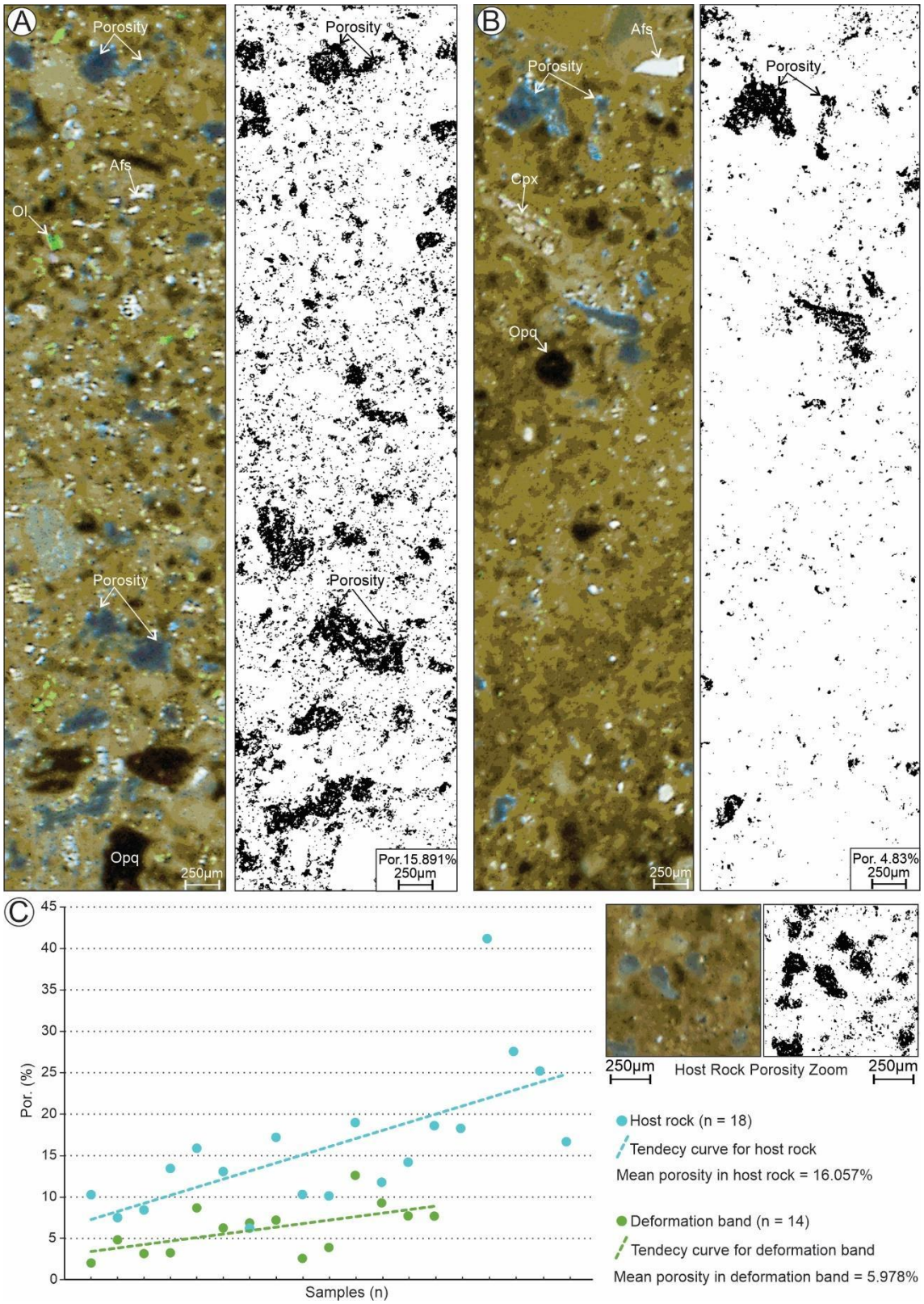

Figure 3.10 - Porosity analysis using photomicrographs and JPor (Ferreira and Rasband, 2012; Schneider et al., 2012). (A) Host rock photomicrography with the application of HSB macro, allowing to observe and estimate the 2D porosity (black and white image), with porosity estimated at 16% to this portion. (B) Deformation band photomicrography with the application of HSB macro. It observes the porosity reduction when compared to the host rock, with porosity estimate in 4%. (C) Comparative graph of porosity in the host rock and the deformation band. The porosity in HR varies between 7 to 25% and in DB varies between 2 to 11%, thus demonstrating a certain

reduction in porosity over DB's. Afs: Alkali Feldspar; Ol: Olivine; Opq: Opaque mineral; Cpx: Clinopyroxene; Zeo: Zeolite.

The microstructures in the deformation seen in SEM images are characterized mainly by grains of smaller sizes than those in the HR (Figures 3.11A,D). Micro faults in some grains are consistent with the same kinematic of the extensional and strike-slip faults (Figures 3.11D), granular flow and to a lesser extent cataclastic flow (Figure 3.12A, B). A decrease in pore space and pore sizes is clear in the DBs relative to the HR. However, all the analyses were made on thin sections and some of the porosity might be an artefact rather than real pores. Grains and fragments observed in DBs are of irregular shapes with sharp edges and variable (Figures 3.11D and 3.12). Grains of rounded contours are rarely observable (Figures 3.11D and 3.12B). All of them are embedded in a massive matrix with random distribution of fragments, about 63% of the band is composed of matrix and the rest of fragments. Another difference between the DB and HR is the fragmentation of phillipsite in the deformation zone, while in the HR the fibroid shape remains unchanged.

Broadly, the DB are not foliated but in zones of more concentrated deformation with a more intense cataclasis a drastic reduction in grain size (<10μm) is observed and some planar and prismatic minerals such as mica and amphibole are oriented with their longest dimensions parallel to the DB walls. The matrix of the reduced size grains wrapped around the large oriented grains giving the DB fluidic aspect (Figures 3.12C,D and 3.11E).

Locally the crystals are marked by the rotation process, where they rotate and fragment, generating a thin matrix around the rotated crystal (Figures 3.12E, 3.12F). The presence of deformed biotite evidenced the normal kinematic of the DB (Figures 3.12C, 3.12E), as well as near the zone of greatest deformation the

mechanical incorporation of larger fragments by the cataclasis and the deformation process (Figure 3.12F).

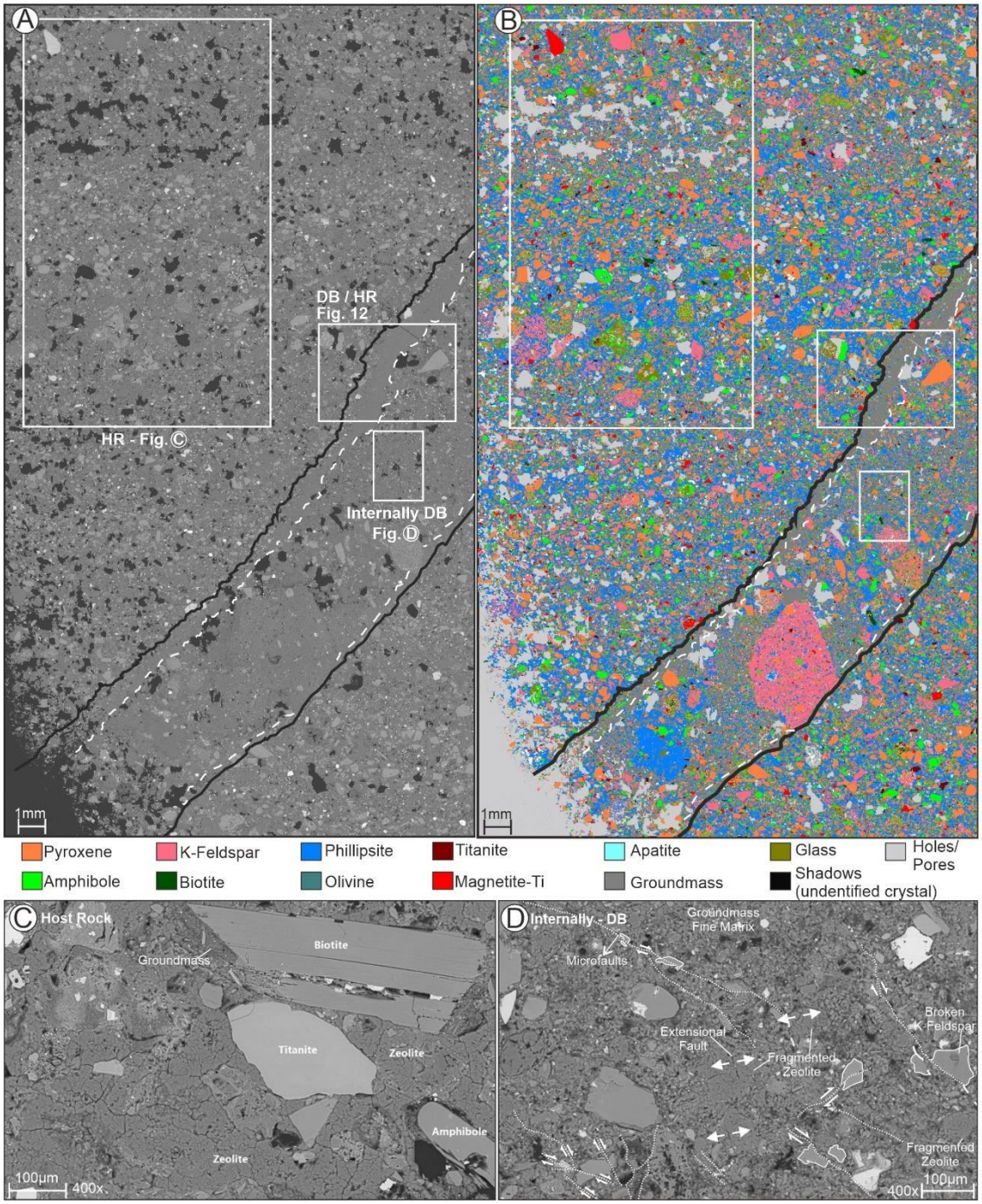

Figure 3.11 - Figure 11: SEM and EDS images acquired. (A) SEM image of the studied thin section, in which the textural difference between de the host rock (HR) and deformation band (DB) is observed. (B) Phase map acquired by EDS, with mineral indication and groundmass (tuffaceous matrix). (C) Zoom of HR where well shaped biotite, titanite and the zeolite (phillipsite) are observed. (D) Internal portion of the deformation band, where groundmass and crystal fragments are dominant, associated with extensional and strike-slip faults.

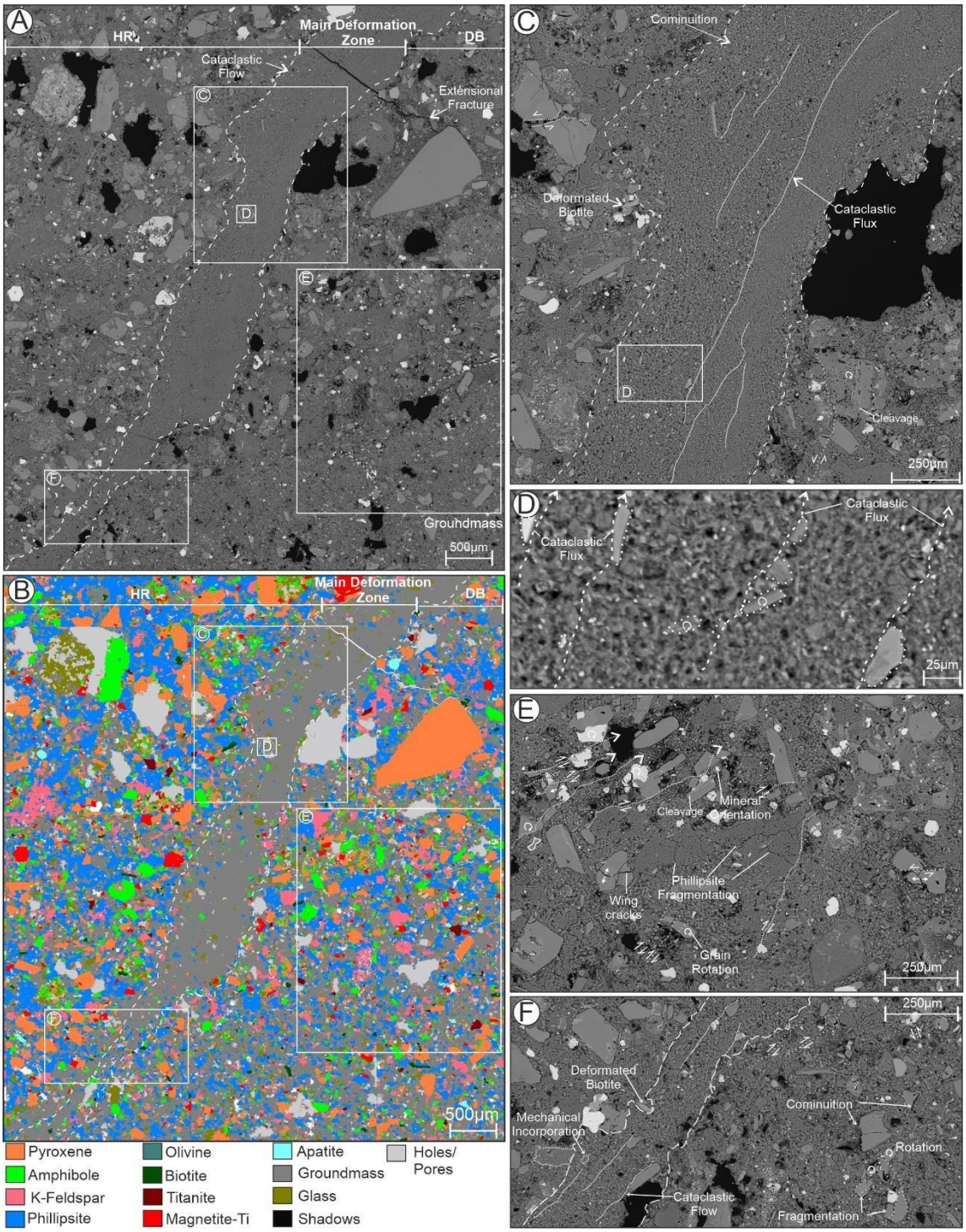

Figure 3.12 - Details of the deformation band in SEM imagens and EDS phase map. (A) The deformation band morphology highlights the main deformation zone, with a different texture marked by intense comminution. (B) Phase map in which the groundmass is identified; some grains may be smaller than the EDS detection limit (gray color). (C) Zoom of the main deformation zone; an intense cataclastic flow and matrix reduction can be observed, marked by intragranular e transgranular fractures. Also, deformed biotite is noted, indicating normal kinematic. (D) cataclastic flow, with an orientation of prismatic and phyllosilicates crystal fragments parallel to the DB direction. (E) Mineral orientation within the deformation band; grain rotation and phillipsite fragmentation can be seen. (F) Fragmentation and mineral rotation process, associated with mechanical incorporation.

6.2. Grain distribution analysis

A reduction in grain size is clear when grain size distribution histrograms are compared for the HR's and the DB's. Grain size distributions are plot for the minerals pyroxene and feldspars (Figure 3.13A to F) (Supplementary Tables 2 – Anexo 3). The pyroxene in the HR has grain size distribution between 5 to 250μm, with a peak between 15 and 45 μm. marking a regular tendency curve, predominate a particle size between 45 to 100μm. A curve for a distribution of grain size for felspar in the HR show a broader range of sizes when compare to the pyroxene in the same rock. Two peaks are more distinct around 15 and 30 μm (Figures 3.13A,B).

On the other hand, the grain size of Pyroxene and K-Feldspar in the DB decreases dramatically, both with peaks in particle sizes smaller than 5μm, with maximum size up to 100μm (Figures 3.13B,C). The same tendency of size reduction is also observed when both minerals are ploted together These reductions also observed when we observe the sum of particle sizes of Pyroxene and K-Feldspar. This difference marks this strong textural change between HR and DB, which leads to the difference observed in the outcrops of the Paredão Volcano.

7. Discussions

7.1. Deformation Mechanism and evolution

In the DB microstructures suggest the operation of two distinct mechanisms of deformation, named granular flow (Adam et al., 2005; Fossen et al., 2007, 2018b) and cataclastic flow. The first observed deformation mechanism is the granular flow, occurring internally in the zone, where a limited presence of

fractures. Grains are rotated (Figures 3.13D,E), generating angular fragments and probably associated to fluid pressure (Fossen et al., 2018b). Possibly this mechanical process is associated with the initial deformation process, leading to the grain reorganization and disaggregation of the crystals and the DB matrix (Rotevatn et al., 2008; Cavailhes and Rotevatn, 2018; Fossen et al., 2018b).

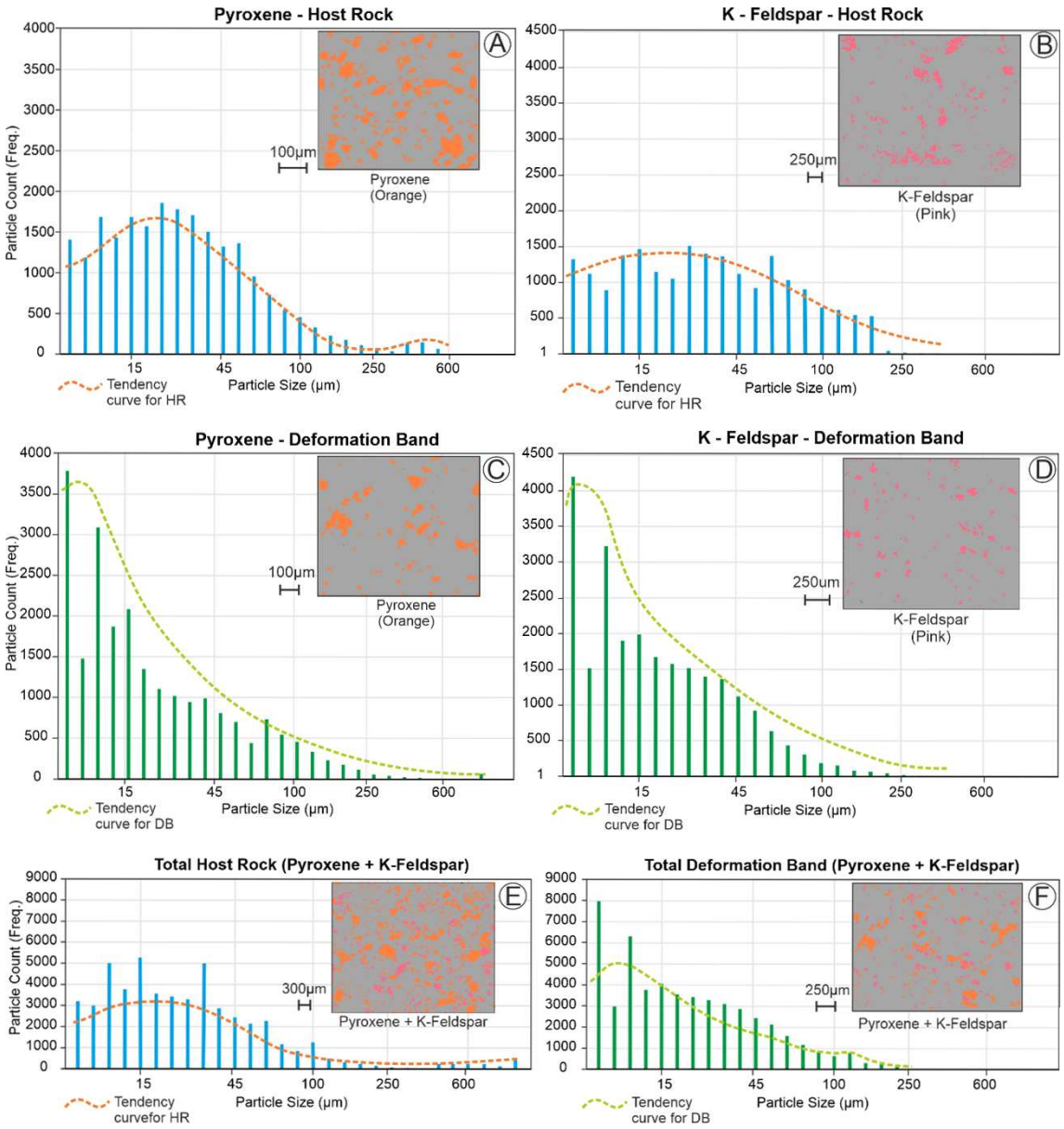

Figure 3.13 - Grain size distribution of Pyroxene and K-Fedspar, obtained using the EDS phase map. (A) and (B) Pyroxene and K-Feldpsar in the host rock demonstrating the concentration of particle size between 15 to 45µm; (C) and (D) Pyroxene and K-Feldpsar in the deformation band demonstrating the concentration of particle size smaller than 15µm; (E) Particle size distribution for Pyroxene and K-Feldspar in the host rock; (F) Particle size distribution for Pyroxene and K-Feldspar in the deformation band.

The cataclastic flow is marked by crystals fragmentation and a generation of a very fine matrix in the main deformation zone, creating a cataclastic fabric (Pizzati et al., 2020) (Figures 3.8 and 3.12). Grains are internally fractured and fracturing are of intra- to transgranular nature where we observe the intragranular and transgranular fracture styles (Figure 3.12C) (Aydin and Johnson, 1978; Balsamo and Storti, 2010; Fossen et al., 2018b; Pizzati et al., 2020). The fractures occur preferentially along cleavage planes, in zeolites (Figures 3.11D and 3.12E), pyroxenes (Figure 3.12E) and amphiboles (Figure 3.12E), such as pre-existing cleavages and fractures. Thus creating a mechanical anisotropy in these rocks, which makes it possible to break into smaller fragments (Cavailhes and Rotevatn, 2018; Fossen et al., 2018b; Pizzati et al., 2020).

These bands can be classified as a cataclastic shear band (CSB), where cataclasis and grain crushing process dominate, similar to what occurs in immature sandstones with a wide mineralogical variety (Fossen et al., 2007a, 2018b; Exner and Tschegg, 2012; Torabi, 2014; Pizzati et al., 2020). The local preferred orientation of the fragments in the main deformation zone and nearby CSB, characterize a cataclastic flow (Figures 3.12A,C and 3.13D). This orientation generates a local foliation (Figure 3.6), probably as a result of the intense cataclasis, which accommodate the displacement along the direction of the DB (Cladouhos, 1999; Del Sole and Antonellini, 2019; Pizzati et al., 2020).

Futhermore, the intense comminution process generates an extreme gran size reduction, for example, observed in the pyroxene and K-Feldspar when compared to HR (Figure 3.13) This reduction is caused by grain crushing during the deformation process (Aydin, 1978; Fossen et al., 2007a), leading to increase the grain angularity .and the shear resistance (Jiaxiang Zhang et al., 1990; Mair

et al., 2002; Fossen et al., 2007a). The porosity reduction observed in CSB is directly associated with the grain reduction, creating a cataclastic fabric that fills and reduces pore space in the CSB (Nogueira et al., 2020; Pizzati et al., 2020).

7.2. Fluid flow and volcano-tectonic history

The evolution of the deformation in the Paredão Formation involves a interaction between five processes: (1) volcanism; (2) hydrothermalism; (3) hydraulic fracturing; (4) the granular; (5) cataclastic flow process. The Paredão Volcano is marked by a complex stratigraphy evolution associated with the phreatomagmatic activity, Strombolian and Hawaiian volcanism (Pires et al., 2016; Pasqualon et al., 2019).

The volcanism process led to a deposition of a planar stratified pyroclastic deposits and lava flows (Figures 3.2 and 3.14A), with intercalation of lapillitic scoria lapillistone, ‘A’a lava and pahoehoe lava flows (Pasqualon et al., 2019) (Figure 14A).

The deposition of volcanic sequences was followed by The second evolutionary phase is marked by hydraulic fracturing (Figure 3.14B) and the hydrothermal process of the lapillistone. This hydrothermal alteration is marked by the transformation of volcanic glass and K-Feldspar to phillipsite (Figures 3.11, 3.12, 3.14B). The mineral transformation occurs along the stratification planes and the fractures (Figure 3.14B) developed by the post magmatic activity (De Rita et al., 1983; Gudmundsson, 2006).

This hydrothermal was responsible for event can be related to a response to two different hypotheses processes: (1) the formation of zeolite phillipsite is closely related to the hydrothermal, post-depositional processes that affected the pyroclastic rocks of Paredão, mainly replacing the volcanic glass of these rocks

(Hernandez et al., 1993; Etame et al., 2012; Mateus et al., 2020); (2) the phillipsite formation os associated to the weathering conditions mainly controlled by the seawater factor. The seawater runs through the system causing the modification of Ph and temperature conditions, leading to complete modification and zeolitization of K-Feldspar and glass (Robert and Goffé, 1993; Ghiara and Petti, 1995). However, both processes can have a certain contribution to the formation of the phillipsite-rich matrix (Mateus et al., 2020).

The zeolitization process and the establishment of a transtensional tectonics during the Middle Pleistocene are associated with VTFZ (Ferrari and Riccomini, 1999; Ribeiro et al., 2019; Barão et al., 2020). This tectonic regime causes the formation of normal faults and conjugate pairs (Figure 3.14C). Possibly, earlier formed structures facilitate the formation of had taken advantage of post-depositional fractures for their installation in Paredão Volcano (Figures 14C).

This tectonic geometry associated with planar intercalation of layers of massive lapilli-breccias and lapillistone, allows establishing a similarity with cataclastic bands developed in arkosic sandstones (e.g. Del Sole and Antonellini, 2019; Nogueira et al., 2020; Pizzati et al., 2020). The deformation starts by fracturing along pre-existing mechanical weakness of minerals, such as cleavages, which causes a reduction of grain size. This processes take advantage of pre-existing structures, such as cleavages (Cavailhes and Rotevatn, 2018; Fossen et al., 2018), leading to granular flow and finally to complete catalysis of the DB (Figure 3.14C).

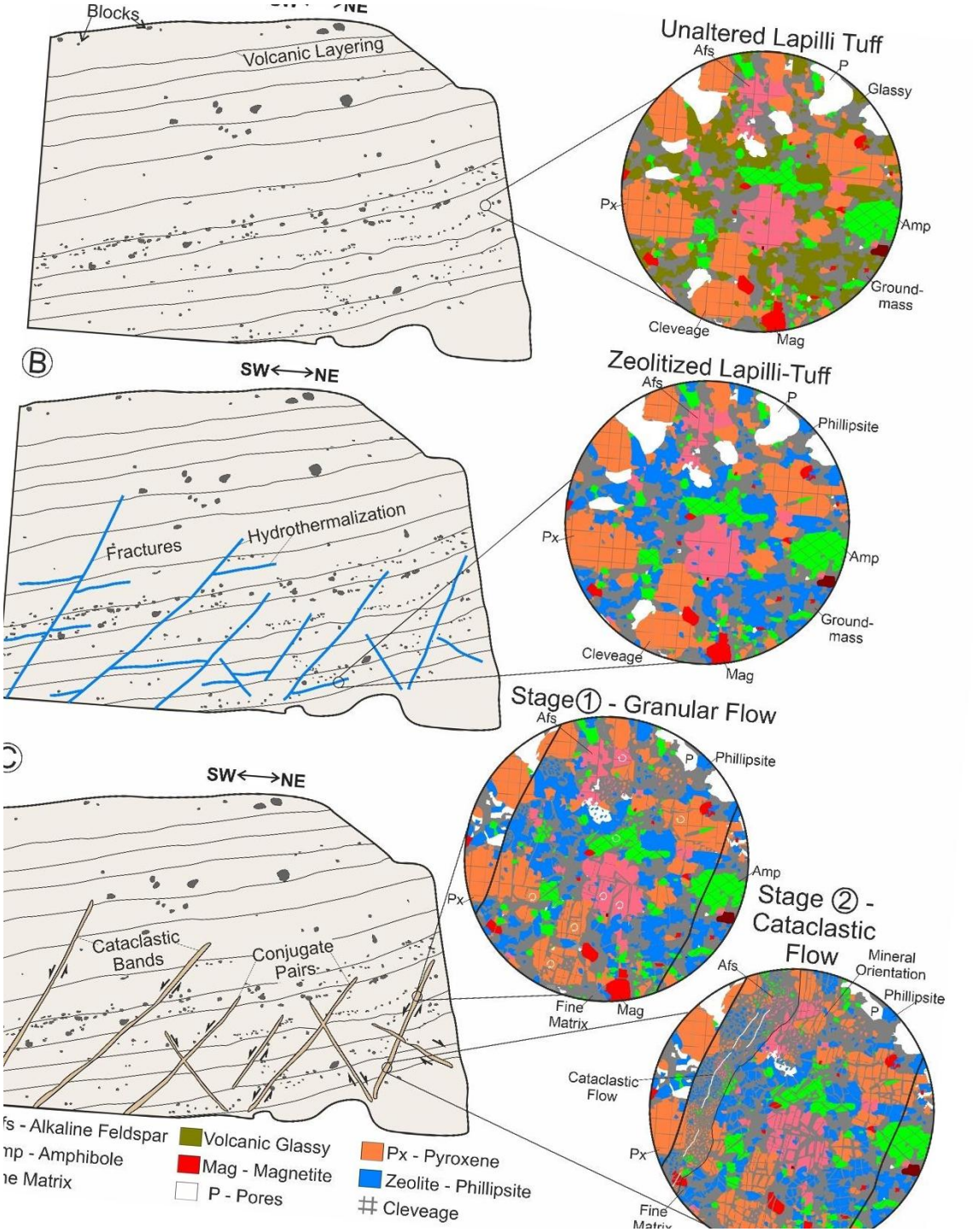

Figure 3.14 - Schematic evolution of hydrothermal and deformation stages of the Paredão Volcano. (A) The first stage is the volcanic event,creating planar stratified pyroclastic deposits and lava flows. The lapilli-tuff facies generated in this process is composed of fragments of pyroxene, alkali feldspar amphibole, glass and magnetite; (B) Second stage is marked by hydraulic fracturing, leading to hydrothermal alteration. This stage is marked by the transformation of volcanic glass and alkali feldspar to phillipsite; (C) The third stage is associated to the tectonics and the formation of cataclastic bands,divided into two stages: the granular flow of particles and the cataclastic flow, reducing grain sizes and generating a cataclysmic matrix.

8. Conclusions

The structutures observed in outcrops as well as in thin sections of Paredão Volcano in Trindade Island allow us to propose a structural evolution, kinematics and deformation mechanisms involved in the formation of deformation bands developed in pyroclastic rocks. Therefore, it is possible to conclude that:

(1) The deformation mechanisms responsible for the first deformational stage is the granular flow. This deformation is associated mainly with the fragmentation and rotation of grains crystals, generating angular fragments associated with the fluid pressure;

(2) The evolution to a cataclastic flow is marked by crystals fragmentation and generation of a fine matrix in the main deformation zone, creating a cataclastic fabric and porosity size reduction of the pyroclastic rocks along the deformation band;

(3) Cataclasis process is controlled according to the different minerals phases, that is, it occurs preferentially along cleavages or microfractures, as occurs for pyroxenes, K-Feldspar and amphiboles where the deformation ins mainly associated with the fractures;

(4) The zeolitization process of the lappilistone is related to the availability of post-volcanic hydrothermal fluids and also to the presence of seawater, which generally constituting a complex hydrogeological system for the rocks of the Volcano Paredão;

(5) Deformation bands are associated with a transtensional context, configuring the geometry of predominantly normal faults and sets of conjugated pairs developed along the rocks of the Paredão volcano.

9. Acknowledgments

We would like to thank CNPq for the financial support through projects 557299/05-5, 557141/2009–5 and 442865/2015–5. To CAPES for the scholarship (88882382075/2019–01), the Brazilian Navy for support and transportation during the fieldwork. To LABAP, LECOST and LAMIR Laboratories for all the infrastructure provided, Geological Survey of Finland (GTK), Laboratory of Process Mineralogy for all analysis and technical support, and analytical technicians Akseli Torppa and Hannu T. Makkonen. RJA is a research fellow of the CNPq (PQ 302913/2018–1) and Fundação Araucária senior fellowship (45725). BT is a CNPq researcher (PQ 306780/2019–4). Also, we thank PPGeol-UFPR for all assistance and support in the continuation and completion of the research.

3.4. Resultados Adicionais

3.4.1. Feições estruturais observadas em Fernando de Noronha

As feições tectono-estruturais também foram observadas no arquipélago de Fernando de Noronha, na qual foram catalogadas zonas de falhas (Figura 13) e a presença de brechas tectônicas nos basanitos da Formação Quixabá e rochas vulcanoclásticas da Formação Remédios.

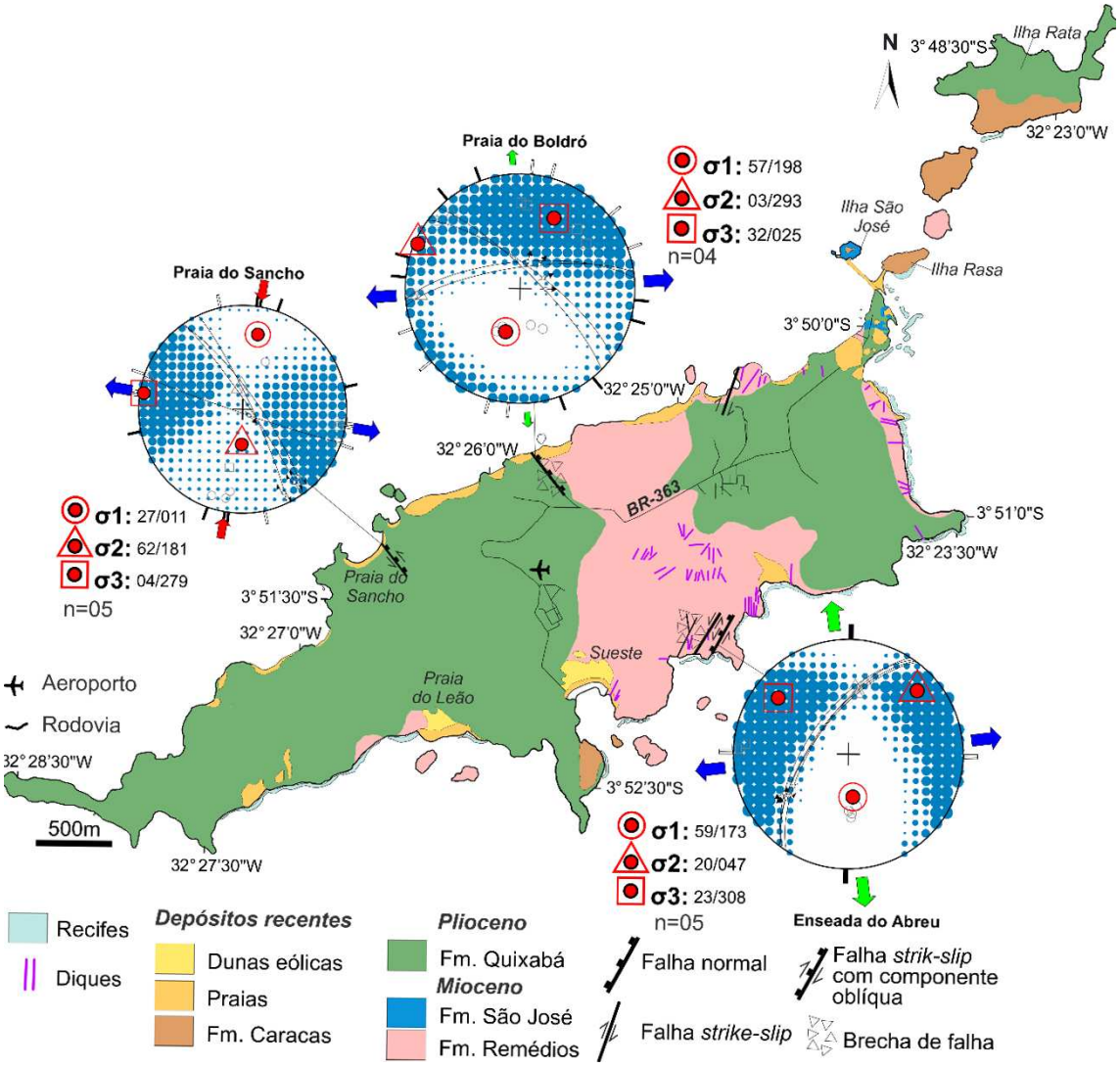

Figura 13 - Mapa das feições estruturais observadas na Ilha de Fernando de Noronha, em que se observa falhas normais e com componente oblíqua nas localidades da Praia do Sancho, Boldró e Enseada dos Abreu. Nessas localidades foi possível se estabelecer as paleotensões envolvidas na formação dos planos de falhas, utilizando o método dos diedros retos.

Os planos de falha observados em geral tratam-se de planos verticalizados em que se desenvolvem *slickenlines* e steps de falha (Figura 14), sendo essas estruturas lineares subverticais (70-90°) (Figura 14A, B), indicando a cinemática normal para essas falhas, sendo possível se observar a presença de óxidos associados a esses planos de falha. Já em alguns casos essas feições lineares são levemente inclinadas (<70°) ou sub-horizontais indicando assim a cinemática direcional exercida sobre esses planos de falha (Figura 14C, D).

Associado aos planos de falha se observou a presença de brechas de falha (Figura 15), essas feições em geral são verticalizadas seguindo os planos de falha, sendo observáveis em rochas com basanitos. As zonas de brecha atingem entre 10 e 50cm (Figuras 15A, B), essas zonas possuem fragmentos angulosos de dimensões variáveis entre 3 e 10cm que são envoltos pela matriz cominuída e presença de argilominerais que acabam por sustentar essas zonas de brecha.

Essas feições também podem ocorrer ao longo de planos inclinados (30-45º), em que se pode estabelecer regiões fortemente afetadas pelo processo de brechação e a zona de dano causada pela falha (Figura 15C). Nesse caso a zona de brecha tende a concentrar a maior deformação, sendo cimentada por argilominerais e óxidos. Quanto a zona de dano verifica-se que fragmentos de maior dimensão (1 - 30cm) são compartimentados por pequenas zonas de fraturas que tendem a ser preenchidas por argilominerais de cor vermelha e carbonatos (Figura 15C).

Levando-se em conta os critérios cinemáticos obtidos em campo foram estabelecidos paleostresses através do método dos diedros retos para cada um dos locais estudados (Figura 13). Os planos de falha possuem *trend* direcional

variável entre N30-45E a N20-45W, apresentando o padrão conjugado das estruturas observadas em campo. Todavia se observa o predomínio da tectônica distensional, principalmente na Praia do Boldró, onde as estrias são verticais com tensões normais (Figura 13).

Já na região da Praia do Sancho e Enseada Abreu ocorre o predomínio de falhas normais com componente oblíqua, em geral marcadas pela cinemática sinistral. Fazendo com tensões principais (σ1) sejam mais horizontalizadas se comparadas as zonas de falha observadas na Praia do Boldró.

Apesar da análise desses dados ser preliminar e da escassez de planos de falha cartografados em campo, ocorre a sugestão de evento distensional de direção E-W (σ3) (Figura 13), similar ao que o ocorre por exemplo na Ilha de Trindade, como provável resposta à tectônica atuante da Zona Fratura de Fernando de Noronha, que deve afetar as ilhas formadas ao longo dessa zona. Sendo sua evolução inicialmente marcada por um momento distensional, gerando falhas normais, evoluindo para o momento transtrativo da zona de fratura.

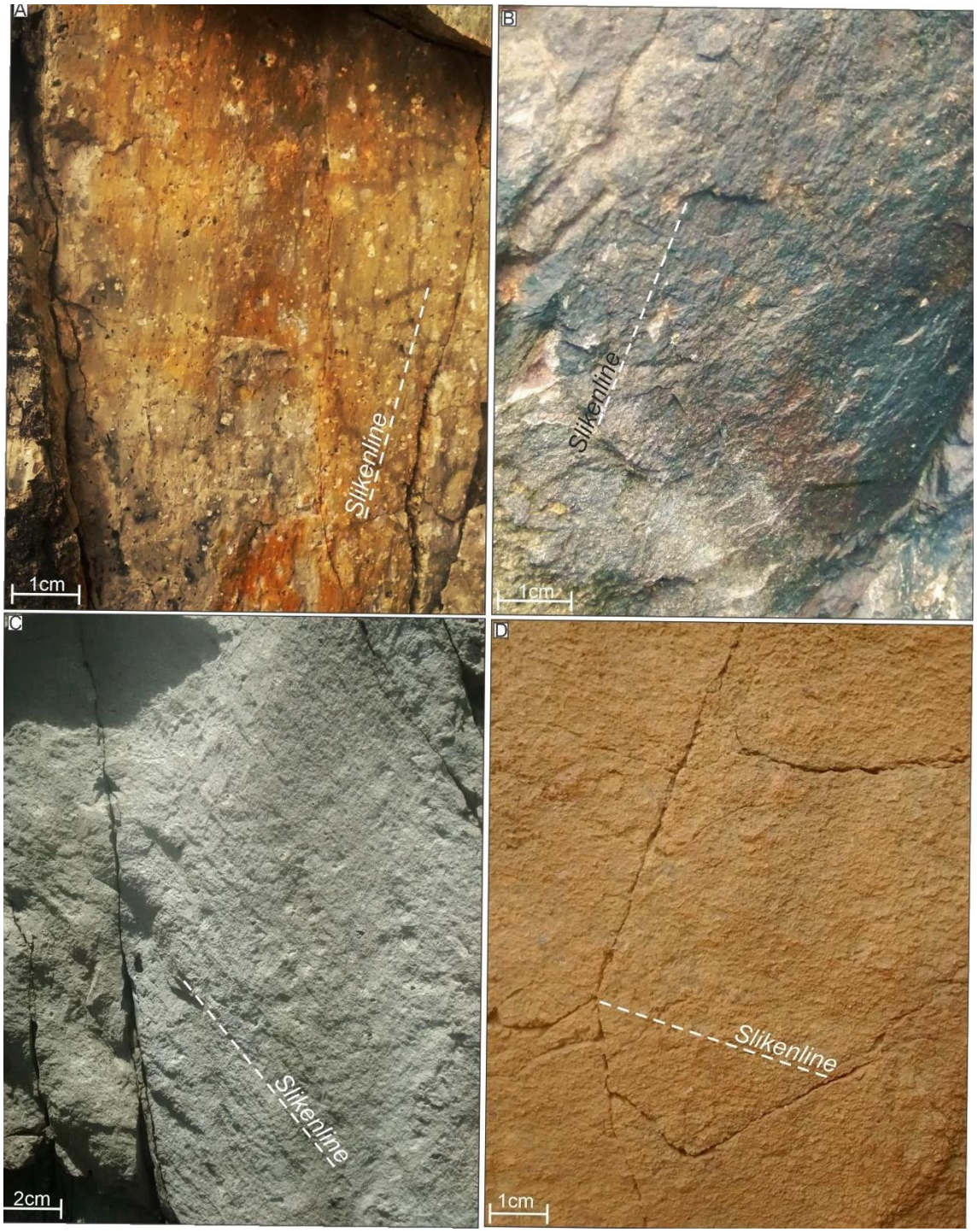

Figura 14 - Planos de falha observados no Arquipélago de Fernando de Noronha. (A, B) Plano de falha com *slickenlines* verticais (70 – 90°) e steps indicando a cinemática normal; (C, D) Planos de falha com estrias horizontais (<70) representando a cinemática indicando a provável componente transtrativa para essas falhas.

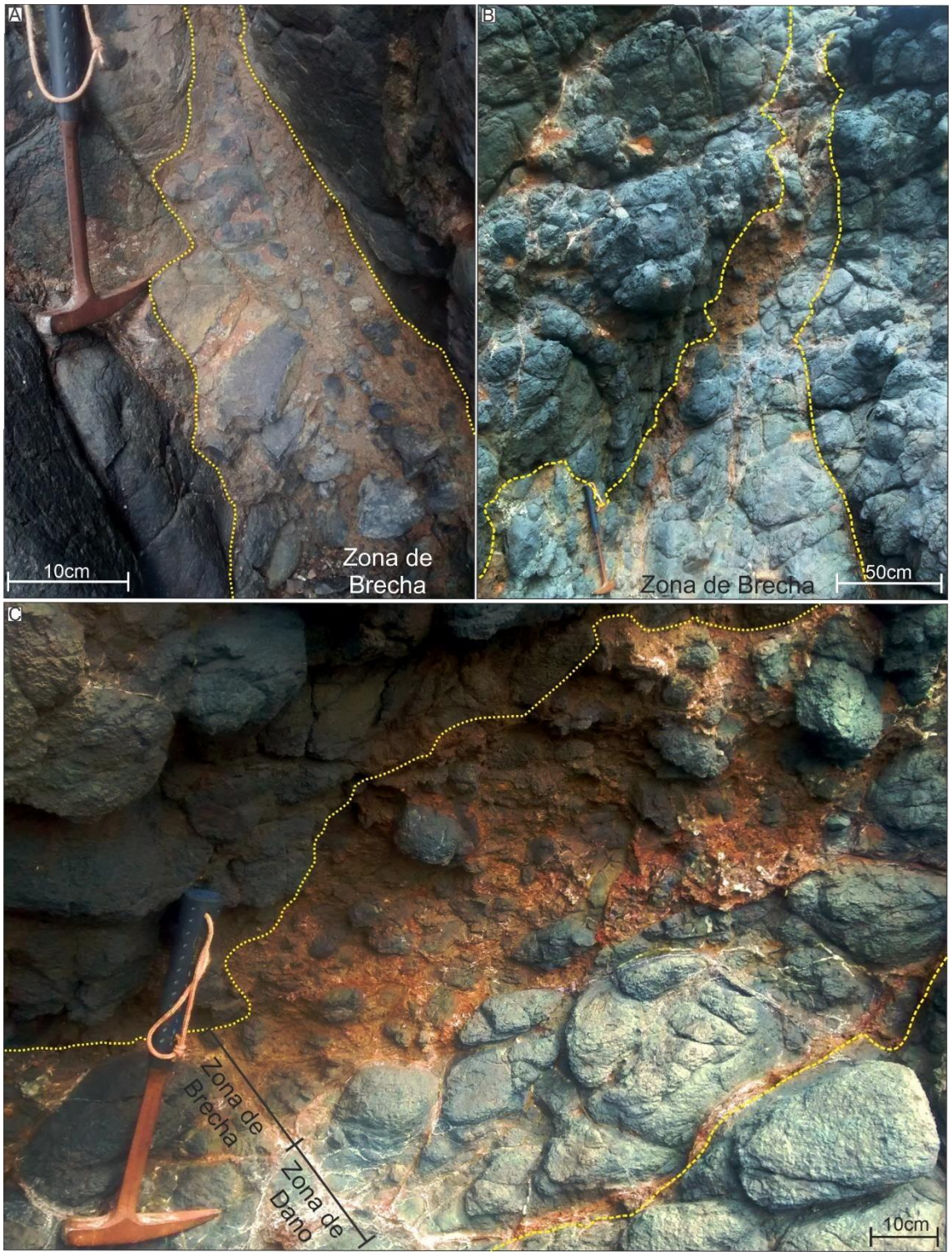

Figura 15 - Fotos de campo de brechas de falhas observadas na Ilha de Fernando de Noronha. (A, B) Zonas de brecha verticalizadas com fragmentos angulares de dimensões variáveis entre 3 e 10cm que são envoltos pela matriz cominuída e argilominerais; (C) Zona de falha inclinada em que se delineia as de brecha e de dano causada pela ação tectônica.

CAPÍTULO IV

4.1. Considerações Finais

As feições deformacionais observadas nos arquipélagos de São Pedro e São Paulo (ASPSP) e ilhas Fernando de Noronha (IFN) e Trindade (IT), apesar de apresentarem distintas peculiaridade geológicas como vulcanismo e variação temporal de formação; são majoritariamente controlados por zonas de fratura transformantes (Figura 16), que propiciam o tectonismo nesses arquipélagos.

Levando-se em conta os eventos deformacionais em planos de falhas observados nos três arquipélagos foi possível constatar distensão tectônica generalizada de direção ESE-WSW, ao longo das zonas transformantes. Sendo, a evolução dessas tensões, intimamente relacionada a eventos sismológicos observados nos arquipélagos, principalmente no ASPSP, o arquipélago mais ativo tectonicamente.

Os movimentos transpressivos relacionados a exumação mantélica do ASPSP (Figura 16B) estão relacionados a íntima relação entre as zonas transformantes e de fraturas, culminando na formação de cadeias de montanhas submarinas distribuídas ao longo de todo o oceano. A compreensão dos esforços primeiramente transpressionais evoluindo para transtrativos coloca esse arquipélago como um dos mais importantes para se observar a interação crosta e manto, além de se conhecer os efeitos das zonas de fraturas sobre a tectônica atlântica.

As ilhas de Trindade e Noronha apesar da certa estabilidade tectônica em que encontram, foi possível estabelecer que a tectônica ainda influencia na formação de falhas e bandas de deformação.

Na Ilha de Trindade se constatou a presença inicial de feições distensionais, formando um conjunto de *horts* e *grabens*, possivelmente associado aos primeiros eventos vulcânicos e tectônicos formadores da ilha. A evolução tectônica e o estabelecimento da tectônica transtrativa (Figura 16C), com a formação de falhas direcionais associadas a dique e falhas, com componente oblíqua, levaram a configuração tectônica atual da IT.

As bandas de deformação observadas na IT são a provável resposta do exercício da tectônica regional na região, por estarem concentradas na unidade mais recente da ilha (Fm. Paredão), devem estar relacionadas a zonas de alívio e a passagem de fluidos e gases durante a formação do Vulcão Paredão.

A coleta de dados estruturais nos três arquipélagos permitiu elucidar e compreender a tectônica regional do Atlântico Sul e a sua íntima relação com as zonas transformantes, que provavelmente agiram desde da formação dessas ilhas oceânicas, que ainda se encontram atuantes na configuração tectônica dos arquipélagos.

A evolução dos trabalhos de cunho tectono-estrutural aliado a outras técnicas, como sísmica de alta resolução, deve proporcionar novas interpretações para a região, contribuindo também para o entendimento da evolução do Oceano Atlântico ao longo do tempo geológico, bem como a compreensão da formação e deformação das ilhas oceânicas pertencentes ao território brasileiro.

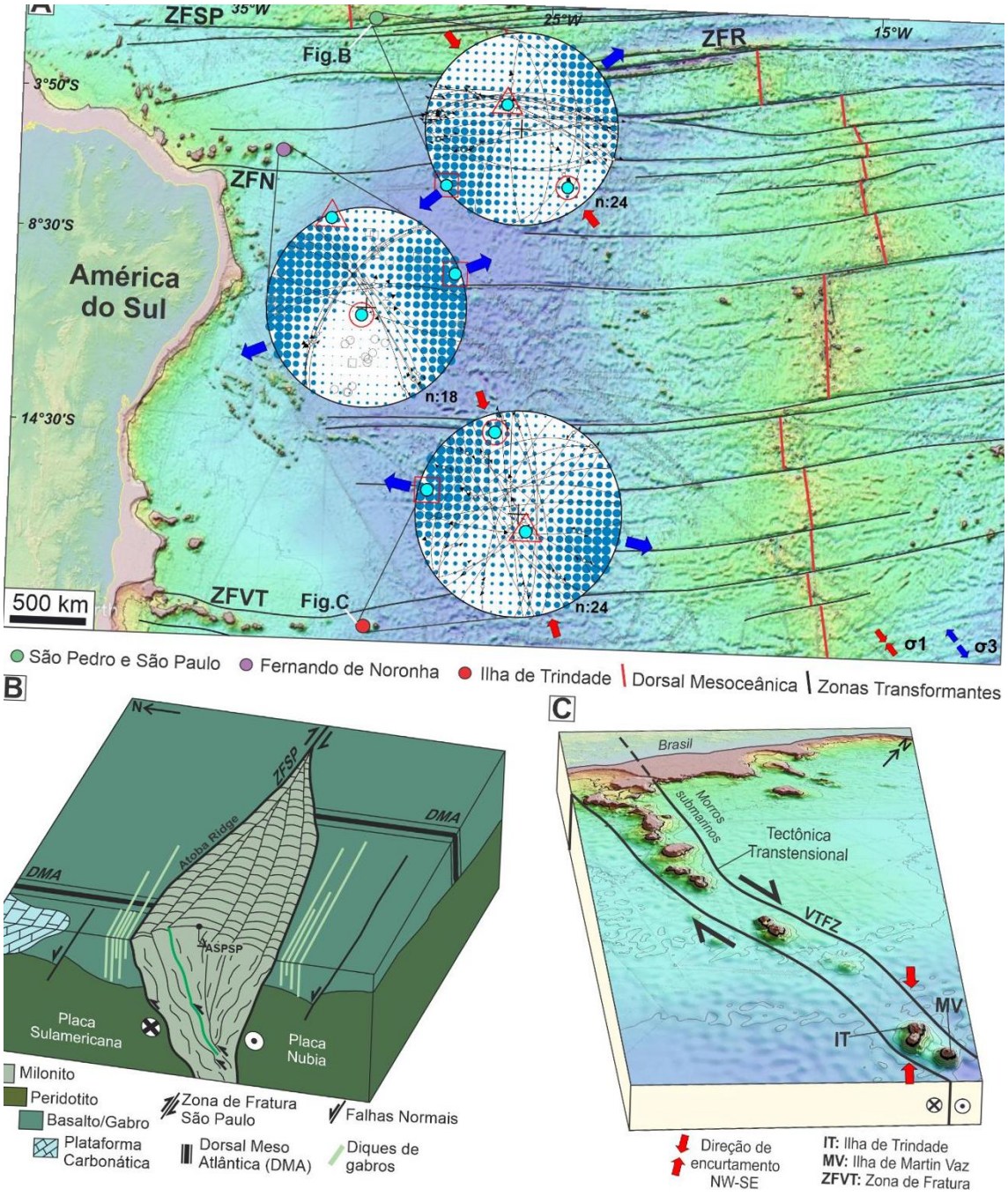

Figura 16 - Ilhas oceânicas e sua relação com a tectônica, destacando-se os arquipélagos de São Pedro e São Paulo (SPSP), Fernando de Noronha (IFN) e Trindade (TI). (A) Distribuição de tensões tectônica para planos de falhas observados nas ilhas de SPSP, FN e IT; (B) Modelo tectônico proposto para o SPSP (Modificado de Barão et al., 2020a); (C) Modelo tectônico proposto para IT (Barão et al., 2020b) .

4.2. Conclusões

A partir do mapeamento e análise microestrutural do arquipélago de São Pedro e São Paulo (ASPSP) e Ilhas de Fernando de Noronha (IFN) e Trindade (IT), foi possível concluir que:

- Ocorre uma contínua evolução da deformação no ASPSP, IFN e IT, que envolve a evolução de Zonas Transformantes, no caso de São Pedro e São Paulo, e de Zonas de Fraturas no caso de Fernando de Noronha e Trindade;
- Em ASPSP fica registrada a rápida transição do momento dúctil, com a deformação e recristalização de minerais como ortopiroxênio e Olivina em temperaturas entre 700 – 800°C;
- A rápida e continua ascenção dessas rochas do manto devido a ação da transpressional da Zona Transformante São Paulo faz com que ocorra a reativação de estruturas formadas anteriormente, evoluindo primeiramente para o estágio *semi-brittle*, e até sua completa assenção para a deformação rúptil com a formação de cataclasitos e brechas de falhas;
- A presença de fluidos é essencial tanto para a deformação, quanto para assenção do bloco mantélico que encontra-se o ASPSP. Formando incialmente níveis ricos em anfibólio e quatro fases de serpentinização;
- Na Ilha de Trindade foi indendificado dois tensores tectônicos distintos, o primeiro marcado pela distenção afetando as rochas vulcânicas formadas no Plesitoceno Inferior, formando principalmente falhas normais nesse contexto;

- Já o segundo evento é marcado pela ação a Zona de Fratura Vitória-Trindade, com tensões principais de direção NW-SE afetando diretamente a formação dos diques fonolíticos, controlando a tectônica da Ilha de Trindade até atualmente;
- No último evento de Trindade fica registrado a formação das bandas de deformação em tufos vulcânicos, principalmente associados a pares conjugados e falhas normais. Essas estruturas são marcadas pela redução drástica da porosidade e pelos mecanismos de deformação fluxo granular e catáclase que predominam ao longo dessas estruturas;

REFERÊNCIAS

Almeida F.F.M.de. 1955. Geologia e petrologia do Arquipélago de Fernando de Noronha. Rio de Janeiro, DGM/IBGE. 181p.

Almeida F.F.M.de. 1961. Geologia e Petrologia da Ilha da Trindade. Rio de Janeiro, DGM/DNPM. 206p.

Almeida, F., 2006. Ilhas oceânicas brasileiras e suas relações com a tectônica atlântica. Terrae Didatica 2, 3–18. https://doi.org/10.1007/BF01915460

Almeida, F.F.M., 2002. Arquipélago de Fernando de Noronha - Registro de monte vulcânico do Atlântico Sul. Sítios Geológicos e Paleontológicos do Brasil 1, 362-368

Alikarami, R., Torabi, A., Kolyukhin, D., Skurtveit, E., 2013. Geostatistical relationships between mechanical and petrophysical properties of deformed sandstone. International Journal of Rock Mechanics and Mining Sciences 63, 27–38. https://doi.org/10.1016/j.ijrmms.2013.06.002

Alves, E.C., Maia, M., Sichel, S.E., De Campos, C.M.P., 2006. Zona de fratura de vitória-trindade no oceano atlântico sudeste e suas implicações tectônicas. Revista Brasileira de Geofisica 24, 117–127. https://doi.org/10.1590/S0102-261X2006000100009

Anderson, E.M., 1936. The Dynamics of the Formation of Cone-sheets , Ring-dykes, and Caldron-subsidences. Hafner Publication Comapny, Edinburgh.

Andrade, F., Simões, L.S.., Navarro, G.R.B., Campos, T.F.C., 2006. Padrão estrutural da foliação milonítica do arquipélago de São Pedro e São Paulo.pdf. Congresso Brasileiro de Geologia, 43. ST04-523.

Andreani, M., Boullier, A., Gratier, J., 2005. Development of schistosity by dissolution – crystallization in a Californian serpentinite gouge. 27, 2256–

2267. https://doi.org/10.1016/j.jsg.2005.08.004

Andreani, M., Luquot, L., Gouze, P., Godard, M., Gibert, B., 2009. Experimental study of carbon sequestration reactions controlled by the percolation of CO_2-rich brine through peridotites. Environmental Science and Technology 43, 1226–1231.

Andreani, M., Mével, C., Boullier, A.M., Escartín, J., 2007. Dynamic control on serpentine crystallization in veins: Constraints on hydration processes in oceanic peridotites. Geochemistry, Geophysics, Geosystems 8, 1–24. https://doi.org/10.1029/2006GC001373

Andreani, M., Muñoz, M., Marcaillou, C., Delacour, A., 2013. Lithos μ XANES study of iron redox state in serpentine during oceanic serpentinization. LITHOS 178, 70–83. https://doi.org/10.1016/j.lithos.2013.04.008

Andreani, M.U., Baronnet, A.L., Boullier, A.., Gratier, J.P., 2004. A microstructural study of a “ crack-seal ” type serpentine vein using SEM and TEM techniques. Eur. J. Mineral. 16, 585–595. https://doi.org/10.1127/0935-1221/2004/0016-0585

Angelier, J., 1994. Fault slip analysis and palaeostress reconstruction. Continental Deformation 53–100.

Angelier, J., Mechler, P., 1977. Sur une methode graphique de recherche des contraintes principales egalement utilisables en tectonique et en seismologie : la methode des diedres droits. Bulletin de La Societe Geologique de France S7-XIX, 1309–1318. https://doi.org/10.2113/gssgfbull.s7-xix.6.1309

Angulo, R.J., Souza, M.C. de, Campos, T.F.C., Bezerra, F.H.R., Fernandes, L.A., Giannini, P.C.F., Pitombo, F.B., Veiga, F.A., 2013. Evidence for late

quaternary episodic uplift of the São Pedro and São Paulo Archipelago, Equatorial Atlantic. Quaternary International 317, 102–111. https://doi.org/10.1016/j.quaint.2013.06.023

Angulo, R. J., Souza, M. C., Barboza, E. G., Rosa, M. L. C., Fernandes, L. A., Guedes, C. C. F., Oliveira, L. H. S., Manzolli, R. P., Disaró, S. T., Ferreira, A. G., Martin, C. M., 2018. Quaternary sealevel changes and coastal evolution of the Island of Trindade,Brazil. J. South Am. Earth Sci. 84, 208–222. https://doi.org/10.1016/j.jsames.2018.04.003.

Antonellini, M., Aydin, A., 1995. Effect of Faulting on Fluid-Flow Geometry and Spatial-Distribution. AAPG Bulletin 79, 642–671. https://doi.org/10.1306/8D2B1B60-171E-11D7-8645000102C1865D

Antonellini, M.A., Pollard, D.D., 1995. Distinct element modeling of deformation bands in sandstone. Journal of Structural Geology 17, 1165–1182. https://doi.org/10.1016/0191-8141(95)00001-T

Assumpcao, M., 1992. The regional intraplate stress field in South America. Journal of Geophysical Research 97, 11889. https://doi.org/10.1029/91JB01590

Aydin, A., 1978. Small faults formed as deformation bands in sandstone. Pure and Applied Geophysics PAGEOPH 116, 913–930. https://doi.org/10.1007/BF00876546

Aydin, A., Johnson, M., 1978. Development of Faults as Zones of Deformation Bands and as Slip Surfaces in Sandstone. Pageoph 116.

Babaie, H.A., La Tour, T.E., 1994. Semibrittle and cataclastic deformation of hornblende-quartz rocks in a ductile shear zone. Tectonophysics 229, 19–30. https://doi.org/10.1016/0040-1951(94)90003-5

Ballas, G., Fossen, H., Soliva, R., 2015. Factors controlling permeability of cataclastic deformation bands and faults in porous sandstone reservoirs. Journal of Structural Geology 76, 1–21. https://doi.org/10.1016/j.jsg.2015.03.013

Balsamo, F., Storti, F. 2010. Grain size and permeability evolution of soft-sediment extensional sub-seismic and seismic fault zones in high-porosity sediments from the Crotone basin, southern Apennines, Italy. Marine and Petroleum Geology 27, 822-837. http://dx.doi.org/10.1016/j.marpetgeo.2009.10.016

Balsamo, F., Storti, F., Salvini, F., Silva, A.T., Lima, C.C., 2010. Structural and petrophysical evolution of extensional fault zones in low-porosity, poorly lithified sandstones of the Barreiras Formation, NE Brazil. Journal of Structural Geology 32, 1806–1826. https://doi.org/10.1016/j.jsg.2009.10.010

Barão, L.M., Trzaskos, B., Angulo, R.J., Souza, M.C. de, 2020a. Deformation and structural evolution of mantle peridotites during exhumation on transform faults: A forced transition from ductile to brittle regime. Journal of Structural Geology 133. https://doi.org/10.1016/j.jsg.2020.103981

Barão, L.M., Trzaskos, B., Angulo, R.J., Souza, M.C. De, 2018a. Análise Qualitativa Fractal das estruturas nas Ilhas Belmonte e Challenger e sua relação com a estruturação local - Arquipélago de São Pedro e São Paulo. In: Lins Oliveira, J.E., Viana, D. de L., Souza, M.A.C. de. V.M. (Eds.), Arquipélago de São Pedro e São Paulo -20 Anos de Pesquisa. Via Design Publicações, Recife, 211–224.

Barão, L.M., Trzaskos, B., Angulo, R.J., Souza, M.C. de, Daufenbach, H.F., Santos, F.A., Gouvêa Vasconcellos, E.M., 2020b. Deformational structures

developed in volcanic sequences as a product of tectonic adjustments in the South Atlantic Ocean. Journal of South American Earth Sciences 104. https://doi.org/10.1016/j.jsames.2020.102812

Barão, L. M., Trzaskos, B., Angulo, R.J., Souza, M.C., Avelar, F., Garcia, M.H., Oliveira, L.S., 2018. Feições estruturais observadas nas ilhas de Trindade e Fernando de Noronha e sua relação com tectônica atual. 49º Congresso Brasileiro de Geologia. Sociedade Brasileira de Geologia, Rio de Janeiro, 1.

Bemis, S.P., Micklethwaite, S., Turner, D., James, M.R., Akciz, S., T. Thiele, S., Bangash, H.A., 2014. Ground-based and UAV-Based photogrammetry: A multi-scale, high-resolution mapping tool for structural geology and paleoseismology. Journal of Structural Geology 69, 163–178. https://doi.org/10.1016/j.jsg.2014.10.007

Bestmann, M., Pennacchioni, G., Nielsen, S., Göken, M., Wall, H. De, 2012. Deformation and ultra fi ne dynamic recrystallization of quartz in pseudotachylyte- bearing brittle faults : A matter of a few seconds. Journal of Structural Geology 38, 21–38. https://doi.org/10.1016/j.jsg.2011.10.001

Birner, S.K., Warren, J.M., Cottrell, E., Davis, F.A., 2016. Hydrothermal alteration of seafloor peridotites does not influence oxygen fugacity recorded by spinel oxybarometry. Geology 44, 535–538. https://doi.org/10.1130/G38113.1

Bistacchi, A., Tibaldi, A., Pasquarè, F.A., Rust, D., 2012. The association of cone-sheets and radial dykes: Data from the Isle of Skye (UK), numerical modelling, and implications for shallow magma chambers. Earth and Planetary Science Letters 339–340, 46–56. https://doi.org/10.1016/j.epsl.2012.05.020

Blaich, O.A., Faleide, J.I., Tsikalas, F., 2011. Crustal breakup and continent-

ocean transition at South Atlantic conjugate margins. Journal of Geophysical Research: Solid Earth 116, 1–38. https://doi.org/10.1029/2010JB007686

Blenkinsop, T.G., Rutter, E.H., 1986. Cataclastic deformation of quartzite in the Moine thrust zone. Journal of Structural Geology 8, 669–681.

Bonatti, E., 1978. Vertical tectonism in oceanic fracture zones. Earth and Planetary Science Letters 37, 369–379. https://doi.org/10.1016/0012-821X(78)90052-3

Bonatti, E., 1971. Ancient continental mantle beneath oceanic ridges. Journal of Geophysical Research 76, 3825–3831. https://doi.org/10.1029/JB076i017p03825

Bonatti, E., Crane, K., 1982. Oscillatory spreading explanation of anomalously old uplifted crust near oceanic transforms., Nature. https://doi.org/10.1038/300343a0

Bonatti, E., Emiliani, C., Ferrara, G., Honnorez, J., Rydell, H., 1974. Ultramafic-carbonate breccias from the equatorial Mid Atlantic Ridge. Marine Geology 16, 83–102. https://doi.org/10.1016/0025-3227(74)90057-7

Bonatti, E. 1990. Subcontinetal mantle exposed in the Atlantic Icean on St Peter-Paul islets. Letters to Nature 345, 800-802

Bonatti, E., Ligi, M., Gasperini, L., Peyve, A., Raznitsin, Y., Chen, Y.J., 1994. Transform migration and vertical tectonics at the Romanche fracture zone, equatorial Atlantic. Journal of Geophysical Research 99802, 779–21. https://doi.org/10.1029/94JB01178

Bonatti, E., Peyve, A., Kepezhinskas, P., Kurentsova, N., Seyler, M., Skolotnev, S., Udintsev, G., 1992. Upper mantle heterogeneity below the Mid-Atlantic Ridge, 0°–15°N. Journal of Geophysical Research 97, 4461.

https://doi.org/10.1029/91JB02838

Bons, P.D., Elburg, M.A., Gomez-Rivas, E., 2012. A review of the formation of tectonic veins and their microstructures. Journal of Structural Geology 43, 33–62. https://doi.org/10.1016/j.jsg.2012.07.005

Borg, I., Handin, J., 1966. Experimental deformation of crystalline rocks. Tectonophysics

3 (4), 249–367. https://doi.org/10.1016/0040-1951(66)90019-9.

Brasil, 1989. Plano de Levantamento da Plataforma Continental Brasilera [WWW Document].

Campos, T.F.., Virgens Neto, J., Amorim, V.A., Hartmann, L.A., Petta, R.A., 2003a. Modificações metassomáticas das rochas milonitizadas do complexo ultramáfico do Arquipélago de São Pedro e São Paulo, Atlântico Equatorial. Geochimica Brasiliensis 17, 81–90.

Campos, T.F.C., Bezerra, F.H.R., Petta, R.A., Virgens Das, J., Srivastava, N.K., Macambira, M., Amaral, R., 2003b. Novos dados Litoestratigráficos da Formação São Pedro e São Paulo (Atlântco Equatorial): Implicações Tectônicas e Eustáticas. II Congresso Sobre Planejamento e Gestão Das Zonas Costeiras Dos Países de Expressão Portuguesa II Congresso Sobre Planejamento e Gestão Das Zonas Costeiras Dos Países de Expressão Portuguesa II Congresso Do Quaternário Dos Países de Língua Ibéricas. 284–285.

Campos, T.F.C., Bezerra, F.H.R., Srivastava, N.K., Vieira, M.M., Vita-Finzi, C., 2010. Holocene tectonic uplift of the St Peter and St Paul Rocks (Equatorial Atlantic) consistent with emplacement by extrusion. Marine Geology 271, 177–186. https://doi.org/10.1016/j.margeo.2010.02.013

Campos, T.F.C., Francisco, H.F., Srivastava, N.K., Petta, R.A., Neto, J.., 2009a. As rochas sedimentares e a formação neogênica de São Pedro e São Paulo. In: Viana, D.L.; Hazin, F.H.V.; Souza, M.A.C. (Ed.), O Arquipélago de São Pedro e São Paulo: 10 Anos de Estação Cientíifica. SECIRM, Brasília-DF, 74–81.

Campos, T.F.C., Petta, R.A., Theye, T., Sichel, S.E., Simões, L.S.A., Srivastava, N.K., Motoki, A., Neto, J.V., Andrade, F.G.G., 2009b. Posição ímpar do Arquipélago de São Pedro e São Paulo na diversidade geológica da Terra. In: Viana, D.L.; Hazin, F.H.V.; Souza, M.A.C. (Ed.), O Arquipélago de São Pedro e São Paulo: 10 Anos de Estação Cientíifica. SECIRM, Brasília-DF, 54–62.

Carioca, A.C., Brandão, P.R.G., 2018. Itabiríticos Principalmente Por Mineral Liberation Analyzer (Mla) Mineralogical Characterization of Itabiritic Iron Ores. Tecnol. Metal. Mater. Miner 15, 415–421.

Carneiro, C. D. R., Hamza, V. M., Almeida, F. F. M. de. 1989. Ativação Tectônica, Fluxo Geotérmico e Sismicidade no Nordeste Oriental Brasileiro – Revista Brasileira de Geociências, São Paulo-SP 19 (3), 310-322.

Carracedo, J.C., 1996. The Canary Islands : an example of structural control on the growth of large oceanic-island volcanoes. Journal of Volcaology and Geothermal Research 60, 225–241.

Carter, N.L., Officer, C.B., Drake, C.L., 1990. Dynamic deformation of quartz and feldspar : clues to causes of some natural crises. Tectonophysics 171, 373–391.

Cavailhes, T., Rotevatn, A., 2018. Deformation bands in volcaniclastic rocks – Insights from the Shihtiping tuffs, Coastal Range of Taiwan. Journal of

Structural Geology 113, 155–175. https://doi.org/10.1016/j.jsg.2018.06.004

Centrella, S., Putnis, A., Lanari, P., Austrheim, H., 2018. Textural and chemical evolution of pyroxene during hydration and deformation: A consequence of retrograde metamorphism. Lithos 296–299, 245–264. https://doi.org/10.1016/j. lithos.2017.11.002.

Ceriani, S., Mancktelow, N.S., Pennacchioni, G., 2003. Analogue modelling of the influence of shape and particle/matrix interfacelubrication on the rotational behaviour of rigid particles in simple shear. Journal of Structural Geology 25, 2005–2021. https://doi.org/10.1016/S0191-8141(03)00098-1

Champness, P.E., Lorimer, G.W., 1973. Precipitation (exsolution) in an orthopyroxene. Journal of Materials Science 8, 467–474. https://doi.org/10.1007/BF00550450

Cilona, A., Baud, P., Tondi, E., Agosta, F., Vinciguerra, S., Rustichelli, A., Spiers, C.J., 2012. Deformation bands in porous carbonate grainstones: Field and laboratory observations. Journal of Structural Geology 45, 137–157. https://doi.org/10.1016/j.jsg.2012.04.012

Cimarelli, C., De Rita, D., 2006. Structural evolution of the Pleistocene Cimini trachytic volcanic complex (Central Italy). Bulletin of Volcanology 68, 538–548. https://doi.org/10.1007/s00445-005-0028-3

Cladouhos, T. T. 1999. Shape preferred orientations of survivor grains in fault gouge. Journal of Structural Geology 21(4), 419 - 436. https://doi.org/10.1016/S0191-8141(98)00123-0

Coelho, S., Passchier, C., Marques, F., 2006. Riedel-shear control on the development of pennant veins: Field example and analogue modelling. Journal of Structural Geology 28, 1658–1669.

https://doi.org/10.1016/j.jsg.2006.05.009

Compton, K.E., Kirkpatrick, J.D., Holk, G.J., 2017. Cyclical shear fracture and viscous flow during transitional ductile-brittle deformation in the Saddlebag Lake Shear Zone, California. Tectonophysics 708, 1–14. https://doi.org/10.1016/j.tecto.2017.04.006

Cordani, U.G., 1970. Idade do vulcanismo no Oceano Atlântico Sul. Boletim IGA 1, 9–75.

Correa-Gomes, L.C., Souza, M.N. De, Correa, D.R., Silva, I.R., Falcão, A.C.S., Cobucci, M.L.P., Ishioka, K.J., Espineira, A.R., Moraes, J.W.O., 1991. Mafic dykes: relationships among geometry, internal fractures and fissural tectonic patterns. Boletim IG-USP. Publicação Especial 1–8. https://doi.org/10.11606/issn.2317-8078.v0i10p01-08

Costa P.R.C., Antunes A.F., Sá E.F.J. de, Amaro V.E., Matos R.M.D.de. 2002. O registro da deforma- ção mesozóica relacionada à abertura da margem equatorial atlântica no litoral do Estado do Ceará (Nordeste do Brasil): evidências a partir da análise de imagens orbitais e de afloramentos. In: Cong. Bras. Geol., 41, João Pessoa. 2002. Anais do Congresso Brasileiro de Geologia, 623.

Crider, J.G., Peacock, D.C.P., 2004. Initiation of brittle faults in the upper crust : a review of field observations. 26, 691–707. https://doi.org/10.1016/j.jsg.2003.07.007

Czertowicz, T.A., Toy, V.G., Scott, J.M., 2016. Recrystallisation, Phase mixing and strain localisation in peridotite during rapid extrusion of sub-arc mantle lithosphere. Journal of Structural Geology 88, 1–19. https://doi.org/10.1016/j.jsg.2016.04.011

Darwin, C., 1844. Geological Observations on the Volcanic Islands and Parts of South America Visited During The Voyage of H.M.S “Beagle,” 1st ed. Smith Elder and Co, London.

Davison, I., 1999. Tectonics and hydrocarbon distribution along the Brazilian South Atlantic margin. Geological Society, London, Special Publications 153, 133–151. https://doi.org/10.1144/gsl.sp.1999.153.01.09

Davy, P., Bour, O., De Dreuzy, J.-R., Darcel, C., 2008. Flow in multiscale fractal fracture networks. Geological Society, London, Special Publications 261, 31–45. https://doi.org/10.1144/gsl.sp.2006.261.01.03

De Rita, D., Funiciello, R., Rossi, U., Sposato, A., 1983. Structure and evolution of the Sacrofano-Baccano caldera, Sabatini volcanic complex, Rome. Journal of Volcanology and Geothermal Research 17, 219–236. https://doi.org/10.1016/0377-0273(83)90069-0

Del Sole, L., Antonellini, M., 2019. Microstructural, petrophysical, and mechanical properties of compactive shear bands associated to calcite cement concretions in arkose sandstone. Journal of Structural Geology 126, 51–68. https://doi.org/10.1016/j.jsg.2019.05.007

Delaney, P.T., Pollard, D.D., 1981. Deformation of Host Rocks and Flow of Magma during Growth of Minette Dikes and Breccia-bearing Intrusions near Ship Rock, New Mexico Library of Congress Cataloging in Publication Data, Intrusions (Geology).

Delvaux, D., 2012. Release of program Win-Tensor 4.0 for tectonic stress inversion: statistical expression of stress parameters. EGU General Assembly Conference Abstracts 14, 5899. https://doi.org/10.13140/RG.2.2.23415.62887

Dering, G.M., Micklethwaite, S., Cruden, A.R., Barnes, S.J., Fiorentini, M.L., 2019. Evidence for dyke-parallel shear during syn-intrusion fracturing. Earth and Planetary Science Letters 507, 119–130. https://doi.org/10.1016/j.epsl.2018.10.024

DHN - Diretoria de Hidrografia e Navegação, 1971. Carta náutica Ilha da Trindade n. 21, scale 1:15,000.

Dick, H.J.B., Sinton, J.M., 1979. Compositional Layering in Alpine Peridotites: Evidence For Pressure Solution. Journal of Geology 87, 403–416.

Dimmen, V., Rotevatn, A., Peacock, D.C.P., Nixon, C.W., Nærland, K., 2017. Quantifying structural controls on fluid flow: Insights from carbonate-hosted fault damage zones on the Maltese Islands. Journal of Structural Geology 101, 43–57. https://doi.org/10.1016/j.jsg.2017.05.012

Dinwiddie, C.L., Bradbury, K.K., McGinnis, R.N., Fedors, R.W., Ferrill, D.A., 2006. Fault zone deformation overprints permeability of nonwelded ignimbrite: Chalk cove fault, Bishop Tuff, Bishop, California. Vadose Zone Journal 5, 610–627. https://doi.org/10.2136/vzj2005.0062

Dinwiddie, C.L., Bradbury, K.K., McGinnis, R.N., Stillman, D.E., Ferrill, D.A., 2012. Hydrogeologic heterogeneity of faulted and fractured Glass Mountain bedded tuffaceous sediments and ash-fall deposits: The Crucifix site near Bishop, California. Lithosphere 4, 40–62. https://doi.org/10.1130/L179.1

Doblas, M., 1998. Slickenside kinematic indicators. Tectonophysics 295, 187–197. https://doi.org/10.1016/S0040-1951(98)00120-6

Dollinger, G., Blacic, J.D., 1975. Deformation mechanisms in experimentally and naturally deformed amphiboles. Earth and Planetary Science Letters 26, 409–416. https://doi.org/10.1016/0012-821X(75)90016-3

Drury, M.R., Avé Lallemant, H.G., Pennock, G.M., Palasse, L.N., 2011. Crystal preferred orientation in peridotite ultramylonites deformed by grain size sensitive creep, étang de Lers, Pyrenees, France. Journal of Structural Geology 33, 1776–1789. https://doi.org/10.1016/j.jsg.2011.10.002

Dungan, M. a, 1979. A microprobe study of antigorite and some serpentine pseudomorphs. Canadian Mineralogist 17, 771–784.

Ernesto, M., 2005. Paleomagnetism of the Post-Paleozoic Alkaline Magmatism in the Brazilian Platform : Questioning the Mantle Plume Model. Mesozoic to Cenozoic Alkaline Magmatism in the Brazilian Platform 689–705. https://doi.org/10.13140/2.1.1240.6725

Evans, J.P., 1988. Deformation mechanisms in granitic rocks at shallow crustal levels Type 1 small-displacement faults Protolith. Journal of Structural Geology 1, 437–443.

Evans, J.P., Bradbury, K.K., 2004. Faulting and fracturing of nonwelded bishop tuff, Eastern California: Deformation mechanisms in very porous materials in the vadose zone. Vadose Zone Journal 3, 602–623. https://doi.org/10.2113/3.2.602

Exner, U., Tschegg, C. 2012. Preferential cataclastic grain size reduction of feldspar in deformation bands in poorly consolidated arkosic sands. Journal of Structural Geology 43, 63-72. http://dx.doi.org/10.1016/j.jsg.2012.08.005

Ferrari, L.A., Riccomini, C., 1999. Campo De Esforços Plio-Pleistocênico Na Ilha Da Trindade (Oceano Atlântico Sul , Brasil) E Sua Relação Com a Tectônica Regional. Revista Brasileira de Geociencias 29, 195–202.

Ferreira, T., Rasband, W., 2012. ImageJ User Guide, Image J user Guide. https://doi.org/10.1038/nmeth.2019

Forslund, T., Gudmundsson, A., 1992. Structure of Tertiary and Pleistocene Normal Faults in Iceland. Tectonics 11, 57–68.

Fossen, H., Cavalcante, G.C.G., Pinheiro, R.V.L., Archanjo, C.J., 2018a. Deformation – Progressive or multiphase? Journal of Structural Geology. https://doi.org/10.1016/j.jsg.2018.05.006

Fossen, H., Schultz, R.A., Shipton, Z.K., Karen, M., 2007. Deformation bands in sandstone: a review. 164, 755–769.

Fossen, H., Soliva, R., Ballas, G., Trzaskos, B., Cavalcante, C., Schultz, R.A., 2018b. A review of deformation bands in reservoir sandstones: Geometries, mechanisms and distribution. Geological Society Special Publication 459, 9–33. https://doi.org/10.1144/SP459.4

Francheteau J., Pichon, X.L., 1972. Marginal Fracture Zones as Structural Framework of Continental Margins in South Atlantic Ocean. AAPG Bulletin 56, 991–1007. https://doi.org/10.1306/819A40A8-16C5-11D7-8645000102C1865D

Frets, E., Tommasi, A., Garrido, C.J., Padrón-navarta, J.A., Amri, I., 2012. Deformation processes and rheology of pyroxenites under lithospheric mantle conditions. Journal of Structural Geology 39, 138–157. https://doi.org/10.1016/j.jsg.2012.02.019

Früh-Green, G.L., Weissert, H., Bernoulli, D., 1990. Multiple Fluid History Recorded. Journal of the Geological Society 147, 959–970.

Gasperini, L., Carrara Marco Ligi, G., Fabretti, P., Brunelli, D., Cipriani, A., Susini, S., Tartarotti, P., 1997. New data on the geology of the Romanche FZ., equatorial Atlantic: PRIMAR-96 cruise report. 3, 1–2.

Genna, A., Jébrak, M., Marcoux, E., Milési, J.P., 1996. Genesis of cockade

breccias in the tectonic evolution of the Cirotan epithermal gold system, West Java. Canadian Journal of Earth Sciences 33, 93–102. https://doi.org/10.1139/e96-010

Getsinger, A.J., Hirth, G., 2014. Amphibole fabric formation during diffusion creep and the rheology of shear zones. Geology 42, 535–538. https://doi.org/10.1130/G35327.1

Gibson, S.A., Thompson, R.N., Day, J.A., 2006. Timescales and mechanisms of plume-lithosphere interactions: 40Ar/39Ar geochronology and geochemistry of alkaline igneous rocks from the Paraná-Etendeka large igneous province. Earth and Planetary Science Letters 251, 1–17. https://doi.org/10.1016/j.epsl.2006.08.004

Godard, M., Luquot, L., Andreani, M., Gouze, P., 2013. Incipient hydration of mantle lithosphere at ridges: A reactive-percolation experiment. Earth and Planetary Science Letters 371–372, 92–102. https://doi.org/10.1016/j.epsl.2013.03.052

Grady, D.E., Kipp, M.E., 1987. The growth of unstable thermoplastic shear with application to steady-wave shock compression in solids*. Journal of the Mechanics and Physics of Solids 35, 95–119. https://doi.org/10.1016/0022-5096(87)90030-5

Grohmann, C.H. and Campanha, G.A.C., 2010. OpenStereo: open source, cross-platform software for structural geology analysis. AGU 2010 Fall Meeting. San Francisco, CA.

Grove, C., Jerram, D.A., 2011. JPOR: An ImageJ macro to quantify total optical porosity from blue-stained thin sections. Computers and Geosciences 37, 1850–1859. https://doi.org/10.1016/j.cageo.2011.03.002

Gudmundsson, A., 2011. Deflection of dykes into sills at discontinuities and magma-chamber formation. Tectonophysics 500, 50–64. https://doi.org/10.1016/j.tecto.2009.10.015

Gumbsch, P., 2001. Modelling brittle and semi-brittle fracture processes. Materials Science and Engineering 319–321, 1–7.

Haddon, I.G., McCarthy, T.S., 2005. The Mesozoic-Cenozoic interior sag basins of Central Africa: The Late-Cretaceous-Cenozoic Kalahari and Okavango basins. Journal of African Earth Sciences 43, 316–333. https://doi.org/10.1016/j.jafrearsci.2005.07.008

Hadizadeh, J., Tullis, J.A.N., 1992. Cataclastic flow and semi-brittle deformation of anorthosite. 14.

Hancock, P.L., 1985. Brittle microtectonics: principles and practice. 7.

Hartman, S.M., Paterson, S.R., Holk, G.J., Kirkpatrick, J.D., 2018. Structural and hydrothermal evolution of a strike-slip shear zone during a ductile-brittle transition, Sierra Nevada, CA. Journal of Structural Geology 113, 134–154. https://doi.org/10.1016/j.jsg.2018.05.010

Hartnady, C.J.H., le Roex, A.P., 1985. Southern Ocean hotspot tracks and the Cenozoic absolute motion of the African, Antarctic, and South American plates. Earth and Planetary Science Letters 75, 245–257. https://doi.org/10.1016/0012-821X(85)90106-2

Hawkesworth, C., Kelley, S., Turner, S., Roex, A.L.E., Storey, B., 1999. Mantle processes during Gondwana break-up and dispersal. Journal of African Earth Sciences 28, 239–261. https://doi.org/10.1016/S0899-5362(99)00026-3

Heidbach, O., Mojtaba, R., Reiter, K., Ziegler, M., 2016. World Stress Map 2016.

70, 1987–1989. https://doi.org/10.5880/WSM.2016.001.0

Heidbach, O., Rajabi, M., Cui, X., Fuchs, K., Müller, B., Reinecker, J., Reiter, K., Tingay, M., Wenzel, F., Xie, F., Ziegler, M.O., Zoback, Mary Lou, Zoback, Mark, 2018. The World Stress Map database release 2016: Crustal stress pattern across scales. Tectonophysics 744, 484–498. https://doi.org/10.1016/j.tecto.2018.07.007

Hekinian, R., Juteau, T., Gràcia, E., Sichler, B., Sichel, S., Udintsev, G., Apprioual, R., Ligi, M., 2000. Submersible observations of equatorial atlantic mantle: The St. Paul Fracture Zone region. Marine Geophysical Researches 21, 529–560. https://doi.org/10.1023/A:1004819701870

Hensen, C., Duarte, J.C., Vannucchi, P., Mazzini, A., Lever, M.A., Terrinha, P., Géli, L., Henry, P., Villinger, H., Morgan, J., Scmidt, M., Gutscher, M., Barolome, R., Tomonaga, Y., Polona, A., Gràcia, E., Tinivella, U., Luppi, M., Çagatay, M.N., Elvert, M., Sakellariou, D., Matias, L., Kipfer, R., Karageorgis, A.P., Ruffine, L., Liebetrau, V., Catherine, P., Schmidt, C., Batista, L., Gasperini, L., Burwicz, E., Neres, M., Nuzzo, M., 2019. Marine Transform Faults and Fracture Zones: A Joint Perspective Integrating Seismicity, Fluid Flow and Life. Frontiers in Earth Science 7, 29. https://doi.org/10.3389/feart.2019.00039

Hirauchi, K., Katayama, I., 2013. Tectonophysics Rheological contrast between serpentine species and implications for slab – mantle wedge decoupling. Tectonophysics 608, 545–551. https://doi.org/10.1016/j.tecto.2013.08.027

Hirose, T., Bystricky, M., Kunze, K., Stünitz, H., 2006. Semi-brittle flow during dehydration of lizardite-chrysotile serpentinite deformed in torsion: Implications for the rheology of oceanic lithosphere. Earth and Planetary

Science Letters 249, 484–493. https://doi.org/10.1016/j.epsl.2006.07.014

Hirth, G., Tullis, J.., 1992. Dislocation creep regimes in quartz aggregates. Journal of Structural Geology 14, 145–159.

Hodgson, C.J.A.Y., 1989. The Structure of Shear-Related, Vein-Type Gold Deposits. 4, 231–273.

Hoek, J.D., 1991. A classification of dyke-fracture geometry with examples from Precambrian dyke swarms in the Vestfold Hills, Antarctica. Geologische Rundschau 80, 233–248. https://doi.org/10.1007/BF01829363

Iseppi, M., Sevin, B., Cluzel, D., Maurizot, P., Benjamin, B., 2018. Supergene nickel ore deposits controlled by gravity-driven faulting and slope failure Peridotite Nappe , New Caledonia. Economic Geology 113, 551–544. https://doi.org/10.5382/econgeo.2018.4561

Iyer, K., Jamtveit, B., Mathiesen, J., Malthe-Sørenssen, A., Feder, J., 2008. Reaction-assisted hierarchical fracturing during serpentinization. Earth and Planetary Science Letters 267, 503–516. https://doi.org/10.1016/j.epsl.2007.11.060

Jébrak, M., 1997. Hydrothermal breccias in vein-type ore deposits: A review of mechanisms, morphology and size distribution. Ore Geology Reviews 12, 111–134. https://doi.org/10.1016/S0169-1368(97)00009-7

Jiaxiang Z., Wong, T.F., Davis, D. M. 1990. Micromechanics of pressure-induced grain crushing in porous rocks. Journal of Gephysical Research 95(B1), 341-352. https://doi.org/10.1029/jb095ib01p00341

Kelemen, P.B., Aines, R., Bennett, E., Benson, S.M., Carter, E., Coggon, J.A., de Obeso, J.C., Evans, O., Gadikota, G., Dipple, G.M., Godard, M., Harris, M., Higgins, J.A., Johnson, K.T.M., Kourim, F., Lafay, R., Lambart, S., Manning,

C.E., Matter, J.M., Michibayashi, K., Morishita, T., Noël, J., Okazaki, K., Renforth, P., Robinson, B., Savage, H., Skarbek, R., Spiegelman, M.W., Takazawa, E., Teagle, D., Urai, J.L., Wilcox, J., 2018. In situ carbon mineralization in ultramafic rocks: Natural processes and possible engineered methods. Energy Procedia 146, 92–102. https://doi.org/10.1016/J.EGYPRO.2018.07.013

Kjenes, M., 2018. The geometry and evolution of deformation bands in volcaniclastic rocks: insights from Eastern Taiwan.

Knipe, R.J., 1989. Deformation mechanisms m recognition from natural tectonites. Journal of Structural Geology 11, 127–146.

Lajtai, E.Z., 1969. Mechanics of Second Order Faults and Tension Gashes. Geological Society of America Bulletin 80, 2253–2272.

Långbacka, B.O., Gudmundsson, A., 1995. Extensional tectonics in the vicinity of a transform fault in north Iceland. Tectonics 14, 294–306. https://doi.org/10.1029/94TC02904

Law, R.D., 2014. Deformation thermometry based on quartz c -axis fabrics and recrystallization microstructures : A review. Journal of Structural Geology 66, 129–161. https://doi.org/10.1016/j.jsg.2014.05.023

Leeder, M., Pérez-arlucea, M., 2006. Physical Process in Earth and Evironmental Sciences. Blackwell Publishing, United Kingdom.

Ligi, M., Bonatti, E., Gasperini, L., Poliakov, A.N.B., 2002. Oceanic broad multifault transform plate boundaries. Geology 30, 11–14. https://doi.org/10.1130/0091-7613(2002)030<0011:OBMTPB>2.0.CO;2

Lloyd, G.., Knipe, R.J., 1992. Deformation mechanisms accommodating faulting of quartzite under upper crustal conditions. Journal of Structural Geology,

14, 127–143.

Lloyd, G.E., 2000. Grain boundary contact effects during faulting of quartzite : an SEM / EBSD analysis. Journal of Structural Geology 22, 1675–1693.

Lorilleux, G., Jébrak, M., Cuney, M., Baudemont, D., 2002. Polyphase hydrothermal breccias associated with unconformity-related uranium mineralization (Canada): From fractal analysis to structural significance. Journal of Structural Geology 24, 323–338. https://doi.org/10.1016/S0191-8141(01)00068-2

MacLeod, C.J., Escartin, J., Banerji, D., Banks, G.J., Gleeson, M., Irving, D.H.B., Lilly, R.M., McCaig, A.M., Niu, Y., Allerton, S., Smith, D.K., 2002. Direct geological evidence for oceanic detachment faulting: The Mid-Atlantic Ridge, 15°45′N. Geology 30, 879–882. https://doi.org/10.1130/0091-7613(2002)030<0879:DGEFOD>2.0.CO;2

Magott, R. Fabbri, O. Fournier, M., 2017. Polyphase ductile / brittle deformation along a major tectonic boundary in an ophiolitic nappe , Alpine Corsica : Insights on subduction zone intermediate-depth asperities. Journal of Structural Geology Journal 94, 240–257. https://doi.org/10.1016/j.jsg.2016.12.002

Maia, M., Sichel, S., Briais, A., Brunelli, D., Ligi, M., Ferreira, N., Campos, T., Mougel, B., Brehme, I., Hémond, C., Motoki, A., Moura, D., Scalabrin, C., Pessanha, I., Alves, E., Ayres, A., Oliveira, P., 2016. Extreme mantle uplift and exhumation along a transpressive transform fault. Nature Geoscience 9, 1–6. https://doi.org/10.1038/ngeo2759

Mainprice, D., Lloyd, G.E., Casey, M., 1993. Individual orientation measurements in quartz polycrystals : advantages and limitations for texture and

petrophysical property determinations. Journal of Structural Geology 15, 1169–1187.

Mair, K., Frye, K. M., Marone, C. 2002. Influence of grain characteristics on the friction of granular shear zones. Journal of Geophysical Research: Solid Earth 107 (B10), ECV 4-1-ECV 4-9. http://dx.doi.org/10.1029/2001JB000516

Manatschal, G., Engström, A., Desmurs, L., Schaltegger, U., Cosca, M., Müntener, O., Bernoulli, D., 2006. What is the tectono-metamorphic evolution of continental break-up: The example of the Tasna Ocean-Continent Transition. Journal of Structural Geology 28, 1849–1869. https://doi.org/10.1016/j.jsg.2006.07.014

Marinha, do B., 2011. Imagem aérea escala 1:10.000.

Marques, L.S., Ulbrich, M.N.C., Ruberti, E., 1999. Petrology , geochemistry and Sr – Nd isotopes of the Trindade and Martin Vaz volcanic rocks ž Southern Atlantic Ocean /. Journal of Volcanology and Geothermal Research 93, 191–216. https://doi.org/10.1016/S0377-0273(99)00111-0

Márquez, A., Herrera, R., Izquierdo, T., Martín-González, F., López, I., Martín-Velázquez, S., 2017. The dyke swarms of the Old Volcanic Edifice of La Gomera (Canary Islands): Implications for the origin and evolution of volcanic rifts in oceanic island volcanoes. Global and Planetary Change 171, 255–272. https://doi.org/10.1016/j.gloplacha.2017.12.004

Mascle, J., Blarez, E., Marinho, M., 1988. The shallow structures of the Guinea and Ivory Coast-Ghana transform margins: Their bearing on the Equatorial Atlantic Mesozoic evolution. Tectonophysics 155, 193–209. https://doi.org/10.1016/0040-1951(88)90266-1

Mathieu, L., van Wyk de Vries, B., 2009. Edifice and substrata deformation induced by intrusive complexes and gravitational loading in the Mull volcano (Scotland). Bulletin of Volcanology 71, 1133–1148. https://doi.org/10.1007/s00445-009-0295-5

Mathieu, L., van Wyk de Vries, B., Holohan, E.P., Troll, V.R., 2008. Dykes, cups, saucers and sills: Analogue experiments on magma intrusion into brittle rocks. Earth and Planetary Science Letters 271, 1–13. https://doi.org/10.1016/j.epsl.2008.02.020

Mcclay, K.R., 1991. The Mapping of Geological Structures, 2nd ed. Wiley, Great Britain.

McDougall, I., 1964. Potassium-Argon Ages from Lavas of the Hawaiian Islands. Geological Society of America Bulletin 75, 107–127.

McDougall, I., Chamalaun, F.H., 1969. Isotopic Dating and Geomagnetic Polarity Studies on Volcanic Rocks from Mauritius, Indian Ocean. Geological Society of America BulletinSociety of AMer 80, 1419–1442.

McGinnis, R.N., Morris, A.P., Ferrill, D.A., Dinwiddie, C.L., 2009. Deformation analysis of tuffaceous sediments in the Volcanic Tableland near Bishop, California. Lithosphere 1, 291–304. https://doi.org/10.1130/L43.1

Mehouachi, F., Singh, S.C., 2018. Water-rich sublithospheric melt channel in the equatorial Atlantic Ocean. Nature Geoscience 11, 65–69. https://doi.org/10.1038/s41561-017-0034-z

Melo, G.W.S., Nascimento, A.F., 2018. Earthquake Magnitude Relationships for the Saint Peter and Saint Paul Archipelago, Equatorial Atlantic. Pure and Applied Geophysics 175, 741–756. https://doi.org/10.1007/s00024-017-1732-6

Melo, G.W.S., Nascimento, A.F., 2015. Análise de escalas de magnitude para eventos sísmicos de estação única : um estudo do Arquipélago de São Pedro e São Paulo . 14th International Congress of the Brazilian Geophysical Society. Brazilian Geophysical Society, Rio de Janeiro.

Melson, W.G.., Hart, S.R., Thompson, G., 1972. St . Paul ' s Rocks , Equatorial Atlantic : Petrogenesis , Radiometric Ages , and Implications on Sea-Floor Spreading. The Geological Society of America 132, 241–272.

Melson, W.G., Jarosewich, E., Bowen, V.T., Thompson, G., 1967. St. Peter and St. Paul's Rocks: a high temperature mantle-derived intrusion. Science 155, 1532–1535.

Menzel, M.D., Garrido, C.J., López Sánchez-Vizcaíno, V., Marchesi, C., Hidas, K., Escayola, M.P., Delgado Huertas, A., 2018. Carbonation of mantle peridotite by CO2-rich fluids: the formation of listvenites in the Advocate ophiolite complex (Newfoundland, Canada). Lithos. https://doi.org/10.1016/j.lithos.2018.06.001

Misra, A.A., Mukherjee, S., 2016. Dyke–brittle shear relationships in the Western Deccan Strike-slip Zone around Mumbai (Maharashtra, India). Geological Society, London, Special Publications 445, 269–295. https://doi.org/10.1144/sp445.4

Mohriak, W., 2020. Genesis and evolution of the South Atlantic volcanic islands offshore Brazil. Geo-Marine Letters. https://doi.org/https://doi.org/10.1007/s00367-019-00631-w

Mohriak, W.U., 2003. Bacias Sedimentares da Margem Continetal Brasileira. In: Bizi, L.A., Schobbenhaus, C., Vidotti, R.M., Gonçalves, J.H. (Eds.), Geologia, Tectônica e Recursos Minerais Do Brasil. Serviço Geológico do

Brasil, Brasília, 87–165.

Mohriak, W.U., Barros, A.Z.N. de, 1990. Novas Evidências De Tectonismo Cenozóico Na Região Sudeste Do Brasil : O Gráben De Barra De , São João Na Plataforma De Cabo Frio , Rj. Revista Brasileira de Geociências 20, 187–196. https://doi.org/10.1016/S0002-9149(02)02366-4

Mohriak, W.U., Rosendahl, B.R., 2003. Transform zones in the South Atlantic rifted continental margins. Geological Society, London, Special Publications 210, 211–228. https://doi.org/10.1144/GSL.SP.2003.210.01.13

Moraes, J.F.S., 1997. Arquipélago de São Pedro e São Paulo – Testemunho do Manto Superior no Atlântico Equatorial.pdf. Anais VI Congresso Brasileiro de Geoquímica. Sociedade Brasileira de Geoquímica, Salvador, 672–675.

Morandi, N., Felice, G., 1979. Serpentine minerals from veins in serpentinite rocks. Mineralogical Magazine 4, 135–140.

Moreira, N., Dias, R., 2018. Domino structures evolution in strike-slip shear zones; the importance of the cataclastic flow. Journal of Structural Geology 110, 187–201. https://doi.org/10.1016/j.jsg.2018.01.010

Morgan, W.J., 1972. Plate motions and deep mantle convection. Memoir of the Geological Society of America 132, 7–22. https://doi.org/10.1130/MEM132-p7

Motoki, A., Sichel, S.., Campos, T.F.., Vargas, T., Soares, R., Motoki, K.F., 2011. Morfologia Abissal Em Torno Do Arquipélago De São Pedro E São Paulo, Oceano Atlântico Equatorial, E Sua Relação Ao Tectonismo De Soerguimento Ativo. Revista de Geografia especial, 318–330.

Motoki, A., Sichel, S.E., Campos, T.F.D.C., Srivastava, N.K., Soares, R., 2009. Taxa de soerguimento atual do arquipélago de São Pedro e São Paulo,

Oceano Atlântico Equatorial. Revista Escola de Minas 62, 331–342. https://doi.org/10.1590/S0370-44672009000300011

Moulin, M., Aslanian, D., Unternehr, P., 2010. A new starting point for the South and Equatorial Atlantic Ocean. Earth-Science Reviews 98, 1–37. https://doi.org/10.1016/j.earscirev.2009.08.001

Nogueira, F. C.C., Nicchio, M. A., Balsamo, F., Souza, J. A.B., Silva, I. V.L., Bezerra, F. H.R., Vasconcelos, D. L., Carvalho, B. R.B.M. 2020. The influence of the cataclastic matrix on the petrophysical properties of deformation bands in arkosic sandstones. Marine and Petroleum Geology 124, 104825. https://doi.org/10.1016/j.marpetgeo.2020.104825

Noort, R. Van, Spiers, C.J., Drury, M.R., Kandianis, M.T., 2013. Peridotite dissolution and carbonation rates at fracture surfaces under conditions relevant for in situ mineralization of CO 2. Geochimica et Cosmochimica Acta 106, 1–24. https://doi.org/10.1016/j.gca.2012.12.001

Okubo, C.H., Schultz, R.A., Chan, M.A., Komatsu, G., 2009. Deformation band clusters on Mars and implications for subsurface fluid flow. Bulletin of the Geological Society of America 121, 474–482. https://doi.org/10.1130/B26421.1

Palmiotto, C., Corda, L., Bonatti, E., 2017. Oceanic tectonic islands. Terra Nova 29, 1–12. https://doi.org/10.1111/ter.12247

Palmiotto, C., Corda, L., Ligi, M., Cipriani, A., Dick, H.J.B., Douville, E., Gasperini, L., Montagna, P., Thil, F., Borsetti, A.M., Balestra, B., Bonatti, E., 2013. Nonvolcanic tectonic islands in ancient and modern oceans. Geochemistry, Geophysics, Geosystems 14, 4698–4717. https://doi.org/10.1002/ggge.20279

Papeschi, S., Musumeci, G., Mazzarini, F., 2018. Evolution of shear zones through the brittle-ductile transition: The Calamita Schists (Elba Island, Italy). Journal of Structural Geology 113, 100–114. https://doi.org/10.1016/j.jsg.2018.05.023

Park, M., Jung, H., 2017. Microstructural evolution of the Yugu peridotites in the Gyeonggi Massif, Korea: Implications for olivine fabric transition in mantle shear zones. Tectonophysics 709, 55–68. https://doi.org/10.1016/j.tecto.2017.04.017

Parry, W.T., Chan, M.A., Beitler, B., 2004. Chemical bleaching indicates episodes of fluid flow in deformation bands in sandstone. American Association of Petroleum Geologists Bulletin 88, 175–191. https://doi.org/10.1306/09090303034

Paschier, C.W., Trouw, R.A.J., 2005. Microtectonics, Springer. ed. Berlin.

Pasqualon, N.G., de Lima, E.F., dos Santos Scherer, C.M., de Magalhães May Rossetti, L., da Luz, F.R., 2019. Lithofacies association and stratigraphy of the Paredão Volcano, Trindade Island, Brazil. Journal of Volcanology and Geothermal Research 380, 48–63. https://doi.org/10.1016/j.jvolgeores.2019.05.011

Pec, M., Stünitz, H., Heilbronner, R., 2012. Semi-brittle deformation of granitoid gouges in shear experiments at elevated pressures and temperatures. Journal of Structural Geology 38, 200–221. https://doi.org/10.1016/j.jsg.2011.09.001

Petit, J.P., 1987. Criteria for the sense of movement on fault surfaces in brittle rocks. Journal of Structural Geology 9, 597–608. https://doi.org/10.1016/0191-8141(87)90145-3

Petronis, M.S., 2013. Magma emplacement into the Lemptégy scoria cone (Chaîne Des Puys , France) explored with structural , anisotropy of magnetic susceptibility , and Paleomagnetic data. https://doi.org/10.1007/s00445-013-0753-y

Peuble, S., Andreani, M., Godard, M., Gouze, P., Barou, F., Van De Moortele, B., Mainprice, D., Reynard, B., 2015. Carbonate mineralization in percolated olivine aggregates: Linking effects of crystallographic orientation and fluid flow. American Mineralogist 100, 474–482. https://doi.org/10.2138/am-2015-4913

Peuble, S., Andreani, M., Gouze, P., Pollet-Villard, M., Reynard, B., Van de Moortele, B., 2018. Multi-scale characterization of the incipient carbonation of peridotite. Chemical Geology 476, 150–160. https://doi.org/10.1016/j.chemgeo.2017.11.013

Piazolo, S., Austrheim, H., Whitehouse, M., 2012. Brittle-ductile microfabrics in naturally deformed zircon: Deformation mechanisms and consequences for U-Pb dating. American Mineralogist 97, 1544–1563. https://doi.org/10.2138/am.2012.3966

Picazo, S., Manatschal, G., Cannat, M., Andréani, M., 2013. Lithos Deformation associated to exhumation of serpentinized mantle rocks in a fossil Ocean Continent Transition : The Totalp unit in SE Switzerland. LITHOS 175–176, 255–271. https://doi.org/10.1016/j.lithos.2013.05.010

Pinheiro, M.R., Cianfarra, P., Villela, F.N.J., Salvini, F., 2019. Tectonics of the Northeastern border of the Parana Basin (Southeastern Brazil) revealed by lineament domain analysis. Journal of South American Earth Sciences 94, 102231. https://doi.org/10.1016/j.jsames.2019.102231

Pinheiro, M.R., Queiroz Neto, J.P. de, 2014. Reflexões Sobre a Gênese Da Serra Geral E Da Depressão Periférica Paulista: O Exemplo Da Região Da Serra De São Pedro E Do Baixo Piracicaba, Sp. Revista Do Instituto Geológico 35, 47–59. https://doi.org/10.5935/0100-929x.20140004

Pires, G.L.C., Bongiolo, E.M., 2016. Journal of South American Earth Sciences The nephelinitic e phonolitic volcanism of the Trindade Island (South Atlantic Ocean): Review of the stratigraphy , and inferences on the volcanic styles and sources of nephelinites. Journal of South American Earth Sciences 72, 49–62. https://doi.org/10.1016/j.jsames.2016.07.008

Pires, G.L.C., Bongiolo, E.M., Neumann, R., 2016. New 40Ar/39Ar ages and revised 40K/40Ar* data from nephelinitic–phonolitic volcanic successions of the Trindade Island (South Atlantic Ocean). Journal of Volcanology and Geothermal Research. https://doi.org/10.1016/j.jvolgeores.2016.09.020

Pizzati, M., Balsamo, F., Storti, F. 2020. Displacement-dependent microstructural and petrophysical properties of deformation bands and gouges in poorly lithified sandstone deformed at shallow burial depth (Crotone Basin, Italy). Journal of Structural Geology 137,1-21. https://doi.org/10.1016/j.jsg.2020.104069

Pollard, D.D., Townsend, M.R., 2018. Fluid-filled fractures in Earth's lithosphere: Gravitational loading, interpenetration, and stable height of dikes and veins. Journal of Structural Geology 109, 38–54. https://doi.org/10.1016/j.jsg.2017.11.007

Post, A., Tullis, J., 1999. A recrystallized grain size piezometer for experimentally deformed feldspar aggregates. Tectonophysics 303, 159–173.

Précigout, J., Prigent, C., Palasse, L., Pochon, A., 2017. Water pumping in mantle

shear zones. Nature Communications 8. https://doi.org/10.1038/ncomms15736

Prigent, .C, Agard, P., Guilot, S., Godard, M., Dubacq, B., 2018a. Mantle wedge deformation during subduction infancy : evidence from the base of the Semail ophiolitic mantle. https://doi.org/10.1093/petrology/egy090

Prigent, C., Warren, J., Kohli, A., Teyssier, A., 2018b. The semi-brittle to ductile transition in oceanic faults in peridotite : mechanisms and P-T conditions. AGU Fall Meeting 2017. 1–2.

Queiroz, G.L., Salamuni, E., Do Nascimento, E.R., 2014. AzimuthFinder: Ferramenta para a extração de dados e apoio na análise estrutural. Geologia USP - Serie Cientifica 14, 69–80. https://doi.org/10.5327/Z1519-874X201400010005

Quesnel, B., Gautier, P., Boulvais, P., Cathelineau, M., Maurizot, P., Cluzel, D., Ulrich, M., Guillot, S., Lesimple, S., Couteau, C., 2013. Syn-tectonic, meteoric water-derived carbonation of the new caledonia peridotite nappe. Geology 41, 1063–1066. https://doi.org/10.1130/G34531.1

Quesnel, B., Gautier, P., Cathelineau, M., Boulvais, P., 2016. The internal deformation of the Peridotite Nappe of New Caledonia : A structural study of serpentine-bearing faults and shear zones in the Koniambo Massif. 85, 51–67. https://doi.org/10.1016/j.jsg.2016.02.006

Rahl, J.M., Skemer, P., 2016. Microstructural evolution and rheology of quartz in a mid-crustal shear zone. Tectonophysics 680, 129–139. https://doi.org/10.1016/j.tecto.2016.05.022

Ramsay, J.G., 1980. The crack-seal mechanism of rock deformation. Nature 284, 135–139. https://doi.org/10.1038/284135a0

Re, G., White, J.D.L., Ort, M.H., 2015. Dikes, sills, and stress-regime evolution during emplacement of the Jagged Rocks Complex, Hopi Buttes Volcanic Field, Navajo Nation, USA. Journal of Volcanology and Geothermal Research 295, 65–79. https://doi.org/10.1016/j.jvolgeores.2015.01.009

Reber, J.E., Pec, M., 2018. Comparison of brittle- and viscous creep in quartzites: Implications for semi-brittle flow of rocks. Journal of Structural Geology 113, 90–99. https://doi.org/10.1016/j.jsg.2018.05.022

Renard, F., Andréani, M., Boullier, A.M., Labaume, P., 2005. Crack-seal patterns: Records of uncorrelated stress release variations in crustal rocks. Geological Society Special Publication 243, 67–79. https://doi.org/10.1144/GSL.SP.2005.243.01.07

Reuber, K., Mann, P., 2019. Control of Precambrian-To-Paleozoic Orogenic Trends on Along-Strike Variations in Early Cretaceous Continental Rifts of the South Atlantic Ocean. Interpretation 1–80. https://doi.org/10.1190/int-2018-0257.1

Ribeiro, C.V.., Patrício, R.L., Hackspacher, P.C., 2019. Evolução Tectono-Magmática da Ilha de Trindade, Atlântico Sul. 28º Simpósio de Geologia Do Nordeste. Aracajú, 1.

Riccomini, C., 1989. O Rift continental do sudeste do Brasil. Universidade de São Paulo.

Riccomini, C., Assumpção, M., 1999. Quaternary tectonics in Brazil. Episodes 22, 221–225.

Riccomini, C., Sant'Anna, L.G., Ferrari, L.A., 2004. Evolução geológica do rift continental do sudeste do Brasil. In: Mantesso-Neto, V., Bartorelli, A., Carneiro, C.D.., Brito Neves, B.B. (Eds.), Geologia Do Continente Sul-

Americano: Evolução Da Obra de Fernando Flávio Marques de Almeida. Beca, São Paulo, 383–405.

Rivalta, E., Taisne, B., Bunger, A.P., Katz, R.F., 2015. A review of mechanical models of dike propagation: Schools of thought, results and future directions. Tectonophysics 638, 1–42. https://doi.org/10.1016/j.tecto.2014.10.003

Rodrigues, M.C.N. de L., Trzaskos, B., Lopes, A.P., 2015a. Influence of deformation bands on sandstone porosity: A case study using three-dimensional microtomography. Journal of Structural Geology 72, 96–110. https://doi.org/10.1016/j.jsg.2015.01.003

Rotevatn, A., Torabi, A., Fossen, H., Braathen, A. 2008. Slipped deformation bands: A new type of cataclastic deformation bands in Western Sinai, Suez rift, Egypt. Journal of Structural Geology 30, 1317-1331. http://dx.doi.org/10.1016/j.jsg.2008.06.010

Rouméjon, S., Cannat, M., Agrinier, P., Godard, M., Andreani, M., 2014. Serpentinization and fluid pathways in tectonically exhumed peridotites from the southwest Indian ridge (62-65°E). Journal of Petrology 56, 703–734. https://doi.org/10.1093/petrology/egv014

Rudge, J.F., Kelemen, P.B., Spiegelman, M., 2010. A simple model of reaction-induced cracking applied to serpentinization and carbonation of peridotite. Earth and Planetary Science Letters 291, 215–227. https://doi.org/10.1016/j.epsl.2010.01.016

Salvador, E.D., Riccomini, C., 1995. Neotectônica da Região do Alto Estrutural de Queluz (SP-RJ, Brasil). Revista Brasileira de Geociências 25, 151–164.

Sandwell, D.T., Smith, W.H.F., 1997. Marine gravity anomaly from Geosat and ERS 1 satellite altimetry. Journal of Geophysical Research 102, 10039.

https://doi.org/10.1029/96JB03223

Schneider, C.A., Rasband, W.S., Eliceiri, K.W., 2012. NIH Image to ImageJ: 25 years of image analysis. Nature Methods 9, 671–675. https://doi.org/10.1038/nmeth.2089

Scholz, C.H., 1988. The brittle-plastic transition and the depth of seismic faulting. Geologische Rundschau 77/1 77, 319–328.

Schroeder, T., John, B., Frost, B.R., 2002. Geologic implications of seawater circulation through peridotite exposed at slow-spreading mid-ocean ridges. Geology 30, 367–370. https://doi.org/10.1130/0091-7613(2002)030<0367:GIOSCT>2.0.CO;2

Schroeder, T., John, B.E., 2004. Strain localization on an oceanic detachment fault system, Atlantis Massif, 30 ° N, Mid-Atlantic Ridge. Geochemistry, Geophysics, Geosystems 5, 1–30. https://doi.org/10.1029/2004GC000728

Searle, M., Avouac, J.P., Elliott, J., Dyck, B., 2017. Ductile shearing to brittle thrusting along the Nepal Himalaya: Linking Miocene channel flow and critical wedge tectonics to 25th April 2015 Gorkha earthquake. Tectonophysics 714–715, 117–124. https://doi.org/10.1016/j.tecto.2016.08.003

Sibrant, A.L.R., Hildenbrand, A., Marques, F.O., Costa, A.C.G., 2015. Volcano-tectonic evolution of the Santa Maria Island (Azores): Implications for paleostress evolution at the western Eurasia-Nubia plate boundary. Journal of Volcanology and Geothermal Research 291, 49–62. https://doi.org/10.1016/j.jvolgeores.2014.12.017

Sibson, R., 1986. Brecciation processes in fault zones. Pure and Applied Geophysics 124, 159–175.

Sibson, R.H., 1983. Continental fault structure and the shallow earthquake source. Journal of the Geological Society 140, 741–767. https://doi.org/10.1144/gsjgs.140.5.0741

Sibson, Richard H., 1977. Fault rocks and fault mechanisms. Journal of the Geological Society 133, 191–213. https://doi.org/10.1144/gsjgs.133.3.0191

Sichel, S.E., Esperança, S., Motoki, A., Maia, M., Horan, M.F., Szatmari, P., Da, E., Alves, C., Mello, S.L.M., 2008. Geophysical and Geochemical Evidence for Cold Upper Mantle Beneath the Equatorial Atlantic Ocean. Revista Brasileira de Geofísica 26, 69–86. https://doi.org/10.1590/S0102-261X2008000100006

Siebel, W., Becchio, R., Volker, F., Hansen, M.A.F., Viramonte, J., Trumbull, R.B., Haase, G., Zimmer, M., 2000. Trindade and Martin Vaz Islands, South Atlantic: Isotopic (Sr, Nd, Pb) and trace element constraints on plume related magmatism. Journal of South American Earth Sciences 13, 79–103. https://doi.org/10.1016/S0895-9811(00)00015-8

Simões, L.S., Andrade, F.G., Campos, T.F., Sichel, S.E., Motoki, A., 2009. Padrão petro-estrutural das rochas e o seu significado no contexto tectônico do Atlântico Equatorial. In: Viana, D.L.; Hazin, F.H.V.; Souza, M.A.C. (Ed.), Arquipélago São Pedro e São Paulo: 10 Anos de Estação Científica. Brasília-DF, 92–97.

Skelton, Y.A.D.L., Valley, J.W., 2000. The relative timing of serpentinisation and mantle exhumation at the ocean–continent transition, Iberia: constraints from oxygen isotopes. Earth and Planetary Science Letters 178, 327–338.

Soda, Y., Takagi, H., 2010. Sequential deformation from serpentinite mylonite to metasomatic rocks along the Sashu Fault, SW Japan. Journal of Structural

Geology 32, 792–802. https://doi.org/10.1016/j.jsg.2010.05.003

Soliva, R., Ballas, G., Fossen, H., Philit, S., 2016. Tectonic regime controls clustering of deformation bands in porous sandstone. Geology 44, 423–426. https://doi.org/10.1130/G37585.1

Souza, K.G., Martins, L.R., Cavalcanti, V.M., Pereira, C. V., Borges, L.F., 2009. Recursos Não-Vivos da Plataforma Continental Brasileira e Áreas Oceânicas Adjacentes. Gravel Edição Esp, 86.

Starkey, J., 1968. The geometry of kink bands in crystals - a simple model. Contrib.

Mineral. Petrol. 19 (2), 133–141. https://doi.org/10.1007/BF00635484.

Stipp, M., Stünitz, H., Heilbronner, R., Schmid, S.M., 2002a. Dynamic recrystallization of quartz: Correlation between natural and experimental conditions. Geological Society Special Publication 200, 171–190. https://doi.org/10.1144/GSL.SP.2001.200.01.11

Stipp, M., Stunitz, H., Sciences, E., 2002b. Dynamic recrystaUization of quartz : correlation between natural and experimental conditions. In: de Meer, S.; Drury, M. R.; D. Bresser, J. H. P.; PENNOCK, G.M. (Ed.), Dynamic RecrystaUization of Quartz: Correlation between Natural and Experimental Conditions. London, 171–190.

Szatmari, P., Mohriak, W.U., 1995. Plate model postbreakup tectono-magmatic activity in SE Brazil and the adjacent Atlantic. Simpósio Nacional de Estudos Tectônicos 5. SBGEO, Gramado, 213–214.

Tilley, C.E., 1947. The dunite-mylonites of Saint Paul's Rocks (Atlantic). American Journal Of Science 483–494.

Tondi, E., Antonellini, M., Aydin, A., Marchegiani, L., Cello, G., 2006. The role of

deformation bands, stylolites and sheared stylolites in fault development in carbonate grainstones of Majella Mountain, Italy. Journal of Structural Geology 28, 376–391. https://doi.org/10.1016/j.jsg.2005.12.001

Torabi, A., Fossen, H., Braathen, A., 2013. Insight into petrophysical properties of deformed sandstone reservoirs. AAPG Bulletin 97, 619–637. https://doi.org/10.1306/10031212040

Torabi, A. 2014. Cataclastic bands in immature and poorly lithified sandstone, examples from Corsica, France. Tectonophysics 630, 91-102. http://dx.doi.org/10.1016/j.tecto.2014.05.014

Tavares, A.C., Castro, D.L., Bezerra, F.H.C., Oliveira, D.C., Vanucchi, P., Iacopini, D., Jovane, L., Vital, H., 2020. The Romanche fracture zone influences the segmentation of the equatorial margin of Brazil. J. S. Am. Earth Sci. https://doi.org/10.1016/j.jsames.2020.102738

Torsvik, T.H., Rousse, S., Labails, C., Smethurst, M.A., 2009. A new scheme for the opening of the South Atlantic Ocean and the dissection of an Aptian salt basin. Geophysical Journal International 177, 1315–1333. https://doi.org/10.1111/j.1365-246X.2009.04137.x

Trommsdorff, V., Evans, B., Pfeifer, H., 1980. Ophicarbonate rocks - Metamorphic reactions and possible origin. Archives Des Sciences 33, 361–364.

Tubía, J.M., Cuevas, J., Esteban, J.J., 2004. Tectonic evidence in the Ronda peridotites, Spain, for mantle diapirism related to delamination. Geology 32, 941–944. https://doi.org/10.1130/G20869.1

Tucholke, E., Lin, J., Kleinrock, C., 1998. Megamullions and mullion structure defining oceanic metamorphic core complexes on the Mid-Atlantic Ridge.

Journal of Geophysical Research 103, 9857–9866.

Tulis, J., 1970. Quartz: Preferred Orientation in Rocks Produced by Dauphiné Twinning. Science 168, 1342–1344.

Ueda, T., Obata, M., Di Toro, G., Kanagawa, K., Ozawa, K., 2008. Mantle earthquakes frozen in mylonitized ultramafic pseudotachylytes of spinel-lherzolite facies. Geology 36, 607–610. https://doi.org/10.1130/G24739A.1

Ulbrich, M.N.C., Marques, L.S., Lopes, R.P., 2004. As ilhas vulcânicas brasileira - Fernando de Noronha e Trindade. In: Mantesso-Neto, V., Bartorelli, A., Carneiro, C.D.R., Brito-Neves, B.B. (Eds.), Geologia Do Continente Sul-Americano: Evolução Da Obra de Fernando Flávio Marques de Almeida. BEca, 555–573.

Urai, J., Means, W.D., Lister, G., 1986. Dynamic recrystallization of minerals. Geophysical Monograph 36, 161–198. https://doi.org/10.1029/GM036p0161

Vasconcelos, D.L., Bezerra, F.H.R., Clausen, O.R., Medeiros, W.E., de Castro, D.L., Vital, H., Barbosa, J.A., 2019. Influence of Precambrian shear zones on the formation of oceanic fracture zones along the continental margin of Brazil. Marine and Petroleum Geology 101, 322–333. https://doi.org/10.1016/j.marpetgeo.2018.12.010

Ventura, G., Vilardo, G., Milano, G., Pino, N.A., 1999. Relationships among crustal structure, volcanism and strike-slip tectonics in the Lipari-Vulcano Volcanic Complex (Aeolian Islands, Southern Tyrrhenian Sea, Italy). Physics of the Earth and Planetary Interiors 116, 31–52. https://doi.org/10.1016/S0031-9201(99)00117-X

Viola, G., Kounov, A., Andreoli, M.A.G., Mattila, J., 2012. Brittle tectonic evolution along the western margin of South Africa: More than 500Myr of continued

reactivation. Tectonophysics 514–517, 93–114. https://doi.org/10.1016/j.tecto.2011.10.009

Virgo, S., Abe, S., Urai, J.L., 2014. Journal of Geophysical Research : Solid Earth Models of fracture sealing. 8708–8727. https://doi.org/10.1002/2014JB011520.Received

Wallace, M., Green, D.H., 1991. The effect of bulk rock composition on the stability of amphibole in the upper mantle: Implications for solidus positions and mantle metasomatism. Mineralogy and Petrology 44, 1–19. https://doi.org/10.1007/BF01167097

Wang, Y.F., Zhang, J.F., Jin, Z.M., Green, H.W., 2012. Mafic granulite rheology: Implications for a weak continental lower crust. Earth and Planetary Science Letters 353–354, 99–107. https://doi.org/10.1016/j.epsl.2012.08.004

White, R.S., Drew, J., Martens, H.R., Key, J., Soosalu, H., Jakobsdóttir, S.S., 2011. Dynamics of dyke intrusion in the mid-crust of Iceland. Earth and Planetary Science Letters 304, 300–312. https://doi.org/10.1016/j.epsl.2011.02.038

Whitney, D.L and Evans, B. W. 2010. Abbreviations for names of rock-forming minerals. American Mineralogist 95, 185-187

Wicks, F J; Whittaker, E.J.W., 1977. Serpentine Textures and Serpentinization. Canadian Mineralogist 15(1), 459–488. https://doi.org/10.2138/am.2010.3371

Wilson, J.E., Goodwin, L.B., Lewis, C.J., 2003. Deformation bands in nonwelded ignimbrites: Petrophysical controls on fault-zone deformation and evidence of preferential fluid flow. Geology 31, 837–840. https://doi.org/10.1130/G19667R.1

Wilson, J.T., 1963. A possible origin of the Hawaiian Islands. Canadian Journal of Earth Sciences 51, 863–870. https://doi.org/10.1139/p63-094

Wilson, J.T., 1965. A new class of faults and their bearing on continental drift. Nature 343–347.

Wintsch, R.P., Christoffersen, R., Kronenberg, a. K., 1995. Fluid-rock reaction weakening of fault zones. Journal of Geophysical Research 100, 13021. https://doi.org/10.1029/94JB02622

Wiseman, J.D.H., 1966. St Paul Rocks and the Problem of the Upper Mantle. Journal of Geophysical Research 11, 519–525.

Wolfe, C.J., Bergman, E. a., Solomon, S.C., 1993. Oceanic transform earthquakes with unusual mechanisms or locations: Relation to fault geometry and state of stress in the adjacent lithosphere. Journal of Geophysical Research 98, 16187. https://doi.org/10.1029/93JB00887

Woods, J., Winder, T., White, R.S., Brandsdóttir, B., 2019. Evolution of a lateral dike intrusion revealed by relatively-relocated dike-induced earthquakes: The 2014–15 Bárðarbunga–Holuhraun rifting event, Iceland. Earth and Planetary Science Letters 506, 53–63. https://doi.org/10.1016/j.epsl.2018.10.032

Zuluaga, L.F., Fossen, H., Rotevatn, A., 2014. Progressive evolution of deformation band populations during laramide fault-propagation folding: Navajo Sandstone, san rafael monocline, Utah, U.S.A. Journal of Structural Geology 68, 66–81. https://doi.org/10.1016/j.jsg.2014.09.008

Ulbrich M.N.C., Marques L.S., Lopes R.P. 2004. As ilhas vulcânicas brasileiras: Fernando de No- ronha e Trindade. In: V. Mantesso-Neto, A. Bartorelli, C.D.R. Carneiro, B.B.de B. Neves (eds.). Geologia do Continente Sul-

Americano: Evolução da Obra de Fernando Flávio Marques de Almeida. São Paulo: Beca, 555-573p.

Vasconcelos, D.L., Bezerra, F.H.R., Clausen, O.R., Medeiros, W.E., de Castro, D.L., Vital, H., Barbosa, J.A., 2019. Influence of Precambrian shear zones on the formation of oceanic fracture zones along the continental margin of Brazil. Marine and Petroleum Geology 101, 322–333. https://doi.org/10.1016/j.marpetgeo.2018.12.010

ANEXO 1 – Figuras Suplementares Artigo 1

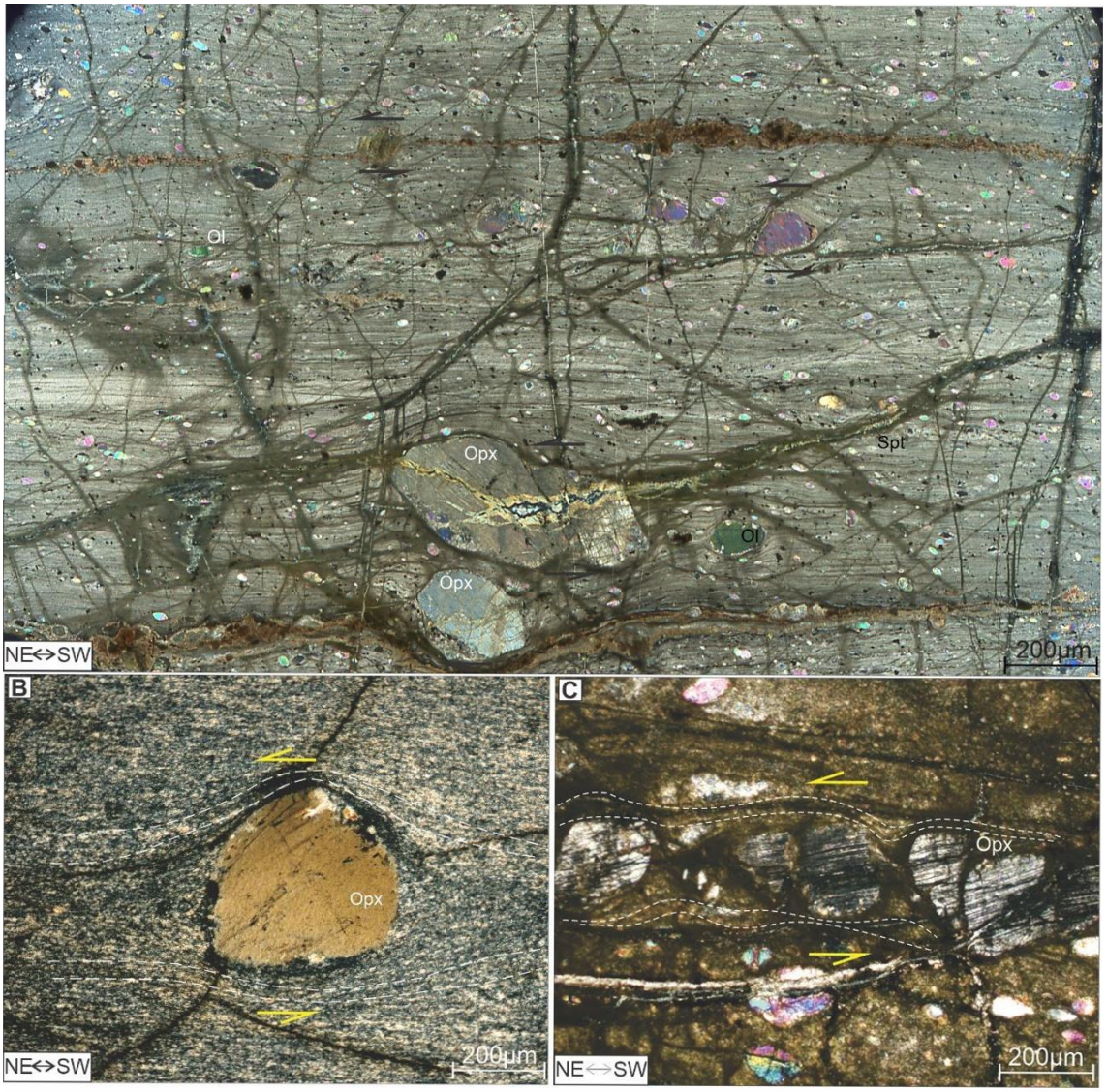

Figure - Photomicrographs of the mylonitic domain. (A) Overview of the ultramylonites, ortopyroxene (Opx) porphyroclasts and olivine (Ol) porphyroclasts surrounded by the fine-grained recrystallized matrix; (B) Ortopyroxene porphyroclasts showing left lateral kinematics; (C) Opx crystal fragmented.

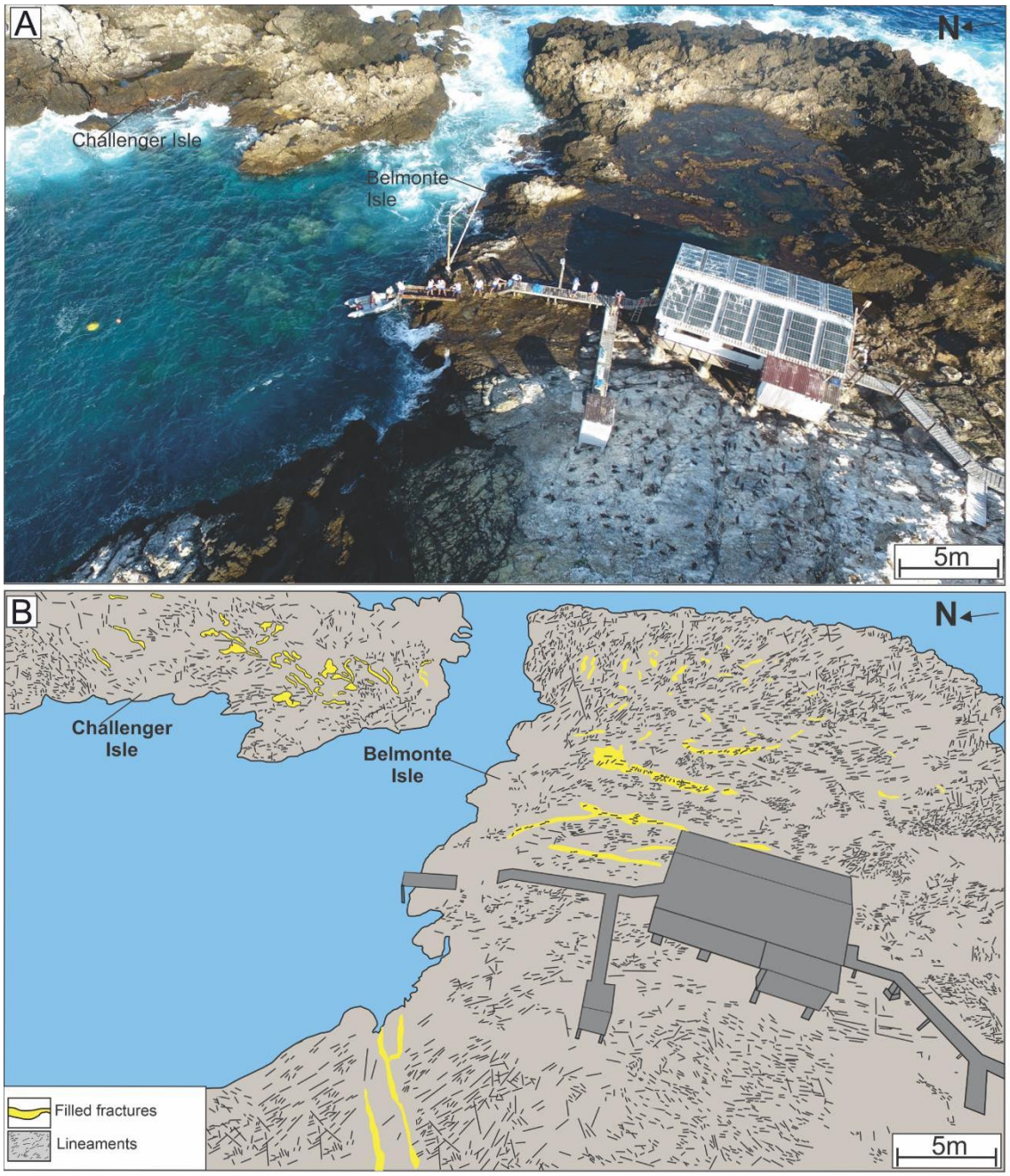

Figure - (A) Drone image of SPSP Challenger and Belmonte Isles. (B) Interpreted drone image (scale - 1:50), highlight the main lineaments observed on SPSP, the structures has the main direction NNW-SSE, probably associated to mylonitic foliation and cataclastic flow. Other structures also delineate the fractures filled by sediments, with strucutre turned to NNE-SSW and E-W structures.

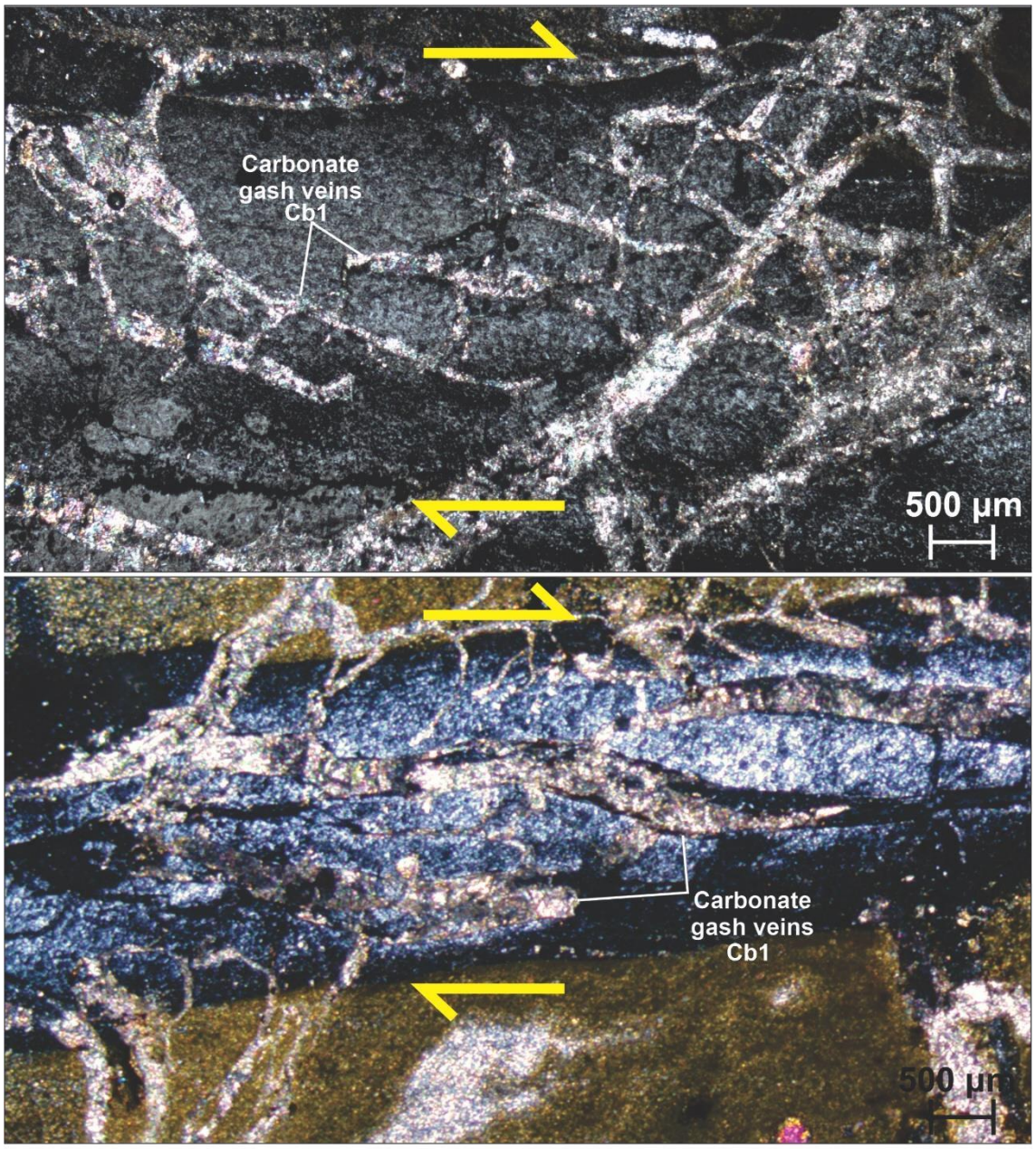

Figure - Carbonate gash veins formed in Cbto 1 phase. Observed dextral kinematic.

ANEXO 2 – Figuras Suplementares Artigo 2

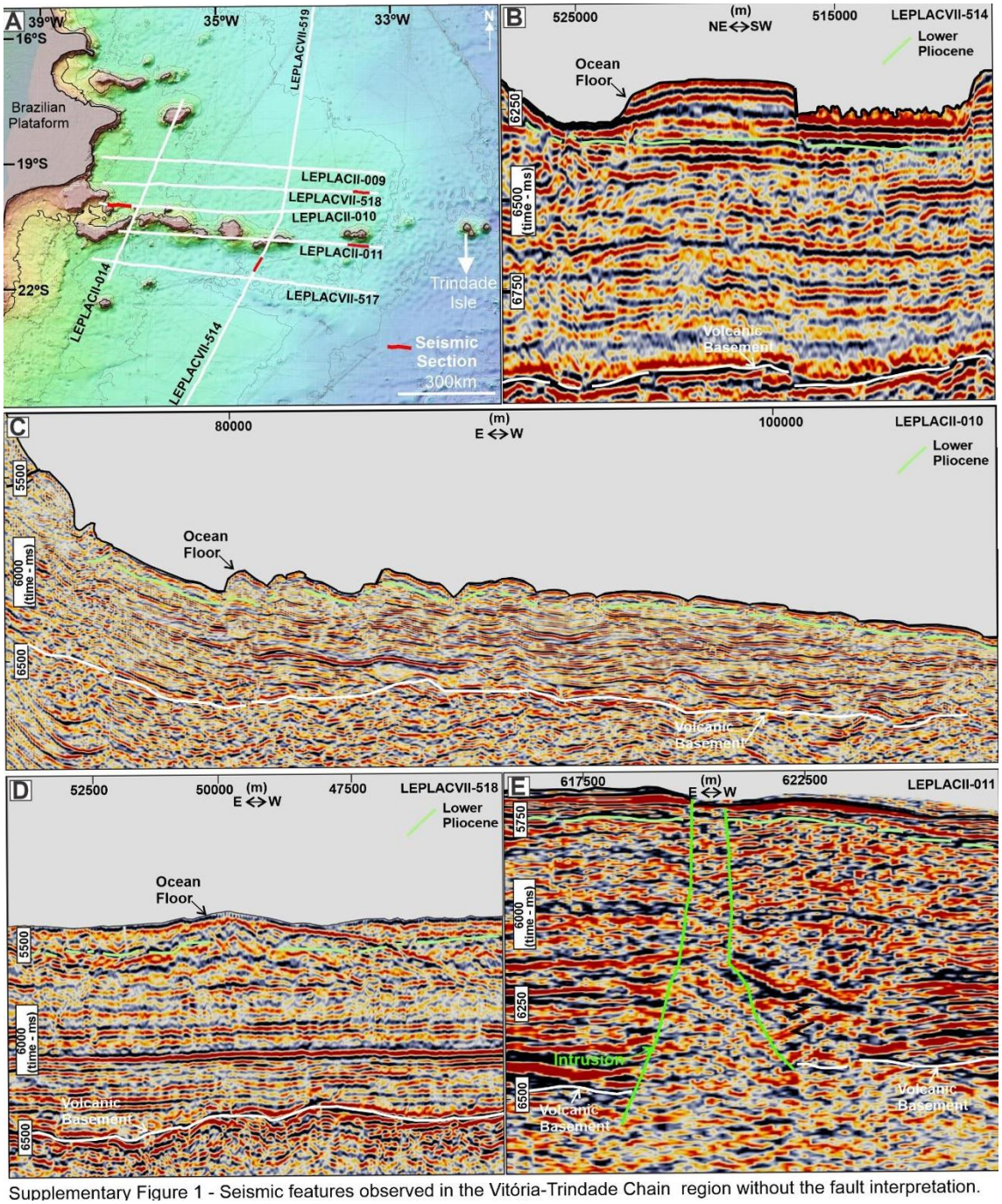

Supplementary Figure 1 - Seismic features observed in the Vitória-Trindade Chain region without the fault interpretation.

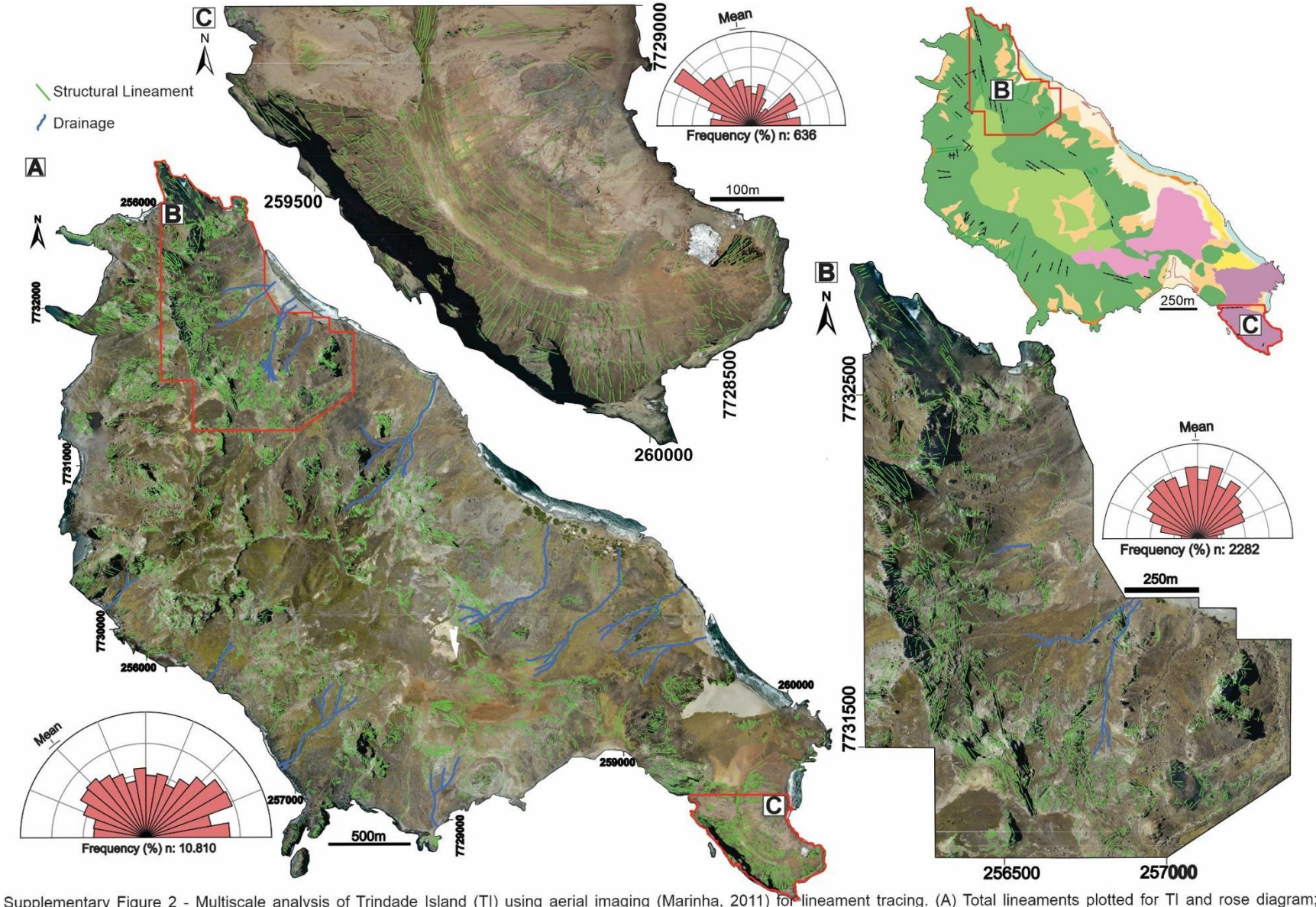

Supplementary Figure 2 - Multiscale analysis of Trindade Island (TI) using aerial imaging (Marinha, 2011) for lineament tracing. (A) Total lineaments plotted for TI and rose diagram; (B) Lineaments traced to the Crista do Galo and Noroesten region with the cumulative frequency of lineaments; (C) Zoom of the Paredão Volcano area with the lineament and rose diagram compiled for this area.

ANEXO 3 –Figuras e tabelas Suplementares Artigo 3

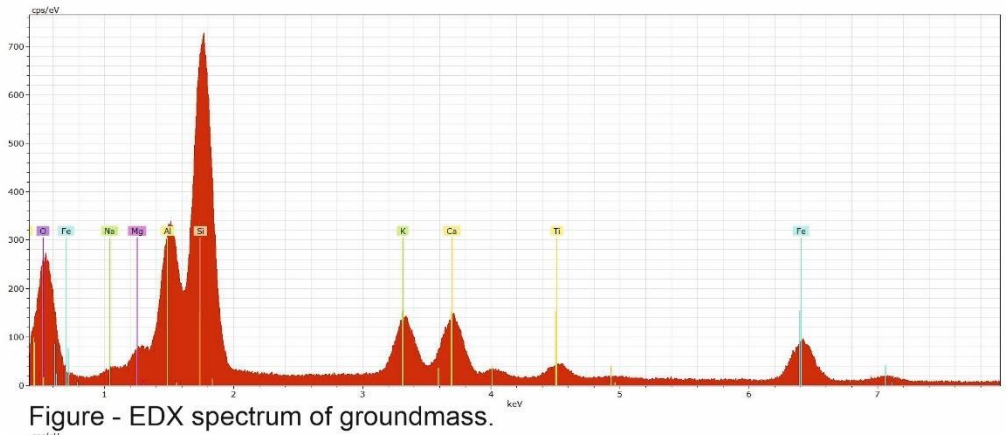

Figure - EDX spectrum of groundmass.

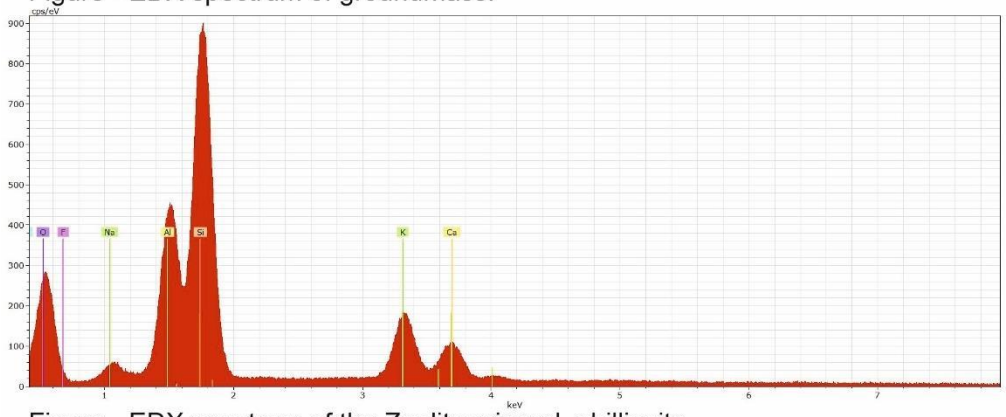

Figure - EDX spectrum of the Zeolite mineral, phillipsite.

Supplementary Figure 1 – EDX spectrum for matrix and zeolite.

Supplementary Table 1 – Mineral contents data for the analysed thin section

Mineral	Area1 - Host Rock - Wt%	Area2 - Deformation Band Wt%
Quartz	0,01	0,00
Pyroxene	15,42	9,04
Amphibole	11,76	6,73
K_feldspar	5,38	3,83
Albite	0,08	0,01
Biotite	5,23	6,33
Phillipsite_Ca_K	13,08	5,89
Titanite	0,49	0,62
Apatite	0,82	0,52
Magnetite_Ti	4,52	2,63
Ilmenite	0,45	0,25
Pyrrhotite	0,00	0,00
Pyrite	0,00	0,00
Glass	0,62	0,51
Groundmass	41,57	63,29
Unclassified	0,57	0,34
Total	100,00	100,00

Number of measured points	28506	8825

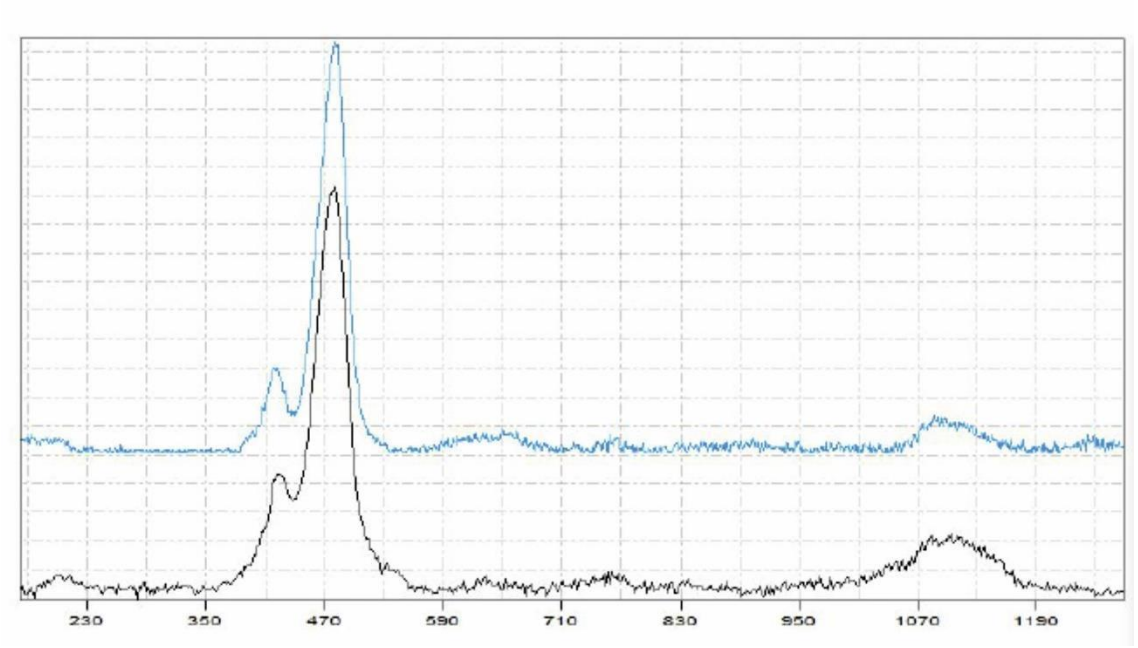

Supplementary Figure 2 - Raman spectrum of the zeolite mineral, phillipsite. The spectrum below (black) is from the studied sample. The upper one (blue) is from RRUFF-database. The matching percentage is 98%. The laser wavelength was 532 nm.

Supplementary Table 2 – Distribuição de tamanho dos grãos na bandas e rocha hospedeira para o Piroxênio e Fedspato Alcalino, respectivamente.

Mineral Size Distribution - [Grain Layer]:[Pyroxene]:[Equivalent Circle]:[SEM Default Sieve Sizes]			
Size	Particle Count	Retained (Wt%)	Cumumation Passing (Wt%)
1009,08	0	0	100,00%
848,53	1	1,05	98,95%
713,52	0	0	98,95%
600	2	1,02	97,93%
504,54	3	1,2	96,73%
424,26	14	3,67	93,05%
356,76	23	4,25	88,80%
300	38	4,98	83,82%
252,27	57	5,47	78,35%
212,13	113	7,45	70,91%
178,38	177	8,23	62,68%
150	230	7,7	54,97%
126,13	333	7,92	47,06%
106,07	455	7,63	39,43%
89,19	544	6,45	32,98%
75	731	6,1	26,88%
63,07	957	5,65	21,23%
53,03	1215	5,08	16,15%
44,6	1323	3,91	12,24%
37,5	1505	3,16	9,08%
31,53	1709	2,54	6,54%
26,52	1781	1,86	4,68%
22,3	1860	1,37	3,31%
18,75	1894	0,98	2,33%
15,77	2085	0,75	1,58%
13,26	1871	0,48	1,09%
11,15	3090	0,55	5,40%
9,38	1476	0,19	3,50%
7,88	3786	0,35	0,00%

Mineral Size Distribution - [Grain Layer]:[K-feldspar]:[Equivalent Circle]:[SEM Default Sieve Sizes]			
Size	Particle Count	Retained (Wt%)	Cum. Passing (Wt%)
1200	1	16,73	83,27
1009,08	0	0	83,27
848,53	0	0	83,27
713,52	2	2,08	81,19
600	1	0,69	80,5
504,54	5	2,77	77,73
424,26	4	1,58	76,15
356,76	12	3,44	72,7
300	13	2,67	70,04
252,27	21	2,9	67,13
212,13	45	4,42	62,71
178,38	67	4,74	57,97
150	83	4,14	53,82
126,13	154	5,41	48,42
106,07	189	4,71	43,71
89,19	307	5,4	38,31
75	438	5,5	32,8
63,07	636	5,66	27,14
53,03	924	5,78	21,36
44,6	1120	4,97	16,39
37,5	1365	4,31	12,08
31,53	1402	3,12	8,96
26,52	1517	2,38	6,58
22,3	1576	1,73	4,85
18,75	1673	1,29	3,55
15,77	1989	1,07	2,48
13,26	1902	0,74	1,74
11,15	3224	0,87	0,87
9,38	1516	0,3	0,58
7,88	4196	0,58	0